

PDF hosted at the Radboud Repository of the Radboud University Nijmegen

The following full text is a publisher's version.

For additional information about this publication click this link.

<http://hdl.handle.net/2066/49201>

Please be advised that this information was generated on 2017-12-06 and may be subject to change.

MAGNETIC RESONANCE SPECTROSCOPY
OF CREATINE-RELATED ENERGY METABOLISM
IN SKELETAL MUSCLE AND BRAIN

MAGNETIC RESONANCE SPECTROSCOPY
OF CREATINE-RELATED ENERGY METABOLISM
IN SKELETAL MUSCLE AND BRAIN

Een wetenschappelijke proeve op het gebied van de Medische Wetenschappen

Proefschrift ter verkrijging van de graad van doctor aan de Radboud Universiteit Nijmegen,
op gezag van de Rector Magnificus Prof. Dr. C.W.P.M. Blom, volgens besluit van het
College van Decanen in het openbaar te verdedigen op
maandag 10 oktober des namiddags om 1:30 uur precies door

Willem Klaas Jans Renema
geboren op 19 augustus 1975 te Winterswijk

Promotores: Prof. Dr. A. Heerschap
Prof. Dr. B. Wieringa

Manuscriptcommissie: Prof. Dr. R.J.M. Bindels
Prof. Dr. D.G. Norris
Dr. P.J.W. Pouwels (Vrije Universiteit Amsterdam)

ISBN-10: 9090197680

ISBN-13: 9789090197685

Printed by Print Partners Ipskamp Enschede, The Netherlands

This project was supported by a program grant from the Dutch Organization for Scientific Research (NWO-ZonMW).

CONTENTS

Abbreviations and symbols	7
1 Introduction	9
1.1 Magnetic resonance spectroscopy of energy metabolism in vivo	10
1.1.1 ATP production and utilization	10
1.1.2 Creatine: formation, utilization and catabolism	11
1.1.3 Occurrence and functions of creatine kinase	13
1.1.4 Uptake of Cr and Cr analogues	14
1.1.5 Functions and isoforms of adenylate kinase	15
1.1.6 Diffusion or compartmentation: CK and AK systems work in concert	15
1.1.7 Energy metabolism of skeletal muscle: metabolic challenges vs. basal activity	17
1.1.8 Energy metabolism of the brain: neurotransmitter cycling activity vs. isoelectric state	18
1.2 Magnetic Resonance Spectroscopy	21
1.2.1 From Nuclear Magnetic Resonance to biomedical Magnetic Resonance	21
1.2.2 Basics of MR	21
1.2.3 In vivo ¹ H MR spectroscopy of brain and muscle	24
1.2.4 In vivo ³¹ P MR spectroscopy of brain and muscle	27
1.2.5 In vivo ¹³ C MR spectroscopy of brain	28
1.2.6 Data processing	29
1.3 Outline of this thesis	31
2. In vivo magnetic resonance spectroscopy of transgenic mouse models with altered high energy phosphoryl transfer metabolism	41
2.1 Introduction	42
2.2 Equipment for MRS of mice	45
2.3 Genetic alterations of high energy phosphoryl transfer systems	47
2.3.1 Key enzymes in phosphoryl transfer	47
2.3.2 Mice lacking one or more CK isoenzymes in skeletal muscle	48
2.3.3 Over-expression of phosphoryl transfer enzymes in skeletal muscle	52

2.3.4	Mice lacking one or more CK isoenzymes in brain	53
2.3.5	Mice lacking one or more CK isoenzymes in heart	56
2.3.6	Transgenic expression of CK in liver	57
2.3.7	Mice lacking guanidinoacetate methyltransferase (GAMT)	58
2.3.8	Knock-outs of the AK system	59
2.4	Concluding remarks	60
3.	Presence of (phospho)creatine in developing and adult skeletal muscle of mice without mitochondrial and cytosolic muscle creatine kinase isoforms	69
4.	Metabolic recovery after ischemic stress is impaired in skeletal muscle of mice that lack both cytosolic creatine kinase and adenylate kinase	93
5.	Cerebral creatine kinase deficiency influences metabolite levels and morphology in the mouse brain: a quantitative in vivo ^1H and ^{31}P magnetic resonance study	113
6.	In vivo ^{13}C MRS recording demonstrates altered glucose metabolism in brain of mice with creatine kinase deficiency	139
7.	MR spectroscopy of muscle and brain in guanidinoacetate methyltransferase (GAMT) deficient mice: validation of an animal model to study creatine	157
8.	Magnetization transfer effect on the creatine methyl resonance studied by CW off-resonance irradiation in human skeletal muscle on a clinical MR system	177
9.	Summary	193
10.	Samenvatting	199
	Dankwoord	206
	Curriculum Vitae	208
	List of publications	209

ABBREVIATIONS AND SYMBOLS

~P	high-energy phosphates
γ	gyromagnetic ratio
ν	precession frequency
¹ H MRS	hydrogen magnetic resonance spectroscopy
¹³ C MRS	carbon magnetic resonance spectroscopy
³¹ P MRS	phosphorous magnetic resonance spectroscopy
β -GPA	β -guanidinopropionic acid
ADP	adenosine diphosphate
AGAT	L-arginine:glycine amidinotransferase
AK	adenylate kinase
AK1	adenylate kinase isoform 1
Ala	alanine
AMP	adenosine monophosphate
Asp	aspartate
ATP	adenosine triphosphate
a.u.	arbitrary units
B ₀	static main magnetic field
B-CK	cytosolic brain-type creatine kinase
BBB	blood brain barrier
Cho	choline containing compounds
CK	creatine kinase
Cr	creatine
Crn	creatinine
G6P	glucose 6-phosphate
GAMT	guanidinoacetate methyltransferase
Glc	glucose
Gln	glutamine
Glu	glutamate
Glx	glutamate + glutamine
Gua	guanidinoacetate
Ins	inositol
Lac	lactate
M-CK	cytosolic muscle-type creatine kinase

MR	magnetic resonance
MRI	magnetic resonance imaging
MRS	magnetic resonance spectroscopy
NAA	N-acetylaspartate
OAA	oxaloacetate
OG	oxaloglutarate
OxPhos	oxidate phosphorylation
PCr	phosphocreatine
PGua	phosphorylated guanidinoacetate
Pi	inorganic phosphate
ppm	parts per million
PME	phosphomonoesters
Pyr	pyruvate
RF	radio frequency
ScCKmit	mitochondrial sarcomeric creatine kinase
T ₁	longitudinal relaxation time
T ₂	transversal relaxation time
Tau	taurine
TMA	trimethyl ammonium
tCr	total creatine (creatine + phosphocreatine)
TE	echo time
TM	mixing time
TR	repetition time
V _{cycle}	glutamate / glutamine cycle rate
V _{Gln}	glutamine synthetase rate
V _{PC}	pyruvate carboxylase rate
V _{PDH}	pyruvate dehydrogenase rate
V _x	multiple reactions which combine to the exchange between oxaloglutarate and glutamate
UbCKmit	mitochondrial ubiquitous creatine kinase
wt	wild-type mouse

1

INTRODUCTION

KlaasJan Renema

1.1 Magnetic resonance spectroscopy of energy metabolism in vivo

Availability of energy is essential for all living organisms. Adenosine triphosphate (ATP) is the most important biochemical energy carrier and the main source of fuel for cellular processes. To control energy homeostasis, elaborate systems for the production, use and distribution of ATP have evolved. In (in)vertebrates, production of ATP via the glycolytic pathway and by oxidative phosphorylation in mitochondria occurs in close conjunction with energy buffering and transmission by creatine kinase (CK) (or arginine kinase) and adenylate kinase (AK) mediated reactions (1, 2). Together, these circuits provide an integrated metabolic network with high flexibility to meet sudden and large fluctuations in energy demand in tissues like muscle and brain. Studies by us and others have shown that disabling one or more enzymes of these circuits by genetic knock-out or knock-down, or pharmacological inhibition, will result in a re-routing of fluxes through the remaining systems to re-establish the balance between energy production and utilization. The general aim of this thesis is to further elucidate the role of the CK and AK systems in energy metabolism of skeletal muscle and brain. The use of mice in which the genes for these enzymes have been deleted (knock-out mice) is crucial for the present work and has helped us to uncover functions of both enzyme systems as well as the physiological adaptations that occur in response to genetic stress in the metabolic energy network upon their deletion. To study these enzyme systems we have used the technique of magnetic resonance spectroscopy (MRS). This technique enables the *in vivo* monitoring of the substrates of these enzymes and gives us a direct view on their action in the natural environment of the intact animal.

This introductory chapter is divided into two sections. The first section will cover the basics of energy metabolism in skeletal muscle and in brain. A more comprehensive description of metabolic energy production and utilization is already given in several biochemical handbooks (see for instance (3-5)). Therefore, this section will only deal with those aspects of energy production and metabolism (and in particular the role of the CK- and AK-systems therein) that are of interest for studies with MRS in general and form a background for the specific studies described in this thesis. The second section of this chapter explains the basic principles of magnetic resonance (MR) and focuses on the specific MR techniques used in this thesis.

1.1.1 ATP production and utilization

ATP stores its energy in high-energy phosphoryl groups at the γ and β positions of the molecule. To release this energy from the γ -position, ATP-ases can hydrolyze ATP to adenosine diphosphate (ADP) and inorganic phosphate (Pi) according to the reaction:

$\text{ATP} + \text{H}_2\text{O} \leftrightarrow \text{ADP} + \text{Pi} + \text{H}^+$. Additional energy can be mobilized by utilizing the β -phosphoryl energy in two ADP molecules in the reaction $2 \text{ADP} \leftrightarrow \text{AMP} + \text{ATP}$ (4).

The main fuels for the generation of ATP are (poly)carbohydrates and lipids, while other compounds like ketone bodies and amino acids can also be used. Use of these fuel substrates depends on physiological conditions and tissue type. Carbohydrates are metabolized to glucose, which enters a chain of metabolic reactions whereby glucose is converted to pyruvate. This process is called glycolysis and takes place in the cytosol, yielding a net synthesis of about 2 ATP molecules per glucose molecule invested (5). Glycolysis is usually considered as an anaerobic process although it takes place in the absence as well as in the presence of oxygen (anaerobic and aerobic glycolysis). The first step of glycolysis, in which glucose is converted to glucose 6-phosphate (G6P) by hexokinase (or glycol kinase), is of particular interest in MRS research as G6P is one of the components of the phosphomonoester signal (PME) observed in ^{31}P MR spectra (see section 1.2.4).

At the end of the glycolytic reaction chain, pyruvate is formed. This important metabolite can be converted to lactate, or to acetyl coenzyme A (acetyl CoA) in mitochondria where it serves a substrate for the citric acid cycle (or Krebs cycle). The citric acid cycle produces NADH and FADH_2 , which are used to transfer electrons to O_2 synthesizing high amounts of ATP in a process called oxidative phosphorylation (OxPhos). OxPhos comprises a respiratory chain (also called electron transport chain) with proton pumps, which build up a proton motive force across the mitochondrial membrane. In turn, this proton motive force drives the yield of ATP, which is variably depending on intrinsic and extrinsic coupling (6). Under normal conditions, OxPhos can yield about 17 times more ATP than glycolysis (6) making it by far the most important process for generating ATP. Upon conditions of oxygen depletion (e.g. during ischemia), however, cells are constrained to (anaerobic) glycolysis which is much more inefficient and leads to acidification of the tissue via the formation of lactic acid.

1.1.2 Creatine: formation, utilization and catabolism

Creatine (Cr) plays a central role in energy metabolism in tissues with high and fluctuating energy demand such as muscle and brain. Phosphorylation of Cr to phosphocreatine (PCr) stores high-energy phosphate groups and is catalyzed in an equilibrium reaction by creatine kinase (CK): $\text{Cr} + \text{ATP} \leftrightarrow \text{PCr} + \text{ADP} + \text{H}^+$ (see also section 1.1.3). To maintain a constant body pool of Cr, its breakdown and build-up via dietary intake and endogenous synthesis must be balanced.

The first step on the synthetic route of Cr is catalyzed by L-arginine:glycine amidinotransferase (AGAT) and involves transfer of the amidino group of arginine to glycine,

to yield ornithine and guanidinoacetate (Gua). Since this process occurs mainly in the kidneys, Gua must subsequently be transported by the blood to the liver, where it is methylated to Cr by guanidinoacetate methyltransferase (GAMT) (7) (figure 1.1). Cr itself is then transported through the blood to the different tissues where it is taken up by Cr transporters (7, 8) situated in the cellular and mitochondrial membrane(s). Finally, a constant fraction of the Cr and PCr pool is catabolized non-enzymatically to creatinine (Crn), which is excreted in the urine (9, 10).

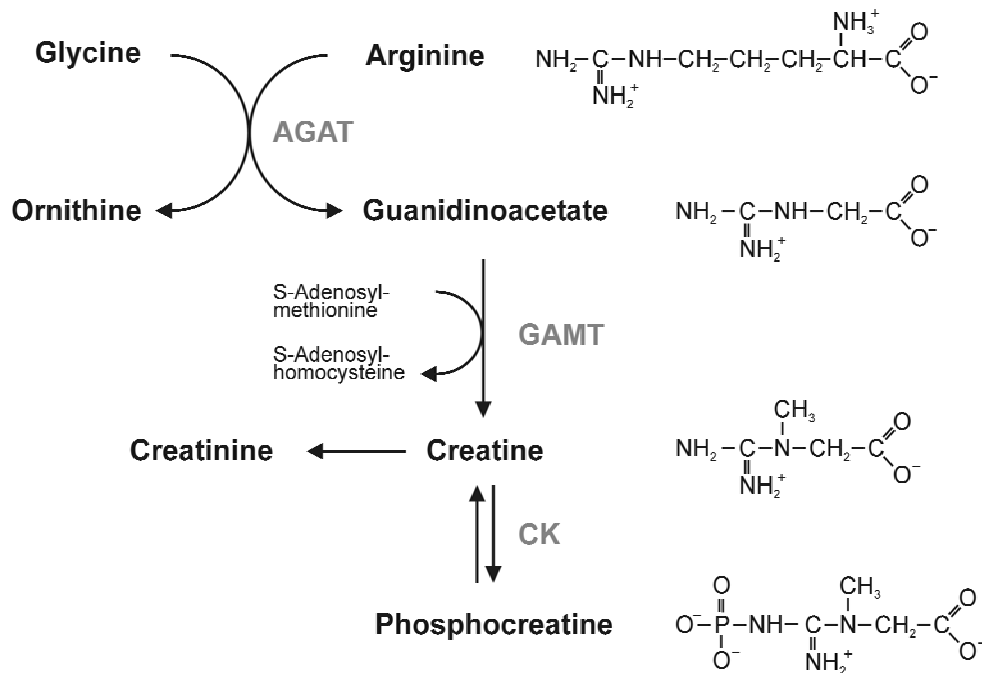


Figure 1.1: Schematic overview of the biosynthesis of Cr.

Several inborn errors of Cr metabolism have recently been reported. The first report was on an infant with extrapyramidal movement disorder (11) which had low Crn in serum and urine (11-14). ^1H MRS played a crucial role in the diagnosis of this patient by revealing low Cr signals and elevated levels of guanidinoacetate in brain which partially normalized upon oral administration of Cr (11). The absence of Cr was attributed to a deficiency of GAMT and since then several case reports on GAMT deficiency have appeared in literature (15-20). Decreased tissue Cr levels are also observed in other forms of inborn errors of Cr metabolism, for example in patients with Cr transporter deficiency (21, 22) or deficiency of AGAT (23, 24).

1.1.3 Occurrence and functions of creatine kinase

In vertebrate brain and muscle, 4 genes of CK are identified coding for the subunits of altogether five different isoenzymes (for a more extended review see (25-27)). M-CK and B-CK subunits can assemble into the hetero- or homodimeric isoenzymes MM-CK, MB-CK and BB-CK which are present in the cytosol. Of those, MM-CK is predominantly expressed in striated and heart muscle, while BB-CK is expressed at high concentrations in brain, but also in kidney, intestine, spermatozoa, smooth muscle and other tissues (28). Trace amounts of BB-CK may be present in skeletal muscle originating from satellite cells ((29) and references therein). MB-CK is a transitional hybrid which is present during differentiation of muscular tissues, but permanently expressed in (adult) heart ((26) and references therein).

Ubiquitous CK (UbCKmit) and sarcomeric CK (ScCKmit) are present as dimeric and octameric isoforms located between the inner and outer membrane of mitochondria (27) and associated with the cardiolipid moieties in these membranes (30). ScCKmit is mainly expressed in striated and heart muscle, while UbCKmit appears to be co-expressed with B-CK. The ratio mitochondrial/cytosolic CK differs for specific tissues and cell-types. Generally, mitochondrial CK will be present at relatively larger amounts in tissues with higher aerobic capacity (27). For skeletal muscle, 1-10 % of total CK activity is of mitochondrial origin (26, 31). Differences reported are due to physiological differences between muscle types examined, since the level of mitochondrial CK is considerably higher in slow twitch compared to fast twitch muscles (27), but cytosolic CK is relatively high in fast muscle. Cardiac muscle shows relatively high amounts of mitochondrial CK, which can be on the order of 30% (26, 27). Brain, a highly oxidative organ, shows mitochondrial CK levels which represent 0.5-15% of total CK activity (27) depending on the cell types investigated. In tissue extracts of the whole brain, even up to 30% of normal CK activity was attributed to mitochondrial UbCKmit (Jost et al., unpublished result).

Several global regulatory and buffering functions are ascribed to the CK system (25, 26). The first and main function is that of a temporal energy buffer. Because the magnitude of free energy (ΔG^0) for hydrolysis of PCr is higher than that of ATP (-10.3 kcal/mol compared to -7.3 kcal/mol, respectively (5)), ~P groups are effectively stored in this compound. In times of energy demand, CK can regenerate ATP by transferring its ~P to ADP to yield additional energy. A second proposed function of the CK system is that of a spatial energy buffer. Cr and PCr are smaller in size than ATP and ADP which, together with the high concentrations of PCr and Cr in comparison to ATP and ADP, make it easier to diffuse through the cell thereby connecting sites of energy production (e.g. mitochondria) and energy demand (e.g. ATP-ases) (see figure 1.2 and the discussion in section 1.1.6 below). Another function is buffering of protons, preventing (local) acidification of tissues when ATP-ase activity is

increased or during anoxia (32-35). The net CK reaction also releases Pi which is of importance to stimulate glycolysis and glycogenolysis (36, 37). Finally, a consequence of the local presence of the CK reaction is that it will keep ATP/ADP ratios locally balanced at sites of energy production and consumption (26, 38, 39).

1.1.4 Uptake of Cr and Cr analogues

Although the above description covers all main aspects of the Cr-CK system, our current picture is certainly not complete. The distribution of Cr among tissues is a complex process and uptake and metabolic conversion rates may differ between tissues, like in the case of muscle and brain. For example, it is generally agreed that the main synthesis of Cr occurs in pancreas and liver (10). However, other tissues like brain, where Cr is suggested to fulfill a neuroprotective role (40), are also capable of synthesizing (part of) their own creatine needs (7, 8, 41). In muscle, GAMT activity appears to be high enough to synthesize all Cr needed (Isbrandt, personal communication).

Additionally, in order for Cr to be absorbed by the brain, it has to pass the blood-brain barrier (BBB) and there is evidence that the BBB is not fully (and perhaps also not equally) permeable for guanidino compounds (see e.g. (7)). Therefore, care has to be taken in drawing conclusions from pharmacological studies with Cr-analogues which can be utilized by CK as a substrate (7, 42, 43). For analogues like β -guanidinopropionic acid (β -GPA), which is often used as a competitor of Cr (36, 44, 45) it is known that uptake and clearance kinetics differs between tissues. Studies in which β -GPA was fed to rats and mice showed an (almost) complete replacement of PCr by phosphorylated β -GPA in muscle (36, 44, 46), but only a partial replacement in brain (47). Long term feeding of β -GPA induced profound physiological changes in muscle (48). Changes (involving alterations in phosphorylated β -GPA and PCr levels) in brain were much slower upon starting of β -GPA feeding or stopping after a period of β -GPA feeding (47). These findings could be explained by the already mentioned limited permeability of the BBB, but also by a slower Cr turnover in brain. The former explanation may be the most likely as it is supported by the observation that in patients with Cr deficiency restoration of Cr levels in brain upon administration of high oral doses of Cr is slow (in the order of months) (11, 12, 15-17, 49, 50). In mice with creatine deficiency, PCr levels in muscle reached approximately 50% of original values after only two days of 1% Cr substitution in the drinking water (51).

To better understand Cr's role it is therefore imperative that we develop a better picture of the integral physiological aspects of metabolic cooperation between organs and tissues, and the effects of nutrient regimes and intrinsic and extrinsic stimulation of energetic

and osmolar activity. Special emphasis is needed for the study of species specific differences in the synthesis and utilization of creatine, before we can extrapolate findings in animal models to those in human patients.

1.1.5 Functions and isoforms of adenylate kinase

For adenylate kinase (AK), which also contributes to cellular energy homeostasis (52) by catalyzing the reaction: $2 \text{ ADP} \leftrightarrow \text{ATP} + \text{AMP}$, five isoforms, labeled AK1 to AK5, are known (53-56). In skeletal muscle, AK1 is the major isoform representing approximately 99% of AK activity (54). The only other AK isoform present at low activity in skeletal muscle is AK3, and is in fact an enzyme which uses GTP and AMP as substrates (54). In contrast to AK1 which is solely expressed in the cytosol of skeletal muscle, a variant of AK1 (AK1 β) is present in a membrane-bound form (53), possibly for quick ATP supply close to ATP-ases or ATP sensitive sites (57).

AK is thought to increase the efficiency of ATP production during high metabolic stress by locally balancing ATP/ADP ratios (58). By further releasing the energy stored in the pool of adenine β -phosphoryls, the AK-mediated circuit allows cellular energy metabolism to occur in a highly efficient mode. In this way, AK increases the tolerance to metabolic stress (59, 60).

1.1.6 Diffusion or compartmentation: CK and AK systems work in concert

Almost two decades ago it was proposed that the AK and CK enzyme systems work in close harmony, forming a shuttle system for exchanging $\sim\text{P}$ groups between compartments of production and utilization (61, 62) (see also chapter 4). A more modern version of this model, acting as a “vectorial ligand conduction” network, was proposed by Goldberg and coworkers (63) and investigated in more detail later (64). This model assumes a dense distribution of enzymes such that substrates can be ‘passed’ from one enzyme to the other, with exchangeability of the CK and AK relay systems. The model also proposes an integrated role for glycolytic pathways (see figure 1.2). Together these enzyme systems form an intertwined network for transport of high energy phosphates only, rather than the entire phosphorylated metabolite itself, forming a circuit that is more efficient in terms of reaction velocity and flux rate than pure diffusion (2).

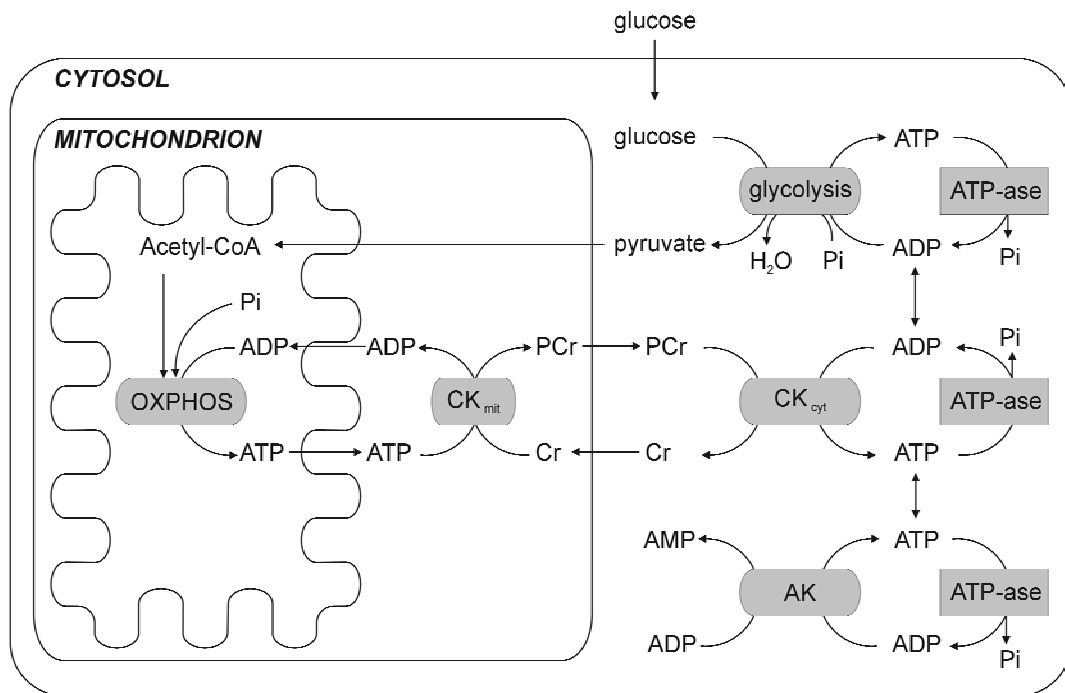


Figure 1.2: Schematic view of high-energy phosphoryl transfer systems in the cell.

Note: enzymatic reactions of CK and AK are equilibrium reactions; the direction of the arrows indicates the main flux of substrates.

Mitochondrial compartmentation of the CK enzyme – and also AK isoenzymes – is a key element in this hypothesis. Mitochondrial CK has preferential access to ATP formed in the mitochondria by OXPPOS (27, 65, 66) and plays an important role in ATP/ADP exchange between the mitochondrial matrix and the cytosol, a process in which also other enzymes like the ANT and VDAC (porin) are involved (67, 68). It is important to note here that not all mitochondrial and cytosolic components of the network as drawn in figure 1.2 occur in all cell types.

Also other hypothetical models have been proposed. Meyer and coworkers proposed a model of facilitated diffusion (69). This model implies that the diffusive flux of PCr is increased when PCr is in equilibrium with ATP through the CK reaction. In their model, buffering of ATP/ADP and diffusion of PCr are closely related, however, physical or functional compartmentation of substrates is not needed (69, 70). In simulations they showed that when diffusion distances are small, CK is not necessary for spatial buffering of ATP/ADP ratios (69). In the PCr-Cr shuttle hypothesis the different isoenzymes are functionally coupled to the physical location, in the diffusion model they are not. Although the pros and cons of both models are still fiercely discussed, often with subjective and selective use of circumstantial evidence of cell biological and kinetic studies, both theories agree on PCr being the main transporter of high-energy phosphoryls.

1.1.7 Energy metabolism of skeletal muscle: metabolic challenges vs. basal activity

Already since the early days of *in vivo* magnetic resonance spectroscopy, a technique which is described in more detail in section 1.2, skeletal muscle has served as one of the best accessible systems to study mammalian energy metabolism. Studies performed have been conducted on a variety of muscles of human patients or healthy individuals and animal models as well. Even in *in vivo* MR studies on small animals like mice, hind leg muscle can easily be spatially constrained to reduce motion artefacts without compromising the space necessary for spontaneous breathing. Although many studies are performed during resting conditions, when the animal that is investigated is under slight anaesthesia, differential effects of genetic or physiological stress conditions are likely to become more apparent in MR spectra under conditions of metabolic challenge (see e.g. chapter 4). For muscle, two general approaches for applying metabolic challenge are used. The first method involves the induction of muscle contraction (i.e. labour) by electric stimulation. The other method is the use of ischemia-reperfusion protocols. Unfortunately, these two methods induce vastly different effects on muscle metabolism, and therefore cannot be easily compared. To better understand these differences we have to draw an adequate picture of the principal metabolic fuels and pathways that play a role in muscle energetics. During the first minutes of a moderate metabolic challenge, in which oxidative phosphorylation is the primary process responsible for generation of ATP, muscle glycogen is the major fuel (71). During prolonged metabolic demand, glucose and fatty acids from the blood will serve as substrate for generating ATP. If the metabolic challenge is more severe or in case there is a lack of oxygen, muscle and other tissues can switch to anaerobic glycolysis (see section 1.1.1). In that case, both muscle glycogen and glucose from the blood can serve as substrates of ATP production (71). Also PCr can serve as fuel, but its main role is in fast buffering of mismatches between ATP production and utilization.

Skeletal muscle fibers can roughly be divided into two groups. Slow twitch fibers (type 1) are adapted for long term exercise with oxidative phosphorylation as its major energy producing pathway. Fast type fibers are more suited for short term work with high metabolic demand, relying mostly on glycolysis (type 2b) and PCr buffering for fast availability of energy, but also on oxidative processes (type 2a). Because metabolite and enzyme levels differ significantly between these muscle types (7, 8, 26), MRS can yield different results depending on the position of the volume of interest. In unlocalized experiments of hind leg muscle, the main contribution to the MR signal comes from the gastrocnemius muscle, which is predominantly composed of fast-type fibers.

1.1.8 Energy metabolism of the brain: neurotransmitter cycling activity vs. isoelectric state

For brain, in contrast to muscle, the arrangement of energy compartmentalization is inherently more complex. Glucose (together with ketone bodies) is virtually the only energy source of the brain (see e.g. (72) and references therein; (73)). From the ratio of utilization of glucose over the utilization of O_2 (CMR_{glc}/CMR_{O_2}), which is about 5.5 for the resting brain, it can be derived that the brain is a highly oxidative organ (74). The numerous cell types present in the brain can be roughly divided in two types: neuronal and glial cells (75). Neurons have long axons and are responsible for impuls transduction while glial cells, e.g. astrocytes, were until recently thought to function only in support of neurons. However, experimental data indicated that astrocytes fulfill much more important functions in neurotransmitter cycling and energy metabolism (76).

Glutamate (Glu), the major excitatory neurotransmitter (77), is recycled from the synaptic cleft by astrocytes and converted to glutamine. Glutamine (Gln) is then transported back to the neurons where it can be converted to Glu (78). This way of recycling Glu reduces the amount of carbon chains needed from the Krebs cycle. Although the anaplerotic pathway through pyruvate carboxylase (see figure 1.3), can replace carbon chains lost from the Krebs cycle to form neurotransmitters, recycling of Glu via astrocyte-neuron cooperation is considered more efficient (79).

Besides its function in recycling Glu, astrocytes have been proposed to play a more general role in energy metabolism of the brain (76) as well as in brain development. As astrocytes are in close vicinity to blood vessels, they can easily take up glucose. This glucose can be converted to lactate by glycolysis, which is assumed to be transferred to neurons, where it is then metabolized further in the Krebs cycle and by oxidative phosphorylation. The energy yielded from glycolysis in the astrocytes can be used to recycle Glu. In this way, Glu has been shown to stimulate glycolysis, creating a tight coupling between neuronal activity and glucose utilization (76, 80-82). Although it has been shown that neurons may preferentially use lactate over glucose, they can also use glucose itself as a substrate for energy production (83). Furthermore, a linear relation has been determined between Glu/Gln cycling and oxidative glucose metabolism in active brain (84), despite the fact that Glu/Gln cycling itself is estimated to account for only 3% of total energy consumption during activation (85). The amount of glucose utilization in the isoelectric brain (when no electric activity is detected in the EEG) is a point of intense debate, as is the percentage of lactate shuttling under isoelectric and more active conditions (86). Certainly not all energy in normal active brain is utilized for neurotransmitter cycling and ion homeostasis activity to sustain de- and repolarization activity. Some reports claim that up to 50% of energy may be spend to

actin related motility processes, including vesicle secretion. Neurogenesis, neuritogenesis and axonal pruning in development may also represent relative large energy challenges (87).

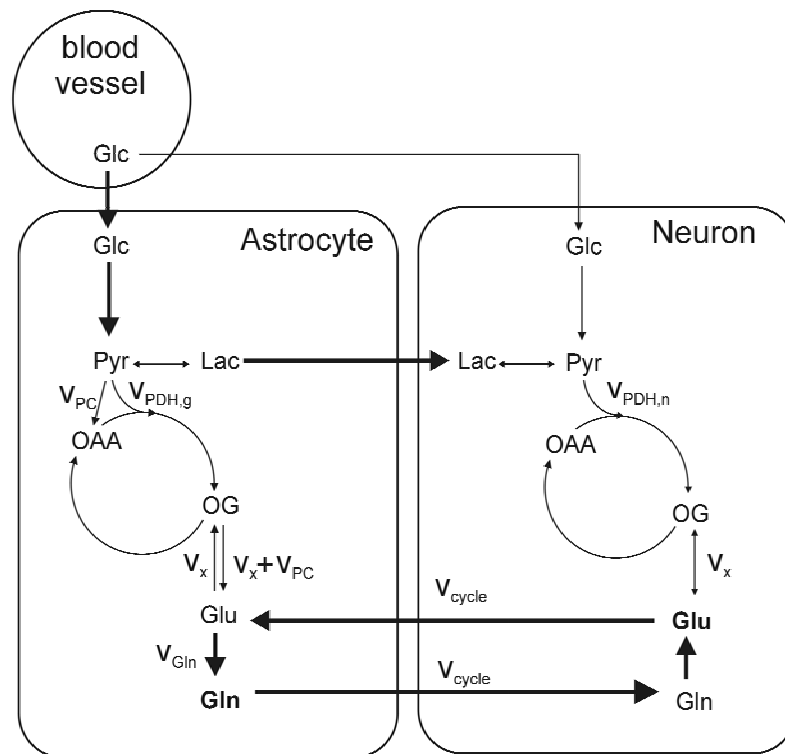


Figure 1.3: Schematic view of metabolic link between astrocytes and neurons, adapted from (88-90). The bold arrows indicate the main flux of substrates when glucose enters the astrocyte-neuron system. Subsequently lactate is transported from the astrocyte to the neuron. Glutamate and glutamine are cycled between the astrocyte and the neuron; the main pool of glutamate is located in the neurons, while the main pool of glutamine is situated in the astrocytes.

Abbreviations of metabolites (see also text for details): OAA, oxaloacetate, OG, oxaloglutarate. Abbreviations of specific fluxes: v_{PC} , pyruvate carboxylase; v_{PDHg} , glial pyruvate dehydrogenase; v_{PDHn} , neuronal pyruvate dehydrogenase, v_x , multiple reactions which combine to the exchange between OG and Glu; v_{cycle} , glu/gln cycle rate; v_{gln} , glutamine synthetase.

Brain energy metabolites and Glu/Gln pools are considered to be distributed over neuronal and glial compartments. A large Glu pool is present in the neuronal compartment and a small Glu pool is present in glial compartments (89-91) (figure 1.3). ^{13}C MR spectroscopy (see also section 1.2.5) has proven to be a powerful tool in elucidating carbon fluxes through the brain and brain compartments. Labeling one of the carbons, in for instance glucose, and following its fate over time when this label is transferred biochemically to other substrates yields information on conversion rates (91-94). By modeling the increase and

decrease of the different ^{13}C labeled compounds which are formed and broken down after infusion of a ^{13}C labeled substance, rates can be derived for the TCA cycle, Glu/Gln cycle, and oxidative metabolism or the anaplerotic pathway (89) depending on position of the label in the infused compound. For example, glucose may be labeled at the C1 or C6 position (or labeled both at the first and 6th carbon position). These carbons will firstly be transferred to the C3 position of pyruvate and then to the C4 position of Glu (Glu₄) after which it is biochemically passed on to the C4 position of Gln (Gln₄). Due to the symmetry in the succinate moiety, an Krebs-cycle intermediate, labeled carbons of pyruvate will be transferred to Glu₂ and Glu₃ with equal probability after it has made a full turn in the TCA cycle (91). Using the incorporation kinetics of these labels into various compounds, rates for the TCA cycle and Glu/Gln cycle rates can be determined (78, 84, 89, 95). A serious drawback in this modelling is that no discrimination is allowed between the extend of coupling and flux rates through glycolytic and mitochondrial systems in neurons and glial cells. The use of 2- ^{13}C or 5- ^{13}C glucose enables calculation of flux through the anaplerotic pathway (79). Other labeled substrates can also be used to determine reaction rates in vivo. 1,2- $^{13}\text{C}_2$ acetate, for instance, is believed to be directly converted to acetyl-CoA, a process that occurs only in glial cells (91, 96).

When calculating fluxes using a biochemical model, care has to be taken which assumptions are used in that model. It has been shown that when the exchange rate between oxoglutarate and glutamine, for instance, is assumed to be fast, this may influence the estimated TCA cycle rate dramatically (Henry, personal communication). Future efforts in this field therefore must be directed to interdisciplinary approaches, in which cell biological and physiological knowledge is joined with biophysical (MRS) knowledge to develop models which reflect in vivo physiology more faithfully.

1.2 Magnetic Resonance Spectroscopy

In the last two decades, magnetic resonance (MR) has become a powerful technique to study anatomy, physiology and metabolism in a non-destructive way in animals and humans. While MR imaging (MRI) provides a non-invasive tool to study anatomy and distribution of biomaterial (fluid, solutes, (bio)molecules) of the body, MR spectroscopy (MRS) provides a window on metabolism, physiology and morphology in selected volumes of interest. This section deals with the basic principles of MR. Firstly, the parameters that play a role in the basic understanding of a general MR experiment will be described. The remaining part focuses on specific MRS techniques of particular interest for this thesis.

1.2.1 From Nuclear Magnetic Resonance to biomedical Magnetic Resonance

The principles of Nuclear Magnetic Resonance (NMR) were firstly demonstrated independently by Bloch et al. and Purcell et al. (97, 98). For this discovery they received the Nobel prize in physics in 1952. They showed that certain atomic nuclei, when placed in a magnetic field, are able to absorb energy in the form of radio frequencies (RF). A set of equations describing the time dependent behavior of magnetization are the Bloch equations (99), in which also the longitudinal and transversal relaxation times are included (see below).

Since its discovery, NMR has been used to determine properties of solid state materials and to elucidate structures of molecules. In 1971 Damadian demonstrated the first potential medical application by showing that the water NMR relaxation times of tumor tissue and healthy tissue are different (100). In 1973, Lauterbur demonstrated the use of MR for imaging by introducing magnetic field gradients (101). Mansfield independently presented a similar MR method for displaying structures of materials (102) and further developed the utilization of magnetic field gradients and the mathematical methods necessary to analyze the MR signals (103-106). For their work, Lauterbur and Mansfield received the 2003 Nobel Prize in Physiology or Medicine. Ernst introduced the use of the Fourier transformation in RF pulsed NMR (107), which is the basis of modern MR spectroscopy, and he was one of the founders of modern MR imaging by proposing phase and frequency encoding (108). For his work he received the Nobel prize in Chemistry in 1991.

In a (bio)medical environment, NMR is abbreviated to MR because of negative associations with the term nuclear, although at chemistry and physics departments the term NMR is still in use. In the remainder of this thesis the term MR will be used.

1.2.2 Basics of MR

The technique of MR is based on the property that certain nuclei possess a spin (see for instance (109)). Protons (^1H nuclei), phosphorus nuclei (^{31}P) and carbon nuclei (^{13}C), the most

common nuclei used in MR experiments in vivo, have spin value of $\frac{1}{2}$. Although spin is a quantum mechanical property, it can be described relatively well in a semi classical context.

Spin can be considered as a rotation of the nucleus around its own axis, giving it an intrinsic angular momentum \mathbf{I} [§], orientated along the axis of that nucleus. This angular momentum induces a magnetic dipole moment $\boldsymbol{\mu}$, which is also an intrinsic property of the nucleus orientated in the same direction as \mathbf{I} . The magnitude of $\boldsymbol{\mu}$, however, is characteristic of that nucleus and is described by the gyromagnetic ratio γ (eq. 1.1).

$$\boldsymbol{\mu} = \gamma \cdot \mathbf{I} \quad [1.1]$$

In the absence of a strong magnetic field, the orientation of all these magnetic dipole momenta is random. In the presence of an external magnetic field, however, a torque arises which causes the magnetic dipole momentum to precess around an axis parallel to the external field (\mathbf{B}_0) (figure 1.4).

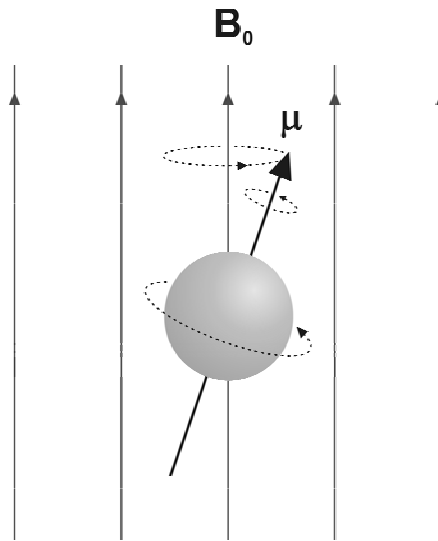


Figure 1.4: Precession movement of a nucleus with magnetic dipole moment $\boldsymbol{\mu}$. The rotational movement is around an axis parallel to the external field \mathbf{B}_0 .

The angular frequency with which the spin precesses (Larmor frequency, ω) is dependent on the external magnetic field strength, and is given by equation 1.2.

$$\omega = \gamma \cdot B_0 \quad [1.2]$$

[§] Vectors are denoted in bold, while the magnitude of the vector is denoted in plain text.

The gyromagnetic constant γ is a characteristic property of a nucleus, determining the Larmor frequency of the nucleus in an external field. For example, at 7 T (the strength of the magnet used for most of the work described in this thesis) protons resonate at a frequency ($\omega / 2\pi$) of 300 MHz, ^{31}P nuclei at 122 MHz and ^{13}C nuclei at 75 MHz.

Apart from the external magnetic field, also small internal magnetic fields have an influence on the resonance frequency. For instance, the main magnetic field may induce a small counter field in the electron cloud surrounding the nucleus. This magnetic field is proportional to B_0 and can partially shield the main magnetic field observed by the nucleus. The local field at the site of the nucleus is given by equation 1.3:

$$B_{\text{eff}} = B_0 (1 - \sigma) \quad [1.3]$$

In eq. 1.3, σ represents a screening factor which is dependent on the chemical environment of the nucleus. Because the effective magnetic field (B_{eff}) causes the resonance frequency of that particular nucleus to be slightly different from nuclei with other σ , a distinction between nuclei in different chemical surroundings can be made. This provides the basis of MR spectroscopy.

The precession motion caused by \mathbf{B}_0 aligns $\boldsymbol{\mu}$ in the parallel or anti-parallel direction with respect to \mathbf{B}_0 . Because parallel is a state of lower energy, more spins will be in the parallel state with a distribution given by the Boltzmann equation (eq. 1.4):

$$\frac{n_a}{n_p} = e^{\frac{-\Delta E}{kT}} = e^{\frac{-\gamma \hbar B_0}{kT}} \quad [1.4]$$

where n_p is the number of spins parallel to the external magnetic field, n_a the number of spins anti-parallel, k the Boltzmann constant, T the absolute temperature, \hbar the constant of Planck divided by 2π and ΔE the difference in energy between the upper and lower energy level. Since the sensitivity of an MR experiment is determined by the ratio n_a / n_p , it can be concluded from this equation that the sensitivity can be increased by increasing B_0 , choosing a nucleus with relatively large γ or lowering the thermal noise (i.e. decreasing T).

When performing an MR experiment, the equilibrium of parallel and anti-parallel spins is perturbed by applying one or more radio frequency (RF) pulses. The macroscopic magnetization \mathbf{M} , that is, the sum vector of all up and down spins, is tilted from its original orientation along \mathbf{B}_0 to the xy -plane by the RF pulse (when \mathbf{B}_0 was in the z -direction). Furthermore, the precession of the ensemble of individual spins obtain a coherent phase.

From this perturbation, the spin system will return to the original state before excitation by two processes which occur simultaneously. Firstly, \mathbf{M} will return to the \mathbf{z} -direction with a rate described by a time constant called the spin-lattice relaxation time, or T_1 . The surplus of energy induces an RF modulation in the detection coil in principle according to Faraday's law. Besides T_1 relaxation, dephasing of the individual spins will result in signal loss, with a characteristic time called spin-spin relaxation time, or T_2 .

The acquired MR signal in the time domain is then Fourier transformed to obtain the frequency information, which is plotted to yield an MR spectrum (see below). The x-axis of the spectrum is denoted in parts per million (ppm) relative to a reference frequency. ^1H is the most sensitive MR nucleus and has a natural abundance of 99.98%. Furthermore, because water is the most abundant compound in the body, the protons in water are by far the most common nuclei used in biomedical MR. Besides water, other molecules can also be detected using ^1H MRS (see section 1.2.3). Moreover, additional metabolites are detectable by ^{31}P MRS (section 1.2.4) or ^{13}C MRS (section 1.2.5). Because of sensitivity limits and other restrictions, generally only small metabolites (molecular weight of 500 or less) at relatively high concentrations (> 0.1 mM) are detectable by *in vivo* MRS. In total, up to about 50 metabolites or ions may be assessed by this approach in living tissue.

1.2.3 *In vivo* ^1H MR spectroscopy of brain and muscle

^1H MRS can be performed on relatively small volumes of interest (voxels) because of the high sensitivity and natural abundance of ^1H compared to other nuclei. At 7 T, voxel sizes down to $1\text{-}2\text{ mm}^3$ can be achieved in the mouse brain, for instance. Good localization is essential, since contamination from signals originating from outside the voxel may lead to biased metabolite concentrations or spectra of poor quality e.g. in the case of lipid signal contamination.

Depending on the research goal, a single voxel or a multi voxel selection pulse sequence method can be applied. Stimulated echo acquisition mode (STEAM) (110) and point resolved spectroscopy (PRESS) (111) are selection methods frequently used in ^1H MRS. STEAM with only 90° pulses enables short echo times (TE) (down to about 10 ms on our scanner), especially of interest when looking at strongly coupled molecules like Glu, Gln and Ins. In PRESS sequences, however, two 180° pulses, which are in general long pulses, make the use of short echo times more difficult. The signal gain of a factor of two in PRESS with respect to STEAM (which gives a stimulated echo), however, motivated the development of short echo PRESS sequences using short asymmetrical 180° pulses (112).

One of the major challenges of ^1H MRS is to measure metabolites at low concentration (down to 1-2 mM) in the presence of the large signal of water (~ 45 M in the body). Because of dynamic range and other problems, the water signal needs to be suppressed. Several techniques are available for this purpose, from specific selection with single Gaussian shaped pulses to more complex schemes like CHESS (113) and VAPOR (114). Essential for proper water suppression is good shimming, which can be performed manually or by automatic procedures like FASTMAP (115). A typical MR spectrum of the brain shows a large variety of molecules (116, 117) including Cr, Glu and Gln (figure 1.5).

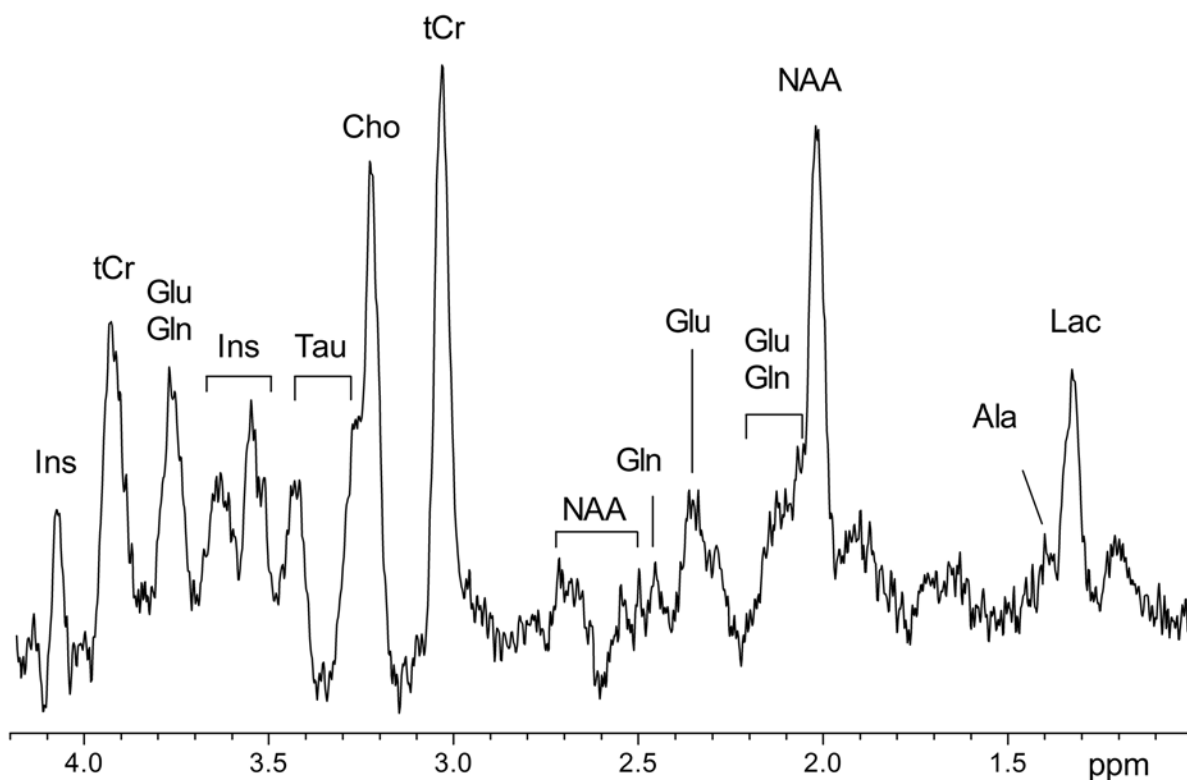


Figure 1.5: Single voxel ^1H MRS of a $3 \times 3 \times 4.5$ mm³ voxel of the mouse brain using a STEAM sequence ($TE=10$ ms, $TM=15$ ms, $TR=5000$ ms, 64 averages) and VAPOR water suppression at 7 T (see text for details).

Abbreviations: Ins, myo-Inositol; tCr, creatine and phosphocreatine; Glu, glutamate; Gln, glutamine; Tau, taurine; Cho, cholines; NAA, N-acetylaspartate; Ala, alanine; Lac, lactate.

MR spectroscopic imaging (MRSI) (or chemical shift imaging; CSI) (118, 119) gives an overview of the distribution of metabolites in a larger area by pre-selecting a volume which is divided into multiple voxels by phase/frequency encoding. This technique can be used in combination with a STEAM or PRESS preselection (figure 1.6) A major advantage of MRSI is that after acquiring the MRSI data the voxels can be shifted such that the position of one of more voxels cover the anatomical region of interest. Disadvantages are the relatively

long minimal measurement time compared to single voxel techniques and contamination from one voxel to another through the point spread function. Dedicated MRSI sequences can partially overcome these problems by applying filters or by specific k-space sampling (120-122).

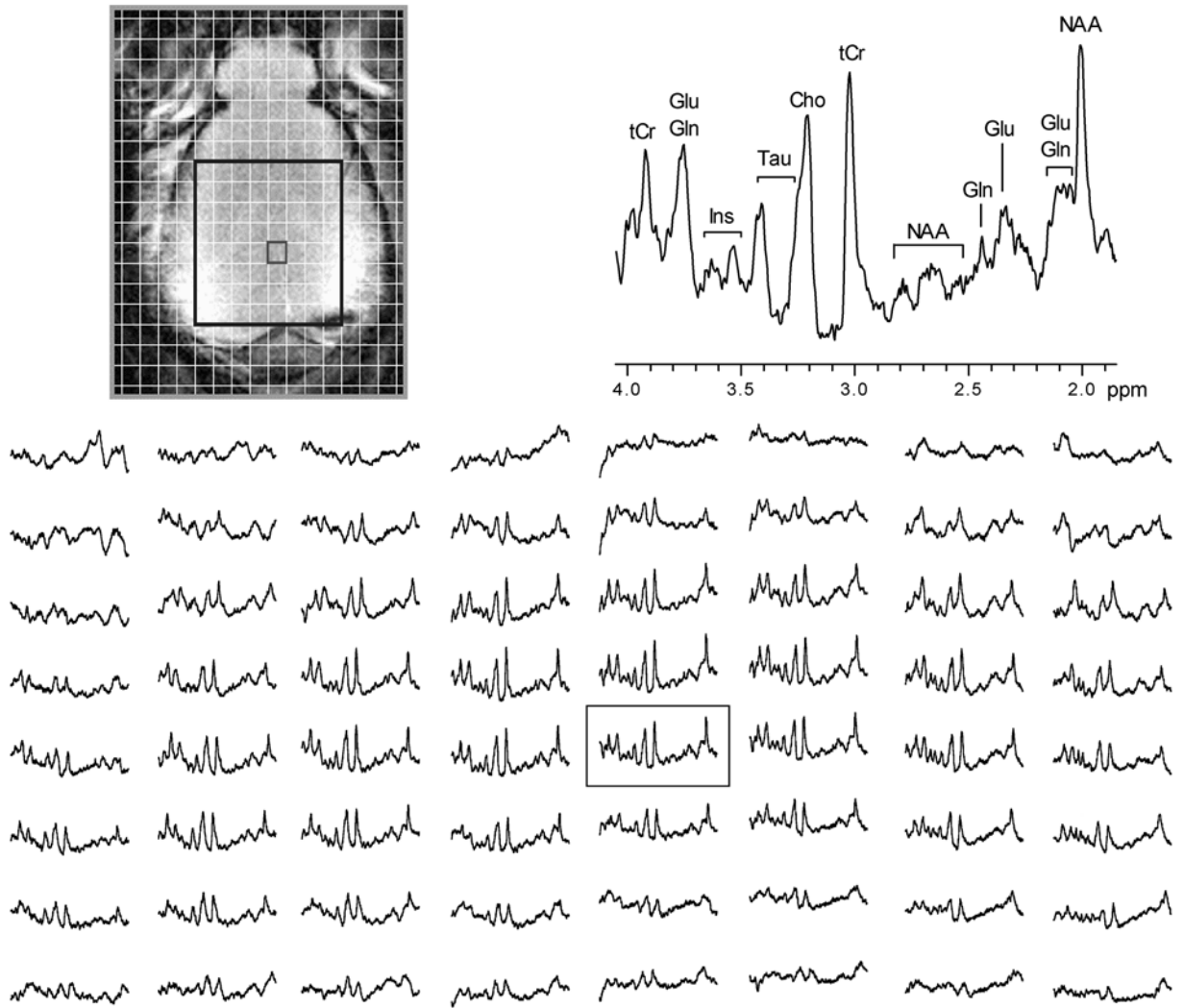


Figure 1.6: ^1H MRSI of a slice through the mouse brain in vivo (adapted from (123)).

Top left: Transversal localizer image showing the grid from which the spectroscopic imaging data set was obtained. A STEAM sequence was used for preselection (large box in the localizer image) while the small voxels were selected using MRSI localization.

Bottom: Individual MR spectra from voxels inside the STEAM selection box

Top right: An enlarged spectrum of the indicated voxel shows the same resonances as the single voxel spectrum in figure 1.5.

MR spectra of both brain and skeletal muscle show characteristic signals for specific metabolites. In the brain, a wide range of overlapping resonances can be detected and although the physiological significance of some metabolites is not exactly known, some

general remarks can be made (117). N-acetylaspartate (NAA) (for a review see: (124)) is one of the major metabolites visible in the ^1H MR spectrum of the brain. It is considered as a marker for healthy neurons and is often decreased in neurodegenerative diseases. The concentration of NAA may vary between different species (125). Choline compounds (Cho) are thought to be markers for cell proliferation and are generally increased in tumors but signal changes may also be associated with myelin breakdown. Myo-Inositol is normally elevated in fetal brain where it may play a role in brain development, and it possibly acts as a cerebral osmolite (117, 126). The role of taurine (Tau) is largely unknown, it has been proposed as osmolite and recently also as a protector of inflammation (127). Lactate (Lac) is one of the end products of glycolysis and is present at relatively high concentrations in mouse brain compared to human and rat brain (fig. 1.6; (128)). Together, these metabolites provide an extensive ‘metabolic fingerprint’ of brain tissue.

In ^1H MR spectra of mouse skeletal muscle signals for Cr and overlapping signals for Tau and trimethylammonium (TMA) compounds are present, of which only Cr is of interest when monitoring energy metabolism. Preferentially, the skeletal muscle is set at an angle of 55° with the main magnetic field to reduce dipolar interactions which will split up the signals making quantification difficult (129).

1.2.4 In vivo ^{31}P MR spectroscopy of brain and muscle

^{31}P has a natural abundance of 100%, but the sensitivity is lower than that of protons (6-7 % of proton sensitivity). Although CSI or ISIS localization is possible with ^{31}P MRS, it sometimes is sufficient to use a pulse-acquire experiment, for instance in hind leg muscle, because the surrounding tissues do not contain large enough concentrations of metabolites measured with ^{31}P MRS to significantly contribute to the acquired ^{31}P MR signal.

Phosphorous MR spectroscopy gives an overview of the levels of phosphates involved in energy metabolism like phosphocreatine (PCr), inorganic phosphate (Pi), and ATP. During special conditions like ischemia in muscle, or in basal spectra of the brain, signals for phosphomonoesters (PME) at approximately 6 ppm are also observed. Phosphodiester (PDE) signals are found in the brain and, for instance, in tumors. Besides the phosphorous metabolites, tissue pH can be calculated from the shift in resonance position between the Pi and PCr signal (130) and the $[\text{Mg}^{2+}]$ from positions of the different ATP signals (131).

A typical ^{31}P MR spectrum of the mouse hind leg muscle is shown in figure 1.7. A pulse acquire sequence was applied yielding signal mainly from the GPS complex, in which the gastrocnemius is the largest muscle.

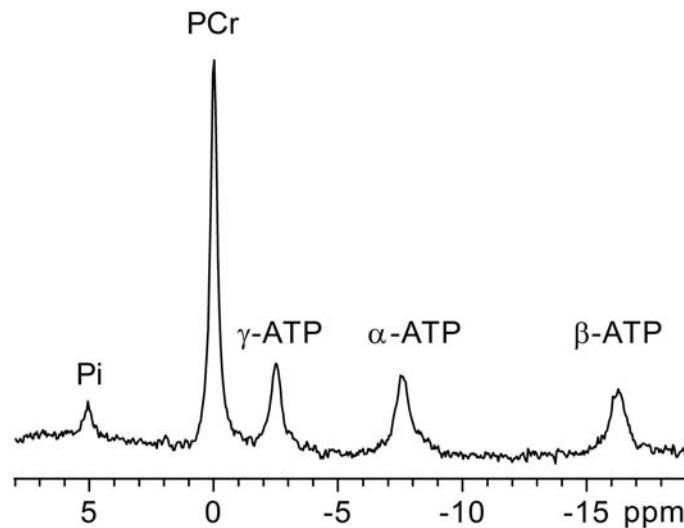


Figure 1.7: ^{31}P MR spectrum under resting conditions using a 3-turn solenoid coil and a pulse-acquire sequence ($TR=7000$ ms, 64 averages).

^{31}P MR measurements of the mouse brain in this thesis are performed using two surface coils, tuned to the ^{31}P frequency and working in quadrature mode (132, 133). Contamination of signals from the brain with signals from the masseter muscles could be severe since PCr signals are relatively high in muscle compared to brain. Therefore, a localization technique, e.g. an ISIS sequence (134), has to be used. Typical voxel sizes achieved are $6.5 \times 6.5 \times 4.5$ mm³ (190 μl).

Measurement times for the acquisition of ^{31}P MR spectra are in the order of minutes for muscle and even longer for brain. Because metabolic changes may appear much faster, these changes will average out and therefore remain undetected in the MR spectrum. One way to avoid this is to use a gated approach which allows a spatial resolution for detecting the PCr signal changes of a few seconds. This time resolution is sufficient to detect differences in PCr levels between wild-type (wt) and M-CK deficient (M-CK $^{-/-}$) mice immediately after a burst of twitch contractions (135).

1.2.5 In vivo ^{13}C MR spectroscopy of brain

^{13}C MR spectroscopy has a low sensitivity ($1.8 \cdot 10^{-2}$ of that of protons) and differs fundamentally from ^1H and ^{31}P MRS in the fact that the ^{13}C isotope has a natural abundance of only 1.1%. Therefore, generally only a few molecules present at high concentrations in the body, like long chain fatty acids and glycogen in muscle, show a natural abundance signal. Recent experiments showed that also signals for neurotransmitters can be detected when acquiring signal over a long period of time (3.5 hours) (136).

Because of this low natural abundance, infusion of ^{13}C labeled compounds, e.g. glucose labeled at the C1 position, enables detection of other molecules by uptake of this labeled compound and transfer of the ^{13}C label to other metabolites dynamically (see also section 1.1.8). After a certain period, the ^{13}C label of glucose is transferred to several carbon positions in Glu, Gln, Lac, alanine (Ala), Aspartate (Asp), NAA and GABA (figure 1.8).

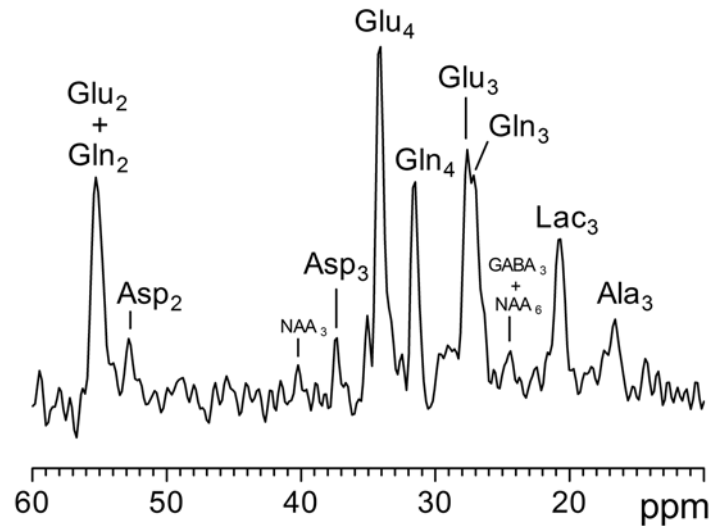


Figure 1.8: Difference spectrum of 30 minutes of the mouse brain, one hour after infusion of 99% enriched 1- ^{13}C glucose. The number in subscript denotes the carbon position of the ^{13}C label in the molecule.

Two major challenges are present when performing ^{13}C MRS on the mouse brain. Firstly, the low sensitivity of the ^{13}C nucleus compared to protons together with the small size of the mouse brain yield a low ^{13}C MR signal. Therefore, a sensitive ^{13}C coil is needed. In our experiments, a ^{13}C surface coil was used. Secondly, the spins of protons connected to the ^{13}C atom split up the energy levels which causes the signal to divide up into multiplets. By using a decoupling scheme, magnetization of protons is randomized making the multiplets collapse into a singlet with higher signal to noise ratio (SNR). One has to be careful in applying decoupling power, however, because too much power could lead to tissue heating (137, 138).

1.2.6 Data processing

In an MR spectrum, the surface area under the signal reflects the amount of resonating nuclei. Therefore, the easiest way to quantify a signal is by integrating the signal area. However, low SNR, overlapping signals, and baseline distortions, which are commonly observed in MR spectra acquired in vivo, may affect proper quantification. This problem is commonly circumvented by introducing prior knowledge (139).

The first way this can be performed is by fitting each single resonance by a Lorentzian or a Gaussian line shape function. From MR theory in liquids, only Lorentzian lineshapes are expected. In practice, however, Gaussian lineshapes may provide a better fit to signals obtained in vivo. This fitting procedure can be performed in the time domain using the software package MRUI (140) by a so called VARPRO (141) or AMARES (142) technique. Further prior knowledge can be enforced on the linewidths and resonance positions making the fitting procedure more robust.

While fitting of single line shapes works well in spectra which consist of a few resolved resonances (^{31}P spectra of brain and muscle, ^1H spectra of skeletal muscle, ^{13}C subtraction spectra), for MR spectra with multiple overlapping resonances, like in ^1H MR spectra of the brain, another approach is more favorable. For instance, LCModel is a software package that fits complete spectra recorded from several metabolites in solution (143). Every metabolite that is expected to be found in vivo has to be measured separately in solution. These solution spectra are then taken together in a so called basis set, of which a linear combination is fitted to the in vivo data. In this way optimal prior knowledge is employed. By setting the proper parameter values for the metabolite concentration in solution and some other parameters like a transmitter reference amplitude, absolute values for the tissue content of the metabolites can be obtained. The new java version of MRUI (jMRUI, (144)) can fit a modeled or measured basis set to the in vivo data through an algorithm named QUEST (145).

Absolute quantification is possible in several ways. As described above, LCModel can directly compare the in vivo data to ^1H MR spectra of solutions with known concentration. Care has to be taken to correct for differences in transmitter amplitude between the acquired metabolite spectrum and the water spectrum. An alternative approach is to compare metabolite signals to the water signal in an MR spectrum acquired without water suppression. Assuming a fixed tissue concentration of water, absolute values for the metabolites can be calculated. When measuring with relatively short repetition time (TR), a correction for T_1 saturation needs to be applied, just as a correction for T_2 decay when acquiring an echo (e.g. when using STEAM). In ^{31}P MRS, the ^1H water signal observed by a separate coil may also be used for quantification but this requires a somewhat complicated approach. A separate measurement performed with equal MR conditions of a phantom filled with a known phosphate containing solution can be used as reference. Alternatively, ATP is often used as an internal reference. It is then assumed to have a constant value for a particular tissue independent of small fluctuations in energetic state of that tissue. Therefore, in ^{31}P MR metabolic concentration values are often calculated assuming a constant ATP pool or are presented as ratio to ATP. In both cases, possible T_1 saturation has to be taken into account.

1.3 Outline of this thesis

MRS is a powerful technique to study transgenic animals *in vivo*, in particular when substrates of the enzymes involved show signals in the MR spectra. In the last decade, several new transgenic mouse models and approaches to generate these models have become available that provide exiting opportunities to study metabolism and metabolic pathways in healthy and pathological conditions. This thesis focuses on the role of CK and AK in a number of strongly interconnected energetics pathways, i.e. the Cr-CK system, the AK system, glycolysis, the mitochondrial TCA cycle and oxidative phosphorylation (OXPHOS). Disabling one or more enzymes may lead to rerouting of fluxes through the remaining energy pathways. Although various approaches with use of pharmacological inhibition or siRNA- or antibody-based interference strategies are now available to ablate enzyme activity, the use of conventional gene knock-out methodology is still the only 100% reliable procedure to achieve complete and specific deficiency. Before turning to the in depth studies of the above mentioned systems, a review will be given in **chapter 2** on the current status of *in vivo* MRS of transgenic mouse models that have a genomic phenotype which affect high-energy phosphoryl transfer.

In the work of this thesis, the following specific issues were addressed. First, a study on postnatal development of mice lacking both CK isoforms in muscle was performed (**chapter 3**) to gain insight into the origin of the PCr signal that was somewhat unexpectedly observed in earlier studies of mice with complete CK deficiency (146). By combining cell-biological, biochemical and biophysical approaches, the fate of PCr, and its relation to specific levels of CK isoenzymes, during maturation and ageing of muscle was examined. Furthermore, in this chapter we address the question whether all Cr is visible in ^1H MRS, an issue that has been a topic of debate for some years, by performing both biochemical and ^1H MR spectral analyses.

One of the reasons that single CK and AK1 knock-out mice display a rather mild phenotype is that there is (partial) overlap and redundancy in function of enzymes in the $\sim\text{P}$ transfer network, including the CK, AK and glycolytic systems. Previous work had demonstrated that both M-CK and AK single knock-out mice were well capable of handling ischemic stress to the hind leg. The question that remained was whether combined knock-out of the cytosolic enzymes M-CK and AK1, in so called MAK $^{-/-}$ mice (61), could provide further clues on the interchangeability of both systems *in vivo*. In **chapter 4** we studied whether energy provision in MAK $^{-/-}$ muscle during an ischemic challenge and upon recovery becomes solely dependent on glycolysis, since no other high-energy sources are available. Comparing the results of this study with similar studies in M-CK $^{-/-}$ and AK $^{-/-}$ single knock-

out mice gives a new perspective on the interaction between the CK and AK enzyme systems *in vivo*.

The metabolic systems that provide energy for proper brain functioning are currently intensely studied. Much emphasis is aimed at a better understanding of the close interaction between neurons and glial cells (81, 82). How B-CK and UbCKmit, the only CK isoforms occurring in brain, are integrated into this complex network is not very well understood. First, to obtain a better picture and make an inventory of anatomical and metabolic consequences of knock-out brains of mice lacking B-CK, UbCKmit, or both enzymes (B-CK/UbCKmit^{-/-}), were investigated with ³¹P and ¹H MRS in **chapter 5**. To study whether CK absence in brain also results in an up-regulation of glycolysis, similar to the situation in muscle, ¹³C MRS techniques were developed on a 7 T MR animal system which were applied to B-CK/UbCKmit^{-/-} mice (**chapter 6**). Although this technique was already used in rat brain, the much smaller size of the mouse brain imposes considerable technical challenges which have not been solved thus far, despite the great interest to study metabolic adaptation in transgenic mice. Using ¹³C MRS, we compared conversion of glucose, formation of lactate and synthesis of other substances including several neurotransmitters between B-CK/UbCKmit^{-/-} and wt animals with high temporal resolution.

In **chapter 7**, mice are investigated which lack guanidinoacetate methyltransferase (GAMT) and, as a result, lack creatine. These animals serve as a faithful model for GAMT deficiency in humans, but were also expected to provide important information on the role of Cr/CK circuit, additional to the data obtained from CK deficient mice. As MRS plays a crucial role in the diagnosis of these patients, MRS of these mice is performed to see whether they show similar metabolic characteristics as patients with GAMT deficiency. Furthermore, additional experiments were performed to get a better fundamental understanding of the mechanisms involved in Cr deficiency.

The last chapter, **chapter 8**, deals with the visibility of Cr in human ¹H MRS. In rat and mice tissues it has already been observed that the proton invisible pool of Cr is very small (147-150). In humans, however, due to technical limitations of clinical MR scanners this was thus far not reliably studied. We retrofitted a clinical MR scanner, and measured the pool size of the MR invisible Cr fraction in human gastrocnemius muscle. In **chapter 9** all findings are integrated in a general summary.

REFERENCES

1. Dzeja, P.P., Terzic, A. and Wieringa, B. Phosphotransfer dynamics in skeletal muscle from creatine kinase gene-deleted mice. *Mol Cell Biochem* 2004;256-257:13-27.
2. Dzeja, P.P. and Terzic, A. Phosphotransfer networks and cellular energetics. *J Exp Biol* 2003;206:2039-47.
3. Hochachka, P.W. and Somero, G.N. *Biochemical adaptation: mechanism and process in physiological evolution*. New York: Oxford University Press; 2002.
4. Atkinson, D.E. *Cellular energy metabolism and its regulation*. New York: Academic press; 1977.
5. Stryer, L. *Biochemistry*. New York: W. H. Freeman and Company; 1975.
6. Kadenbach, B. Intrinsic and extrinsic uncoupling of oxidative phosphorylation. *Biochim Biophys Acta* 2003;1604:77-94.
7. Wyss, M. and Kaddurah-Daouk, R. Creatine and creatinine metabolism. *Physiol Rev* 2000;80:1107-213.
8. Wyss, M. and Wallimann, T. Creatine metabolism and the consequences of creatine depletion in muscle. *MolCellBiochem* 1994;133-134:51-66.
9. Borsook, H. and Dubnoff, J.W. The hydrolysis of phosphocreatine and the origin of urinary creatine. *J Biol Chem* 1947;168:493-510.
10. Walker, J.B. Creatine: biosynthesis, regulation, and function. *Adv Enzymol* 1979;50:177-242.
11. Stöckler, S., Holzbach, U., Hanefeld, F., Marquardt, I., Helms, G., Reuart, M., Hanicke, W. and Frahm, J. Creatine deficiency in the brain: a new, treatable inborn error of metabolism. *Pediatr Res* 1994;36:409-13.
12. Stöckler, S., Hanefeld, F. and Frahm, J. Creatine replacement therapy in guanidinoacetate methyltransferase deficiency, a novel inborn error of metabolism. *Lancet* 1996;348:789-90.
13. Stöckler, S., Isbrandt, D., Hanefeld, F., Schmidt, B. and von Figura, K. Guanidinoacetate methyltransferase deficiency: the first inborn error of creatine metabolism in man. *Am J Hum Genet* 1996;58:914-22.
14. Stöckler, S., Marescau, B., De Deyn, P.P., Trijbels, J.M. and Hanefeld, F. Guanidino compounds in guanidinoacetate methyltransferase deficiency, a new inborn error of creatine synthesis. *Metabolism* 1997;46:1189-93.
15. Ganesan, V., Johnson, A., Connelly, A., Eckhardt, S. and Surtees, R.A. Guanidinoacetate methyltransferase deficiency: new clinical features. *Pediatr Neurol* 1997;17:155-7.
16. Leuzzi, V., Bianchi, M.C., Tosetti, M., Carducci, C., Cerquiglini, C.A., Cioni, G. and Antonozzi, I. Brain creatine depletion: guanidinoacetate methyltransferase deficiency (improving with creatine supplementation) [In Process Citation]. *Neurology* 2000;55:1407-9.
17. Schulze, A., Hess, T., Wevers, R., Mayatepek, E., Bachert, P., Marescau, B., Knopp, M.V., De Deyn, P.P., Bremer, H.J. and Rating, D. Creatine deficiency syndrome caused by guanidinoacetate methyltransferase deficiency: diagnostic tools for a new inborn error of metabolism [see comments]. *J Pediatr* 1997;131:626-31.
18. Thiel, T., Ensenauer, R., Hennig, J. and Lehnert, W. In vivo magnetic resonance spectroscopy in a patient with Creatine deficiency syndrome: new aspects on mechanism of Creatine uptake in brain and muscle. *Proc Intl Soc Mag Reson Med* 9 2001;582.
19. van der Knaap, M.S., Verhoeven, N.M., Maaswinkel-Mooij, P., Pouwels, P.J., Onkenhout, W., Peeters, E.A., Stöckler-Ipsiroglu, S. and Jakobs, C. Mental retardation and behavioral problems as presenting signs of a creatine synthesis defect. *Ann Neurol* 2000;47:540-3.
20. Schulze, A., Bachert, P., Schlemmer, H., Harting, I., Polster, T., Salomons, G.S., Verhoeven, N.M., Jakobs, C., Fowler, B., Hoffmann, G.F. and Mayatepek, E. Lack of creatine in muscle and brain in an adult with GAMT deficiency. *Ann Neurol* 2003;53:248-51.
21. de Grauw, T.J., Cecil, K.C., Salomons, G.S., van Doornen, S.J.M., Verhoeven, N.M., Ball, W.S. and Jakobs, C., The clinical syndrome of creatine transporter deficiency, in "Abstracts of 6th international conference on guanidino compounds in biology and medicine, Cincinnati, Ohio, VS, 2001.

22. Cecil, K.M., Salomons, G.S., Ball, W.S., Jr., Wong, B., Chuck, G., Verhoeven, N.M., Jakobs, C. and DeGrauw, T.J. Irreversible brain creatine deficiency with elevated serum and urine creatine: a creatine transporter defect? *Ann Neurol* 2001;49:401-4.
23. Bianchi, M.C., Tosetti, M., Fornai, F., Alessandri, M.G., Cipriani, P., De Vito, G. and Canapicchi, R. Reversible brain creatine deficiency in two sisters with normal blood creatine level. *Ann Neurol* 2000;47:511-3.
24. Item, C.B., Stockler-Ipsiroglu, S., Stromberger, C., Muhl, A., Alessandri, M.G., Bianchi, M.C., Tosetti, M., Fornai, F. and Cioni, G. Arginine:glycine amidinotransferase deficiency: the third inborn error of creatine metabolism in humans. *Am J Hum Genet* 2001;69:1127-33.
25. Wallimann, T. Bioenergetics. Dissecting the role of creatine kinase. *Curr Biol* 1994;4:42-6.
26. Wallimann, T., Wyss, M., Brdiczka, D., Nicolay, K. and Eppenberger, H.M. Intracellular compartmentation, structure and function of creatine kinase isoenzymes in tissues with high and fluctuating energy demands: the phosphocreatine circuit for cellular energy homeostasis. *Biochem J* 1992;281:21-40.
27. Wyss, M., Smeitink, J., Wevers, R.A. and Wallimann, T. Mitochondrial creatine kinase: a key enzyme of aerobic energy metabolism. *Biochim Biophys Acta* 1992;1102:119-66.
28. Wallimann, T. and Hemmer, W. Creatine kinase in non-muscle tissues and cells. *Mol Cell Biochem* 1994;133-134:193-220.
29. in 't Zandt, H.J., Groof, A.J., Renema, W.K., Oerlemans, F.T., Klomp, D.W., Wieringa, B. and Heerschap, A. Presence of (phospho)creatine in developing and adult skeletal muscle of mice without mitochondrial and cytosolic muscle creatine kinase isoforms. *J Physiol* 2003;548:847-58.
30. Schlattner, U., Gehring, F., Vernoux, N., Tokarska-Schlattner, M., Neumann, D., Marcillat, O., Vial, C. and Wallimann, T. C-terminal lysines determine phospholipid interaction of sarcomeric mitochondrial creatine kinase. *J Biol Chem* 2004;279:24334-42.
31. Bittl, J.A., DeLayre, J. and Ingwall, J.S. Rate equation for creatine kinase predicts the in vivo reaction velocity: 31P NMR surface coil studies in brain, heart, and skeletal muscle of the living rat. *Biochemistry* 1987;26:6083-6090.
32. Adams, G.R., Foley, J.M. and Meyer, R.A. Muscle buffer capacity estimated from pH changes during rest-to-work transitions. *J Appl Physiol* 1990;69:968-72.
33. Kemp, G.J., Roussel, M., Bendahan, D., Le Fur, Y. and Cozzone, P.J. Interrelations of ATP synthesis and proton handling in ischaemically exercising human forearm muscle studied by 31P magnetic resonance spectroscopy. *J Physiol* 2001;535:901-28.
34. Crowther, G.J., Carey, M.F., Kemper, W.F. and Conley, K.E. Control of glycolysis in contracting skeletal muscle. I. Turning it on. *Am J Physiol Endocrinol Metab* 2002;282:E67-73.
35. in 't Zandt, H.J., Oerlemans, F., Wieringa, B. and Heerschap, A. Effects of ischemia on skeletal muscle energy metabolism in mice lacking creatine kinase monitored by in vivo 31P nuclear magnetic resonance spectroscopy. *NMR Biomed* 1999;12:327-34.
36. Meyer, R.A., Brown, T.R., Krilowicz, B.L. and Kushmerick, M.J. Phosphagen and intracellular pH changes during contraction of creatine depleted rat muscle. *Am J Physiol* 1986;250:C264-C274.
37. Bose, S., French, S., Evans, F.J., Joubert, F. and Balaban, R.S. Metabolic network control of oxidative phosphorylation: multiple roles of inorganic phosphate. *J Biol Chem* 2003;278:39155-65.
38. Dzeja, P.P. and Terzic, A. Phosphotransfer reactions in the regulation of ATP-sensitive K⁺ channels. *Faseb J* 1998;12:523-9.
39. Wallimann, T., Pelloni, G., Turner, D.C. and Eppenberger, H.M. Monovalent antibodies against MM-creatine kinase remove the M line from myofibrils. *Proc Natl Acad Sci U S A* 1978;75:4296-300.
40. Wyss, M. and Schulze, A. Health implications of creatine: can oral creatine supplementation protect against neurological and atherosclerotic disease? *Neuroscience* 2002;112:243-60.
41. Braissant, O., Henry, H., Loup, M., Eilers, B. and Bachmann, C. Endogenous synthesis and transport of creatine in the rat brain: an in situ hybridization study. *Brain Res Mol Brain Res* 2001;86:193-201.
42. Boehm, E.A., Radda, G.K., Tomlin, H. and Clark, J.F. The utilisation of creatine and its analogues by cytosolic and mitochondrial creatine kinase. *Biochim Biophys Acta* 1996;1274:119-28.

43. Fitch, C.D. and Chevli, R. Inhibition of creatine and phosphocreatine accumulation in skeletal muscle and heart. *Metabolism* 1980;29:686-90.
44. van Deursen, J., Jap, P., Heerschap, A., ter Laak, H., Ruitenbeek, W. and Wieringa, B. Effects of the creatine analogue beta-guanidinopropionic acid on skeletal muscles of mice deficient in muscle creatine kinase. *Biochim Biophys Acta* 1994;1185:327-35.
45. O'Gorman, E., Beutner, G., Wallimann, T. and Brdiczka, D. Differential effects of creatine depletion on the regulation of enzyme activities and on creatine-stimulated mitochondrial respiration in skeletal muscle, heart, and brain. *Biochim Biophys Acta* 1996;1276:161-70.
46. Shoubridge, E.A. and Radda, G.K. A ³¹P-nuclear magnetic resonance study of skeletal muscle metabolism in rats depleted of creatine with the analogue beta-guanidinopropionic acid. *Biochim Biophys Acta* 1984;805:79-88.
47. Holtzman, D., McFarland, E., Moerland, T., Koutcher, J., Kushmerick, M.J. and Neuringer, L.J. Brain creatine phosphate and creatine kinase in mice fed an analogue of creatine. *BrainRes* 1989;483:68-77.
48. Shoubridge, E.A., Challiss, R.A., Hayes, D.J. and Radda, G.K. Biochemical adaptation in the skeletal muscle of rats depleted of creatine with the substrate analogue beta-guanidinopropionic acid. *Biochem J* 1985;232:125-31.
49. von Figura, K., Hanefeld, F., Isbrandt, D. and Stöckler-Ipsiroglu, S. Guanidinoacetate methyltransferase deficiency. in: *The Metabolic and Molecular Bases of Inherited Disease* Eds.: C. R. Scriver, A. L. Beaudet, W. S. Sly, D. Valle and V. Childs 2001.
50. Frahm, J., Requardt, M., Helms, G., Hänicke, W., Stöckler, S., Holzbach, U. and Hanefeld, F., Creatine deficiency in the brain. A new treatable inborn error of metabolism identified by proton and phosphorous MR spectroscopy in vivo, *Society of Magn Res, San Francisco*, 1994.
51. Kan, H.E., Renema, W.K., Isbrandt, D. and Heerschap, A. Phosphorylated guanidinoacetate partly compensates for the lack of phosphocreatine in skeletal muscle of mice lacking guanidinoacetate methyltransferase. *J Physiol* 2004;560:219-29.
52. Noda, L. Adenylate Kinase. in: *The enzymes* Eds.: P. D. Boyer; New York: Academic Press: 1973. 279-305
53. Collavin, L., Lazarevic, D., Utrera, R., Marzinotto, S., Monte, M. and Schneider, C. wt p53 dependent expression of a membrane-associated isoform of adenylate kinase. *Oncogene* 1999;18:5879-88.
54. Tanabe, T., Yamada, M., Noma, T., Kajii, T. and Nakazawa, A. Tissue-specific and developmentally regulated expression of the genes encoding adenylate kinase isozymes. *J Biochem (Tokyo)* 1993;113:200-7.
55. Van Rompay, A.R., Johansson, M. and Karlsson, A. Identification of a novel human adenylate kinase. cDNA cloning, expression analysis, chromosome localization and characterization of the recombinant protein. *Eur J Biochem* 1999;261:509-17.
56. Yoneda, T., Sato, M., Maeda, M. and Takagi, H. Identification of a novel adenylate kinase system in the brain: cloning of the fourth adenylate kinase. *Brain Res Mol Brain Res* 1998;62:187-95.
57. Janssen, E.E.W., Kuiper, J., Hodgson, D., Zingman, L.V., Alekseev, A.E., Terzic, A. and Wieringa, B. Two structurally distinct and spatially compartmentalized adenylate kinases are expressed from the AK1 gene in mouse brain. *Mol Cell Biochem* 2003;in press.
58. Janssen, E.E.W. *The role of Adenylate kinase 1 in energy transfer: a study of mice lacking adenylate kinase 1*. Nijmegen: University of Nijmegen; 2003.
59. Janssen, E., Dzeja, P.P., Oerlemans, F., Simonetti, A.W., Heerschap, A., de Haan, A., Rush, P.S., Terjung, R.R., Wieringa, B. and Terzic, A. Adenylate kinase 1 gene deletion disrupts muscle energetic economy despite metabolic rearrangement. *Embo J* 2000;19:6371-81.
60. Pucar, D., Janssen, E., Dzeja, P.P., Juranic, N., Macura, S., Wieringa, B. and Terzic, A. Compromised energetics in the adenylate kinase AK1 gene knockout heart under metabolic stress. *J Biol Chem* 2000;275:41424-9.
61. Janssen, E., Terzic, A., Wieringa, B. and Dzeja, P.P. Impaired intracellular energetic communication in muscles from creatine kinase and adenylate kinase (M-CK/AK1) double knock-out mice. *J Biol Chem* 2003;278:30441-9.

62. Bessman, S.P. and Carpenter, C.L. The creatine-creatine phosphate energy shuttle. *Annu Rev Biochem* 1985;54:831-62.
63. Zeleznikar, R.J., Dzeja, P.P. and Goldberg, N.D. Adenylate kinase-catalyzed phosphoryl transfer couples ATP utilization with its generation by glycolysis in intact muscle. *J Biol Chem* 1995;270:7311-9.
64. Dzeja, P.P., Zeleznikar, R.J. and Goldberg, N.D. Adenylate kinase: kinetic behavior in intact cells indicates it is integral to multiple cellular processes. *Mol Cell Biochem* 1998;184:169-82.
65. Wegmann, G., Zanolla, E., Eppenberger, H.M. and Walliman, T. In situ compartmentation of creatine kinase in intact sarcomeric muscle: the acto-myosin overlap zone as a molecular sieve. *J Muscle Res Cell Motil* 1992;13:420-435.
66. Wallimann, T., Dolder, M., Schlattner, U., Eder, M., Hornemann, T., O'Gorman, E., Ruck, A. and Brdiczka, D. Some new aspects of creatine kinase (CK): compartmentation, structure, function and regulation for cellular and mitochondrial bioenergetics and physiology. *Biofactors* 1998;8:229-34.
67. Beutner, G., Ruck, A., Riede, B., Welte, W. and Brdiczka, D. Complexes between kinases, mitochondrial porin and adenylate translocator in rat brain resemble the permeability transition pore. *FEBS Lett* 1996;396:189-95.
68. Schlattner, U. and Wallimann, T. Octamers of mitochondrial creatine kinase isoenzymes differ in stability and membrane binding. *J Biol Chem* 2000;275:17314-20.
69. Meyer, R.A., Sweeney, H.L. and Kushmerick, M.J. A simple analysis of the "phosphocreatine shuttle". *Am J Physiol* 1984;15:C365-C377.
70. Wiseman, R.W. and Kushmerick, M.J. Creatine kinase equilibration follows solution thermodynamics in skeletal muscle. ³¹P NMR studies using creatine analogs. *J Biol Chem* 1995;270:12428-12438.
71. Vander, A.J., Sherman, J.H. and Luciano, D.S. *Human Physiology*. New York, NY: McGraw-Hill; 1998.
72. Magistretti, P.J. Brain Energy metabolism. in: *Fundamental neuroscience* Eds.: M. J. Zigmond, F. E. Bloom, S. C. Landis, J. L. Roberts and L. R. Squire San Diego, CA: Academic Press: 2003. 339-360
73. Shepherd, G.M. *Neurobiology*. New York: Oxford University Press; 1983.
74. Herz, L. and Diemel, G.A. International Review of neurobiology. in: *Glucose metabolism in the brain* Eds.: D. S. Dwyer San Diego, CA: Academic Press: 2002.
75. Zigmond, M.J., Bloom, F.E., Landis, S.C., Roberts, J.L. and Squire, L.R. *Fundamental Neuroscience*. 1999;1600.
76. Pellerin, L. and Magistretti, P.J. Glutamate uptake into astrocytes stimulates aerobic glycolysis: a mechanism coupling neuronal activity to glucose utilization. *Proc Natl Acad Sci U S A* 1994;91:10625-9.
77. Erecinska, M. and Silver, I.A. Metabolism and role of glutamate in mammalian brain. *Prog Neurobiol* 1990;35:245-96.
78. Sibson, N.R., Dhankhar, A., Mason, G.F., Behar, K.L., Rothman, D.L. and Shulman, R.G. In vivo ¹³C NMR measurements of cerebral glutamine synthesis as evidence for glutamate-glutamine cycling. *Proc Natl Acad Sci U S A* 1997;94:2699-704.
79. Sibson, N.R., Mason, G.F., Shen, J., Cline, G.W., Herskovits, A.Z., Wall, J.E., Behar, K.L., Rothman, D.L. and Shulman, R.G. In vivo (¹³C) NMR measurement of neurotransmitter glutamate cycling, anaplerosis and TCA cycle flux in rat brain during. *J Neurochem* 2001;76:975-89.
80. Magistretti, P.J., Pellerin, L., Rothman, D.L. and Shulman, R.G. Energy on demand. *Science* 1999;283:496-7.
81. Pellerin, L. and Magistretti, P.J. Neuroscience. Let there be (NADH) light. *Science* 2004;305:50-2.
82. Kasischke, K.A., Vishwasrao, H.D., Fisher, P.J., Zipfel, W.R. and Webb, W.W. Neural activity triggers neuronal oxidative metabolism followed by astrocytic glycolysis. *Science* 2004;305:99-103.
83. Bouzier-Sore, A.K., Voisin, P., Canioni, P., Magistretti, P.J. and Pellerin, L. Lactate is a preferential oxidative energy substrate over glucose for neurons in culture. *J Cereb Blood Flow Metab* 2003;23:1298-306.

84. Sibson, N.R., Dhankhar, A., Mason, G.F., Rothman, D.L., Behar, K.L. and Shulman, R.G. Stoichiometric coupling of brain glucose metabolism and glutamatergic neuronal activity. *Proc Natl Acad Sci U S A* 1998;95:316-21.
85. Attwell, D. and Laughlin, S.B. An energy budget for signaling in the grey matter of the brain. *J Cereb Blood Flow Metab* 2001;21:1133-45.
86. Pellerin, L. and Magistretti, P.J. Food for thought: challenging the dogmas. *J Cereb Blood Flow Metab* 2003;23:1282-6.
87. Bernstein, B.W. and Bamburg, J.R. Actin-ATP hydrolysis is a major energy drain for neurons. *J Neurosci* 2003;23:1-6.
88. Gruetter, R., Seaquist, E.R., Kim, S. and Ugurbil, K. Localized in vivo ¹³C-NMR of glutamate metabolism in the human brain: initial results at 4 tesla. *Dev Neurosci* 1998;20:380-8.
89. Gruetter, R. In vivo ¹³C NMR studies of compartmentalized cerebral carbohydrate metabolism. *Neurochem Int* 2002;41:143-54.
90. Gruetter, R., Seaquist, E.R. and Ugurbil, K. A mathematical model of compartmentalized neurotransmitter metabolism in the human brain. *Am J Physiol Endocrinol Metab* 2001;281:E100-12.
91. Cruz, F. and Cerdan, S. Quantitative ¹³C NMR studies of metabolic compartmentation in the adult mammalian brain. *NMR Biomed* 1999;12:451-62.
92. Kunnecke, B. and Cerdan, S. Multilabeled ¹³C substrates as probes in in vivo ¹³C and ¹H NMR spectroscopy. *NMR Biomed* 1989;2:274-7.
93. Rothman, D.L., Sibson, N.R., Hyder, F., Shen, J., Behar, K.L. and Shulman, R.G. In vivo nuclear magnetic resonance spectroscopy studies of the relationship between the glutamate-glutamine neurotransmitter cycle and functional neuroenergetics. *Philos Trans R Soc Lond B Biol Sci* 1999;354:1165-77.
94. van Zijl, P.C. and Rothman, D. NMR studies of brain ¹³C-glucose uptake and metabolism: present status. *Magn Reson Imaging* 1995;13:1213-21.
95. Sibson, N.R., Shen, J., Mason, G.F., Rothman, D.L., Behar, K.L. and Shulman, R.G. Functional energy metabolism: in vivo ¹³C-NMR spectroscopy evidence for coupling of cerebral glucose consumption and glutamatergic neuronal activity. *Dev Neurosci* 1998;20:321-30.
96. Muir, D., Berl, S. and Clarke, D.D. Acetate and fluoroacetate as possible markers for glial metabolism in vivo. *Brain Res* 1986;380:336-40.
97. Bloch, F., Hansen, W.W. and Packard, M. The nuclear induction experiment. *Phys Rev* 1946;70:474-485.
98. Purcell, E.M., Torrey, H.C. and Pound, R.V. Resonance absorption by nuclear magnetic moments in a solid. *Phys Rev* 1946;69:37-38.
99. Bloch, F. Nuclear induction. *Phys Rev* 1946;70:460-474.
100. Damadian, R. Tumor detection by nuclear magnetic resonance. *Science* 1971;171:1151-3.
101. Lauterbur, P.C. Image formation of induced local interactions: examples employing NMR. *Nature* 1973;242:190-191.
102. Mansfield, P. and Grannell, P.K. NMR 'diffraction' in solids? *J Phys* 1973;C 6:L422-L426.
103. Mansfield, P. and Maudsley, A.A. Line scan proton spin imaging in biological structures by NMR. *Phys Med Biol* 1976;21:847-52.
104. Mansfield, P. Multi-planar image formation using NMR spin echoes. *J Phys C: Solid State Phys* 1977;10:55-58.
105. Mansfield, P. and Maudsley, A.A. Medical imaging by NMR. *Br J Radiol* 1977;50:188-94.
106. Mansfield, P. and Chapman, B. Active magnetic screening of gradient coils in NMR imaging. *J Magn Reson* 1986;66:573-576.
107. Ernst, R.R. and Anderson, W.A. Application of Fourier Transform Spectroscopy to Magnetic Resonance. *Rev Sci Instrum* 1966;37:84-93.
108. Kumar, A., Welti, D. and Ernst, R.R. NMR zeugmatography. *J Magn Reson* 1975;18:69-83.

109. Macomber, R.S. A complete introduction to modern NMR spectroscopy. New York: John Wiley & Sons; 1998.
110. Frahm, J., Merboldt, K.D. and Hänicke, W. Localised proton spectroscopy using stimulated echoes. *J Magn Reson* 1987;72:502-08.
111. Ordidge, R.J., Bendall, M.R., Gordon, R.E. and Connelly, A. Volume selection for in-vivo biological spectroscopy. in: *Magnetic resonance in biology and medicine* Eds.: G. Govil, D. L. Khetrapal and A. Saran New Delhi: Tata McGraw-Hill: 1985. 387-97
112. Geppert, C., Dreher, W. and Leibfritz, D. PRESS-based proton single-voxel spectroscopy and spectroscopic imaging with very short echo times using asymmetric RF pulses. *Magma* 2003;
113. Haase, A., Frahm, J., Hanicke, W. and Matthaei, D. 1H NMR chemical shift selective (CHESS) imaging. *Phys Med Biol* 1985;30:341-4.
114. Tkac, I., Starcuk, Z., Choi, I.Y. and Gruetter, R. In vivo 1H NMR spectroscopy of rat brain at 1 ms echo time. *Magn Reson Med* 1999;41:649-56.
115. Gruetter, R. Automatic, localized in vivo adjustment of all first- and second-order shim coils. *Magn Reson Med* 1993;29:804-11.
116. Pfeuffer, J., Tkac, I., Provencher, S.W. and Gruetter, R. Toward an in vivo neurochemical profile: quantification of 18 metabolites in short-echo-time (1)H NMR spectra of the rat brain. *J Magn Reson* 1999;141:104-20.
117. Ross, B. and Bluml, S. Magnetic resonance spectroscopy of the human brain. *Anat Rec* 2001;265:54-84.
118. Brown, T.R. Practical Applications of Chemical Shift Imaging. *NMR Biomed* 1992;5:238-243.
119. Brown, T.R., Kincaid, B.M. and Ugurbil, K. NMR chemical shift imaging in three dimensions. *Proc Natl Acad Sci U S A* 1982;79:3523-6.
120. Klomp, D.W., Van Laarhoven, H.W., Kentgens, A.P. and Heerschap, A. Optimization of localized 19F magnetic resonance spectroscopy for the detection of fluorinated drugs in the human liver. *Magn Reson Med* 2003;50:303-8.
121. Pohmann, R. and von Kienlin, M. Accurate phosphorus metabolite images of the human heart by 3D acquisition-weighted CSI. *Magn Reson Med* 2001;45:817-26.
122. Scheenen, T.W., Klomp, D.W., Roll, S.A., Futterer, J.J., Barentsz, J.O. and Heerschap, A. Fast acquisition-weighted three-dimensional proton MR spectroscopic imaging of the human prostate. *Magn Reson Med* 2004;52:80-8.
123. Heerschap, A., Sommers, M.G., in 't Zandt, H.J., Renema, W.K., Veltien, A.A. and Klomp, D.W. Nuclear magnetic resonance in laboratory animals. *Methods Enzymol* 2004;385:41-63.
124. Baslow, M.H. N-acetylaspartate in the vertebrate brain: metabolism and function. *Neurochem Res* 2003;28:941-53.
125. Birken, D.L. and Oldendorf, W.H. N-acetyl-L-aspartic acid: a literature review of a compound prominent in 1H-NMR spectroscopic studies of brain. *Neurosci Biobehav Rev* 1989;13:23-31.
126. Kok, R.D., Steegers-Theunissen, R.P., Eskes, T.K., Heerschap, A. and van den Berg, P.P. Decreased relative brain tissue levels of inositol in fetal hydrocephalus. *Am J Obstet Gynecol* 2003;188:978-80.
127. Schuller-Levis, G.B. and Park, E. Taurine: new implications for an old amino acid. *FEMS Microbiol Lett* 2003;226:195-202.
128. Tkac, I., Henry, P.G., Andersen, P., Keene, C.D., Low, W.C. and Gruetter, R. Highly resolved in vivo 1H NMR spectroscopy of the mouse brain at 9.4 T. *Magn Reson Med* 2004;52:478-84.
129. in 't Zandt, H.J.A., Klomp, D.W.J., Oerlemans, F., Wieringa, B., Hilbers, C.W. and Heerschap, A. Proton MR Spectroscopy of wild-type and creatine kinase deficient mouse skeletal muscle: dipole-dipole coupling effects and post-mortem changes. *Magn Reson Med* 2000;43:517-524.
130. Moon, R.B. and Richards, J.H. Determination of intracellular pH by 31P magnetic resonance. *J Biol Chem* 1973;248:7276-8.
131. Gupta, R.K. and Moore, R.D. 31P NMR studies of intracellular free Mg²⁺ in intact frog skeletal muscle. *J Biol Chem* 1980;255:3987-93.

132. Klomp, D.W.J., in 't Zandt, H.J.A., van den Boogert, H.J., Oerlemans, F., Wieringa, B. and Heerschap, A. Optimized probe design for localized in vivo mouse brain ³¹P NMR spectroscopy. *Proc Intl Soc mag Reson Med* 7 1999;2069.
133. Heerschap, A., Sommers, M.G., in 't Zandt, H.J.A., Renema, W.K.J., Veltien, A.A. and Klomp, D.W.J. NMR in laboratory animals. in: *Methods in Enzymology*. 2003.
134. Ordidge, R.J., Connely, A. and Lohman, J.A.B. Image-selected in vivo spectroscopy (ISIS). A new technique for spatially selective NMR spectroscopy. *J Magn Reson* 1986;66:293-294.
135. Roman, B.B., Meyer, R.A. and Wiseman, R.W. Phosphocreatine kinetics at the onset of contractions in skeletal muscle of MM creatine kinase knockout mice. *Am J Physiol Cell Physiol* 2002;283:C1776-83.
136. Henry, P.G., Tkac, I. and Gruetter, R. ¹H-localized broadband ¹³C NMR spectroscopy of the rat brain in vivo at 9.4 T. *Magn Reson Med* 2003;50:684-92.
137. van den Bergh, A.J., van den Boogert, H.J. and Heerschap, A. Skin temperature increase during local exposure to high-power RF levels in humans. *Magn Reson Med* 2000;43:488-90.
138. <http://www.fda.gov/cdrh/ode/95.html>
139. in 't Zandt, H., van Der Graaf, M. and Heerschap, A. Common processing of in vivo MR spectra. *NMR Biomed* 2001;14:224-32.
140. <http://www.mrui.uab.es/mrui/>
141. van der Veen, J.W., de Beer, R., Luyten, P.R. and van Ormondt, D. Accurate quantification of in vivo ³¹P NMR signals using the variable projection method and prior knowledge. *Magn Reson Med* 1988;6:92-8.
142. Vanhamme, L., van den Boogaart, A. and Van Huffel, S. Improved method for accurate and efficient quantification of MRS data with use of prior knowledge. *J Magn Reson* 1997;129:35-43.
143. Provencher, S.W. Estimation of metabolite concentrations from localized in vivo proton NMR spectra. *Magn Reson Med* 1993;30:672-9.
144. Naressi, A., Couturier, C., Devos, J.M., Janssen, M., Mangeat, C., de Beer, R. and Graveron-Demilly, D. Java-based graphical user interface for the MRUI quantitation package. *Magma* 2001;12:141-52.
145. Ratiney, H., Coenradie, Y., Cavassila, S., van Ormondt, D. and Graveron-Demilly, D., Time-domain quantitation with a Metabolite Basis Set, in "Proc Intl Soc mag Reson Med 11, Toronto, Canada, 2003.
146. Steeghs, K., Benders, A., Oerlemans, F., de Haan, A., Heerschap, A., Ruitenbeek, W., Jost, C., van Deursen, J., Perryman, B., Pette, D., Bruckwilder, M., Koudijs, J., Jap, P., Veerkamp, J. and Wieringa, B. Altered Ca²⁺ responses in muscles with combined mitochondrial and cytosolic creatine kinase deficiencies. *Cell* 1997;89:93-103.
147. de Graaf, R.A., van Kranenburg, A. and Nicolay, K. Off-resonance metabolite magnetization transfer measurements on rat brain in situ. *Magn Reson Med* 1999;41:1136-44.
148. Dreher, W., Norris, D.G. and Leibfritz, D. Magnetization transfer affects the proton creatine/phosphocreatine signal intensity: in vivo demonstration in the rat brain. *Magn Reson Med* 1994;31:81-4.
149. Kruiskamp, M., Vliet, G.v. and Nicolay, K. Creatine kinase deficiency alters the off-resonance magnetization transfer effect of creatine methyl ¹H-MR signal from mouse skeletal muscle. 6th Scientific Meeting of the International Society for Magnetic Resonance in Medicine, Abstract 1998;384.
150. Kruiskamp, M.J., de Graaf, R.A., van Vliet, G. and Nicolay, K. Magnetic coupling of creatine/phosphocreatine protons in rat skeletal muscle, as studied by (¹H)-magnetization transfer MRS. *Magn Reson Med* 1999;42:665-672.

2

IN VIVO MAGNETIC RESONANCE SPECTROSCOPY OF TRANSGENIC MOUSE MODELS WITH ALTERED HIGH ENERGY PHOSPHORYL TRANSFER METABOLISM

KlaasJan Renema

Bé Wieringa

Arend Heerschap

2.1 Introduction

The ability to generate and use genetically altered mice has opened up a broad range of new possibilities for the study of the biological role of specific enzymes or even complete pathways involved in cell signaling, metabolism, or structural assembly of organismal form and function. For a complete appreciation of this work, several types of alterations that can be introduced in the mouse genome must be distinguished. At the one end of the spectrum there are the spontaneous genetic changes that result as an effect of naturally occurring DNA-replication/repair errors or spontaneous (retroviral) transposon (re)integrations, or are induced by radiation or genotoxic agents. A broad range of mice with these types of changes have been identified during the last 2-3 decades and exploited as model systems for various human disorders (1), including inheritable neuro-muscular diseases (e.g. the mdx mice (2)), immunodeficiencies (e.g. the NOD mouse model (3, 4)), diabetes (5, 6) and cancer (7, 8).

To date, various centers in the world have started entirely new efforts to produce this type of mice at high rate, by using huge cohorts of animals and biological (random insertion), chemical or physical (radiation) procedures for forced induction of ‘spontaneous’ mutations. Because mutations produced are random and can occur anywhere in the genome, massive breeding and elaborate high-throughput screening programs are needed to identify recessive or dominant-mutant animals with a potentially interesting phenotype or a hit in the particular gene of interest (9, 10).

At the opposite end of the spectrum, we have transgenesis or targeted mutagenesis that can be used to create pre-designed alterations into the mouse genome. A transgenic mouse, or in fact any transgenic animal, is one in which there has been a deliberate and stable modification of the genome via artificial DNA introduction into one or more of its cells. The transgene is thereby randomly integrated or precisely targeted into the chromosomal DNA and may be inherited through the germ line upon breeding. Random integration is usually achieved upon injection of the transgene construct (as a recombinant DNA insert grown in bacterial vectors *in vitro*) into the male pronucleus of a fertilized mouse egg, followed by intra-oviduct transplantation of the zygote into a foster mother and maturation to term. Also viral transduction procedures, for example with lentiviral vectors containing a transgene insert, can be used. This approach has been applied in many studies where mouse models for human dominant genetic disorders were developed (11, 12). Excellent reviews, describing the different procedures for introducing the transgene as well as the fate of the injected DNA and the genetic consequences of this ‘classic’ transgenic route, have appeared in literature and we here refer the reader to those papers (13, 14).

Use of yet another strategy, homologous DNA recombination in *in vitro* cultured mouse embryonic stem (ES) cells in order to precisely engineer a pre-designed mutation into

one of the parental genes of interest, offers one of the most elegant approaches for mimicking human mutations in a mouse model. By following this route, changes can be engineered very precisely. Strategies used regularly involve replacement of endogenous allele segments of the mouse genome by cognate segments of another organism, usually human, with or without mutation. Functional knock-out of genes is achieved by replacing an essential gene region (usually a coding segment, or essential promoter or RNA-processing signals) by a (selectable) cassette. Gene knock-in may involve replacement of genomic DNA domains by para- or orthologous domains from other organisms or by cDNA segments. Finally, by applying so-called knock-in-knock-out procedures, very subtle alterations, even changes of only one DNA base-pair, can be introduced. The identity of the mutation is usually already verified and studied when still at the ES cell stage, in cell culture. Only if the mutation is genuine and no other undesired alterations have been introduced, the ES cells will be used for reintroduction in vivo, by injection into blastocysts ex vivo followed by intra-uterine implantation into foster mothers and growth of the embryos to term. A high level of sophistication is possible, with build-in features to render expression of the transgene conditionally or specifically restricted to particular cell types or tissues (15-17).

Already quickly after the principle of ES-cell transgenesis was developed by Capecchi and co-workers, and other procedural groundwork was published, a virtual explosion of activity emerged. There are now excellent reviews and commentaries on the topic (18-20) and long lists of knock-out and knock-in mice that have been generated via ES cells. Unfortunately, application of homologous DNA targeting in ES cells for use in transgenesis with other mammals than mouse, is much less well established or often even completely impossible, mainly due to lack of pluripotent ES cell lines amenable for manipulation (21, 22) or lack of sophistication in embryo manipulation procedures for other species.

Various non invasive bioimaging techniques are available to study tissue of living transgenic mice (23), including fluorescence imaging, optical or near infrared spectroscopy (24), radionuclei techniques (e.g. PET) (25) and magnetic resonance (MR) methods. One of the many branches of MR is MR Spectroscopy (MRS) which provides a unique tool to investigate metabolism in vivo and in vitro. MRS can be performed on several MR sensitive nuclei, e.g. ^{31}P , ^1H and ^{13}C , each offering specific information on distinct metabolic and physiologic processes or conditions. When the genetic modification of interest has an effect on enzymes that interact directly with MR-visible metabolites (e.g. in case of the creatine kinase (CK) knockout mice), MRS is most powerful. Phosphorus MRS, i.e. ^{31}P MRS, enables one to monitor the energetic status of the tissue under normal or artificial physiological challenges. From ^{31}P MR data fluxes through some phosphotransfer reactions in cellular energetic

pathways and other physiological relevant parameters like intracellular tissue pH can be inferred (26, 27). Proton MRS offers information on metabolite concentrations of a larger and different set of metabolites (28-30) at higher relative sensitivity. Carbon MRS gained more momentum recently (see for instance the special issue on ^{13}C MRS in NMR Biomed, vol 16, 2003) and opened up the possibility to assess several metabolic fluxes simultaneously. For example, fluxes through glycolysis and the Krebs cycle were determined by following the flow of label in ^{13}C glucose into the metabolic network (31). Natural abundance ^{13}C MR spectroscopy was already applied to a spontaneous rat model in 1982 (32). In general, MRS is now also regarded a tool that can offer new opportunities in the area of metabolomics, the generation of complete metabolite profiles of animal and plant tissues. In this context, MRS will become integrated in future multidisciplinary approaches, together with genomics and proteomics studies, to obtain a third level of understanding of integral physiology.

One of the first MRS studies on genetically altered mice – in this case a spontaneous model - was performed on the ReJ 129 dy/dy strain, a model for human myopathy (33). Since then, MRS studies were published that were conducted with classical transgenic mice (34) and finally also in metabolic knock-out mice with a mutation in muscle CK created with the ES cell technology (35)). Use of transgenesis for metabolic studies, including effects on glucose transport and CK -mediated phosphotransfer, has already been reviewed by Koretsky (36). Since then, however, several new studies on transgenic mice and MR spectroscopy techniques have appeared. We focus here on animal models with alterations in high-energy phosphoryl ($\sim\text{P}$) metabolism or associated metabolic pathways, like the Cr-PCr circuits, ADP-ATP exchange reactions and glycolytic and mitochondrial pathways. It has been shown that distinct enzymes involved in the $\sim\text{P}$ transfer pathways corroborate closely (see e.g. (37, 38))

First, a brief outline of practical aspects of *in vivo* NMR in mice will be presented, followed by a review of MRS studies on mouse models with altered cellular energetics. Furthermore, quantitative and qualitative information on findings from *in vivo* MRS studies of mouse skeletal muscle, heart, liver and brain will be provided.

2.2 Equipment for MRS of mice

In MR spectroscopy of small animals two practical issues are of primary interest: sensitivity and field homogeneity. Therefore, much of the MR hardware components and software that is described in this thesis are especially designed for particular applications and home build according to our own specifications. Proportional spatial downscaling from rat to mice requires approximately a tenfold increase in sensitivity. To a large extent this can be achieved by the use of smaller radiofrequency coils, although too small a coil may reduce tissue coverage and adequate probe building for mice requires skilled miniaturization. In principle, sensitivity can also be increased by going to higher magnetic fields. Common field strengths for mice studies range from 4.7 to 9.4 T (39).

Proper imaging and localization requires a sufficiently strong magnetic field gradient set. For high spectral resolution, the optimization of the field homogeneity is needed by shim coils of sufficient strength (40). Especially in the mouse, field in-homogeneities may be relatively severe since most tissue is in close vicinity of air due the small size of the animal. Therefore strong shim coils including 2nd order terms are desirable (41).

For reliable measurement of the anatomical structures of interest in the mouse, they have to be ‘immobilized’ without suppressing respiratory motion or other basal physiological functions. Commonly, the animal is kept under anesthesia using inhalation or injection anesthetics. Possible ways of securing the mouse head, for instance, are the use of stereotactic earbars, teethbars and tight attachment of a surface coil on top of the head. As mice are not able to maintain body temperature when under anesthetics a warming device, like a warm water bed, is needed. Furthermore, temperature has to be monitored continuously, just as breathing frequency, to adjust the depth of the narcosis when needed since this can influence the MR results.

For measurements of a clean and distortion free signal, radio frequencies (RF; i.e. noise) from outside the MR scanner has to be prevented to interfere with the MR signal. At our MR facility, we use copper disks on the front and rear ends of the perspex MR tube containing the mouse, which close the cage of Faraday when the tube is slit into the magnet. Perspex tube and match sticks, just as tubes for the warm water bed, the optical thermometer, and the devise for monitoring the breathing frequency are fed through long cylindrical copper pipes of specific length which function as an RF filter. The RF signal enters directly through connectors in the copper disks. A proton coil was always present for shimming, imaging and, in case of ¹H MRS, for transmitting or receiving the RF signal for the MR spectroscopy. For the analysis of other nuclei, however, a second coil was employed orthogonal to the proton coil such that both coils did not interact with each other.

As an example, the experimental setup of ^{13}C measurements of the mouse brain is shown. In this case, ^{13}C MR signal was acquired using a surface coil, while imaging, shimming and decoupling were performed using a birdcage ^1H coil (figure 2.1).

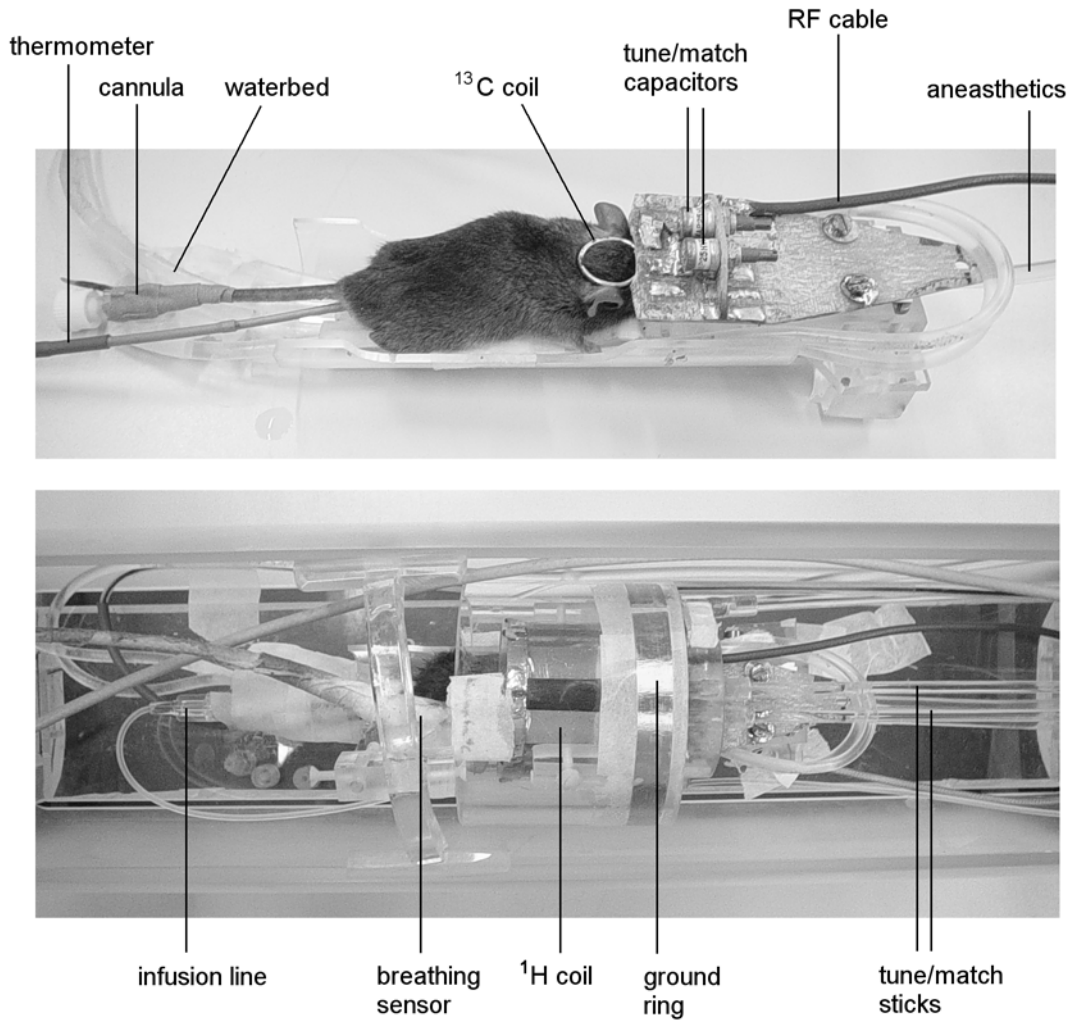


Figure 2.1: Setup of a ^{13}C MR measurement of the mouse brain. Top: mouse in basic setup on warm water bed, only the ^{13}C surface coil present. Bottom: Final setup when the basic setup is slit inside the ^1H birdcage coil and fixed in the perspex MR tube.

2.3 Genetic alterations of high-energy phosphoryl transfer systems

The next section reviews MRS studies on mice with genetic alterations that influence one or more of the \sim P transfer pathways. It starts with a short introduction on Cr/CK and AK systems to place the further subsections into context. For a more detailed description, the reader is referred to chapter 1.

2.3.1 Key enzymes in phosphoryl transfer

Creatine is a small metabolite that fulfills a central role in energy metabolism. The enzyme guanidinoacetate methyltransferase (GAMT) plays a key role in the biosynthesis of Cr, by catalyzing the methylation of guanidinoacetate to form Cr. Phosphorylation of Cr to phosphocreatine (PCr) in the reaction catalyzed by CK: $\text{Cr} + \text{ATP} \leftrightarrow \text{PCr} + \text{ADP} + \text{H}^+$ buffers the levels of high energy phosphates and balances local ATP/ADP ratios (for more comprehensive reviews see (42-45)). In vertebrate tissues, four genes of CK are identified coding for altogether five different isoenzymes. M-CK and B-CK subunits can form the hetero- and homodimeric isoenzymes MM-CK, MB-CK and BB-CK which are present in the cytosol. MM-CK is expressed at high levels in muscle, representing between 85% and 95% of total CK activity depending on fiber type (42), and stage of development. In embryonic or young skeletal muscle, trace amounts of BB-CK also appear (46). MB-CK is a transitional isoform which is present in immature stages of skeletal muscle. In heart, this isoform is permanently expressed at rather low amounts. BB-CK is expressed at high concentrations in brain and various other tissues in adults. Expression of the other class of CKs, ubiquitous CK (UbCKmit) and sarcomeric CK (ScCKmit), is also cell type dependent. UbCKmit is mostly found in tissues where also BB-CK occurs. Recent studies indicate that in the brain B-CK is preferentially expressed in astrocytes and inhibitory neurons, while mitochondrial CK nearly only occurs in neurons (47). The expression of ScCKmit is confined to muscle. UbCKmit and ScCKmit isoforms occur as dimeric or octameric enzymes and reside between the inner and outer membranes of mitochondria (42).

Another \sim P transfer reaction, catalyzed by adenylate kinase (AK), serves to balance ADP/ATP ratios by catalyzing the reaction $2\text{ADP} \leftrightarrow \text{ATP} + \text{AMP}$. Several isoforms of AK exist, labeled AK1 to AK5, all expressed in specific tissues (48-51). In skeletal muscle, AK1 is the major isoform expressing 99% of AK activity while in heart besides AK1 as major isoform also minor isoforms like AK2 and AK3 are present (48). Finally, also glycolytic enzymes and enzyme systems in the mitochondrial network in the cell can be considered distinct \sim P transfer networks. For a schematic overview of cellular \sim P transfer systems see figure 1.2 in chapter 1.

2.3.2 Mice lacking one or more CK isoenzymes in skeletal muscle

Research on high energy phosphoryl transfer in skeletal muscle benefited enormously from the availability of mice with null mutations in the M-CK gene (M-CK^{-/-}) (35), ScCKmit gene (ScCKmit^{-/-}) (52), both CK genes (M-CK/ScCKmit^{-/-}) (53) and animals with a leaky mutation in the M-CK gene (and graded levels of MM-CK activity) (54). Surprisingly, ³¹P MRS studies in skeletal muscle of mice with reduced or absent M-CK expression revealed no significant difference in PCr-, inorganic phosphate (Pi)- or ATP levels, nor in tissue pH, compared to control mice (table 2.1) (35, 54). The method of measurement appeared to be of influence on the measured PCr levels: chemically determined PCr/ATP ratios were somewhat lower than PCr/ATP ratios determined by *in vivo* MRS (35). Furthermore, chemical determination also demonstrated that absolute PCr levels were significantly higher in M-CK^{-/-} mice than in control mice. Discrepancy between *in vivo* MR and *in vitro* chemical measurements is commonly observed and can be ascribed to hydrolysis effects that will occur during the isolation and freezing of tissues or generation of cell extracts (55, 56). In M-CK^{-/-} mice this hydrolysis of PCr during the freezing procedure was partially blocked, further illustrating that CK activity is a difficult to control parameter in invasive approaches where tissue fractionation or extraction is used. Results may also be clouded, if the measurement time frame does not match properly with the physiological event that is studied. Contractile experiments unequivocally demonstrated lack of burst activity in M-CK^{-/-} muscles, however, MRS analysis with stimulation with 1 or 5 Hz (35) or challenge by ischemia reperfusion (57) did not show differences in M-CK^{-/-} mice compared to wt mice in breakdown of PCr and accumulation of Pi within the time resolution of the experiments (~140 s per spectrum). It is of note here, that the residual CK activity in these animals was contributed by remaining mitochondrial CK activity. If the time interval of measurement was shortened, however, like in case of gated ³¹P MRS experiments, an initial decrease of PCr in CK mutants was found during the first few seconds of 5 Hz stimulation in wt (58). This decrease is also observed in M-CK^{-/-} mice, but of smaller magnitude which is in good agreement with the lack of burst activity in the latter mice (35). The impaired capacity of the CK system in M-CK^{-/-} mice was demonstrated already during resting conditions by inversion transfer (35) and saturation transfer (59) experiments which revealed that, in M-CK^{-/-} mice, no high energy phosphates transfer from PCr to ATP or *visa versa* was detectable. In fact, transfer from ATP to PCr appeared already blocked in mice expressing 34% or less MM-CK activity (54) indicating that either this amount of CK activity is necessary to maintain enzymatic kinetics in skeletal muscle or that the transfer rate was below the detection threshold of the MR experiment.

Table 2.1: Tissue metabolite concentrations and ratios of metabolites in mouse skeletal muscle

	in 't Zandt et al. (46)		Steeghs et al. (53)			van Deursen et al. (35)		
	wt	M-CK/ScCKmit double k.o.	wt	ScCKmit-/-	M-CK-/-	M-CK/ScCKmit double k.o.	wt	M-CK-/-
Ratios (by MR) ^{a, b}								
PCr / ATP	2.9 ± 0.2	2.4 ± 0.2*	3.0 ± 0.1 ^g	3.0 ± 0.2 ^g	3.4 ± 0.1 ^g	2.1 ± 0.1 ^g	2.8 ± 0.3 ^g	2.9 ± 0.2 ^g
PGua / ATP	-	-	-	-	-	-	-	-
Pi / ATP	-	-	0.36 ± 0.06 ^g	0.31 ± 0.05 ^g	0.32 ± 0.06 ^g	0.51 ± 0.04* ^g	0.37 ± 0.11 ^g	0.32 ± 0.06 ^g
pH	7.22 ± 0.03	7.24 ± 0.04	7.29 ± 0.07	7.17 ± 0.05	7.24 ± 0.02	7.21 ± 0.05	7.18 ± 0.08	7.19 ± 0.09
Concentrations (mM) ^c								
[tCr]	30.5 ± 2.0 ^d	31.4 ± 2.8 ^d	29.9 ± 1.0 ^{h, j}	29.9 ± 1.3 ^{h, j}	29.9 ± 1.3 ^{h, j}	29.9 ± 2.3 ^{h, j}	27.0 ± 1.8	30.2 ± 2.2
[PCr]	22.5 ± 1.9 ^d	17.6 ± 2.2 ^d	19.7 ± 0.7 ^h	20.6 ± 0.9 ^h	21.8 ± 1.0* ^h	16.4 ± 1.7* ^h	17.2 ± 1.5	23.0 ± 1.9*
[Pi]	-	-	-	-	-	-	-	-
[ATP]	7.8 ± 0.8 ^d	7.5 ± 1.1 ^d	7.8 ± 1.5 ^h	7.3 ± 0.6 ^h	6.1 ± 0.7 ^h	5.8 ± 0.8* ^h	8.4 ± 0.5	7.4 ± 0.6
Other values in vivo								
PCr / tCr	0.74 ± 0.04	0.56 ± 0.05*	-	-	-	-	-	-
[ADP]	0.037	(0.083) ^e	-	-	-	-	-	-

Table 2.1, continued

	Renema et al. (29)		Kan et al.(100)		Renema et al., chapter 4	
	wt	GAMT -/-	wt	GAMT -/-	wt	MAK-/-
Ratios (by MR) ^{a, b}						
PCr / ATP	2.7 ± 0.1	0.8 ± 0.3*	3.2 ± 0.3	n.d.	2.9 ± 0.4	3.0 ± 0.3
PGua / ATP	-	1.8 ± 0.4*	n.d.	3.0 ± 0.2		
Pi / ATP	0.40 ± 0.06	0.40 ± 0.08	0.40 ± 0.04	0.65 ± 0.04*	0.48 ± 0.11	0.50 ± 0.12
pH	7.24 ± 0.09	7.18 ± 0.06	7.20 ± 0.02	7.19 ± 0.04	7.24 ± 0.04	7.24 ± 0.04
Concentrations (mM) ^c						
[tCr]	28.4 ± 2.6 ^d	8.9 ± 3.8* ^d	-	-	-	-
[PCr]	-	-	-	-	-	-
[Pi]	-	-	-	-	-	-
[ATP]	-	-	5.0 ± 0.9 ^h	3.5 ± 0.9 ^h	-	-
Other values in vivo						
PCr / tCr	-	-	-	-	-	-
[ADP]	-	-	-	-	0.040 ± 0.003	0.040 ± 0.003

Notes on table 2.1:

Concentrations are expressed in mmol / (l tissue), except [ADP] which is expressed as mmol / (l intracellular water). Values that are expressed per l tissue can be converted to values per l intracellular water by using a factor of 0.73 for the intracellular water fraction (60, 61)

* significantly different from wt animals; § significantly different from value before supplementation

^a Ratios are determined from fully relaxed MR spectra. Studies which use not fully relaxed spectra to compare wt and transgenic animals are not included in this table for comparability reasons.

^b Unless stated otherwise, ratio's are with respect to β -ATP

^c concentrations are determined by chemical methods in $\mu\text{mol}/(\text{g wet weight})$ and calculated to mM by assuming a tissue density of 1.06, unless stated otherwise

^d concentrations derived from in vivo MR spectra

^e equilibrium condition necessary for calculation of ADP may not be valid in this knockout mouse

^f after 1 month of Cr supplementation

^g Calculated from other values

^h concentrations are determined by chemical methods in $\mu\text{mol}/(\text{g dry weight})$ and calculated to mM by assuming the fraction dw:ww to be 0.3:0.7 (which appears correct since tCr values are in accordance to in vivo measurements in the same mouse model) and a tissue density of 1.06 (62)

ⁱ Cr + PCr were in this study normalized over all muscles.

After an ischemic period of 20 minutes, a somewhat larger acidification was observed in M-CK-/- compared to wt muscle (57), which may be due to diminished proton buffering. A striking observation in studies of M-CK-/- mice was the disability to phosphorylate β -GPA in vivo. This finding suggested that cytosolic MM-CK is the only CK isoform which is able to phosphorylate this Cr analogue (63) in muscle. Similar findings from in vitro study had been reported (64, 65).

Just as with M-CK-/- mice, ScCKmit-/- mice showed no difference in PCr, Pi and pH levels compared to wild-type mice during resting conditions. Both inversion transfer (52) and saturation transfer (66) revealed no difference in the flux through the CK reaction. Small differences compared to wt animals were observed in ischemia experiments: recovery of PCr and Pi levels were faster than in wt animals and the hydrolysis of PCr was not completely compensated for by Pi and PME increases. This may be related to changes in the mitochondrial membrane microenvironment (57).

Inbreeding of M-CK-/- and ScCKmit-/- resulted in mice lacking both isoenzymes: M-CK/ScCKmit-/- double knockout mice, which have virtually no CK activity in skeletal

muscle (53). Total Cr (tCr) level (i.e. the addition of Cr and PCr levels) rose in parallel during aging in M-CK/ScCKmit^{-/-} and wt mice as was shown by ¹H MRS and biochemical methods (46), both yielding the same concentrations. This latter finding convincingly demonstrated that virtually all Cr is MR visible in ¹H MR spectra if measured under the proper conditions (46, 67). Remarkably, the postnatal increase of PCr levels in these knockout mice was the same as in wt animals, which is likely due to the residual BB-CK activity present in muscle of M-CK/ScCKmit^{-/-} mice the first weeks postnatal (46). In muscle of mature M-CK/ScCKmit^{-/-} mice, PCr /ATP ratio's decreased with age. When M-CK/ScCKmit^{-/-} mice were three weeks old they still were able to fully hydrolyze PCr (46). At older age this CK activity decreased to an undetectable low level and as a consequence, conversion through the CK reaction became gradually very low (46) until in adult mice the MR detectable flux through the CK reaction was fully absent (53, 66). The silencing of the CK reaction was reflected by a decrease of ATP levels and a profound decline of tissue pH during 20 minutes of ischemia (57).

By using ¹³C MRS and ¹³C-4 labeled creatine, simultaneous observation of Cr and PCr became possible. Injection with ¹³C labeled Cr in adult M-CK/ScCKmit^{-/-} mice showed uptake and phosphorylation of Cr demonstrating that very low CK activity is sufficient for this process (46). Using this ¹³C MR data it was possible to calculate PCr/total Cr (tCr) ratios. This PCr/tCr ratio, together with the absolute tCr value yielded from the ¹H MR spectra and the metabolite ratios determined from the ³¹P MR spectra, enabled determination of the tissue concentrations of ATP and PCr in vivo (table 2.1) (46).

In general, it appears that CK in normal mouse muscle is abundantly present. Reducing CK content does not affect the concentrations of ~P metabolites, and muscles of mice with less CK perform reasonably well during metabolic challenges if at least a small amount of CK remains present. However, disruption of local ~P equilibrium or sudden changes in ~P metabolites on a short time scale are very well possible in mice with less CK activity, but may be averaged out in the signals acquired during an MR experiment. Furthermore, more challenging conditions may uncover further defects.

2.3.3 Over-expression of phosphoryl transfer enzymes in skeletal muscle

Converse experiments, with overexpression of CK, were also performed. Ectopic over-expression of the B-CK isoform in muscle of transgenic mice resulted in the formation of the stable dimers MB-CK and BB-CK, and increased total muscle CK activity as assessed under maximal velocity conditions in tissue extract (up to 150% of that of controls) (68, 69). Using saturation transfer techniques, the in vivo CK activity appeared to be up regulated by a factor of two (69). Interestingly, this up-regulation of CK had no effect on PCr/ATP or

Pi/ATP ratios as measured by ^{31}P MRS, or the ATP or Cr concentration as measured by HPLC. This provided further evidence for the contention that the CK reaction is at equilibrium under resting conditions. The above studies were initially performed in animals that were heterozygous for the transgene, but subsequent analysis of homozygous transgenics showed similar effects (70). The only difference between wt and these homozygous transgenic mice was a decrease in the rise time of force of a 5 s tetanic stimulation, which showed that only during severe metabolic demand extra CK may increase performance (70). Besides an up-regulation in CK activity, AK activity appeared to be decreased by 9% (70), which may reflect the close harmony in which CK and AK work.

To test whether the proposed specific localization of MM-CK in muscle, close to the M line and the sarcoplasmic reticulum, is important, M-CK $^{-/-}$ mice (35) were mated with mice expressing B-CK in muscle (69) to generate mice in which M-CK has been 'replaced' by B-CK although now the cytosolic CK has no specific localization (71). In vivo, ^{31}P saturation transfer experiments showed a decrease of CK activity at rest to only 58% of that of wt animals (71). Together with the observation that the contractile phenotype of M-CK $^{-/-}$ mice returned to normal in the mice containing only B-CK, these results indicated that compartmentation of CK to the myofibril is not an (absolutely) essential condition for proper contractile function. Another implication of these results is that the CK shuttle, as originally proposed by Bessman and coworkers (72, 73), may be beneficial to skeletal muscle but it is not of vital importance.

Besides CK, also other phosphotransfer enzymes can be expressed intentionally in skeletal muscle. Using the method of adenoviral transduction, arginine kinase (ArgK), which works analogous to CK but with arginine instead of Cr, was expressed in hind leg muscle of mice (74). The phosphorylated arginine (PArg) was detected in vivo using ^{31}P MRS, at a resonance position of 0.49 ppm upfield of PCr up to 8 months after injection. PArg was observed as a singlet of equal linewidth compared to the signal of PCr, where (PArg + PCr)/ γ -ATP in the injected leg was equal to PCr/ γ -ATP in the control leg with PArg:PCr of approximately 1:1. Using an ischemia reperfusion protocol it was shown that PArg is used during energy demand, although the decrease in PArg was less and slower compared to PCr. This study is of particular interest as it demonstrated elegantly that an MR spectroscopy signal can be exploited as a non-invasive detectable marker of transgene expression and can be used to investigate the role of other $\sim\text{P}$ transfer systems in corroboration with the traditional ones.

2.3.4 Mice lacking one or more CK isoenzymes in brain

Mice lacking either the cytosolic B-CK (B-CK $^{-/-}$ mice) (75), the mitochondrial ubiquitous isoenzyme (UbCKmit $^{-/-}$ mice) (76) or both enzymes (B-CK/UbCKmit $^{-/-}$ mice)

(30) have been generated to study the role of the CK reaction in other tissues than muscle, notably in brain. B-CK^{-/-} mice had normal PCr, Pi, ATP and pH levels, but the flux of ~P transfer through the CK reaction measured by saturation transfer experiments was dramatically lowered, although still measurable (75). Because the brain is an oxidative organ, the mitochondrial content and fractional contribution of the mitochondrial CK activity (up to 30% of total CK activity, unpublished result Wieringa et al.) is much higher than in muscle. Unlike in muscle, the mitochondrial CK in brain may therefore be present at large enough quantities to mediate a visible exchange between the high energy phosphates of γ -ATP and PCr. Direct comparison of the relevance of the cytosolic and mitochondrial end points of the CK shuttle in brain and muscle is therefore difficult. Comparison is also difficult because the cellular infrastructure and anatomy of these tissues differ profoundly. Brain is composed of a very heterogeneous mixture of cell types, and not much is known about the cell-type distribution and co-expression of B-CK and UbCKmit isoforms in glial and neuronal cells over various brain regions. Recent evidence showed close metabolic collaboration between glial and neuronal systems for brain energetics (77, 78), in an arrangement that is very much different from the communication between individual myofibers in muscle. This makes it intrinsically difficult to know how the PCr shuttle – if any – is integrated into the energetic network of brain. Recently, creatine and the CK reaction have been proposed for a neuron-glial shuttle (47).

In our own studies, UbCKmit^{-/-} mice appeared to have rather normal basal PCr, Pi, ATP and pH levels (30), although Kekelidze and coworkers report a significant lower PCr/ATP ratio in homozygous UbCKmit^{-/-} mice (76). During seizure induction by PTZ injection, UbCKmit^{-/-} mice showed a more pronounced decrease in PCr and β -ATP signals while the PCr/ β -ATP remained always lower than in wt mice (76).

PCr in brains of double mutant B-CK/UbCKmit^{-/-} mice appeared to be fully depleted, while Pi, ATP and pH levels were virtually normal (30). In addition, a decrease in total creatine (tCr) was observed (30) in contrast to muscle, where it remained constant upon near depletion of CK. In this respect it may be of interest that the brain is able to synthesize (part of) its own Cr (79, 80) and that the blood-brain barrier may not be fully permeable for Cr (43). In addition to decreased tCr levels, increased levels of N-acetyl aspartate (NAA) and glutamate were observed in B-CK/UbCKmit^{-/-} mice (table 2.2) (30) which points to physiological or morphological adaptations (81) that could be the result of the lack of CK during brain development.

Table 2.2: Tissue concentrations of brain metabolites in several transgenic mice and their corresponding littermates measured in vivo

	Renema et al. (29)		Natt et al. (106) Schwarcz et al. (107)		Tkac et al. (41)	in 't Zandt et al. (30)			
	GAMT- /- (n=7)	wt (n=5)	NMRI (n=8)	BALB/c (n=7)	C57BL/6J (n=8)	wt ^{e,f} (n=6-8)	B-CK-/- ^f (n=5)	UbCKmit-/- ^f (n=6)	B-CK/UbCKmit-/- ^f (n=5)
taurine	5.7 ± 1.6	5.8 ± 1.3	-	-	-	7.7 – 12.9	-	-	-
total choline ^a	1.9 ± 0.4	1.9 ± 0.4	-	-	-	1.2 – 1.9	0.9 – 2.3	1.4 – 3.0	0.8 – 2.8
choline	-	-	2.2 ± 0.5	1.8 ± 0.2	2.6 ± 0.7	-	-	-	-
NAA	5.4 ± 0.8	5.3 ± 1.3	-	-	-	7.4 – 9.0	-	-	-
total NAA ^b	7.2 ± 0.9 ^d	6.4 ± 1.8 ^d	7.1 ± 1.7	6.5 ± 0.5	7.9 ± 1.5	8.2 – 10.5	6.3 – 7.3	6.3 – 7.0	8.1 – 8.8
total creatine ^e	1.4 ± 0.4	8.2 ± 1.2	7.8 ± 1.6	7.2 ± 0.6	9.2 ± 1.6	7.9 – 13.0	8.5 – 10.0	8.4 – 11.2	6.5 – 7.9
myo-inositol	2.7 ± 0.9	2.2 ± 1.7	6.0 ± 1.2	5.2 ± 1.4	6.6 ± 1.4	4.4 – 7.1	2.9 – 4.3	2.9 – 3.8	2.0 – 2.9
glutamate	4.4 ± 0.6	3.9 ± 0.3	-	-	-	9.2 – 12.4	6.1 – 6.6	7.4 – 8.3	7.0 – 8.8
glutamine	2.4 ± 0.7	1.8 ± 0.5	-	-	-	3.4 – 3.8	-	-	-
glucose	-	-	6.2 ± 2.3	5.4 ± 2.7	9.8 ± 3.9	3.2 – 4.2	-	-	-
lactate	-	-	1.9 ± 1.4	1.1 ± 1.0	2.8 ± 0.8	2.5 – 4.8	-	-	-

All concentrations are presented in mM (mean ± s.d. or range over different brain regions).

^a phosphocholine + glycerol- phosphocholine; ^b NAA + NAAG; ^c creatine + phosphocreatine; ^d not published result;

^e extrapolated from bar diagram; ^f average over different brain regions.

2.3.5 Mice lacking one or more CK isoenzymes in heart

Cardiac muscle cells possess a relatively high mitochondrial capacity compared to skeletal muscle cells, and therefore have a more oxidative character with smaller diffusion distances between energy producing and energy consuming sites. Although the total CK activity (activity units per mg tissue) is only between 10-30% of that in skeletal muscle, the relative contribution by mitochondrial ScCKmit activity is much higher. Moreover, a small fraction of cytosolic CK activity stems from MB-CK (82).

³¹P MRS has revealed that M-CK^{-/-} hearts displayed normal PCr/ATP ratios as well as normal absolute PCr and ATP levels, thus keeping phosphorylation potential high (83, 84). During different workloads (i.e. at different pacing frequencies), changes in PCr and other ³¹P MRS detectable metabolites appeared to be equal in M-CK^{-/-} and wt mice, however, differences in very fast events may have been missed in these studies as rather long acquisition times were used. Free ADP levels were also equal or somewhat higher in transgenic mice at a workload of 600 beats per minute (83, 84). In contrast to skeletal muscle without M-CK, saturation transfer clearly demonstrated phosphoryl transfer from PCr to ATP. Again, this is most easily explained by the presence of relatively large amounts of mitochondrial CK (59, 84). At higher workloads, however, CK flux could not keep up and increased less than the CK flux in wt mice (84). From these studies it was concluded that mitochondrial CK activity is sufficient to maintain most of the CK functions. The authors hypothesized that mitochondrial CK, although quantitatively present at lower concentrations than cytosolic CK, has a contribution to the total measured CK flux that is higher than that in skeletal muscle (84). This conclusion was further corroborated by ³¹P MR experiments performed on ScCKmit^{-/-} hearts which showed that mitochondrial CK was necessary to maintain normal high energy phosphate levels (85). Mice lacking only mitochondrial CK showed 20-30% lower PCr-levels (85, 86), which is in contrast to the situation in skeletal muscle, where PCr levels remained unaltered (52). Furthermore, ScCKmit^{-/-} hearts showed elevated ADP levels by a factor of two while Pi and ATP levels appeared normal (85). This latter finding is rather remarkable, and underlines the role of ScCKmit in maintaining (local) ADP concentrations. During increased workload the mice were still able to break down PCr, although hydrolysis of PCr was somewhat less in ScCKmit^{-/-} mice (24%) than in wt mice (37%). When recovering from this higher workload, ScCKmit^{-/-} mice resynthesized PCr. Therefore it was concluded that ~P transfer is maintained even if CK is lacking from the inter-membrane compartment of mitochondria (85). A similar conclusion had already been drawn from study of skeletal muscle without ScCKmit earlier (57).

The basal PCr level was also lower in intact hearts of M-CK/ScCKmit^{-/-} mice, as was demonstrated by ³¹P MRS. In sharp contrast to skeletal muscle, hearts of double knockout

M-CK/ScCKmit^{-/-} mice are able to hydrolyze PCr even better than in M-CK^{-/-} or wt hearts during increased cardiac work (83, 87). Since the [PCr] is a balance between Cr phosphorylation and PCr breakdown, this is attributed to impaired synthesis (normally primarily mediated by ScCKmit) during cardiac work. In addition, the presence of BB-CK in cardiac muscle may contribute to this conversion, although this remaining CK activity is only ~2 times higher than that in muscle of CK double knockouts (1.9 mM^s⁻¹ vs. 0.5-1.0 mM^s⁻¹). Localization of the enzyme and substrates in different muscle compartments may also play a role here (46, 83). [ADP], as calculated using the CK reaction equilibrium constant (88), was increased by 95% in hearts of M-CK/ScCKmit^{-/-} mice, which may also be the result of the disrupted functioning of mitochondrial CK in balancing ADP/ATP levels.

2.3.6 Transgenic expression of CK in liver

Liver is an ideal model to study creatine metabolism and CK function in a null background, since it normally does not express CK. Transgenic expression of CK in liver can therefore be used as a marker for successful expression (89). When CK is ectopically expressed from a transgene, differences with the normal situation in liver can provide direct information on the working mechanisms and importance of CK. Moreover, as the CK reaction in equilibrium enables to calculate free ADP levels, its presence opens up a possibility to study free ADP in liver.

One of the first genetic manipulations involving the CK system was by expressing the B subunit of CK in liver (34). Livers were measured using an ³¹P RF probe adjacent to a surgically exposed liver. The ability to phosphorylate Cr was only observed after Cr feeding and the concentration of PCr measured correlated with the quantity of Cr ingested (90). ADP levels were calculated to remain constant with different CK activities and Cr concentrations (68, 90). In studies of the perfused liver during an ischemia protocol, ³¹P MRS showed that the introduced CK system prevented a dramatic decrease in ATP and pH (91), thus rescuing the liver tissue from the adverse effects of the ischemic challenge. This role has striking parallels with the role in muscle, where also hydrolysis of ATP and a severe decline of pH was observed when both isoforms of CK were knocked out (57). Later, the pH of the perfusate was also shown to have a large influence on the amount and rate of PCr formed with several Cr concentrations in the buffer (92). Tissue pH levels decreased immediately upon application of ischemia in wt livers, while in CK containing livers tissue pH remained constant during the initial period of ischemia. Again this confirmed our own observations in the muscle studies (57, 93, 94). Pi was increasing more during ischemia in CK expressing livers than in wt livers. After reperfusion, the CK expressing livers appeared to have gained the ability return to pre-ischemia values of ~P within 80 minutes (91). Besides protecting the

liver from ischemia, the CK system could also protect the liver from anoxia, depending on the amount of PCr present (91).

A fructose load is a severe challenge of energy metabolism in the liver due to the consumption of ATP and Pi in the conversion to fructose-1-phosphate. When fructose was injected intraperitoneally, ^{31}P MRS revealed that PME levels rose two-three fold, and Pi and ATP levels decreased by 60% and 50%, respectively, similarly in wt type mice and in transgenic mice not fed Cr. Pi returned to resting levels in approximately 30 minutes, while ATP and PME were not back at these levels after one hour. Upon feeding of Cr, the fall in ATP levels was prevented and only a small decrease of ATP was observed for relatively low PCr values ($\text{PCr}/\text{ATP} = 1 - 1.5$) (95). Both Pi decrease and PME increase were diminished in the presence of PCr. ADP levels as calculated from MR spectra, however, changed independently of Cr feeding (95). The authors concluded that prevention of decline in ATP must be due to the new available source of high energy phosphates of PCr (95). Interestingly, these results also demonstrate that only small amounts of PCr are sufficient to play a significant role in the buffering of high energy phosphates, a finding that was confirmed in later studies on Cr deficient mice (see below).

In addition to mice expressing cytosolic CK, mice have been generated that express the mitochondrial UbCKmit isoenzyme in liver (96). These mice were able to synthesize PCr upon Cr feeding, and during ischemia of perfused livers PCr decreased, indicating that it is utilized (96). Furthermore, mice were generated which express both cytosolic and mitochondrial CK in liver, in this way providing a series of mice expressing a range of CK activities (B-CK, UbCKmit or both, ranging in activity from 28 – 1635 $\mu\text{mol}\cdot\text{g wet wt}^{-1}\cdot\text{min}^{-1}$) (97). Saturation transfer experiments on perfused livers showed a linear relation between the CK rate in vivo and the biochemically determined CK activity. Furthermore, it was demonstrated that the forward and backward flux through the CK reaction were similar because the $k_{\text{for}}/k_{\text{rev}}$ is equal to $[\text{ATP}]/[\text{PCr}]$, even in mouse liver expressing only mitochondrial CK. Expression of CK also had a large effect on ADP levels: only in the mice expressing very low levels of CK ADP levels were relatively high. When a certain threshold in CK activity was reached, apparent ADP levels dropped significantly. The authors attributed this effect to functional incorporation of the mitochondrial CK isoform in the livers of these transgenic mice. (97).

2.3.7 Mice lacking guanidinoacetate methyltransferase (GAMT)

Recently, mice lacking GAMT were generated (98) as a model for human Cr deficiency (99). As these animals were not able to synthesize their own Cr, they were completely deprived of Cr unless Cr was orally ingested.

Localized proton MRS of *GAMT*^{-/-} mice showed reduced levels of Cr in muscle and brain although residual Cr may still be present due to oral intake (29). In skeletal muscle, a broad signal of guanidinoacetate (Gua) was observed, however this signal was only present in cases when Cr was decreased to almost complete depletion. Gua was shown to be phosphorylated and metabolic active in skeletal muscle (29). In ischemia-reperfusion ³¹P MR experiments PGua decrease showed similar time evolution as the PCr signal. The recovery of the PGua signal, however, was significantly reduced and because recovery rate did not change upon Cr feeding, it was concluded that this may be a result from the lower affinity of CK to Gua (100). Accordingly, saturation transfer experiments on the γ -ATP showed negligible transfer of ATP to PGua indicating slower enzymatic kinetics (100).

Brain and heart, just as skeletal muscle, showed a phosphorylated Gua (PGua) signal (29, 98). The PGua signal from brain had much lower intensities than in skeletal muscle and, since in skeletal muscle the PGua signal showed striking fluctuations, oral ingestion of Cr appeared to be an important factor (29, 100). In mice with no detectable PCr, after a few days of Cr feeding the PCr signal in muscle already exceeded the PGua signal (100). In contrast, large fluctuations of the PGua signal were not observed in brain, suggesting limited permeability of the blood brain barrier, which was already suspected from the slow recovery of the Cr signal after long term feeding of high amounts of Cr to *GAMT* deficient patients (43, 101). Feeding of Cr to *GAMT*^{-/-} mice could in the future elucidate the extent of permeability of the blood brain barrier for Cr.

Another interesting phenotype of *GAMT*^{-/-} mice was an increased Pi signal which was similar as observed in *M-CK/ScCK*^{mit-/-} mice (table 2.1) (100). This increased Pi was only detected when PCr was fully absent for a longer time period. Upon (intentional) Cr feeding the Pi signal normalized (100). Despite the lower affinity of CK for PGua, it functions surprisingly well in vivo to match moderate energy demands. Only small amounts of PCr were necessary to prevent elevated levels of Pi, and increased levels of Pi itself may also be a adaptation to stimulate glycolysis, yet another pathway for relatively fast energy production. Taken combined, these findings confirm a model with cooperativity in function between various \sim P pathways.

2.3.8 Knock-outs of the AK system

Parallel to these studies also the role of yet another \sim P pathway, the AK-mediated ADP \leftrightarrow ATP exchange reaction, was assessed in mice lacking the cytosolic isoform AK1 (*AK*^{-/-} mice). In these mice the cytosolic capacity to maintain local ADP/ATP ratios (94) was changed. Ischemia reperfusion experiments showed no difference in PCr breakdown and restoration, which was not surprising because CK activity was not changed. PME, however,

accumulated more during the ischemic period. This was explained by an increased glycolytic flux accompanied by higher glucose 6-phosphate levels, as measured by ^{18}O labeling studies in AK $^{-/-}$ mice (94). The lower tissue pH measured at the end of the ischemic period may also be a result thereof (94).

Double knock-out mice lacking both AK1 and cytosolic M-CK enzymes (MAK $^{-/-}$ mice) had a severely impaired cytosolic phosphoryl transfer capacity (102). This was evident from the much delayed recovery of both PCr and Pi after an ischemic challenge compared to wt animals (93). This delayed recovery of high energy phosphoryls appeared, at first sight, similar to the response of GAMT $^{-/-}$ mice to an ischemic challenge (100), but probably has a different origin. In MAK $^{-/-}$ mice, it could be attributed to re-establishment of mitochondrial $\sim\text{P}$ metabolism which may be accompanied by local unfavourable ADP concentrations, while in GAMT $^{-/-}$ mice the reduced enzyme kinetics were the most likely explanation for the reduced recovery rate.

2.4 Concluding remarks

The use of MRS methodology in combination with new procedures for the generation of transgenic mice have opened up entirely new opportunities to study metabolism under normal (i.e. healthy) and pathological conditions *in vivo*. Especially when the genetic modification has an effect on enzymes that interact directly with MR visible metabolites, or on the presence of MR visible metabolites, the tools that different MRS techniques offer to study these mice *in vivo* are very potent. Mario Capecchi's statement 'if you give me a gene, I could knock it out and tell you what its function is' (20), however, appeared to be overly optimistic, since in a complex biological system the functions of a protein may not be straightforward (103) due to partial redundancy or overlap with functions of other proteins.

Knockout mice show a remarkable plasticity in coping with the effects of gene deficiency. For CK, which was long considered essential in tissues with high energy demand, it has now been demonstrated that it is not absolutely indispensable under laboratory conditions since CK knockout mice are viable. As was shown in several studies altering CK, AK or any related pathway, metabolic intervention in energy metabolism will always result in a global response, preventing a direct or expected alteration in metabolism. Therefore, changes may be subtle and remain unnoticed. When the metabolic system is sufficiently stressed, however, alterations may become apparent.

When making a phenotypic comparison between a knockout and control mouse, care should be taken in selecting the proper strain for reference. Differences may be large between strains with different genetic backgrounds, obscuring small changes resulting from the genetic alteration of interest. Furthermore, cellular heterogeneity in tissues may be an issue of

concern, especially when the tissue composition changes due to the mutation. Moreover, unexpected secondary adaptations may occur, which may have a larger influence on the metabolism than the direct (primary) effect of knockout itself. This was shown for example in muscle CK double knock-out mice, which showed a shift in fibertype and up-regulation of glycolytic and oxidative potential (104).

Another important consideration is that the phenotypic consequences may also not be 100% penetrant, as was shown in imaging of ventricles of HD and B-CK mice (30, 105). Although detectable in MRI, when this occurs in MRS studies in which only average values are presented, changes may remain unnoticed. Despite these challenges, in vivo MRS has proven to be a valuable and powerful tool in the study of mice with genetic alterations in the high energy phosphoryl transfer systems.

REFERENCES

1. Darling, S. Mice as models of human developmental disorders: natural and artificial mutants. *Curr Opin Genet Dev* 1996;6:289-94.
2. Bulfield, G., Siller, W.G., Wight, P.A. and Moore, K.J. X chromosome-linked muscular dystrophy (mdx) in the mouse. *Proc Natl Acad Sci U S A* 1984;81:1189-92.
3. Kataoka, S., Satoh, J., Fujiya, H., Toyota, T., Suzuki, R., Itoh, K. and Kumagai, K. Immunologic aspects of the nonobese diabetic (NOD) mouse. Abnormalities of cellular immunity. *Diabetes* 1983;32:247-53.
4. Makino, S., Kunimoto, K., Muraoka, Y., Mizushima, Y., Katagiri, K. and Tochino, Y. Breeding of a non-obese, diabetic strain of mice. *Jikken Dobutsu* 1980;29:1-13.
5. Sarvetnick, N., Liggitt, D., Pitts, S.L., Hansen, S.E. and Stewart, T.A. Insulin-dependent diabetes mellitus induced in transgenic mice by ectopic expression of class II MHC and interferon-gamma. *Cell* 1988;52:773-82.
6. Chen, H., Charlat, O., Tartaglia, L.A., Woolf, E.A., Weng, X., Ellis, S.J., Lakey, N.D., Culpepper, J., Moore, K.J., Breitbart, R.E., Duyk, G.M., Tepper, R.I. and Morgenstern, J.P. Evidence that the diabetes gene encodes the leptin receptor: identification of a mutation in the leptin receptor gene in db/db mice. *Cell* 1996;84:491-5.
7. Harvey, M., Vogel, H., Morris, D., Bradley, A., Bernstein, A. and Donehower, L.A. A mutant p53 transgene accelerates tumour development in heterozygous but not nullizygous p53-deficient mice. *Nat Genet* 1995;9:305-11.
8. <http://web.ncifcrf.gov/researchresources/mmhcc/>
9. Bock, N.A., Konyer, N.B. and Henkelman, R.M. Multiple-mouse MRI. *Magn Reson Med* 2003;49:158-67.
10. <http://bio.lsd.ornl.gov/mgd/phenotype/>
11. Searle, A.G., Edwards, J.H. and Hall, J.G. Mouse homologues of human hereditary disease. *J Med Genet* 1994;31:1-19.
12. Meisler, M.H. Insertional mutation of 'classical' and novel genes in transgenic mice. *Trends Genet* 1992;8:341-4.
13. Shuldiner, A.R. Transgenic animals. *N Engl J Med* 1996;334:653-5.
14. Jaenisch, R. Transgenic animals. *Science* 1988;240:1468-74.
15. Metzger, D. and Feil, R. Engineering the mouse genome by site-specific recombination. *Curr Opin Biotechnol* 1999;10:470-6.
16. Tsien, J.Z., Chen, D.F., Gerber, D., Tom, C., Mercer, E.H., Anderson, D.J., Mayford, M., Kandel, E.R. and Tonegawa, S. Subregion- and cell type-restricted gene knockout in mouse brain. *Cell* 1996;87:1317-26.
17. Lois, C., Hong, E.J., Pease, S., Brown, E.J. and Baltimore, D. Germline transmission and tissue-specific expression of transgenes delivered by lentiviral vectors. *Science* 2002;295:868-72.
18. Pascoe, W.S., Kemler, R. and Wood, S.A. Genes and functions: trapping and targeting in embryonic stem cells. *Biochim Biophys Acta* 1992;1114:209-21.
19. Misra, R.P. and Duncan, S.A. Gene targeting in the mouse: advances in introduction of transgenes into the genome by homologous recombination. *Endocrine* 2002;19:229-38.
20. Travis, J. Scoring a technical knockout in mice. *Science* 1992;256:1392-4.
21. Charreau, B., Tesson, L., Soulillou, J.P., Pourcel, C. and Anegon, I. Transgenesis in rats: technical aspects and models. *Transgenic Res* 1996;5:223-34.
22. Capecchi, M.R. How close are we to implementing gene targeting in animals other than the mouse? *Proc Natl Acad Sci U S A* 2000;97:956-7.
23. Budinger, T.F., Benaron, D.A. and Koretsky, A.P. Imaging transgenic animals. *Annu Rev Biomed Eng* 1999;1:611-48.
24. Ntziachristos, V., Bremer, C. and Weissleder, R. Fluorescence imaging with near-infrared light: new technological advances that enable in vivo molecular imaging. *Eur Radiol* 2003;13:195-208.

25. MacLaren, D.C., Toyokuni, T., Cherry, S.R., Barrio, J.R., Phelps, M.E., Herschman, H.R. and Gambhir, S.S. PET imaging of transgene expression. *Biol Psychiatry* 2000;48:337-48.
26. Brindle, K.M. NMR methods for measuring enzyme kinetics in vivo. *Progress in NMR spectroscopy* 1988;20:257-293.
27. Moon, R.B. and Richards, J.H. Determination of intracellular pH by ³¹P magnetic resonance. *J Biol Chem* 1973;248:7276-8.
28. Pfeuffer, J., Tkac, I., Provencher, S.W. and Gruetter, R. Toward an in vivo neurochemical profile: quantification of 18 metabolites in short-echo-time (1)H NMR spectra of the rat brain. *J Magn Reson* 1999;141:104-20.
29. Renema, W.K., Schmidt, A., Van Asten, J.J., Oerlemans, F., Ullrich, K., Wieringa, B., Isbrandt, D. and Heerschap, A. MR spectroscopy of muscle and brain in guanidinoacetate methyltransferase (GAMT)-deficient mice: Validation of an animal model to study creatine deficiency. *Magn Reson Med* 2003;50:936-43.
30. in 't Zandt, H.J., Renema, W.K., Streijger, F., Jost, C., Klomp, D.W., Oerlemans, F., Van der Zee, C.E., Wieringa, B. and Heerschap, A. Cerebral creatine kinase deficiency influences metabolite levels and morphology in the mouse brain: a quantitative in vivo 1H and ³¹P magnetic resonance study. *J Neurochem* 2004;90:1321-30.
31. Gruetter, R., Seaquist, E.R. and Ugurbil, K. A mathematical model of compartmentalized neurotransmitter metabolism in the human brain. *Am J Physiol Endocrinol Metab* 2001;281:E100-12.
32. Stevens, A.N., Iles, R.A., Morris, P.G. and Griffiths, J.R. Detection of glycogen in a glycogen storage disease by ¹³C nuclear magnetic resonance. *FEBS Lett* 1982;150:489-93.
33. Heerschap, A., Bergman, A.H., van Vaals, J.J., Wirtz, P., Loermans, H.M. and Veerkamp, J.H. Alterations in relative phosphocreatine concentrations in preclinical mouse muscular dystrophy revealed by in vivo NMR. *NMR Biomed* 1988;1:27-31.
34. Koretsky, A.P., Brosnan, M.J., Chen, L. and Van Dyke, T. NMR detection of creatine kinase expressed in liver of transgenic mice: Determination of free ADP levels. *Proc Natl Acad Sci USA* 1990;87:3112-3116.
35. van Deursen, J., Heerschap, A., Oerlemans, F., Ruitenbeek, W., Jap, P., ter Laak, H. and Wieringa, B. Skeletal muscles of mice deficient in muscle creatine kinase lack burst activity. *Cell* 1993;74:621-31.
36. Koretsky, A.P. Insights into cellular energy metabolism from transgenic mice. *Physiol Rev* 1995;75:667-88.
37. Zeleznikar, R.J., Dzeja, P.P. and Goldberg, N.D. Adenylate kinase-catalyzed phosphoryl transfer couples ATP utilization with its generation by glycolysis in intact muscle. *J Biol Chem* 1995;270:7311-9.
38. Dzeja, P.P. and Terzic, A. Phosphotransfer networks and cellular energetics. *J Exp Biol* 2003;206:2039-47.
39. Heerschap, A., Sommers, M.G., in 't Zandt, H.J.A., Renema, W.K.J., Veltien, A.A. and Klomp, D.W.J. NMR in laboratory animals. in: *Methods in Enzymology* Eds.: 2003.
40. Gruetter, R., Weisdorf, S.A., Rajanayagan, V., Terpstra, M., Merkle, H., Truwit, C.L., Garwood, M., Nyberg, S.L. and Ugurbil, K. Resolution improvements in in vivo 1H NMR spectra with increased magnetic field strength. *J Magn Reson* 1998;135:260-4.
41. Tkac, I., Henry, P.G., Andersen, P., Keene, C.D., Low, W.C. and Gruetter, R. Highly resolved in vivo 1H NMR spectroscopy of the mouse brain at 9.4 T. *Magn Reson Med* 2004;52:478-84.
42. Wallimann, T., Wyss, M., Brdiczka, D., Nicolay, K. and Eppenberger, H.M. Intracellular compartmentation, structure and function of creatine kinase isoenzymes in tissues with high and fluctuating energy demands: the phosphocreatine circuit for cellular energy homeostasis. *Biochem J* 1992;281:21-40.
43. Wyss, M. and Kaddurah-Daouk, R. Creatine and creatinine metabolism. *Physiol Rev* 2000;80:1107-213.
44. Wallimann, T. Bioenergetics. Dissecting the role of creatine kinase. *Curr Biol* 1994;4:42-6.
45. Wyss, M., Smeitink, J., Wevers, R.A. and Wallimann, T. Mitochondrial creatine kinase: a key enzyme of aerobic energy metabolism. *Biochim Biophys Acta* 1992;1102:119-66.
46. in 't Zandt, H.J., Groof, A.J., Renema, W.K., Oerlemans, F.T., Klomp, D.W., Wieringa, B. and Heerschap, A. Presence of (phospho)creatine in developing and adult skeletal muscle of mice without mitochondrial and cytosolic muscle creatine kinase isoforms. *J Physiol* 2003;548:847-58.

47. Tachikawa, M., Fukaya, M., Terasaki, T., Ohtsuki, S. and Watanabe, M. Distinct cellular expressions of creatine synthetic enzyme GAMT and creatine kinases uCK-Mi and CK-B suggest a novel neuron-glia relationship for brain energy homeostasis. *Eur J Neurosci* 2004;20:144-60.
48. Tanabe, T., Yamada, M., Noma, T., Kajii, T. and Nakazawa, A. Tissue-specific and developmentally regulated expression of the genes encoding adenylate kinase isozymes. *J Biochem (Tokyo)* 1993;113:200-7.
49. Collavin, L., Lazarevic, D., Utrera, R., Marzinotto, S., Monte, M. and Schneider, C. wt p53 dependent expression of a membrane-associated isoform of adenylate kinase. *Oncogene* 1999;18:5879-88.
50. Van Rompay, A.R., Johansson, M. and Karlsson, A. Identification of a novel human adenylate kinase. cDNA cloning, expression analysis, chromosome localization and characterization of the recombinant protein. *Eur J Biochem* 1999;261:509-17.
51. Yoneda, T., Sato, M., Maeda, M. and Takagi, H. Identification of a novel adenylate kinase system in the brain: cloning of the fourth adenylate kinase. *Brain Res Mol Brain Res* 1998;62:187-95.
52. Steeghs, K., Heerschap, A., de Haan, A., Ruitenbeek, W., Oerlemans, F., van Deursen, J., Perryman, B., Pette, D., Brueckwilder, M., Koudijs, J., Jap, P. and Wieringa, B. Use of gene targeting for compromising energy homeostasis in neuro-muscular tissues: The role of sarcomeric mitochondrial creatine kinase. *J Neurosci Methods* 1997;71:29-41.
53. Steeghs, K., Benders, A., Oerlemans, F., de Haan, A., Heerschap, A., Ruitenbeek, W., Jost, C., van Deursen, J., Perryman, B., Pette, D., Bruckwilder, M., Koudijs, J., Jap, P., Veerkamp, J. and Wieringa, B. Altered Ca²⁺ responses in muscles with combined mitochondrial and cytosolic creatine kinase deficiencies. *Cell* 1997;89:93-103.
54. van Deursen, J., Ruitenbeek, W., Heerschap, A., Jap, P., ter Laak, H. and Wieringa, B. Creatine kinase (CK) in skeletal muscle energy metabolism: a study of mouse mutants with graded reduction in muscle CK expression. *Proc Natl Acad Sci U S A* 1994;91:9091-5.
55. Ackerman, J.J., Grove, T.H., Wong, G.G., Gadian, D.G. and Radda, G.K. Mapping of metabolites in whole animals by ³¹P NMR using surface coils. *Nature* 1980;283:167-70.
56. Meyer, R.A., Brown, T.R. and Kushmerick, M.J. Phosphorus nuclear magnetic resonance of fast- and slow-twitch muscle. *Am J Physiol* 1985;248:C279-C287.
57. in 't Zandt, H.J., Oerlemans, F., Wieringa, B. and Heerschap, A. Effects of ischemia on skeletal muscle energy metabolism in mice lacking creatine kinase monitored by in vivo ³¹P nuclear magnetic resonance spectroscopy. *NMR Biomed* 1999;12:327-34.
58. Roman, B.B., Meyer, R.A. and Wiseman, R.W. Phosphocreatine kinetics at the onset of contractions in skeletal muscle of MM creatine kinase knockout mice. *Am J Physiol Cell Physiol* 2002;283:C1776-83.
59. van Dorsten, F.A., Reese, T., Gellerich, J.F., van Echteld, C.J., Nederhoff, M.G., Muller, H.J., van Vliet, G. and Nicolay, K. Fluxes through cytosolic and mitochondrial creatine kinase, measured by P-31 NMR. *Mol Cell Biochem* 1997;174:33-42.
60. Sjogaard, G. and Saltin, B. Extra- and intracellular water spaces in muscles of man at rest and with dynamic exercise. *Am J Physiol* 1982;243:R271-80.
61. Forsberg, A.M., Nilsson, E., Werneman, J., Bergstrom, J. and Hultman, E. Muscle composition in relation to age and sex. *Clin Sci (Lond)* 1991;81:249-56.
62. Mendez, J. and Keys, A. Density and composition of mammalian muscle. *Metabolism* 1960;9:184-188.
63. van Deursen, J., Jap, P., Heerschap, A., ter Laak, H., Ruitenbeek, W. and Wieringa, B. Effects of the creatine analogue beta-guanidinopropionic acid on skeletal muscles of mice deficient in muscle creatine kinase. *Biochim Biophys Acta* 1994;1185:327-35.
64. Boehm, E.A., Radda, G.K., Tomlin, H. and Clark, J.F. The utilisation of creatine and its analogues by cytosolic and mitochondrial creatine kinase. *Biochim Biophys Acta* 1996;1274:119-28.
65. Clark, J.F., Khuchua, Z., Kuznetsov, A.V., Vassil'eva, E., Boehm, E., Radda, G.K. and Saks, V. Actions of the creatine analogue beta-guanidinopropionic acid on rat heart mitochondria. *Biochem J* 1994;300 (Pt 1):211-6.

66. Nicolay, K., van Dorsten, F.A., Reese, T., Kruiskamp, M.J., Gellerich, J.F. and van Echteld, C.J. In situ measurements of creatine kinase flux by NMR. The lessons from bioengineered mice [In Process Citation]. *Mol Cell Biochem* 1998;184:195-208.
67. in 't Zandt, H.J.A., Klomp, D.W.J., Oerlemans, F., Wieringa, B., Hilbers, C.W. and Heerschap, A. Proton MR Spectroscopy of wild-type and creatine kinase deficient mouse skeletal muscle: dipole-dipole coupling effects and post-mortem changes. *MRM* 2000;43:517-524.
68. Brosnan, M.J., Halow, J.M. and Koretsky, A.P. Manipulating creatine kinase activity in transgenic mice to study control of energy metabolism. *Biochem Soc Trans* 1991;19:1010-4.
69. Brosnan, M.J., Raman, S.P., Chen, L. and Koretsky, A.P. Altering creatine kinase isoenzymes in transgenic mouse muscle by overexpression of the B subunit. *Am J Physiol* 1993;264:C151-60.
70. Roman, B.B., Foley, J.M., Meyer, R.A. and Koretsky, A.P. Contractile and metabolic effects of increased creatine kinase activity in mouse skeletal muscle. *Am J Physiol Cell Physiol* 1996;270:C1236-45.
71. Roman, B.B., Wieringa, B. and Koretsky, A.P. Functional equivalence of creatine kinase isoforms in mouse skeletal muscle. *J Biol Chem* 1997;272:17790-4.
72. Bessman, S.P. and Fonyo, A. The possible role of the mitochondrial bound creatine kinase in regulation of mitochondrial respiration. *Biochem Biophys Res Commun* 1966;22:597-602.
73. Bessman, S.P. Hexokinase acceptor theory of insulin action. New evidence. *Isr J Med Sci* 1972;8:344-52.
74. Walter, G., Barton, E.R. and Sweeney, H.L. Noninvasive measurement of gene expression in skeletal muscle. *Proc Natl Acad Sci U S A* 2000;97:5151-5.
75. Jost, C.R., Van Der Zee, C.E., In 't Zandt, H.J., Oerlemans, F., Verheij, M., Streijger, F., Fransen, J., Heerschap, A., Cools, A.R. and Wieringa, B. Creatine kinase B-driven energy transfer in the brain is important for habituation and spatial learning behaviour, mossy fibre field size and determination of seizure susceptibility. *Eur J Neurosci* 2002;15:1692-706.
76. Kekelidze, T., Khait, I., Togliatti, A., Benzecry, J.M., Wieringa, B. and Holtzman, D. Altered brain phosphocreatine and ATP regulation when mitochondrial creatine kinase is absent. *J Neurosci Res* 2001;66:866-72.
77. Kasischke, K.A., Vishwasrao, H.D., Fisher, P.J., Zipfel, W.R. and Webb, W.W. Neural activity triggers neuronal oxidative metabolism followed by astrocytic glycolysis. *Science* 2004;305:99-103.
78. Pellerin, L. and Magistretti, P.J. Neuroscience. Let there be (NADH) light. *Science* 2004;305:50-2.
79. Wyss, M. and Wallimann, T. Creatine metabolism and the consequences of creatine depletion in muscle. *Mol Cell Biochem* 1994;133-134:51-66.
80. Braissant, O., Henry, H., Loup, M., Eilers, B. and Bachmann, C. Endogenous synthesis and transport of creatine in the rat brain: an in situ hybridization study. *Brain Res Mol Brain Res* 2001;86:193-201.
81. Streijger, F., Jost, C.R., Oerlemans, F., Ellenbroek, B.A., Cools, A.R., Wieringa, B. and Van der Zee, C.E. Mice lacking the UbCKmit isoform of creatine kinase reveal slower spatial learning acquisition, diminished exploration and habituation, and reduced acoustic startle reflex responses. *Mol Cell Biochem* 2004;256-257:305-18.
82. Veksler, V.I., Kuznetsov, A.V., Anflous, K., Mateo, P., van Deursen, J., Wieringa, B. and Ventura-Clapier, R. Muscle creatine kinase-deficient mice. II. Cardiac and skeletal muscles exhibit tissue-specific adaptation of the mitochondrial function. *J Biol Chem* 1995;270:19921-9.
83. Saupe, K.W., Spindler, M., Tian, R. and Ingwall, J.S. Impaired cardiac energetics in mice lacking muscle-specific isoenzymes of creatine kinase. *Circ Res* 1998;82:898-907.
84. Van Dorsten, F.A., Nederhoff, M.G., Nicolay, K. and Van Echteld, C.J. ³¹P NMR studies of creatine kinase flux in M-creatine kinase-deficient mouse heart. *Am J Physiol* 1998;275:H1191-9.
85. Spindler, M., Niebler, R., Remkes, H., Horn, M., Lanz, T. and Neubauer, S. Mitochondrial creatine kinase is critically necessary for normal myocardial high-energy phosphate metabolism. *Am J Physiol Heart Circ Physiol* 2002;283:H680-7.
86. Spindler, M., Engelhardt, S., Niebler, R., Wagner, H., Hein, L., Lohse, M.J. and Neubauer, S. Alterations in the myocardial creatine kinase system precede the development of contractile dysfunction in beta(1)-adrenergic receptor transgenic mice. *J Mol Cell Cardiol* 2003;35:389-97.

87. Ingwall, J.S. Creatine kinase knockout mice--what is the phenotype: heart. *Magma* 1998;6:120-1.
88. Veech, R.L., Lawson, J.W., Cornell, N.W. and Krebs, H.A. Cytosolic phosphorylation potential. *J Biol Chem* 1979;254:6538-47.
89. Auricchio, A., Zhou, R., Wilson, J.M. and Glickson, J.D. In vivo detection of gene expression in liver by ³¹P nuclear magnetic resonance spectroscopy employing creatine kinase as a marker gene. *Proc Natl Acad Sci U S A* 2001;98:5205-10.
90. Brosnan, M.J., Chen, L., Van Dyke, T.A. and Koretsky, A.P. Free ADP levels in transgenic mouse liver expressing creatine kinase. Effects of enzyme activity, phosphagen type, and substrate concentration. *J Biol Chem* 1990;265:20849-55.
91. Miller, K., Halow, J. and Koretsky, A.P. Phosphocreatine protects transgenic mouse liver expressing creatine kinase from hypoxia and ischemia. *Am J Physiol* 1993;265:C1544-C1551.
92. Masson, S. and Quistorff, B. Kinetics of creatine uptake in the perfused mouse liver: a ³¹P-n.m.r. study of transgenic mice expressing creatine kinase (CKBB) in the liver. *Biochem J* 1994;303 (Pt 2):531-8.
93. Renema, W.K.J., Janssen, E.E.W., Jansen, J.F.A., Oerlemans, F., Wieringa, B. and Heerschap, A. ³¹P MRS reveals a compromised phosphoryl transfer system in mice lacking both cytosolic CK and AK. *Proc Intl Soc mag Reson Med* 10 2002;1869.
94. Janssen, E., Dzeja, P.P., Oerlemans, F., Simonetti, A.W., Heerschap, A., de Haan, A., Rush, P.S., Terjung, R.R., Wieringa, B. and Terzic, A. Adenylate kinase 1 gene deletion disrupts muscle energetic economy despite metabolic rearrangement. *Embo J* 2000;19:6371-81.
95. Brosnan, M.J., Chen, L.H., Wheeler, C.E., Van Dyke, T.A. and Koretsky, A.P. Phosphocreatine protects ATP from a fructose load in transgenic mouse liver expressing creatine kinase. *Am J Physiol* 1991;260:C1191-200.
96. Miller, K., Sharer, K., Suhan, J. and Koretsky, A.P. Expression of functional mitochondrial creatine kinase in liver of transgenic mice. *Am J Physiol* 1997;272:C1193-C1202.
97. Askenasy, N. and Koretsky, A.P. Transgenic livers expressing mitochondrial and cytosolic CK: mitochondrial CK modulates free ADP levels. *Am J Physiol Cell Physiol* 2002;282:C338-46.
98. Schmidt, A., Marescau, B., Boehm, E.A., Renema, W.K., Peco, R., Das, A., Steinfeld, R., Chan, S., Wallis, J., Davidoff, M., Ullrich, K., Waldschutz, R., Heerschap, A., De Deyn, P.P., Neubauer, S. and Isbrandt, D. Severely altered guanidino compound levels, disturbed body weight homeostasis and impaired fertility in a mouse model of guanidinoacetate N-methyltransferase (GAMT) deficiency. *Hum Mol Genet* 2004;13:905-21.
99. Stöckler, S., Holzbach, U., Hanefeld, F., Marquardt, I., Helms, G., Requate, M., Hanicke, W. and Frahm, J. Creatine deficiency in the brain: a new, treatable inborn error of metabolism. *Pediatr Res* 1994;36:409-13.
100. Kan, H.E., Renema, W.K., Isbrandt, D. and Heerschap, A. Phosphorylated guanidinoacetate partly compensates for the lack of phosphocreatine in skeletal muscle of mice lacking guanidinoacetate methyltransferase. *J Physiol* 2004;560:219-29.
101. von Figura, K., Hanefeld, F., Isbrandt, D. and Stöckler-Ipsiroglu, S. Guanidinoacetate methyltransferase deficiency. in: *The Metabolic and Molecular Bases of Inherited Disease* Eds.: C. R. Scriver, A. L. Beaudet, W. S. Sly, D. Valle and V. Childs 2001. chapter 84
102. Janssen, E., Terzic, A., Wieringa, B. and Dzeja, P.P. Impaired intracellular energetic communication in muscles from creatine kinase and adenylate kinase (M-CK/AK1) double knock-out mice. *J Biol Chem* 2003;278:30441-9.
103. Bailey, J.E. Lessons from metabolic engineering for functional genomics and drug discovery. *Nat Biotechnol* 1999;17:616-8.
104. Steeghs, K., Oerlemans, F., de Haan, A., Heerschap, A., Verdoodt, L., de Bie, M., Ruitenbeek, W., Benders, A., Jost, C., van Deursen, J., Tullson, P., Terjung, R., Jap, P., Jacob, W., Pette, D. and Wieringa, B. Cytoarchitectural and metabolic adaptations in muscles with mitochondrial and cytosolic creatine kinase deficiencies. *Mol Cell Biochem* 1998;184:183-94.
105. Auerbach, W., Hurlbert, M.S., Hilditch-Maguire, P., Wadghiri, Y.Z., Wheeler, V.C., Cohen, S.I., Joyner, A.L., MacDonald, M.E. and Turnbull, D.H. The HD mutation causes progressive lethal neurological disease in mice expressing reduced levels of huntingtin. *Hum Mol Genet* 2001;10:2515-23.

106. Natt et al Quantitative proton MRS detects different cerebral metabolic responses of mouse strains to global ischemia. Proc Intl Soc Mag Reson Med 11 2003;1960.
107. Schwarcz, A., Natt, O., Watanabe, T., Boretius, S., Frahm, J. and Michaelis, T. Localized proton MRS of cerebral metabolite profiles in different mouse strains. Magn Reson Med 2003;49:822-7.

3

PRESENCE OF (PHOSPHO)CREATINE IN DEVELOPING AND ADULT SKELETAL MUSCLE OF MICE WITHOUT MITOCHONDRIAL AND CYTOSOLIC MUSCLE CREATINE KINASE ISOFORMS

René in 't Zandt
Ad de Groof
KlaasJan Renema
Frank Oerlemans
Dennis Klomp
Bé Wieringa
Arend Heerschap

This chapter is in slightly modified form published as:

H.J. in 't Zandt, A.J. Groof, W.K. Renema, F.T. Oerlemans, D.W. Klomp, B. Wieringa, and A. Heerschap, Presence of (phospho)creatine in developing and adult skeletal muscle of mice without mitochondrial and cytosolic muscle creatine kinase isoforms. *J Physiol* 2003; 548: 847-58.

ABSTRACT

We assessed the relationship between phosphocreatine (PCr) and creatine (Cr) content and creatine kinase (CK) activity in skeletal muscle of mice. Therefore, PCr and total Cr (tCr) concentration as well as CK activity in hind-limb muscles of mice with or without the cytosolic and mitochondrial isoforms of muscle creatine kinase (wild-type and M-CK/ScCKmit^{-/-} mice) were determined by *in vivo* MR spectroscopy and by biochemical means during postnatal growth and adulthood. In wild-type muscle [tCr], the PCr/ATP ratio and CK activity increased rapidly in the first 4 - 7 weeks of age. Remarkably, M-CK/ScCKmit^{-/-} mice showed a similar increase in the PCr/ATP ratio during the first month of age in the presence of only minor brain-type BB-CK activity. Uptake of Cr in muscle was seemingly unrelated to CK activity as tCr increased in the same way in the muscles of both mice types. At older age the PCr/ATP ratio decreased in M-CK/ScCKmit^{-/-} muscles in contrast to wild-type where it still slowly increased, whereas [tCr] was similar for muscle of both mice. Using a new *in vivo* MR approach with application of ¹³C-4 labeled Cr, also a lower PCr/tCr ratio was observed in M-CK/ScCKmit^{-/-} muscle. From these data it followed that *in vivo* global ATP levels at rest are similar in presence or absence of CK. Although Cr could still be converted to PCr in mature M-CK/ScCKmit^{-/-} muscle, the immediate availability of PCr decreased, and PCr became partly inconvertible at older age. Apparently catalysis of the CK reaction by BB-CK, although significant in muscles of newborn mice, gradually declines to very low levels in adulthood. Part or all of this BB-CK may arise from satellite cells fusing with myotubes, a process which is most active during the first months of life. Finally, our observation that the MR and the chemical assessment of muscle [tCr] and PCr/tCr ratio were similar for all mice does not support the existence of a significant MR-invisible or immobile pool of Cr, with a role of CK in this phenomenon.

INTRODUCTION

Creatine kinases (CKs; EC 2.7.3.2) form a small family of isoenzymes which catalyze the reaction $\text{Creatine (Cr)} + \text{MgATP}^{2-} \leftrightarrow \text{Phosphocreatine (PCr}^{2-}) + \text{MgADP}^- + \text{H}^+$. These proteins play a key role in the energetics of excitable tissues, such as muscle and brain, by keeping ATP/ADP ratios balanced and the adenylate pool highly charged (1, 2). Apart from forming a temporal energy buffer, the CK circuit may also act as an intermediate in spatial energy networks (3). Other roles of the CK system, which follow from the presence of other CK reactants, are intracellular regulation of pH (1, 4) and inorganic phosphate (Pi) levels (5).

To study the overall physiological significance of the CK/PCr-system in muscle, we have generated mice with null mutations in the muscle-specific cytosolic M-CK and mitochondrial ScCKmit genes (6-8). Apart from specific functional losses, also some remarkable metabolic adaptations were observed in muscles of CK lacking animals (e.g. (7, 9, 10)). Early in life a significant part of total skeletal muscle CK activity comes from the BB-CK isoform and it has been shown for some species that the expression of this isoform becomes gradually suppressed during maturation of skeletal muscle, leaving only trace amounts at adulthood (11, 12). Skeletal muscle of adult mice with combined null mutations for M-CK and ScCKmit (M-CK/ScCKmit^{-/-}) showed no up-regulation of BB-CK activity. Nevertheless, substantial amounts of PCr were found in these muscles. However, this pool was not accessible for energy buffering (8, 13) and moreover, the exchange-flux of phosphate between the PCr and ATP pools measured in MR transfer experiments had dropped to below detection levels in adult animals (9, 13).

The main purpose of the present study was to obtain a more precise characterization of the origin and fate of the PCr pool in muscle without muscle-type CKs as compared to PCr in muscle of wild-type mice. It is of particular interest to know what happens with the muscle PCr content in relation to CK activity and total Cr levels. These key parameters in the setting of PCr tissue levels are expected to change in skeletal muscle of mice during postnatal development and aging. To address how they relate to PCr levels in wild-type and M-CK/ScCKmit^{-/-} mice the total content of Cr (tCr) and PCr in hind-limb muscle was assessed by in vivo MR spectroscopy in parallel with biochemical determinations of muscle Cr levels and CK activity as a function of age. To identify whether uptake and phosphorylation of creatine indeed occur in muscle of adult M-CK/ScCKmit^{-/-} mice we introduce a new approach involving the administration of ¹³C-4 labeled Cr to monitor its phosphorylation in vivo by ¹³C MR spectroscopy. From this approach also the muscle [PCr]/[tCr] ratio can be determined which, together with tCr content and [PCr]/[ATP] ratios, allows for an assessment of in vivo ATP levels in a novel way. Finally, we also compared the

potential to de-phosphorylate PCr in muscle of wild-type and of double knock-out mice as a function of age. The results provided further clues on the presence of PCr in (developing) skeletal muscle of wild-type mice and of mice without cytosolic MM-CK and mitochondrial ScCKmit. Moreover, the particular results of this study on metabolite levels also have interesting implications for views on Cr mobility and visibility as seen by MR spectroscopy in skeletal muscle.

MATERIALS AND METHODS

Animals

In this study a comparison was made between mice lacking cytosolic M-CK and sarcomeric mitochondrial ScCKmit (i.e. M-CK/ScCKmit--/--) and wild-type C57Bl/6 controls. All procedures were approved by the Animal Care Committee of the University of Nijmegen and conformed to the Dutch Council for Animal Care. Animals were anesthetized with 1.2% isoflurane in a gas mixture of 50% O₂/ 50% N₂O delivered through a facemask. Their body temperature was monitored using a fluoroptic thermometer (Luxtron 712, California, USA) and was maintained at $36.8 \pm 0.5^\circ\text{C}$ using a warm water circuit.

Magnetic Resonance (MR) equipment

The MR experiments were performed on a horizontal 7.0 T magnet (Magnex Scientific, Abingdon, UK), which was equipped with 150 mT/m shielded gradients, and interfaced to a SMIS (Surrey Medical Imaging Systems, Surrey, UK) spectrometer, operating at 300.22 MHz for ¹H, at 121.53 MHz for ³¹P and at 75.49 MHz for ¹³C. The receiver channel was slightly modified by using home-built ultra-low noise preamplifiers and a low-loss active transmit/receive switch.

Phosphorus (³¹P) MR study of postnatal development

For non-localized ³¹P MR measurements, a three-turn solenoid coil with a diameter of 8 mm was used with an Alderman-Grant type ¹H coil surrounding it (14). For young mice (7 – 14 days of age), a special plastic insert was used to ensure that only the hind limb muscles were measured. After the shimming procedure, a scout image was obtained in three perpendicular directions to ensure that only the hind limb was situated in the radiofrequency (RF) field of the coil. Experiments on a phantom (100 mM inorganic phosphate solution) showed that the field of view of the ¹H coil corresponded to that of the ³¹P coil. This was verified by the combined application of localized ³¹P MR spectroscopy (15) and ¹H MRI which showed the absence of ³¹P MR signals outside the phantom. MR spectra were acquired

using a 90° RF pulse of 40 μ s with a repetition time of 7 seconds and were obtained from the hind limb of mice starting at ages of 7 days up to ages of 300 days (N= 3 – 6 for each data point). Additional spectra were obtained with a repetition time of 25 sec from animals at ages of 90 and 110 days to obtain metabolite levels under fully relaxed conditions and to assess saturation factors (N= 3 for each mouse type).

Post mortem study

³¹P MR spectra were acquired from wild-type mice aged 21 days and 12 months (n=2 each), and M-CK/ScCKmit^{-/-} mice aged 21 days (n=3) and 6, 9 and 12 months (n=1 per time point). The ³¹P MR spectra (TR=7 s, 128 scans) were acquired using the same coil setup as used in the postnatal development study. After the acquisition of a reference spectrum, the animal was killed with an overdose of isoflurane and the PCr resonance was monitored until its level became constant.

In vivo monitoring of [4-¹³C] creatine by ¹³C magnetic resonance spectroscopy (MRS)

M-CK/ScCKmit^{-/-} (n=5) and wild-type (n=5) mice between 3 and 6 months of age were injected intravenously with 100% ¹³C-4 labeled Cr (11.25 mg/ml, 200 μ l), three times a week, for three weeks. The labeled Cr was obtained from Mercachem (Mercachem, Nijmegen, The Netherlands) synthesized according to (16). Hind-limb muscles of these mice were analyzed weekly by ¹³C MR spectroscopy, using a 4-turn solenoid ¹³C coil with a diameter of 8 mm surrounded by an Alderman-Grant ¹H coil. ¹³C MR spectra were acquired with a 90° RF pulse of 40 μ s, a repetition time of 3 seconds, and Waltz-4 ¹H decoupling (40 W, duty cycle 0.7%) to ensure that the resonances of PCr and Cr are maximally resolved. Heating caused by decoupling power was evaluated by monitoring the temperature of the hind limb and of the body by a two-channel fluoroptic thermometer (Luxtron 712); no warming of the animal could be detected during 1.5 hours.

Ischemia protocol

To make hind-limb muscles ischemic the MR probe was provided with a diaphragm plate, which allows reversible and reproducible occlusion of the hind limb (17). Before, during and after ischemia sequential ¹³C MR measurements were made essentially as described above, except that the number of scans was reduced to 600 with a repetition time of one second. These experiments were performed on mice between 3 and 6 months of age.

Quantification of the total Cr pool in muscle using localized ^1H MR spectroscopy

Creatine levels were determined by quantitative localized ^1H MRS in gastrocnemius muscle, oriented at 55° with respect to the static magnetic field (B_0) direction (magic angle) to avoid complications due to dipolar coupling (18). Localized ^1H MRS was performed as described previously (18). A stimulated echo pulse sequence with an echo time of 10 ms and a repetition time of 5 s was used to select a voxel (typical size $2 \times 2 \times 2 \text{ mm}^3$) in the gastrocnemius muscle, guided by MR images acquired in three oblique, perpendicular directions. Localized shimming on this (oblique) voxel was performed until a H_2O peak with full width at half maximum of less than 22 Hz was reached. Creatine levels were estimated from the peak area of its methyl protons using the ^1H signal of water as an internal reference and assuming a muscle water content of 76% (19). Corrections were made for T_2 transverse relaxation times. The relaxation time T_2 for Cr methyl and water proton spins was estimated by the acquisition of ^1H MR spectra at different echo times and applying a mono-exponential fit to the signal intensities obtained at increasing echo times. At a repetition time of 5 seconds, the proton spin system was considered to be fully relaxed and hence no correction for T_1 was applied. Creatine content was determined in this way at the ages of 60, 120 and 200 days ($n=3$ each).

Biochemical determination of CK activity and metabolite levels

Mice were killed by cervical dislocation and hind limb muscles snapshot frozen and stored at -80°C . Muscles were homogenized in a Teflon-glass Potter-Elvehjem using 10 volumes of an ice-cold buffer containing 200 mM sucrose, 2 mM EDTA, 10 mM TrisHCl (pH 7.4), supplemented with heparin (50 Units/ml) and protease inhibitors (Boehringer Mannheim, Germany). The suspension was diluted 1:1 in a 30 mM phosphate buffer (pH 7.4), with 0.2 mM DTT, 0.05% (v/v) Triton X-100 and protease inhibitors. Extracts were incubated at room temperature for 20 minutes and subsequently centrifuged at 14,000 rpm (Eppendorf) at 4°C for 20 minutes. Total CK activity was measured at 37°C using a CK-NAC activated kit (Boehringer) and expressed in $\text{mmol} \cdot \text{L}^{-1}$ (intracellular water) $\cdot \text{s}^{-1}$ assuming 20% protein content in skeletal muscle (20) and 1 g of muscle being equivalent to 0.69 ml intracellular water. For zymogram analysis, total protein extracts (5 μg) were resolved on a 0.7% (v/v) Seakem ME agarose gel (FMC Bioproducts, Rockland, ME, USA). Enzyme activities were visualized by a CK isoenzyme colorimetric detection kit (Sigma Diagnostics, St. Louis, USA, (8)).

For chemical analysis of the Cr content in the gastrocnemius-plantaris-soleus (GPS) complex, tissues were extracted by 0.6 M HClO_4 and neutralized with 3 M KOH. Total Cr levels were assayed via coupled enzymatic reactions using a spectrophotometer operating at

340 nm (21). Cr levels were determined in $\mu\text{mol/g}$ wet weight and mmol/l tissue, assuming a muscle density of 1.06 g/ml (22). These were converted to mmol/l intracellular water assuming a cellular water fraction of 0.73 (19, 23). PCr was determined as described previously (8, 9).

MR data analysis

MRS data was evaluated in the time domain using MR user interface (MRUI) 97.1 software (24). The processing of ^1H MR spectra was performed as described previously (18). The creatine peak at a chemical shift of 3.03 parts per million (ppm) was fitted assuming a Gaussian line shape model function. Resonances in ^{31}P MR spectra were also fitted with a Gaussian line shape model function. No further prior knowledge was used. For the assessment of ATP content only the γATP and the βATP signals were considered. Intracellular pH was derived from the chemical shift difference between P_i and PCr peaks (25).

In ^{13}C MR spectra, all signals originating from carbons in lipids were filtered using Hankel Lanczos singular value decomposition (26), leaving Cr and PCr signals around 157 ppm for further analysis. As prior knowledge, a chemical shift difference of 0.8 ppm (16) and equal damping for these resonances was assumed. Differences between mean parameter values were analyzed by the Student's unpaired t-test.

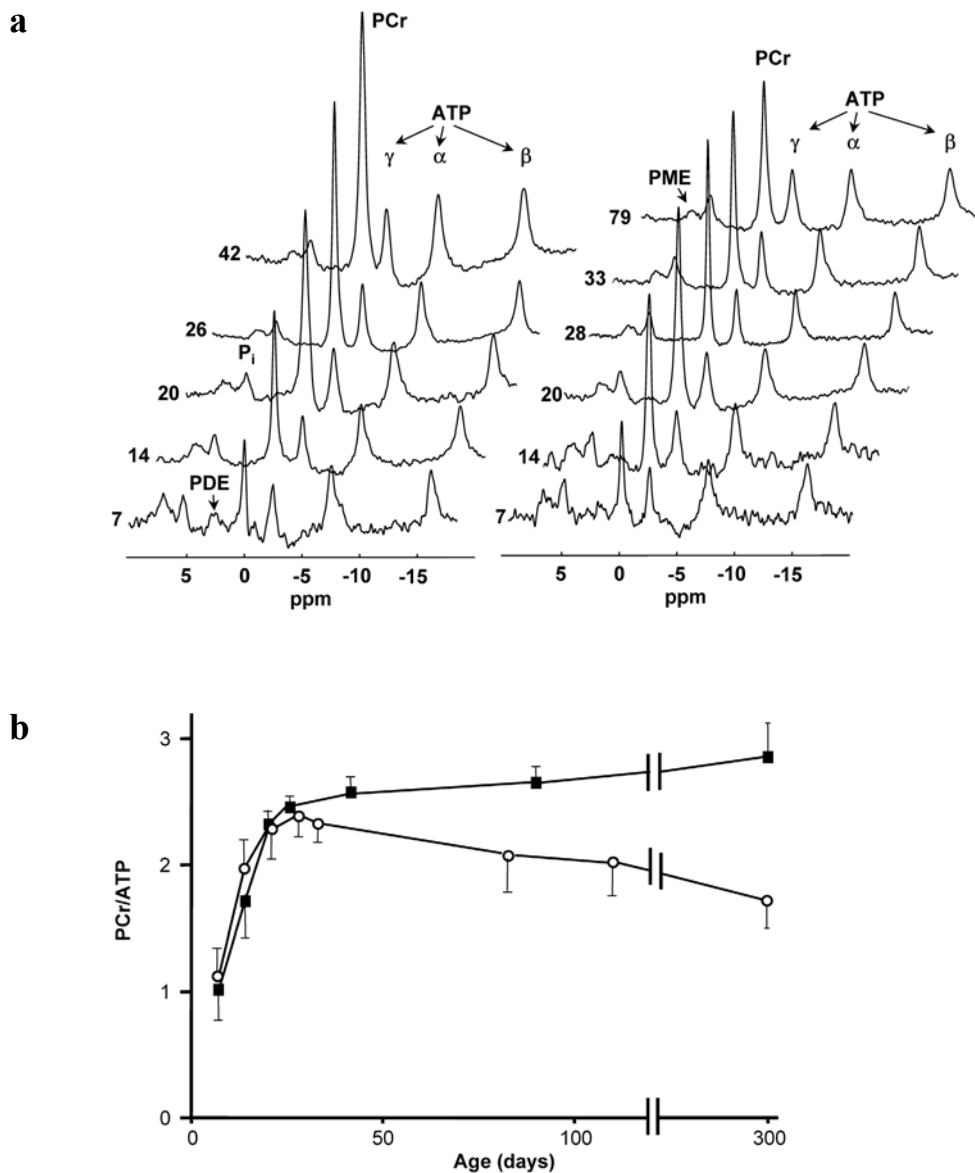


Figure 3.1: ^{31}P MRS of hind-limb skeletal muscle as a function of age. (a) Spectral changes for a wild-type (a, left panel) and a $M\text{-CK}/Sc\text{CKmit}^{-/-}$ mouse (a, right panel) reflect postnatal development of high-energy phosphate metabolism. Spectra are vertically scaled to the ATP content. The age of the animals (days) is indicated at the left. Assignments: PME, phosphomonoesters; Pi, inorganic phosphate; PDE, phosphodiester; PCr, phosphocreatine; ATP, adenosine triphosphate. (b) The PCr to ATP signal ratio as a function of the age for $M\text{-CK}/Sc\text{CKmit}^{-/-}$ (o) and control (■) mice. Ratios are not corrected for partial signal saturation. Each data point represents the average of at least 3 different mice. Standard deviations are indicated when outside the symbol sizes.

RESULTS

Postnatal development of (phospho)creatine levels

Energy metabolites in developing hind-limb muscles of control and M-CK/ScCKmit^{-/-} mice aged 7-300 days were monitored by ³¹P MR spectroscopy. All ³¹P MR spectra (figure 3.1a) showed signals for PCr, γ -, α - and β -ATP, inorganic phosphate (Pi) and phosphomonoesters (PME). During the first four weeks of life the PCr/ATP signal ratio gradually increased to a value of about 2.5 (uncorrected for spin saturation), with a similar slope for wild-types and mutants (figure 3.1b). Thereafter, this ratio slightly increased further in controls, but gradually declined in M-CK/ScCKmit^{-/-} mice.

To assess how the size of the cellular Cr pool determines the ratio of PCr over ATP we measured total Cr levels as a function of age, in the same cohort of mice as studied by ³¹P MRS. Using a chemical assay the creatine content appeared to increase similarly in both wild-type and M-CK/ScCKmit^{-/-} mice during postnatal development and leveled off after about 7 weeks of age at values between 27 and 35 mmol/l tissue (see figure 3.2).

Total creatine was also determined by quantitative localized ¹H MRS, with the muscle oriented at the so-called magic angle (18, 27), from the peak area of its methyl protons and using the water peak as a reference. The T₂ relaxation times used for signal correction were estimated to be 83 ± 4 ms (n=6) for creatine methyl protons and 21.9 ± 0.1 ms (n=6) for water proton spins. At 60 and 120 days of age tCr levels were determined in this way by MRS and also chemically, in the same skeletal muscles (n=3). At 60 days of age total creatine concentration was 27.9 ± 0.9 mmol/l tissue by MRS, which is not different from the creatine tissue content determined chemically (27.3 ± 1.4 mmol/l tissue). Although the average value determined by MRS at 120 days (32.5 ± 0.7 mmol/l tissue) is somewhat higher than that determined chemically (30.3 ± 0.9 mmol/l tissue) it is within the range of chemically determined values between 90 and 160 days of age (see figure 3.2). ¹H MRS analysis at 200 days of age found tCr to be 33.2 ± 1.1 mmol/l tissue in controls (n=3) and 34.5 ± 1.2 mmol/l tissue in M-CK/ScCKmit^{-/-} muscles (n=3).

Postnatal changes in creatine kinase activity

During postnatal development of mammalian skeletal muscles a gradual repression of B-CK gene expression takes place. In order to assess the possible involvement of this CK-family member in PCr pool build-up and depletion, we quantified the residual level of BB-CK isoenzyme in M-CK/ScCKmit^{-/-} muscles in relation to normal wild-type CK activity over time. The zymogram assay confirmed complete absence of MM-CK and ScCKmit in double mutant muscle, whereas the BB-CK isoenzyme was clearly visible in both

wild-type and mutant muscle extracts at 7 and 14 days of age (figure 3.3a). During further progression to adulthood, isoenzyme staining on zymograms dropped to undetectable low levels, but the corresponding residual BB-CK enzyme activity could still be assessed with spectro-photometric analysis of tissue lysates. In wild-type hind-limb skeletal muscle CK activity increases during the first month of life from about 75 mM/s at an age of 7 days to a value of about 200 mM/s at adulthood (figure 3.3b). In 7-day-old M-CK/ScCKmit^{-/-} muscles this activity was about 2.5 mM/s or 4% of the normal overall CK activity (combined BB-CK, MM-CK and ScCKmit activities in wild-type controls) and decreased to values of less than 1 mM/s within about 40 days (figure 3.3c).

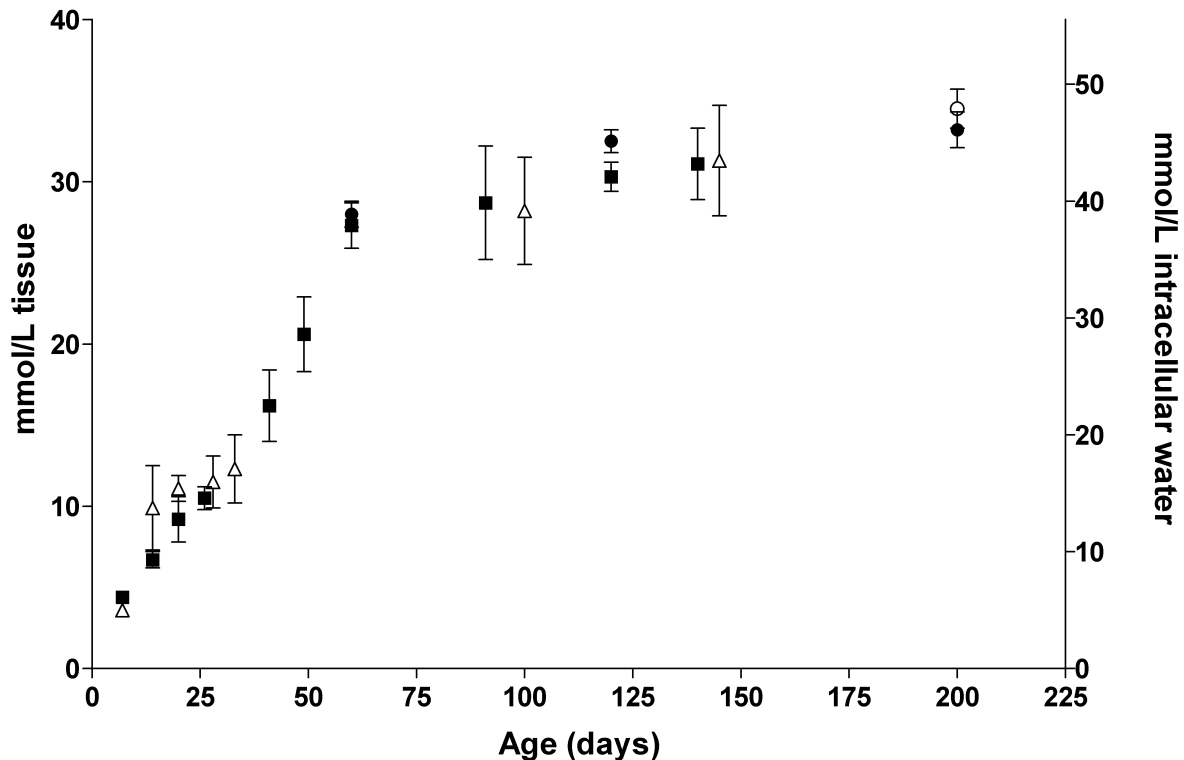


Figure 3.2. Creatine levels in hind-limb skeletal muscle as a function of mouse age. Data is presented as mmol/l tissue (left axis) and as mmol/l intracellular water (right axis) assuming an intracellular water fraction of 0.73 (see materials and methods section). Values for M-CK/ScCKmit^{-/-} mice are indicated by open symbols and for wild-type control mice by closed symbols. Data points at 60, 120 and 200 days, indicated by filled circles, were obtained by quantitative ¹H MRS of wild-type gastrocnemius muscle (n=3) and at 200 days of age also in M-CK/ScCKmit^{-/-} muscle (n=3), indicated by an open circle. The other data points have been obtained by biochemical means from the muscle GPS complex. The data points at 60 and 120 days (n=3) have been determined from the same leg on which the MRS quantification was performed. The data points at 140 and 145 days are averages of 6 and 5 mice, respectively, varying in age between 120 – 160 days. Each other point represents an average of 3 – 6 mice, except at 7 days postpartum, which are single measurements. Standard deviations are indicated if extending beyond the symbol size.

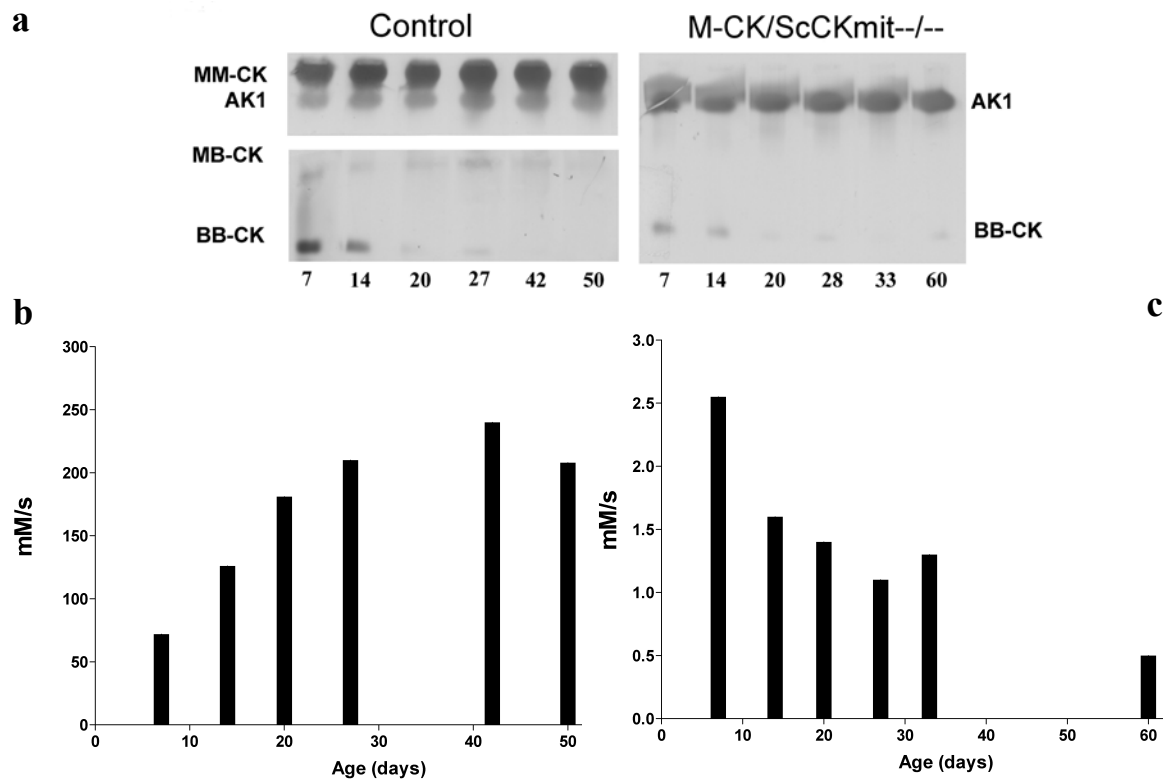


Figure 3.3: CK isoenzyme and adenylate kinase 1 (AK1) distribution in skeletal muscle as a function of mouse age (days)

(a) Zymogram analysis of extracts from wild-type (left panel) and M-CK/ScCKmit^{-/-} mouse muscle (right panel) reveals low levels of BB-CK activity during the first 2 weeks. Note the complete absence of MM-CK activity in M-CK/ScCKmit^{-/-} animals. AK1 activity staining appears different in the right and left panels due to the use of differential staining protocols, necessary to avoid overexposure of MM-CK signal and blurring of the AK1 band by the presence of vast amounts of MM-CK in wild-type muscles. Staining of (low) ScCKmit activity is not visible under the present conditions. (b) CK enzyme activity measured as a function of age in wild-type muscle. Activities are given as mmol/l intracellular water /s. (c) CK activity in M-CK/ScCKmit^{-/-} muscle, which is the non-MM-CK/ScCKmit activity, expressed as mmol (l intracellular water)⁻¹ s⁻¹. Note the difference in vertical scaling with respect to b.

Uptake and phosphorylation of ¹³C-labeled creatine in muscle of adult mice

To assess the uptake and phosphorylation of creatine in mature wild-type and M-CK/ScCKmit^{-/-} mice we explored a new approach by which we could assess Cr and PCr simultaneously in muscle in vivo using ¹³C MR spectroscopy after injection of ¹³C-labeled Cr. After one week, this resulted in well-resolved signals in the ¹³C MR spectrum of wild-type muscle for Cr and PCr (figure 3.4a). Strikingly, uptake and phosphorylation of ¹³C labeled Cr were also detectable in M-CK/ScCKmit^{-/-} mice (figure 3.4b). The phosphorylated fraction

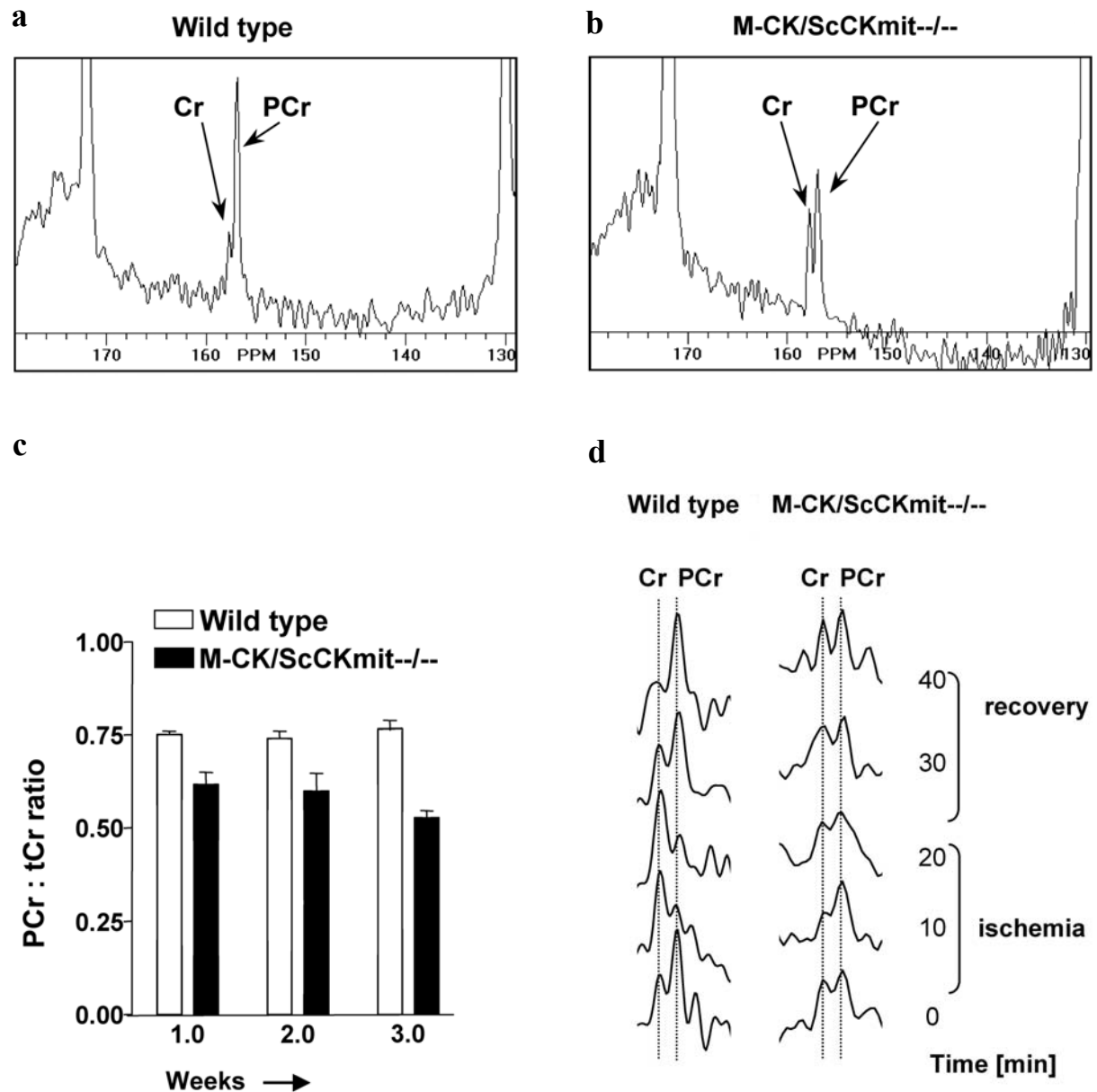


Figure 3.4: ^{13}C -MRS of adult hind limb muscle, after administration of ^{13}C -4 labeled Cr. ^{13}C MR spectra (128 – 180 ppm spectral range) of (a) wild-type control and (b) M-CK/ScCKmit $^{-/-}$ mice. (c) PCr/tCr ratios derived from these spectra assessed over a 3 week period. (d) Zoomed ^{13}C MR spectra obtained before and during 20 minutes of ischemia and recovery. Hydrolysis of PCr and rephosphorylation of Cr are evident in wild-type muscles, while in M-CK/ScCKmit $^{-/-}$ muscles no conversion was detected within the limits set by the signal to noise ratio.

of the Cr pool remained constant during three weeks of creatine injection in both mouse strains (figure 3.4c). The average PCr/tCr ratio as determined by ^{13}C MRS in M-CK/ScCKmit $^{-/-}$ mice (0.56 ± 0.05) is significantly lower than in wild-type muscle (0.74 ± 0.04). In a determination by chemical analysis (8) similar values were found for M-CK/ScCKmit $^{-/-}$ mice (0.55 ± 0.06) and slightly lower values for wild-types (0.66 ± 0.07), which likely is due to some PCr breakdown during the extraction procedure because of the high CK activity.

To verify whether the ^{13}C -labeled PCr in muscle is metabolically active, we applied ischemia to the hind limb muscle. ^{13}C MR spectra were acquired at a time resolution of 10 minutes, during a total ischemic period of 20 minutes. In wild-type mice we observed a clear conversion of PCr to Cr during this time interval, and full recovery of PCr levels occurred after reperfusion (figure 3.4d). In M-CK/ScCKmit $^{-/-}$ mice, no changes in PCr and Cr levels could be observed, within limits set by the signal to noise ratio.

Non-invasive estimation of intracellular ATP and ADP content at rest

Usually the in vivo levels of compounds in skeletal muscle involved in the CK reaction are assessed by ^{31}P MRS by taking the chemically determined contents of ATP and total creatine as starting points. The availability in this study of absolute Cr levels and of the [PCr]/[tCr] and [PCr]/[ATP] ratios allowed the non-invasive estimation of PCr and ATP levels. The average [tCr] for muscle of wild-type mice between 60 and 200 days of age was 30.5 ± 2.0 mmol/l tissue (see Table 3.1).

With a PCr/tCr ratio of 0.74 ± 0.04 we calculate an average value for [PCr] of 22.5 ± 1.9 mmol/l tissue and with a PCr/ATP ratio of 2.90 ± 0.19 we arrive at an average [ATP] of 7.8 ± 0.8 mmol/l tissue. In previous studies we obtained similar [ATP] values for wild-type skeletal muscle (GPS complex) by chemical means: i.e. 8.2 ± 0.8 mmol/l tissue (28) and 8.3 ± 0.5 mmol/l tissue (7). [ATP] in M-CK/ScCKmit $^{-/-}$ muscle derived by the MRS approach was not different from wild-types, but it was substantially lower in the chemical determination. Assuming a fraction of 73% for intracellular water the intracellular concentrations of tCr, PCr and ATP were also determined (Table 3.1). Free intracellular ADP levels were derived from these concentrations and the CK reaction assuming this reaction to be at near-equilibrium with an equilibrium constant of $1.66 \cdot 10^9$ (29) and including intracellular pH data from ^{31}P MR spectra of skeletal muscle. The near-equilibrium condition generally seems valid for skeletal muscle at rest, e.g. (29). This condition also appears to occur in muscle of wild-type mice (7), but may not necessarily be valid for M-CK/ScCKmit $^{-/-}$ muscle.

Table 3.1: Average metabolite concentrations, ratios and tissue pH for adult mouse skeletal muscle.

		wt		M-CK/ScCKmit ^{-/-}	
		mmol / l tissue	mmol / l intracellular water	mmol / l tissue	mmol / l intracellular water
[tCr]	(1)	30.5 ± 2.0	41.8 ± 2.7	31.4 ± 2.8	43.0 ± 3.8
[PCr]		22.5 ± 1.9	30.8 ± 2.6	17.6 ± 2.2	24.1 ± 3.0
[ATP] _{MRS}		7.8 ± 0.8	10.7 ± 1.1	7.5 ± 1.1	10.3 ± 1.5
[ATP] _{chem} *	(2)	8.2 ± 0.8	11.2 ± 1.1	5.7 ± 0.6	7.8 ± 0.8
[ADP]	(3)		0.037		(0.083)
PCr/ATP *	(4)	2.90 ± 0.19		2.36 ± 0.21	
PCr/tCr *	(5)	0.74 ± 0.04		0.56 ± 0.05	
pH	(6)	7.22 ± 0.03		7.24 ± 0.04	

Notes: All the data (\pm SD) is obtained from measurements of animals between 60 to 200 days of age. Metabolite concentrations in mmol/ l tissue (left column for each mouse type) were converted to mmol / l intracellular water (right columns) assuming a fraction of 0.73 for intracellular water. [PCr] and [ATP]_{MRS} were derived from the PCr/tCr and PCr/ATP ratios respectively.

* difference comparison between wt and M-CK/ScCKmit^{-/-} by unpaired t-test: two tailed p value < 0.0001.

(1) tCr = phosphorylated + unphosphorylated creatine. Data from chemical and ¹H MRS determinations have been taken together. n=24 for WT and 12 for M-CK/ScCKmit^{-/-}.

(2) Data taken from (28) in μ mol/g wet weight and converted to mmol/L intracellular water assuming a muscle density of 1.06 and an intracellular water fraction of 0.73. n=5 for WT and n=6 for M-CK/ScCKmit^{-/-}.

(3) ADP is estimated as described in the text, using the [ATP]_{MRS} values and assuming the CK reaction at equilibrium. This may not be valid for M-CK/ScCKmit^{-/-}.

(4) Ratios obtained from ³¹P MR spectra measured under relaxed spin conditions (TR > 20 s) or corrected for spin saturation if obtained at a pulse repetition time of 7 s. n=9 for WT and M-CK/ScCKmit^{-/-}.

(5) Data from ¹³C MRS of the hind-limb, averaged from measurements obtained 1, 2 and 3 weeks after the start of ¹³C-4 creatine administration for 4 WT and 4 M-CK/ScCKmit^{-/-} mice. n= 11 for each mouse species.

(6) Determined from ³¹P MRS data. n=6 for WT and n=5 for M-CK/ScCKmit^{-/-}.

Postmortem de-phosphorylation of phosphocreatine as a function of age

Having demonstrated that Cr phosphorylation can occur in both developing and mature muscle of M-CK/ScCKmit^{-/-} mice at rest, we next investigated to what extent also the inverse reaction, i.e. de-phosphorylation of the PCr pool, could still ensue in these animals. We therefore quantified this activity as a function of age by measuring the rate of PCr signal decay in hind-limbs after a maximal physiological challenge, the onset of death in the MR magnet. Post-mortem PCr breakdown occurs at the same rate in 21 day and 12 month old wild-type mice (figure. 3.5). In contrast, M-CK/ScCKmit^{-/-} mice showed delayed depletion of PCr at the age of 21 days, while de-phosphorylation of PCr was further slowed down at 3, 9 and 12 months of age (figure 3.5). In these latter measurements, the PCr signal did not drop to zero, but reached a plateau at about 50% of the initial concentration, indicating that on the time scale of the experiment a significant portion of PCr had become metabolically inactive.

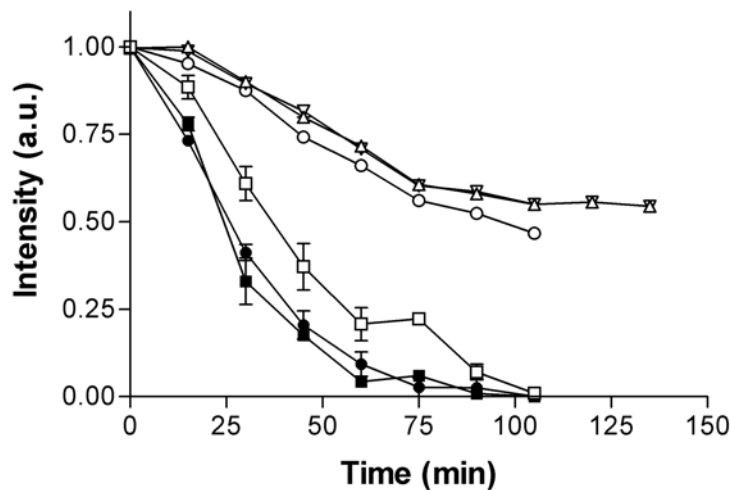


Figure 3.5: Postmortem depletion of PCr in mouse skeletal muscle followed by ³¹P MRS. The animals were killed at $t=0$ as described in the text. Data point symbols for wild-type are ■ : 21 days ($n=2$); ● : 12 months ($n=3$); and for CK^{-/-} : □ : 21 days ($n=3$); ▽: 3 months ($n=1$); △: 9 months ($n=2$); ○: 12 months ($n=1$). In control mice at 21 days and 12 months of age the decay is the same. In M-CK/ScCKmit^{-/-} muscle, the ability to hydrolyze PCr decreases with age. In 21-day-old M-CK/ScCKmit^{-/-} mice, PCr gets completely depleted, but at 3 months or older, PCr appears to decrease only to 50% and at a lower rate.

DISCUSSION

Differences in PCr, total Cr content and CK activity during development and at adulthood

The increase of the CK activity and of the PCr/ATP ratio during postnatal development of skeletal muscle in wild-type mice confirms results of previous studies in rodents (e.g. (20, 25)). In the present study we also observed a postnatal increase for total muscle creatine (tCr) content in these mice, which in the first 4 weeks occurs in parallel with increasing CK activity and PCr/ATP ratios. In general for different tissues there appears to be a positive correlation between CK activity and Cr content (2). However, it is clear that this correlation does not hold strictly. An increasing tCr level paralleled a minor and steadily decreasing CK activity in the M-CK/ScCKmit^{-/-} mice, which declined to levels below 1 mM/s. A decline of BB-CK activity has also been observed for the hearts of these mice (30). Interestingly, the PCr/ATP ratio in skeletal muscle of M-CK/ScCKmit^{-/-} mice increased in a very similar fashion to in wild-type mice during the first four weeks after birth, despite the fact that the total CK activity differed profoundly between mutants and controls. It appears that the initial increase in PCr levels relates to the postnatal increase in the tCr pool, which is largely identical in wild-type and M-CK/ScCKmit^{-/-} mice. While beyond 30 days of age the PCr/ATP ratio increased more slowly in wild-type or even decreased in M-CK/ScCKmit^{-/-} mice, the increase of the muscle tCr content leveled off somewhat later. Resting PCr/ATP ratios are not only determined by the tCr level and CK activity (see below), but also by the intracellular energy charge and total adenylate levels which may change during the postnatal development of skeletal muscle, e.g. (31). The present study indicates that Cr uptake in skeletal muscle is independent from its phosphorylation by CK. This uptake is an active process, regulated by specific Na⁺/Cr co-transporters (2, 32), the activity of which is coupled to energy- and Na⁺, K⁺ and Ca²⁺-homeostasis. Creatine transporter activity shows regional and developmental differences (33, 34), but it seems unaffected in CK lacking mutants.

Once M-CK/ScCKmit^{-/-} mice become older than four weeks, they display lower PCr/ATP and PCr/tCr ratios than wild-type mice. To put this in the proper perspective we first consider how CK activity, the in vivo flux through the CK reaction and ATPase activity relate to each other. The maximum activity (V_{max}) of CK from adult wild-type GPS muscle is about 200 mM/s at 37 °C (see Fig 3B). This is in agreement with other studies on rodent (fast twitch) skeletal muscle, e.g. (20, 35, 36), but it is in contrast to the actual resting CK flux in vivo as derived from ³¹P MRS magnetization transfer in our earlier studies (7), which is approximately 8 mM/s and thus only about 5% of the in vitro values. Similar discrepancies

have been noted previously for skeletal muscle and are explained by specific kinetic behavior of CK enzymes under *in vivo* conditions (35, 37, 38). Still, these fluxes are well above maximum values of ATPase activity so that adequate backup during the early phase of muscle contraction is ensured. In the cytosolic M-CK single knock-out mice the *in vitro* CK activity at 37 °C drops to about 5 mM/s and the *in vivo* CK flux to below 0.4 mM/s (7, 36, 39, 40). These mice lack muscle burst activity as demonstrated by electrical stimulation at 5 Hz. As the rate of ATP breakdown may easily increase above 1 mM/s at such muscle activity (calculated from data in (41, 42)), the CK flux cannot follow ATP breakdown during the first 10 s of contraction when ATP regeneration nearly completely relies on PCr (42). The concomitant ADP increase may explain why burst activity is lacking in the muscle of these mice (43). In muscle of adult M-CK/ScCKmit^{-/-} mice the *in vitro* CK activity is further reduced to less than 1 mM/s. These mice not only lack burst activity but in addition showed lower muscle force and slower relaxation compared to the single M-CK knock-out mice (8). If the *in vivo* activity is also only 5% of the *in vitro* value (i.e. ~ 0.02 mM/s) this comes close to ATPase flux rates as estimated for resting rat skeletal muscle, which are between about 0.01 – 0.04 mM/s (35, 37, 41, 44). With similar ATPase fluxes occurring in resting M-CK/ScCKmit^{-/-} muscle the CK reaction might be out of equilibrium upon work transitions, which, at comparable total Cr and adenylate pools, would result in an altered PCr/ATP ratio. In addition this altered ratio could represent a situation in which the (entire) muscle pool of CK substrates no longer is in continuous open contact with the, now only sparsely present, CK molecules, for instance due to compartmentalization such as discussed for the presumed role of satellite cells below. If, on the other hand, the residual CK activity would still be sufficient to keep the overall CK reaction at or near equilibrium in the resting state, it follows that the concentration of ADP must differ between wild-type and mutant muscle as tissue pH, total creatine and ATP levels are similar. Under equilibrium conditions we estimate an increase of resting free ADP levels by a factor of about 2 in M-CK/ScCKmit^{-/-} muscle (see table 3.1). As resting PCr content may vary with fiber type (45), the different PCr levels might be related to an overall change in fiber type composition in the mutant mouse compared to control. Moreover, postnatal changes in CK activity appear to correlate with changes in myosin heavy chain phenotype (46). However, the myosin heavy chain distribution did not appear to differ much in skeletal muscle of M-CK/ScCKmit^{-/-} mice, although a shift towards a more oxidative character of mainly the type-II fast-twitch glycolytic muscles in M-CK/ScCKmit^{-/-} mice was identified (9, 10).

On the origin of the Cr (de)phosphorylation activity in mature muscle of M-CK/ScCKmit^{-/-} mice

As the ¹³C MRS experiments showed that even in mature M-CK/ScCKmit^{-/-} muscle older than 3 months, Cr can be converted to PCr the question remains of what the origin of this catalytic activity is. It is conceivable that BB-CK activity arises from non-muscle cells, such as vascular endothelium, or that some unknown Cr phosphorylating activity is present in muscle cells. These possibilities seem rather unlikely, in particular as mice with combined deficiency of cytosolic BB-CK and mitochondrial ubiquitous CK (UbCKmit) isoforms completely lack PCr in the brain (47). This provides indirect evidence for the supposition that Cr ↔ PCr conversion in mammalian tissues becomes fully blocked if activity of all CK isoforms is completely ablated.

If we assume that Na⁺/Cr co-transporters do not transport PCr, formed elsewhere and transported by circulation, into muscle directly, and that the negatively charged PCr (PCr²⁻) will not freely pass the sarcolemma against a concentration gradient, we can only explain our results by assuming that trace CK activity in adult CK double mutant muscles causes PCr to occur. Two possibilities remain for this residual CK activity. The first is that even in mature myotubes the expression of the B-CK gene, although decreasing with age, is still not completely blocked. Another interesting explanation for the build-up of a PCr pool in mature hind-limb muscle would be the deposition of BB-CK molecules from satellite cells in the process of fusion (48). Muscle satellite cells are prominently present and active in the growing muscles of young animals, but their population decreases with age (48). Satellite cell nuclei are 30% of the total muscle nuclei at birth, 4% at 8 months and 2.4% at 30 months of age in mouse soleus muscle. Moreover, at adult age when muscle growth has slowed down the remaining satellite cells become quiescent, only being re-activated when myofibers are over-challenged. Thus in the adult stage when little satellite fusion is occurring, a considerable fraction of myofibers may hardly have any BB-CK left. This view is corroborated by the post-mortem data of M-CK/ScCKmit^{-/-} muscle, which shows that at older age the rate of PCr de-phosphorylation is slower and that 50% of the total PCr pool size virtually is unaffected during the observation period. If a significant part of the total cellular Cr pool has no access to the enzyme, this would indeed explain the lower PCr/tCr ratio in adult mutants. In this context M-CK/ScCKmit^{-/-} mice could become a convenient model to study the role of satellite cells, using BB-CK and PCr as sensitive reporters for their fate under different physiological conditions.

Estimation of in vivo ATP content using ^{13}C -4 PCr/tCr ratios

From the experiments with ^{13}C labeled creatine the in vivo PCr/tCr ratio was derived for skeletal muscle. Because we also have total Cr levels and PCr/ATP ratios available this gives the opportunity to estimate in vivo ATP levels in a novel manner. The tissue concentration derived in this way (~ 8 mmol/l tissue) is on the order of ATP values for (fast twitch) skeletal muscle that have been reported by others, e.g. (44, 45, 49) and conforms with ATP tissue concentrations determined by chemical means in wild-type mouse skeletal muscle (7, 28). Moreover, in this way we demonstrate that ATP levels in wild-type and M-CK/ScCKmit $^{-/-}$ muscle are similar, and that differences seen previously in chemical analysis (8, 28) can be explained by rapid breakdown of ATP during the clamping procedure for the extraction (44), which cannot be compensated in M-CK/ScCKmit $^{-/-}$ muscle, because it has a very inefficient CK reaction. In contrast in wild-type muscle PCr is more depleted during this procedure, thus sustaining ATP levels, which is reflected in a slightly lower PCr/ATP ratio when determined by chemical means (8).

The MR visibility of creatine

The present results also bear on the issue of MR visibility of the cellular Cr pool, and the presumed existence of significant free Cr pools that do not participate in the CK reaction. Based on experiments using ^{14}C -labeled Cr in heart muscle (50, 51) and in fast-twitch muscle of fish (52) it has been proposed that a significant fraction of Cr (about 30%) is not immediately available for the CK reaction in these tissues. MR magnetization transfer experiments on skeletal muscle indeed revealed a pool of Cr that may be bound to matrix or cellular macromolecules, but this pool is in exchange with “mobile”, MRS visible creatine and comprises only about 2% of total creatine (53, 54). The observation in human skeletal muscle that the methylene peak of Cr in ^1H MR spectra disappears during exercise (55) further stimulated the discussion that a significant immobile Cr pool may exist, which is not readily accessible to creatine kinase. In another study a decrease in T_2 relaxation time of creatine methyl proton spins was observed during ischemic fatigue in humans (56), suggesting reduced mobility of creatine. In contrast, ^1H MRS investigations of mouse skeletal muscle indicated that changes in Cr signals, observed immediately after death of the animal, mainly result from altered dipolar interactions related to removal of the phosphate moiety of this compound and not from changes in its cyto-architectural environment (18). After eliminating the spectral appearance of these interactions by orienting the fiber direction of the muscle at 55° with the main magnetic field (magic angle), the Cr signal did not change in the early postmortem phase. Interestingly, a recent study indicated that the electric charge of small molecules and proteins affects dipolar coupling interactions in skeletal muscle (57).

Our quantification of total Cr content in adult mouse skeletal muscle, by ^1H MRS of muscles placed at the magic angle to avoid complications by dipolar interactions (27), yielded similar values to those obtained by chemical means. In the GPS complex of animals at an age from 2 to about 6 months the intracellular total creatine concentrations were about 40 mM. This is close to the values published for type 2a/b muscles in mouse and rat (45), which is what can be expected as the gastrocnemius muscle is dominating in this complex. Altogether these results do not point to a significant MR invisible Cr pool (i.e. more than the error of the measurements, which is less than 10%) in mouse skeletal muscle as was already concluded for PCr in these muscles (58). Further support for ‘full MR visibility’ of the total Cr pool comes from the observation that PCr/tCr ratios determined by ^{13}C MRS resemble the chemically determined values. Ischemia experiments indicate that the MR visible PCr and free Cr pools are in direct contact with each other in wild-type mouse skeletal muscle. Finally, the similarity of creatine levels in wild-type and mutant muscles as detected by ^1H MRS indicates that the mere presence of CK itself does not affect the MR visibility at rest of the Cr pool and hence its mobility.

ACKNOWLEDGEMENT

This work was supported by a program grant from the Netherlands Organization for Scientific Research (Medical Sciences) .

REFERENCES

1. Wallimann, T., Wyss, M., Brdiczka, D., Nicolay, K. and Eppenberger, H.M. Intracellular compartmentation, structure and function of creatine kinase isoenzymes in tissues with high and fluctuating energy demands: the phosphocreatine circuit for cellular energy homeostasis. *Biochem J* 1992;281:21-40.
2. Wyss, M. and Kaddurah-Daouk, R. Creatine and creatinine metabolism. *Physiol Rev* 2000;80:1107-213.
3. Walsh, B., Tonkonogi, M., Soderlund, K., Hultman, E., Saks, V. and Sahlin, K. The role of phosphorylcreatine and creatine in the regulation of mitochondrial respiration in human skeletal muscle. *J Physiol* 2001;537:971-8.
4. Edstrom, L., Hultman, E., Sahlin, K. and Sjöholm, H. The contents of high-energy phosphates in different fibre types in skeletal muscles from rat, guinea-pig and man. *J Physiol* 1982;332:47-58.
5. Meyer, R.A., Sweeney, H.L. and Kushmerick, M.J. A simple analysis of the "phosphocreatine shuttle". *Am J Physiol* 1984;15:C365-C377.
6. van Deursen, J. and Wieringa, B. Targeting of the creatine kinase M gene in embryonic stem cells using isogenic and nonisogenic vectors. *Nucl Acids Res* 1992;20:3815-3820.
7. van Deursen, J., Heerschap, A., Oerlemans, F., Ruitenbeek, W., Jap, P., ter Laak, H. and Wieringa, B. Skeletal muscles of mice deficient in muscle creatine kinase lack burst activity. *Cell* 1993;74:621-31.
8. Steeghs, K., Benders, A., Oerlemans, F., de Haan, A., Heerschap, A., Ruitenbeek, W., Jost, C., van Deursen, J., Perryman, B., Pette, D., Bruckwilder, M., Koudijs, J., Jap, P., Veerkamp, J. and Wieringa, B. Altered Ca²⁺ responses in muscles with combined mitochondrial and cytosolic creatine kinase deficiencies. *Cell* 1997;89:93-103.
9. Steeghs, K., Oerlemans, F., de Haan, A., Heerschap, A., Verdoodt, L., de Bie, M., Ruitenbeek, W., Benders, A., Jost, C., van Deursen, J., Tullson, P., Terjung, R., Jap, P., Jacob, W., Pette, D. and Wieringa, B. Cytoarchitectural and metabolic adaptations in muscles with mitochondrial and cytosolic creatine kinase deficiencies. *Mol Cell Biochem* 1998;184:183-94.
10. de Groof, A.J., Smeets, B., Groot Koerkamp, M.J., Mul, A.N., Janssen, E.E., Tabak, H.F. and Wieringa, B. Changes in mRNA expression profile underlie phenotypic adaptations in creatine kinase-deficient muscles. *FEBS Lett* 2001;506:73-8.
11. Eppenberger, H.M., Perriard, J.C. and Wallimann, T. Analysis of creatine kinase during muscle differentiation. in: *Current topics in biological and medical research* Eds.: M. Rattazi, J. C. Scandalios and G. S. Whitt New York: Alan Liss: 1983. 19-38
12. Trask, R.V. and Billadello, J.J. Tissue-specific distribution and developmental regulation of M and B creatine kinase mRNAs. *Biochim Biophys Acta* 1990;1049:182-8.
13. Heerschap, A., Houtman, C., Zandt, H.J.A.v., Bergh, A.J.v.d. and Wieringa, B. Introduction to in vivo 31P magnetic resonance spectroscopy of (human) skeletal muscle. *Proceedings of the Nutrition Society* 1999;58:1-10.
14. Alderman, D.W. and Grant, D.M. An efficient decouple coil design which reduces heating in conductive samples in superconducting spectrometers. *J Magn Reson* 1979;36:447-451.
15. Ordidge, R.J., Connely, A. and Lohman, J.A.B. Image-selected in vivo spectroscopy (ISIS). A new technique for spatially selective NMR spectroscopy. *J Magn Reson* 1986;66:293-294.
16. Han, C.H. and Sillerud, L.O. Synthesis of [guanidino-¹³C]creatine and measurement of the creatine phosphokinase reaction in vivo by ¹³C nmr spectroscopy. *Magn Reson Med* 1986;3:626-633.
17. in 't Zandt, H.J., Oerlemans, F., Wieringa, B. and Heerschap, A. Effects of ischemia on skeletal muscle energy metabolism in mice lacking creatine kinase monitored by in vivo 31P nuclear magnetic resonance spectroscopy. *NMR Biomed* 1999;12:327-34.
18. in 't Zandt, H.J.A., Klomp, D.W.J., Oerlemans, F., Wieringa, B., Hilbers, C.W. and Heerschap, A. Proton MR Spectroscopy of wild-type and creatine kinase deficient mouse skeletal muscle: dipole-dipole coupling effects and post-mortem changes. *Magn Reson Med* 2000;43:517-524.
19. Sjogaard, G. and Saltin, B. Extra- and intracellular water spaces in muscles of man at rest and with dynamic exercise. *Am J Physiol* 1982;243:R271-80.

20. Zuurveld, J.G., Wirtz, P., Loermans, H.M. and Veerkamp, J.H. Postnatal growth and differentiation in three hindlimb muscles of the rat. Characterization with biochemical and enzyme-histochemical methods. *Cell Tissue Res* 1985;241:183-92.
21. Bergmeyer, H.U. *Methods of Enzymatic Analysis*. New York: Academic Press; 1974.
22. Mendez, J. and Keys, A. Density and composition of mammalian muscle. *Metabolism* 1960;9:184-188.
23. Forsberg, A.M., Nilsson, E., Werneman, J., Bergstrom, J. and Hultman, E. Muscle composition in relation to age and sex. *Clin Sci (Lond)* 1991;81:249-56.
24. <http://www.mrui.uab.es/mrui/mruiHomePage.html>
25. Heerschap, A., Bergman, A.H., van Vaals, J.J., Wirtz, P., Loermans, H.M. and Veerkamp, J.H. Alterations in relative phosphocreatine concentrations in preclinical mouse muscular dystrophy revealed by in vivo NMR. *NMR Biomed* 1988;1:27-31.
26. de Beer, R. and van Ormondt, D. In-Vivo magnetic resonance spectroscopy I: probeheads and radiofrequency pulses spectrum analysis. in: *NMR Eds.*: P. Diehl, E. Fluck, H. Gunther, R. Kosfeld and J. Seelig New York: Springer Verlag: 1992. 201-258
27. Kreis, R., Koster, M., Kamber, M., Hoppeler, H. and Boesch, C. Peak Assignment in localized ¹H MR spectra of human muscle based on oral creatine supplementation. *Magn Reson Med* 1997;37:159-163.
28. Steeghs, K. Consequences of creatine deficiencies in mice Medical faculty, university of Nijmegen, Nijmegen, the Netherlands; 1995.
29. Veech, R.L., Lawson, J.W., Cornell, N.W. and Krebs, H.A. Cytosolic phosphorylation potential. *J Biol Chem* 1979;254:6538-47.
30. Saupe, K.W., Spindler, M., Hopkins, J.C., Shen, W. and Ingwall, J.S. Kinetic, thermodynamic, and developmental consequences of deleting creatine kinase isoenzymes from the heart. Reaction kinetics of the creatine kinase isoenzymes in the intact heart. *J Biol Chem* 2000;275:19742-6.
31. Isselhard, W., Fischer, J.H., Kapune, H. and Stock, W. Metabolic patterns of several tissues of rabbits and guinea pigs during postnatal development. *Biol Neonate* 1973;22:201-21.
32. Guerrero-Ontiveros, M.L. and Wallimann, T. Creatine supplementation in health and disease. Effects of chronic creatine ingestion in vivo: down-regulation of the expression of creatine transporter isoforms in skeletal muscle [In Process Citation]. *Mol Cell Biochem* 1998;184:427-37.
33. Kekelidze, T., Khait, I., Togliatti, A., Benzycry, J., Mulkern, R. and Holtzman, D. Maturational changes in rabbit brain phosphocreatine and creatine kinase. *Ann N Y Acad Sci* 1999;893:309-13.
34. Murphy, R., McConell, G., Cameron-Smith, D., Watt, K., Ackland, L., Walzel, B., Wallimann, T. and Snow, R. Creatine transporter protein content, localization, and gene expression in rat skeletal muscle. *Am J Physiol Cell Physiol* 2001;280:C415-22.
35. Bittl, J.A., DeLayre, J. and Ingwall, J.S. Rate equation for creatine kinase predicts the in vivo reaction velocity: ³¹P NMR surface coil studies in brain, heart, and skeletal muscle of the living rat. *Biochemistry* 1987;26:6083-6090.
36. van Dorsten, F.A., Reese, T., van Echteld, C.J.A., Nederhoff, M.G.J. and Nicolay, K. In vivo fluxes through mitochondrial and cytoplasmic creatine kinase. ³¹P NMR of skeletal and cardiac muscle from transgenic mice. *Proc Intl Soc Mag Reson Med* 4 1996;
37. McFarland, E.W., Kushmerick, M.J. and Moerland, T.S. Activity of creatine kinase in a contracting mammalian muscle of uniform fiber type. *Biophys J* 1994;67:1912-1924.
38. Nicolay, K., van Dorsten, F.A., Reese, T., Kruiskamp, M.J., Gellerich, J.F. and van Echteld, C.J. In situ measurements of creatine kinase flux by NMR. The lessons from bioengineered mice [In Process Citation]. *Mol Cell Biochem* 1998;184:195-208.
39. van Deursen, J., Ruitenbeek, W., Heerschap, A., Jap, P., ter Laak, H. and Wieringa, B. Creatine kinase (CK) in skeletal muscle energy metabolism: a study of mouse mutants with graded reduction in muscle CK expression. *Proc Natl Acad Sci U S A* 1994;91:9091-5.
40. Saupe, K.W., Spindler, M., Tian, R. and Ingwall, J.S. Impaired cardiac energetics in mice lacking muscle-specific isoenzymes of creatine kinase. *Circ Res* 1998;82:898-907.

41. Hood, D.A., Gorski, J. and Terjung, R.L. Oxygen cost of twitch and tetanic isometric contractions of rat skeletal muscle. *Am J Physiol* 1986;250:E449-56.
42. Foley, J.M. and Meyer, R.A. Energy cost of twitch and tetanic contractions of rat muscle estimated in situ by gated ³¹P NMR. *NMR Biomed* 1993;6:32-8.
43. Roman, B.B., Wiseman, R.W., Jayaraman, R. and Meyer, R. Gated ³¹P NMR demonstrates profound energy deficit at the onset of contractions in MM creatine kinase knockout mice. *Proc Intl Soc mag Reson Med* 10 2002;1876.
44. Meyer, R.A., Brown, T.R. and Kushmerick, M.J. Phosphorus nuclear magnetic resonance of fast- and slow-twitch muscle. *Am J Physiol* 1985;248:C279-C287.
45. Kushmerick, M.J., Moerland, T.S. and Wiseman, R.W. Mammalian skeletal muscle fibers distinguished by contents of phosphocreatine, ATP, and Pi. *Proc Natl Acad Sci U S A* 1992;89:7521-5.
46. Watchko, J.F., Daood, M.J. and LaBella, J.J. Creatine kinase activity in rat skeletal muscle relates to myosin phenotype during development. *Pediatr Res* 1996;40:53-8.
47. in 't Zandt, H.J.A., Jost, C., Oerlemans, F., Klomp, D.W.J., Wieringa, B. and Heerschap, A. Brains of creatine kinase deficient mice lack phosphocreatine and exhibit an increased NAA level. *Proc Intl Soc mag Reson Med* 8 2000;174.
48. Schultz, E. and McCormick, K.M. Skeletal muscle satellite cells. *Rev Physiol Biochem Pharmacol* 1994;123:213-57.
49. Shoubridge, E.A., Bland, J.L. and Radda, G.K. Regulation of creatine kinase during steady-state isometric twitch contraction in rat skeletal muscle. *Biochim Biophys Acta* 1984;805:72-8.
50. Lee, Y.C.P. and Visscher, M.B. On the state of creatine in heart muscle. *PNAS* 1961;47:1510-1515.
51. Savabi, F. Free creatine available to the creatine phosphate energy shuttle in isolated rat atria. *Proc Natl Acad Sci USA* 1988;85:7476-7480.
52. Hochachka, P.W. and Mossey, M.K.P. Does muscle creatine phosphokinase have access to the total pool of phosphocreatine plus creatine? *Am J Physiol* 1998;274:R868-R872.
53. Kruiskamp, M.J., de Graaf, R.A., van Vliet, G. and Nicolay, K. Magnetic coupling of creatine/phosphocreatine protons in rat skeletal muscle, as studied by (1)H-magnetization transfer MRS. *Magn Reson Med* 1999;42:665-672.
54. Renema, W.K.J., Klomp, D.W.J., van den Bergh, A.J., Wieringa, B. and Heerschap, A. Off-resonance magnetization transfer of creatine in human gastrocnemius muscle studied by CW irradiation. *MAGMA* 2002;15 suppl. 1:272.
55. Kreis, R., Jung, B., Felblinger, J. and Boesch, C. Effect of exercise on the creatine resonance in 1H MR spectra of human skeletal muscle. *J Mag Reson* 1999;137:350-357.
56. Trump, M.E., Hanstock, C.C., Allen, P.S., Gheorghiu, D. and Hochachka, P.W. An (1)H-MRS evaluation of the phosphocreatine/creatine pool (tCr) in human muscle. *Am J Physiol Regul Integr Comp Physiol* 2001;280:R889-96.
57. Asslani, I., Shankland, E. and Kushmerick, M.J. Charge influences dipolar coupling interactions of lactate and alanine in skeletal muscle. *Proc Intl Soc mag Reson Med* 9 2001;329.
58. Wiseman, R.W. and Kushmerick, M.J. Creatine kinase equilibration follows solution thermodynamics in skeletal muscle. ³¹P NMR studies using creatine analogs. *J Biol Chem* 1995;270:12428-12438.

4

METABOLIC RECOVERY AFTER ISCHEMIC STRESS IS IMPAIRED IN SKELETAL MUSCLE OF MICE THAT LACK BOTH CYTOSOLIC CREATINE KINASE AND ADENYLATE KINASE

KlaasJan Renema

Edwin Janssen

Hermien Kan

Arjan Simonetti

Rene in 't Zandt

Bé Wieringa

Arend Heerschap

ABSTRACT

Creatine kinases (CK) and adenylate kinases (AK) are high-energy phosphoryl (~P) transfer enzymes with a complementary role in the homeostasis and compartmentalization of cellular energetics in tissues like muscle and brain. Here we report on the use of ^{31}P MRS at 7 T to study energy-metabolite behavior in hind-leg muscles of mice lacking both cytosolic creatine kinase (M-CK) and Adenylate Kinase (AK1) (MAK $^{-/-}$) before, during and after an ischemic challenge. Data of similar MR experiments in M-CK and AK1 single knockout mice were reevaluated and compared to MAK $^{-/-}$ mice.

During the ischemic period, both inorganic phosphate (Pi) accumulation and phosphocreatine (PCr) depletion in MAK $^{-/-}$ were faster than in wild-type mice, but total [PCr + Pi] remained constant in both types of animals. After ischemia, MAK $^{-/-}$ mice had a significant slower recovery of PCr and Pi than wild-type mice, reflecting a severely compromised phosphoryl transfer efficiency. Although basal tissue pH levels were similar, upon ischemia pH started to decline immediately in MAK $^{-/-}$ mice while in wt mice basal tissue pH was initially maintained. Therefore, MAK $^{-/-}$ mice had a lower intracellular pH during most of the ischemic period, suggesting earlier turn-on of glycolysis. As ATP levels appeared similar and were essentially homeostatic in both types of animals, our results suggest that the communication between supply-demand pathways for ~P metabolites, reflected by the pool-dynamics thereof, is deviant in MAK $^{-/-}$ mice.

INTRODUCTION

The enzymes creatine kinase (CK) and adenylate kinase (AK) play important roles in tissues with high energy demand by providing an efficient network for high-energy phosphoryl (\sim P) transfer between sites of energy production and consumption (1-5).

By catalyzing the reaction $\text{Cr} + \text{ATP} \leftrightarrow \text{phosphocreatine (PCr)} + \text{ADP} + \text{H}^+$, CKs are generally thought to act as a spatial and temporal energy buffer, and as regulator of tissue pH (1, 5). Several CK isoforms are tissue specifically expressed and located in distinct cellular compartments. In muscle, two major isoforms of CK are present, namely as dimeric MM-CK in the cytosol (representing approximately 85%-95% of total CK activity) and octameric ScCKmit in the space between the inner and outer membranes of mitochondria (representing the remaining 15-5% of CK activity) (5).

Besides CK, AK also contributes to the energy homeostasis by catalyzing the reaction $2 \text{ADP} \leftrightarrow \text{ATP} + \text{AMP}$ (6). In skeletal muscle, AK1 is the major isoform representing approximately 99% of all AK activity (7) and is present as a soluble molecule in the cytosol or as splice variant (designated AK1 β) bound to the cell membrane (8, 9). The only other AK isoform available in skeletal muscle is AK3. It is present at low activity and is in fact an enzyme which uses GTP and AMP as substrates (7). It has been shown in cardiac muscle that AK phosphotransfer is involved in regulating the response of K_{ATP} channels to metabolic changes (10). A more general function of AK may be to increase the efficiency of ATP turnover by releasing the energy that is stored in β -phosphoryls (11).

Our group has generated knockout mice lacking M-CK (M-CK $^{-/-}$ mice) (2), ScCKmit (ScCKmit $^{-/-}$ mice) (12) or both CK isoforms (M-CK/ScCKmit $^{-/-}$ mice) (13) as well as AK1 deficient mice (AK $^{-/-}$ mice) (3) to study the significance of these individual enzymes in cellular energetics. In one series of biochemical and cell biological studies (2, 3, 12, 13) we have monitored the role of the enzymes under conditions of rest and contractile force production in skeletal muscles. In an independent approach we have applied *in vivo* ^{31}P MR spectroscopy (MRS) to investigate the specific coupling of phosphotransfer reactions to ischemic stress conditions in hind-leg muscle. The focus of these studies was on the monitoring of effects of CK or AK absence on the levels of PCr, inorganic phosphate (Pi), phosphomonoesters (PME) and ATP, and on tissue pH (3, 14, 15).

Our studies (3, 16, 17) and studies of others (18-23) point to a model for muscle in which the proper maintenance of ADP/ATP ratios and transport of \sim P is safeguarded by concerted action of the CK and AK circuits and enzymes in the glycolytic pathway, with partial redundant functions of the separate enzymes. Thus a flexible network is created which

provides plasticity and enables muscle to dynamically respond to sudden and highly fluctuating metabolic challenges.

In the current paper we present new data on the effects of ischemia in muscles with combined deficiencies of the cytosolic M-CK and AK1 (MAK^{-/-} mice). Skeletal muscles of MAK^{-/-} mice (24) have only about 8% of the CK activity remaining (attributable to ScCKmit activity in mitochondria), whilst β -ATP turnover due to AK has decreased by 85% (remaining activity is due to combined activities of AK3 and nucleoside diphosphokinases) (24). Based on these observations, phosphotransfer in MAK^{-/-} muscle was expected to rely heavily on glycolytic activity. We demonstrate here that this led to a situation in which recovery of PCr and Pi levels upon termination of ischemic stress was dramatically delayed, a phenomenon that was never observed in single mutant M-CK^{-/-} or AK^{-/-} mice.

MATERIALS AND METHODS

Animals

MAK^{-/-} mice were compared to wild-type (wt) animals of the same mixed genetic background (50% C57BL/6 and 50% 129 Ola) and age (3-4 months). All animals were anesthetized using 1-2 % isoflurane in a gas mixture of 50% O₂ and 50% N₂O delivered through a facemask, while the breathing frequency was monitored. Rectal temperature was monitored during the experiments using a fluoroptic thermometer (Luxtron 712, Santa Clara, California, USA) and maintained at 36.8±0.5 °C using a warm water circuit. Experiments were in accordance with rules of the local animal ethics committee.

MR equipment and methods

The experiments were performed on a horizontal 7.0 T magnet (MagneX Scientific, Abingdon, England) with a free bore size of 120 mm. The MR probe consisted of two coils: a ¹H Alderman-Grant type of coil (25) for shimming and a 3-turn 9 mm solenoid coil for ³¹P acquisition which were interfaced to a S.M.I.S spectrometer (Surrey Medical Systems, Guildford, England) operating at 300 MHz for ¹H and at 122 MHz for ³¹P. All ³¹P MR spectra were obtained using a pulse-acquire sequence. As the gastrocnemius has the largest volume of the mouse hind-leg calf muscles, this muscle contributed most to the signal intensity in ³¹P MR spectra.

Firstly, to get an overview of basal metabolite ratios and tissue pH, ³¹P MR spectra were obtained with low temporal resolution but with a good signal-to-noise ratio (SNR) from six MAK^{-/-} and six wt mice during resting conditions (TR=7 s, 128 averages). Furthermore, fully relaxed spectra (TR=25 s, 64 averages) and spectra with the same repetition time as during ischemia (TR=1400 ms, 512 averages) were acquired in six wt animals to correct PCr and Pi metabolite ratios for T₁ saturation. Since it is unlikely that T₁ values of PCr and Pi will be different in MAK^{-/-} mice compared to wt animals, the T₁ correction factors derived in this way were applied to both wt and knock-out animals.

Ischemic occlusion of skeletal muscle was applied in a separate group of eight MAK^{-/-} and eight wt mice by clamping with a diaphragm plate, which allowed reversible and reproducible obstruction of blood flow through the hind limb (26, 27). Spectra were obtained with high temporal resolution (106 s) using a pulse-acquire sequence (TR=1400ms, 76 averages). After four reference spectra were acquired, an ischemic period of 25 minutes was applied (14 spectra), succeeded by a recovery period of 16 minutes (9 spectra).

Data processing

Data was processed in the time domain using the AMARES method from the MRUI software package (28). When processing the basal spectra, no prior knowledge was used. Signal intensities were fitted assuming Lorentzian lineshape functions and are presented as ratio to the fit of the β -ATP signal.

For the spectra acquired during the ischemia protocol, Pi and PME were constrained during the fit by setting the linewidths of these signals 1.5 times to the linewidth of PCr, which was determined empirically from spectra during ischemia which have higher Pi and PME signal intensities. The individual fitted signals and residues were evaluated and metabolite values from obvious wrong fits (i.e. when the signal could not be fitted or was fitted at a wrong frequency), especially from low SNR signals like PME and sometimes Pi, were discarded. All metabolite signals measured were normalized per mouse to the mean value of the four β -ATP signal integrals measured before applying the ischemic clamp in the same mouse (β -ATP₀).

Although our ischemia protocol was designed to induce ischemia without moving the hind leg by clamping with a diaphragm plate, small changes in position of the hind leg did lead to small alterations in line shape. This, in turn, could lead to errors in the quantification. Therefore, changes in lineshape during ischemia were corrected for by using the assumption that the total ATP signal during the first 3.5 min. of ischemia did not change from resting values.

In all experiments the tissue pH was calculated from the shift in resonance position (S) of the Pi signal compared to the resonance position of PCr (29) using the equation $\text{pH}=6.75 + \log((3.27-S)/(S-5.63))$. ADP levels were calculated assuming that the CK reaction was at equilibrium, with a equilibrium constant of $K=1.66 \cdot 10^9$ (30). Previously, tissue ATP values in hind-leg skeletal muscle of this wt mouse strain were calculated from in vivo MRS data to be 7.8 ± 0.08 mM (27), and MAK^{-/-} mice were assumed to have equal in vivo ATP levels. Furthermore, a fraction of 0.73 for intracellular water was assumed to calculate intracellular ATP (31, 32). Cr levels, also necessary for the calculation of ADP concentrations, were derived from the PCr/ATP levels and the measurement that during resting conditions 74 ± 4 % of the total Cr pool is phosphorylated in these wt mice (27). During the ischemia protocol, however, the percentage of the phosphorylated Cr pool changes. Therefore, the concentration of the total Cr pool (41.8 ± 2.7 mmol per l intracellular water) was used to calculate ADP levels in these experiments (27).

Analysis of time constants

A monoexponential function was fitted (15, 33) to the recovery profile of PCr and Pi using a non-linear least square method with a Levenberg-Marquardt algorithm (GraphPad Prism, San Diego CA, USA). This fit yielded a time constant for signal recovery (τ) for PCr (τ_{PCr}) and Pi (τ_{Pi}). No constraints were applied other than fixing the begin time of the exponential to the start point of recovery.

Reevaluation of M-CK-/- and AK-/- data

To provide a complete overview of the implications of knocking out M-CK, AK or both, data of M-CK -/- (n=6) (15) and AK-/- (n=9) (3) mice, together with wt animals for both knockouts (n=6 and n=10 for comparison with M-CK-/- and AK-/-, respectively) were reevaluated in light of the current results. Several additional plots were generated, including Pi/ATP_0 and $(\text{PCr} + \text{Pi})/\text{ATP}_0$ in AK-/- mice and Pi/PCr in both M-CK-/- and AK-/- mice. Furthermore, τ_{Pi} and τ_{PCr} were calculated in AK-/- mice and recalculated in M-CK-/- mice using identical algorithms as in AK-/- and MAK-/- mice. Because the M-CK-/- mice were measured on a MR scanner with a vertical bore magnet and different occlusion system than the AK-/- and MAK-/- mice, time constants of recovery are not compared quantitatively between different knockouts. Instead, every knockout is compared to the wt group measured in the same study.

Although temporal resolution in the ischemic experiments of M-CK-/- mice was somewhat lower, the ischemic period and the observation period for recovery are of equal length in all three experiments (25 min and 16 min, respectively). For easy comparison, $t=0$ is set at the start of ischemia in all time curves at the same vertical position.

Statistics

A student t-test was used to test differences in metabolite levels between wt and MAK-/- mice for significance before ischemia or at specific time points. Differences in τ between wt and knockout mice, but also between the different wt mice used as control for the M-CK-/-, AK-/- and MAK-/- mice, were tested for significance using an F-test (GraphPad Prism, San Diego CA, USA). Differences were considered significant when $p < 0.05$. Data is presented as mean \pm SEM unless stated otherwise.

RESULTS

MAK^{-/-} and wt mice at resting conditions

Basal ³¹P MR spectra of mouse hind-leg muscle at resting conditions (as given for MAK^{-/-} muscle in Figure 1a) showed resonances for PCr, Pi and three resonances for the three phosphate groups of ATP. In some cases a signal of very low intensity for PME could be distinguished in the reference spectra.

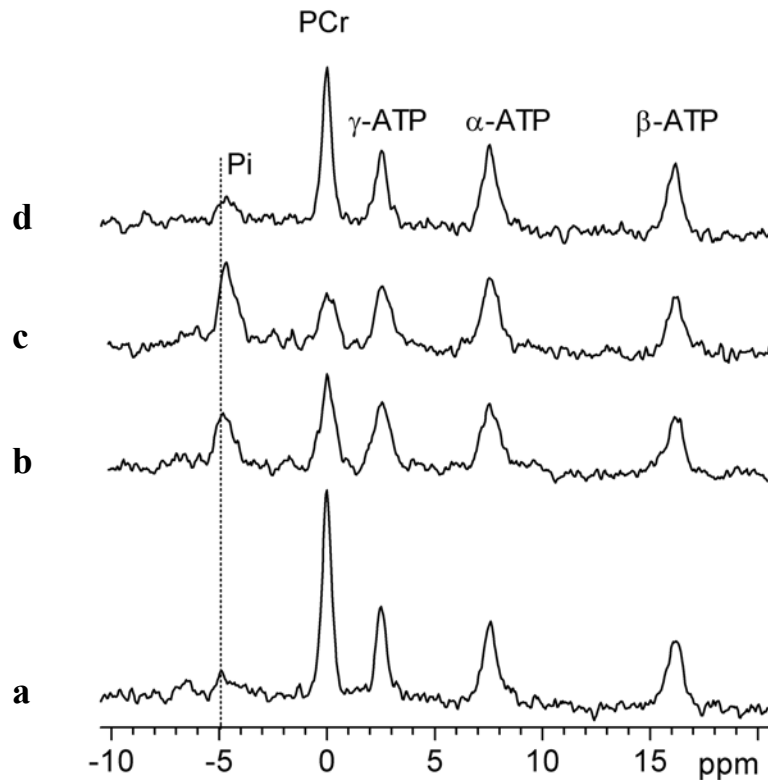


Figure 4.1: representative spectra of MAK^{-/-} hind-leg muscle before (a), during (at 10 min. (b) and 25 min. (c)) and at 15 min. after (d) the period of ischemia.

At a repetition time of 25 seconds, ³¹P MR spectra were assumed to be fully relaxed at 7 T. Measurement of the same wt mouse at resting conditions with TR of 1400 ms, 7 s and 25 s enabled the estimation of T₁ saturation factors necessary to correct for partial saturation at TR of 1400 ms and 7s. T₁ correction factors for PCr/ATP are 1.8 ± 0.1 and 1.09 ± 0.07 , and for Pi/ATP are 2.3 ± 0.7 and 1.6 ± 0.7 for TR=1400 ms and TR=7 s, respectively.

The ratio of the PCr and Pi signal to the β-ATP signal, and the Pi / PCr ratio itself, appeared to be similar in MAK^{-/-} and wt mice since t-tests showed no significant differences (table 4.1). Also no significant differences could be determined in tissue pH, or the ADP concentration (calculated from the CK equilibrium reaction; table 4.1) between these mice.

Table 4.1: Ratios of integral values of phosphorous metabolite signals.

	PCr/ATP ^a	Pi/ATP ^a	Pi/PCr ^a	ADP (mmol/l) ^b	pH
wt	2.9 ± 0.4	0.48 ± 0.11	0.16 ± 0.02	0.040 ± 0.003	7.24 ± 0.04
MAK ^{-/-}	3.0 ± 0.3	0.50 ± 0.12	0.17 ± 0.04	0.040 ± 0.003	7.24 ± 0.04

All values are presented as mean ± s.d.

^a T_1 corrected values acquired at a repetition time of 7 s.

^b ADP value is expressed as mmol/(l intracellular water), and calculated using the equilibrium CK reaction (see materials and methods for details).

Ischemia of hind-leg muscle

During ischemia, we observed a pronounced decrease for both mice in the signal of PCr. Concomitantly, the signal of Pi increased and shifted slightly towards the PCr signal due to a lower pH (figure 4.1). PME levels also increased during the ischemic period, however, the SNR remained low in MAK^{-/-} and wt animals. After the challenge, the signal intensities returned to their original values (figure 4.1d).

Fitting of the PCr and Pi signals at various time points before, during and after ischemia revealed remarkable differences between MAK^{-/-} and wt mice (figures 4.2, 4.3) in comparison to previously reported findings in M-CK^{-/-} and AK^{-/-} single knockout mice. Towards the end of the ischemic period, PCr levels were significantly lower in MAK^{-/-} mice than in wt animals. Pi levels showed the opposite tendency (figure 4.3c). Differences between MAK^{-/-} and wt animals became even more apparent when looking at the ratio of Pi / PCr (figure 4.4), which is a measure for the energetic status of the muscular tissue (34, 35). During the ischemic period, Pi / PCr ratios increased rapidly in MAK^{-/-} mice and much more slowly in wt animals (figure 4.4c) while the total PCr and Pi pool remained constant (figure 4.5).

In wt animals, tissue pH first stayed at basal levels during the first 10 minutes of the ischemic interval (figure 4.6c), but declined at a constant rate during the entire period thereafter. In MAK^{-/-} mice, tissue pH started to decline earlier, however, pH subsequently decreased during the ischemic period with a slope similar to that in wild-types. This created a situation in which, from a fixed time point in the ischemic period onwards (approximately at t = 5 min and beyond), tissue pH became significantly lower in MAK^{-/-} mice (figure 4.6).

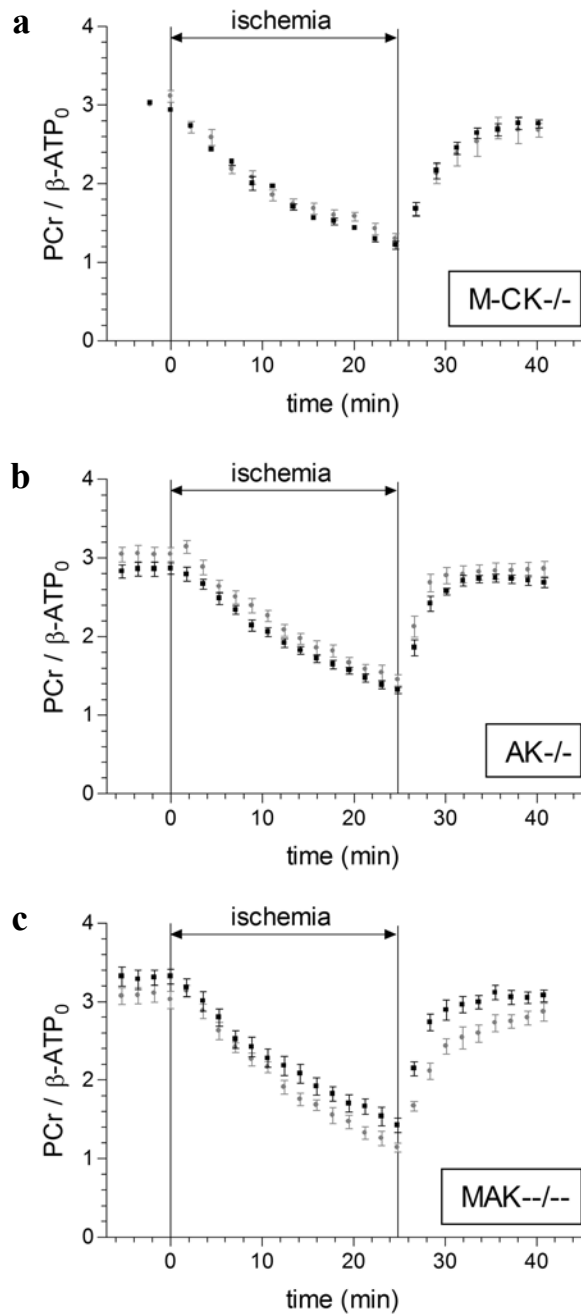


Figure 4.2: time plots of PCr signal intensities normalized to the β -ATP signal before, during and after ischemia in the hind leg of M-CK-/- (a), AK-/- (b) and MAK-/-/- (c) mice and their wt controls. Knock-outs are presented by grey dots, wt mice are presented by black squares.

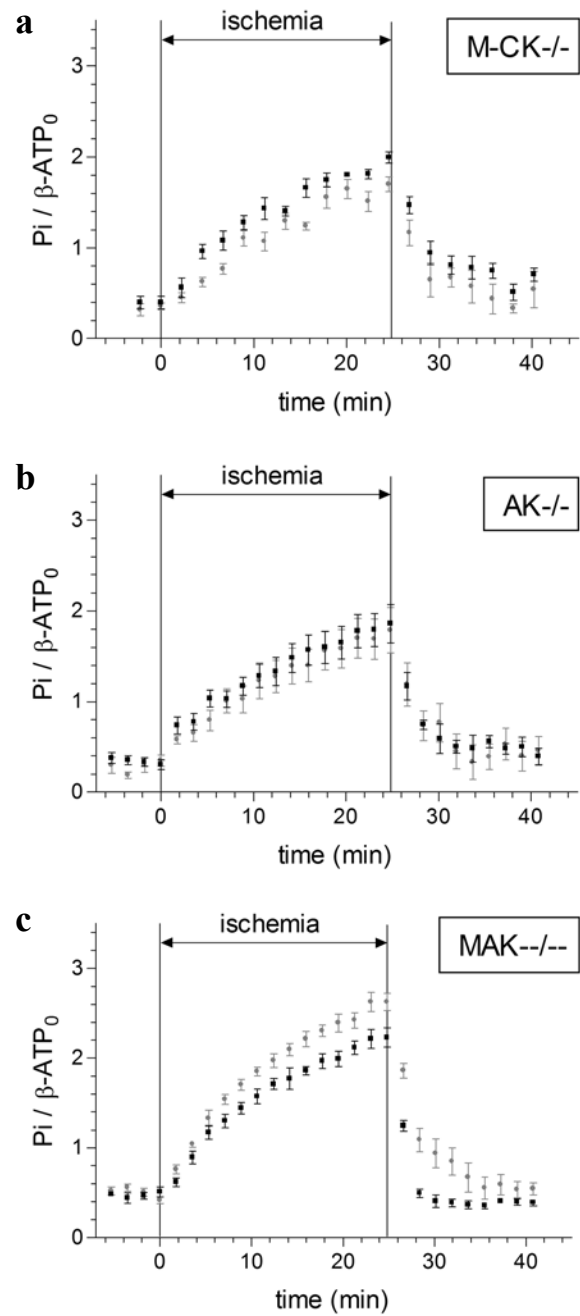


Figure 4.3: time plots of Pi signal intensities normalized to the β -ATP signal before, during and after ischemia in the hind leg of M-CK-/- (a), AK-/- (b) and MAK-/-/- (c) mice and their wt controls (for annotations see figure 4.2).

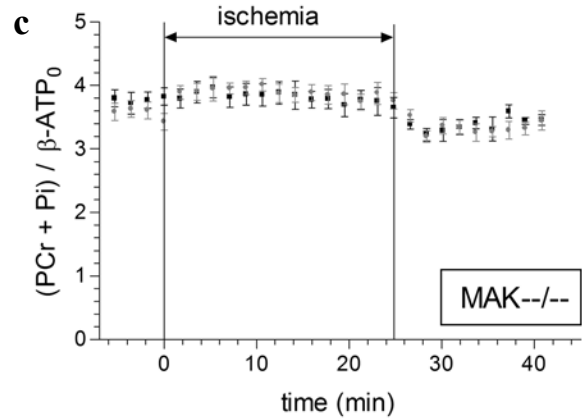
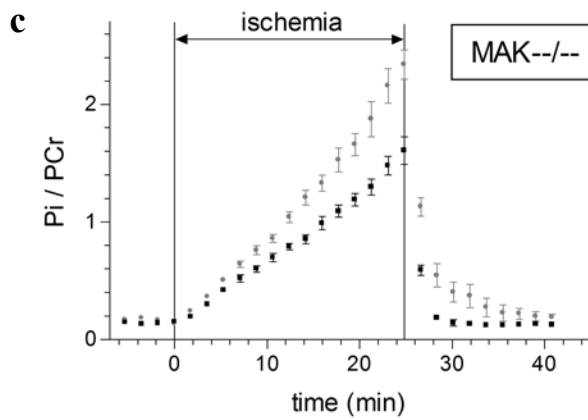
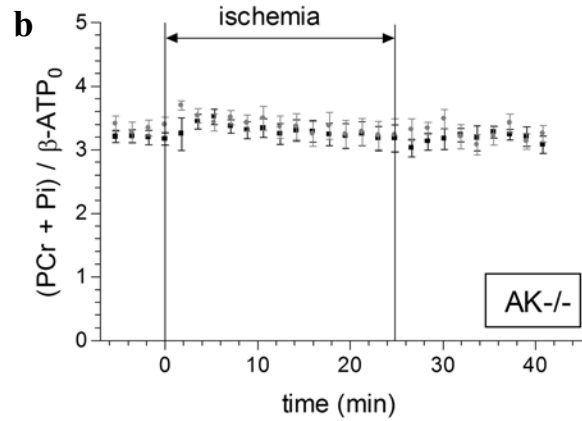
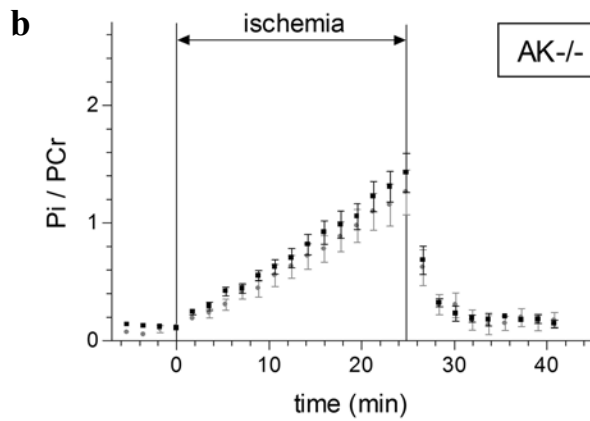
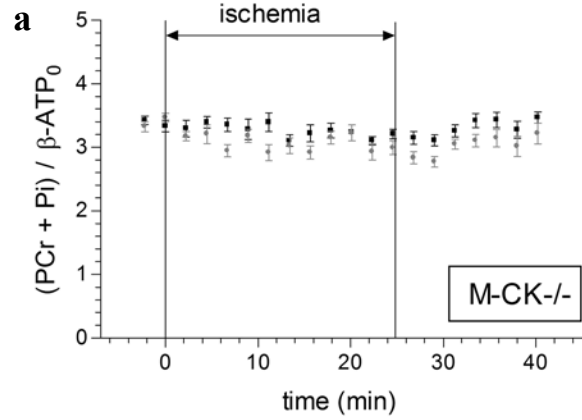
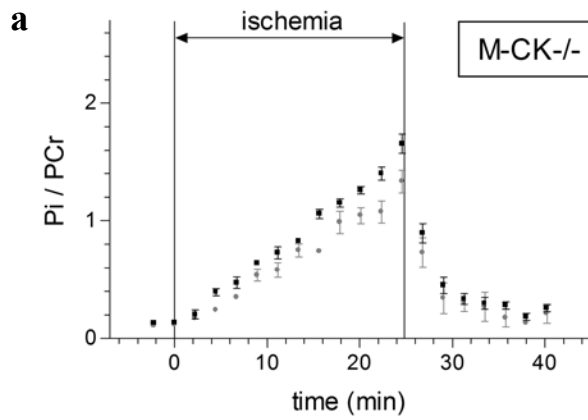


Figure 4.4: time plots of Pi/PCr before, during and after ischemia in the hind leg of M-CK^{-/-} (a), AK^{-/-} (b) and MAK^{-/-} (c) mice and their wt controls (for annotations see figure 4.2).

Figure 4.5: time plots of PCr + Pi intensities normalized to the β -ATP signal before, during and after ischemia in the hind leg of M-CK^{-/-} (a), AK^{-/-} (b) and MAK^{-/-} (c) mice and their wt controls (for annotations see figure 4.2).

ADP concentrations were calculated from the CK reaction (assuming this reaction to be at equilibrium) and, just as PME levels, did not show differences between wt and MAK^{-/-} mice before, during or after ischemia (data not shown). At the end of the ischemic period ADP increased to 0.13 ± 0.05 mmol/(l intracellular water) and 0.15 ± 0.03 mmol / (l intracellular water) for wt and MAK^{-/-} mice, respectively. Finally, ATP levels remained, as expected, constant in both wt and MAK^{-/-} mice during ischemia (data not shown).

Recovery of ischemia

When releasing the ischemic clamp, a pronounced and significantly slower recovery of the PCr pool was observed in MAK^{-/-} mice (figure 4.2c), with time constants of recovery of 2.7 ± 0.4 min and 4.5 ± 0.7 min in wt and MAK^{-/-} mice, respectively (table 4.2). The recovery of the Pi signal was also significantly slower in MAK^{-/-} mice (3.2 ± 0.5 min) compared to wt mice (1.9 ± 0.2 min). These results are in contrast to PCr and Pi recovery in M-CK^{-/-} and AK^{-/-} mice, which show no differences in recovery of PCr with respect to their wt controls (Figures 4.2a,b 4.3a,b). Recovery of the Pi / PCr ratios was, like recovery of the Pi and PCr levels, slower in MAK^{-/-} mice. In both M-CK^{-/-} and AK^{-/-} single knockout mice, the Pi / PCr ratio was similar to that in wt animals before and during the ischemic period and during the recovery thereafter.

Table 4.2: time constants for signal recovery (τ) after ischemia of PCr/ATP₀ and Pi/ATP₀ (min).

	wt	M-CK ^{-/-}	wt	AK ^{-/-}	wt	MAK ^{-/-}
τ_{PCr}	5.3 ± 0.8	5.8 ± 1.7	2.8 ± 0.3	2.3 ± 0.4	2.7 ± 0.4	4.6 ± 0.7 *
τ_{Pi}	3.7 ± 0.7	3.4 ± 1.1	2.4 ± 0.5	2.9 ± 1.0	1.9 ± 0.2	3.2 ± 0.5 **

Recovery rates are presented as fitted value \pm SEM.

M-CK^{-/-}: mouse lacking cytosolic M-CK; AK^{-/-}: mice lacking AK1 ; MAK^{-/-}: mice lacking both M-CK and AK1; wt: wild type animals.

Note: every knockout mouse has to be compared to wt controls measured in the same experiment (see text for details).

* significantly different ($p < 0.02$) from wt animals.

** significantly different ($p < 0.01$) from wt animals.

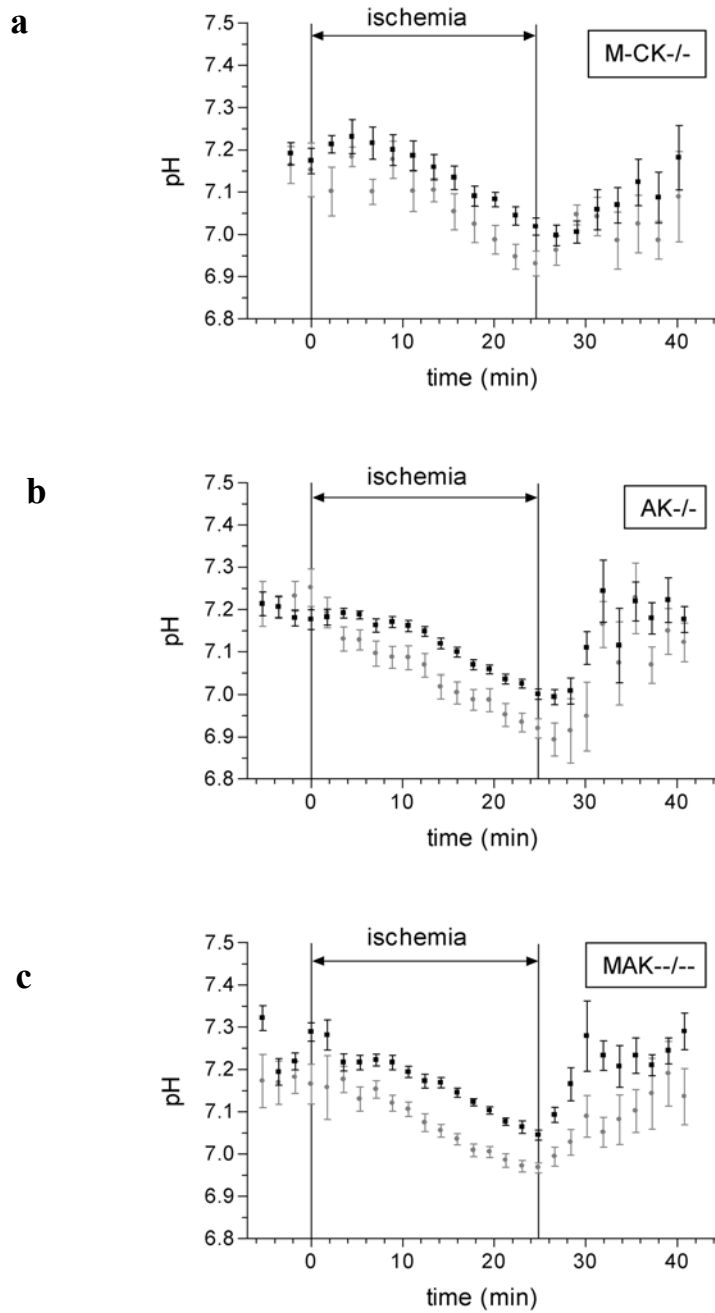


Figure 4.6: profiles of changes in tissue pH before, during and after ischemia in M-CK-/- (a), AK-/- (b) and MAK-/- (c) mice and their wt controls (for annotations see figure 4.2).

DISCUSSION

In the present study we showed that knocking out both cytosolic CK and AK1 enzymes does not have any influence on the resting levels of high-energy phosphoryl ratios in skeletal muscle. Nevertheless, it had a profound effect on the rate of recovery of high-energy phosphoryl levels after an ischemic challenge, something that was not observed before in MRS studies of single M-CK and AK1 knockout mice. Therefore, the current results confirm earlier findings from *ex vivo* and *in vitro* studies suggesting that CK and AK can work in concert, fulfilling partially redundant overlapping functions in the communication between \sim P pools.

Muscles of MAK^{-/-} mice appear normal under resting conditions *in vivo*

Our *in vivo* data presented here are in good agreement with biochemical measurements reported elsewhere (24), and showed that hind-leg muscles which lack two of the major enzymes involved in balancing high-energy phosphates have fully normal phosphate-metabolite ratios (PCr/ATP and Pi/ATP) and intracellular tissue pH when kept under conditions where blood circulation is normal and muscle activity is low. Although MR spectroscopy does not provide an absolute quantification of the level of ATP, our current findings provide strong evidence for global ATP levels being entirely normal in MAK^{-/-} muscle, because Pi/PCr ratios in MAK^{-/-} and wt mice were also identical.

Metabolic stress by means of ischemia

Since, during resting conditions, no overt differences were revealed between MR spectra of MAK^{-/-} and wild-type muscles we challenged the phosphotransfer circuit in these muscles by means of reversible ischemia of the whole hind-leg. To understand the effect of such a challenge on phosphorous metabolites in time, it is important to distinguish two distinct phases in the protocol. One phase starts immediately after muscle clamping and involves the relatively slow progression towards complete ischemia. Oxygen in the muscles rapidly decreases (36) but also entrance of nutrients into the muscle and drainage of waste products are blocked. The other relevant phase is that of recovery after the ischemic period (see below). Because an ischemia-reperfusion protocol is physiologically different from a protocol in which muscles are stimulated to contract, like used in the study of Janssen et al. (24), it is difficult to compare our results directly to these previous findings. However, direct comparison to other MRS studies on ischemia in M-CK^{-/-} and AK^{-/-} single knockout mice (3, 15) is possible.

Here we observed that the PCr signal dropped to significantly lower values in MAK^{-/-} mice than in wt animals during the ischemic period. Studies of M-CK^{-/-} mice already had indicated that in muscle with only ScCKmit the PCr energy buffer can still be fully utilized (15). Although knocking out AK itself did not have any effect on the rate of PCr depletion during ischemic stress ((3) and figure 4.2), it has an effect if tested in combination with M-CK deficiency. This is demonstrated by the higher rate of Pi formation and the reciprocal increase in PCr utilization, with unaltered values for the [PCr + Pi] pool (figure 4.5). Imbalance in ATP levels could theoretically underlie our results as both PCr and Pi levels (figures 4.2,4.3) are normalized to ATP. Direct comparison of ATP signal intensities, however, showed that ATP values remained essentially constant, whereas the Pi/PCr ratio showed significant elevation during the experiment (figure 4.5). This strongly suggests that the enhanced rates of [Pi] and [PCr] changes are genuine. The increase in Pi accumulation in MAK^{-/-} mice during the ischemic interval can therefore be best explained by a balanced PCr breakdown. Additionally, we cannot rule out differences in mitochondrial and cytosolic pool sizes, or differences in coupling between glycolytic and mitochondrial activity, between MAK^{-/-} and wt animals. The fact that ADP levels seem to be homeostatic can be explained by a higher glycolytic rate in MAK^{-/-} animals.

Compromised recovery from ischemic stress in MAK^{-/-} mice

Recovery is a relatively fast process compared to events during the phase of ischemia. Restoration of blood circulation causes myoglobin saturation to reach pre-ischemia levels almost instantaneously (36). PCr recovers quickly, due to mitochondrial ATP production, which also contributes to normalizing pH and Pi levels.

Still, the recovery of PCr and Pi after ischemia was much slower in MAK^{-/-} mice than in single knockout M-CK^{-/-} and AK^{-/-} mice. Both MAK^{-/-} and M-CK^{-/-} mice fully rely for their PCr recovery on the mitochondrial isoform of CK, with a remaining CK activity which is low in muscles of both mice (in the order of 2-8% (24, 37)). Thus, the relative slower recovery in MAK^{-/-} mice must be due to an indirect effect of AK1 deficiency on the activation of flux through the mitochondrial CK-PCr circuit. The recovery of PCr levels after exercise is assumed to be a measure of mitochondrial capacity in skeletal muscle (e.g. Kemp et al. (38)). If we may compare effects of ischemia and exercise, these results would imply a decreased mitochondrial capacity in MAK^{-/-} mice. This is in contrast to reported findings in isolated skeletal muscle, which suggest the opposite, namely an up-regulation of this capacity in MAK^{-/-} muscles (24) (corroborated by an increase in mitochondrial volume; data not shown). An alternative explanation would be that the PCr output by ScCKmit activity necessary for reactivation is firstly and primarily directed towards protection of

compartmentalized homeostasis of ATP and reactivation of primary mitochondrial functions. This, or mitochondrial coupling, may differ in MAK^{-/-} animals. Therefore, the kinetic and qualitative aspects of these reactions would overrule effects of mitochondrial capacity on PCr replenishment and would therefore take longer in muscles with the most profoundly compromised local ATP/ADP ratios and/or ~P pool distributions, i.e. in MAK^{-/-} muscles which have undergone the most extensive cytoarchitectural adaptations. Although global ADP ratios calculated from the CK equilibrium reaction were not different between MAK^{-/-} and wt mice (table 2), local changes in ATP/ADP ratios or cellular ATP gradients across the cytosol may go unnoticed in MR spectroscopy. It is therefore very well possible that reaction pathway preferences may become only visible as a delayed response in PCr and Pi signal recovery upon the sudden release of the ischemic clamp, associated with fast changes in oxygen and metabolite supply. Also other explanations are possible. Other factors, like the deviant pH at the end of the ischemic period (see below), may also have influenced the recovery rate (39, 40). In our previous studies we did, however, not observe similar effects in AK^{-/-} mice, which also show a lower pH compared to wt animals at the end of the ischemic period. Combined, our previous and present results demonstrate that AK presence affects the mitochondrial ScCKmit mediated Cr ↔ PCr reaction and helps in preserving normal ~P levels after an metabolic challenge.

The role of AK in maintaining tissue pH

No differences in basal tissue pH were observed between MAK^{-/-} and wt mice. This is in agreement with the fact that basal lactate concentrations were the same in MAK^{-/-} mice and wt (24), although this does not necessarily imply a similarity in glycolytic flux (41). After the onset of ischemia, pH started declining due to an increase in net proton production. This acidification started earlier in MAK^{-/-} than in wt mice, but thereafter occurred at similar rate in both animals. Changes in pH can be attributed to anaerobic glycolysis and/or ATPase activity, or to PCr hydrolysis, main reactions which produce or consume protons, respectively (41, 42). There is no a-priori reason why ATPase activity would differ between wt and MAK^{-/-} mice. We therefore assume that effects of anaerobic glycolysis will become dominant and explain the larger decrease in tissue pH during the period of full ischemia. Once ischemia is complete, the magnitude of H⁺ production is most likely solely driven by energy demand, explaining why the rate of acidification has similar characteristics in wt and knockout muscle, despite the possible differences in glycolytic capacity between MAK^{-/-} and wt muscles (24). Feedback inhibition of [H⁺] on glycolysis could also result in a similar tissue pH course during ischemia, only with a time delay (43).

Study of exercise as a metabolic challenge demonstrated that changes in pH level and shifts in glycolytic flux need not always be exactly synchronized, due to interfering effects of switches between aerobic-anaerobic glycolysis, and the CK-PCr reaction proper (42). Differential initial use of the CK reaction and/or shifts in the flux ratio through CK and glycolytic pathways, may therefore explain the earlier onset of acidification in MAK^{-/-} muscle.

In summary, in previous studies we have shown that metabolic and cytoarchitectural adaptations, including changes in mitochondrial volume, have a role in masking the effects of mutation in AK1 and M-CK mutant mice. Although M-CK^{-/-}, AK1^{-/-} and MAK^{-/-} mice each have a distinctly altered glycolytic and mitochondrial capacity, a systematic comparison of how mutation type correlates with the nature and extend of individual macromolecular changes has not been done. We conclude here, from the differential metabolic responses during the onset of ischemia and the phase of recovery, that also the distribution of phosphometabolites ATP, PCr and Pi over subcellular pools and the communication between cytosolic and mitochondrial reactions must be distinctly correlated with genotype. Explaining how adaptational changes in the “macromolecular world” (i.e. the proteome) and the “micromolecular world” (i.e. the metabolome) are reciprocally connected is a challenge for future research.

ACKNOWLEDGEMENTS

The study was supported by the Netherlands Organization for Scientific Research (NWO-ZONMW).

REFERENCES

1. Wyss, M. and Kaddurah-Daouk, R. Creatine and creatinine metabolism. *Physiol Rev* 2000;80:1107-213.
2. van Deursen, J., Heerschap, A., Oerlemans, F., Ruitenbeek, W., Jap, P., ter Laak, H. and Wieringa, B. Skeletal muscles of mice deficient in muscle creatine kinase lack burst activity. *Cell* 1993;74:621-31.
3. Janssen, E., Dzeja, P.P., Oerlemans, F., Simonetti, A.W., Heerschap, A., de Haan, A., Rush, P.S., Terjung, R.R., Wieringa, B. and Terzic, A. Adenylate kinase 1 gene deletion disrupts muscle energetic economy despite metabolic rearrangement. *Embo J* 2000;19:6371-81.
4. Dzeja, P.P. and Terzic, A. Phosphotransfer reactions in the regulation of ATP-sensitive K⁺ channels. *Faseb J* 1998;12:523-9.
5. Wallimann, T., Wyss, M., Brdiczka, D., Nicolay, K. and Eppenberger, H.M. Intracellular compartmentation, structure and function of creatine kinase isoenzymes in tissues with high and fluctuating energy demands: the phosphocreatine circuit for cellular energy homeostatis. *Biochem J* 1992;281:21-40.
6. Atkinson, D.E. Adenylate control and the adenylate energy charge. in: *Cellular energy metabolism and its regulation*. New York: Academic press: 1977. 85-107
7. Tanabe, T., Yamada, M., Noma, T., Kajii, T. and Nakazawa, A. Tissue-specific and developmentally regulated expression of the genes encoding adenylate kinase isozymes. *J Biochem (Tokyo)* 1993;113:200-7.
8. Collavin, L., Lazarevic, D., Utrera, R., Marzinotto, S., Monte, M. and Schneider, C. wt p53 dependent expression of a membrane-associated isoform of adenylate kinase. *Oncogene* 1999;18:5879-88.
9. Janssen, E.E.W., Kuiper, J., Hodgson, D., Zingman, L.V., Alekseev, A.E., Terzic, A. and Wieringa, B. Two structurally distinct and spatially compartmentalized adenylate kinases are expressed from the AK1 gene in mouse brain. *Mol Cell Biochem* 2004;256-257:59-72.
10. Carrasco, A.J., Dzeja, P.P., Alekseev, A.E., Pucar, D., Zingman, L.V., Abraham, M.R., Hodgson, D., Bienengraeber, M., Puceat, M., Janssen, E., Wieringa, B. and Terzic, A. Adenylate kinase phosphotransfer communicates cellular energetic signals to ATP-sensitive potassium channels. *Proc Natl Acad Sci U S A* 2001;98:7623-8.
11. Janssen, E.E.W. *The role of Adenylate kinase 1 in energy transfer: a study of mice lacking adenylate kinase 1*. Nijmegen: University of Nijmegen; 2003.
12. Steeghs, K., Heerschap, A., de Haan, A., Ruitenbeek, W., Oerlemans, F., van Deursen, J., Perryman, B., Pette, D., Bruckwilder, M., Koudijs, J., Jap, P. and Wieringa, B. Use of gene targeting for compromising energy homeostasis in neuro-muscular tissues: The role of sarcomeric mitochondrial creatine kinase. *J Neurosci Methods* 1997;71:29-41.
13. Steeghs, K., Benders, A., Oerlemans, F., de Haan, A., Heerschap, A., Ruitenbeek, W., Jost, C., van Deursen, J., Perryman, B., Pette, D., Bruckwilder, M., Koudijs, J., Jap, P., Veerkamp, J. and Wieringa, B. Altered Ca²⁺ responses in muscles with combined mitochondrial and cytosolic creatine kinase deficiencies. *Cell* 1997;89:93-103.
14. Simonetti, A.W., Janssen, E.E.W., in 't Zandt, H.J.A., Oerlemans, F., Wieringa, B. and Heerschap, A., Effect of ischemia on skeletal muscle in wildtype mice and mice lacking adenylate kinase monitored by ³¹P-MRS, in "ISMRM 7th Sci meeting, Philadelphia, 1999.
15. in 't Zandt, H.J., Oerlemans, F., Wieringa, B. and Heerschap, A. Effects of ischemia on skeletal muscle energy metabolism in mice lacking creatine kinase monitored by in vivo ³¹P nuclear magnetic resonance spectroscopy. *NMR Biomed* 1999;12:327-34.
16. de Groof, A.J., Oerlemans, F.T., Jost, C.R. and Wieringa, B. Changes in glycolytic network and mitochondrial design in creatine kinase-deficient muscles. *Muscle Nerve* 2001;24:1188-96.
17. Janssen, E., de Groof, A., Wijers, M., Fransen, J., Dzeja, P.P., Terzic, A. and Wieringa, B. Adenylate kinase 1 deficiency induces molecular and structural adaptations to support muscle energy metabolism. *J Biol Chem* 2003;278:12937-45.
18. Dzeja, P.P., Redfield, M.M., Burnett, J.C. and Terzic, A. Failing energetics in failing hearts. *Curr Cardiol Rep* 2000;2:212-7.

19. Dzeja, P.P., Zeleznikar, R.J. and Goldberg, N.D. Adenylate kinase: kinetic behavior in intact cells indicates it is integral to multiple cellular processes. *Mol Cell Biochem* 1998;184:169-82.
20. Savabi, F. Interaction of creatine kinase and adenylate kinase systems in muscle cells. *Mol Cell Biochem* 1994;133-134:145-52.
21. Zeleznikar, R.J., Dzeja, P.P. and Goldberg, N.D. Adenylate kinase-catalyzed phosphoryl transfer couples ATP utilization with its generation by glycolysis in intact muscle. *J Biol Chem* 1995;270:7311-9.
22. Zeleznikar, R.J., Heyman, R.A., Graeff, R.M., Walseth, T.F., Dawis, S.M., Butz, E.A. and Goldberg, N.D. Evidence for compartmentalized adenylate kinase catalysis serving a high energy phosphoryl transfer function in rat skeletal muscle. *J Biol Chem* 1990;265:300-11.
23. Veksler, V.I., Kuznetsov, A.V., Anflous, K., Mateo, P., van Deursen, J., Wieringa, B. and Ventura-Clapier, R. Muscle creatine kinase-deficient mice. II. Cardiac and skeletal muscles exhibit tissue-specific adaptation of the mitochondrial function. *J Biol Chem* 1995;270:19921-9.
24. Janssen, E., Terzic, A., Wieringa, B. and Dzeja, P.P. Impaired intracellular energetic communication in muscles from creatine kinase and adenylate kinase (M-CK/AK1) double knock-out mice. *J Biol Chem* 2003;278:30441-9.
25. Alderman, D.W. and Grant, D.M. An efficient decouple coil design which reduces heating in conductive samples in superconducting spectrometers. *J Magn Reson* 1979;36:447-451.
26. Heerschap, A., Sommers, M.G., in 't Zandt, H.J., Renema, W.K., Veltien, A.A. and Klomp, D.W. Nuclear magnetic resonance in laboratory animals. *Methods Enzymol* 2004;385:41-63.
27. in 't Zandt, H.J., de Groof, A.J., Renema, W.K., Oerlemans, F.T., Klomp, D.W., Wieringa, B. and Heerschap, A. Presence of (phospho)creatine in developing and adult skeletal muscle of mice without mitochondrial and cytosolic muscle creatine kinase isoforms. *J Physiol* 2003;548:847-58.
28. <http://www.mrui.uab.es/mrui/>
29. Moon, R.B. and Richards, J.H. Determination of intracellular pH by ³¹P magnetic resonance. *J Biol Chem* 1973;248:7276-8.
30. Veech, R.L., Lawson, J.W., Cornell, N.W. and Krebs, H.A. Cytosolic phosphorylation potential. *J Biol Chem* 1979;254:6538-47.
31. Forsberg, A.M., Nilsson, E., Werneman, J., Bergstrom, J. and Hultman, E. Muscle composition in relation to age and sex. *Clin Sci (Lond)* 1991;81:249-56.
32. Sjogaard, G. and Saltin, B. Extra- and intracellular water spaces in muscles of man at rest and with dynamic exercise. *Am J Physiol* 1982;243:R271-80.
33. Meyer, R.A. A linear model of muscle respiration explains monoexponential phosphocreatine changes. *Am J Physiol* 1988;254:C548-C553.
34. Chance, B., Leigh, J.S., Jr., Kent, J., McCully, K., Nioka, S., Clark, B.J., Maris, J.M. and Graham, T. Multiple controls of oxidative metabolism in living tissues as studied by phosphorus magnetic resonance. *Proc Natl Acad Sci U S A* 1986;83:9458-62.
35. Chance, B., Eleff, S., Leigh, J.S., Jr., Sokolow, D. and Sapega, A. Mitochondrial regulation of phosphocreatine/inorganic phosphate ratios in exercising human muscle: a gated ³¹P NMR study. *Proc Natl Acad Sci U S A* 1981;78:6714-8.
36. Marcinek, D.J., Schenkman, K.A., Ciesielski, W.A. and Conley, K.E. Mitochondrial coupling in vivo in mouse skeletal muscle. *Am J Physiol Cell Physiol* 2004;286:C457-63.
37. van Deursen, J., Ruitenbeek, W., Heerschap, A., Jap, P., ter Laak, H. and Wieringa, B. Creatine kinase (CK) in skeletal muscle energy metabolism: a study of mouse mutants with graded reduction in muscle CK expression. *Proc Natl Acad Sci U S A* 1994;91:9091-5.
38. Kemp, G.J., Taylor, D.J. and Radda, G.K. Control of phosphocreatine resynthesis during recovery from exercise in human skeletal muscle. *NMR Biomed* 1993;6:66-72.
39. Iotti, S., Lodi, R., Frassinetti, C., Zaniol, P. and Barbiroli, B. In vivo assessment of mitochondrial functionality in human gastrocnemius muscle by ³¹P MRS. The role of pH in the evaluation of phosphocreatine and inorganic phosphate recoveries from exercise. *NMR Biomed* 1993;6:248-53.

40. Paganini, A.T., Foley, J.M. and Meyer, R.A. Linear dependence of muscle phosphocreatine kinetics on oxidative capacity. *Am J Physiol* 1997;272:C501-10.
41. Kemp, G.J., Roussel, M., Bendahan, D., Le Fur, Y. and Cozzone, P.J. Interrelations of ATP synthesis and proton handling in ischaemically exercising human forearm muscle studied by ³¹P magnetic resonance spectroscopy. *J Physiol* 2001;535:901-28.
42. Crowther, G.J., Carey, M.F., Kemper, W.F. and Conley, K.E. Control of glycolysis in contracting skeletal muscle. I. Turning it on. *Am J Physiol Endocrinol Metab* 2002;282:E67-73.
43. Hochachka, P.W. and Somero, G.N. *Biochemical adaptation, mechanism and process in physiological evolution* New York: Oxford university press; 2002.

5

CEREBRAL CREATINE KINASE DEFICIENCY INFLUENCES METABOLITE LEVELS AND MORPHOLOGY IN THE MOUSE BRAIN: A QUANTITATIVE IN VIVO ^1H AND ^{31}P MAGNETIC RESONANCE STUDY

Rene in 't Zandt
KlaasJan Renema
Femke Streijger
Carolina Jost
Dennis Klomp
Frank Oerlemans
Ineke van der Zee
Bé Wieringa
Arend Heerschap

This chapter is in slightly modified form published as:
in 't Zandt, H.J., Renema, W.K., Streijger, F., Jost, C., Klomp, D.W., Oerlemans, F., Van der Zee, C.E.,
Wieringa, B. and Heerschap, A. Cerebral creatine kinase deficiency influences metabolite levels and
morphology in the mouse brain: a quantitative in vivo ^1H and ^{31}P magnetic resonance study. J
Neurochem 2004; 90: 1321-30.

ABSTRACT

Creatine kinase (CK) catalyzed ATP - phosphocreatine (PCr) exchange is considered to play a key role in energy homeostasis of the brain. This study assessed the metabolic and anatomical consequences of partial or complete depletion of this system in transgenic mice without cytosolic B-CK (B-CK^{-/-}), mitochondrial ubiquitous CK (UbCK^{mit-/-}), or both isoenzymes (B-CK/UbCK^{mit-/-}), using non-invasive quantitative magnetic resonance (MR) imaging and spectroscopy.

MR imaging revealed an increase in ventricle size in a subset of B-CK^{-/-} mice, but not in animals with UbCK^{mit} or compound CK mutations. Mice lacking single CK isoenzymes had normal levels of high-energy metabolites and tissue pH. In the brains of CK double knockouts pH and ATP and Pi levels were also normal, even though PCr had become completely undetectable. Moreover, a 20 – 30% decrease was observed in the level of total creatine and a similar increase in the level of neuronal N-acetyl-aspartate compounds. Although CKs themselves are not evenly distributed throughout the CNS, these alterations were uniform and concordant across different brain regions. Changes in myo-inositol and glutamate peaks did appear mutation-type and brain area specific. Our results challenge current models for the biological significance of the PCr/CK energy system and suggest a multifaceted role for creatine in the brain.

INTRODUCTION

Creatine kinases (CKs; EC 2.7.3.2) form a set of isoenzymes which catalyze the reaction: Creatine (Cr) + MgATP²⁻ ↔ phosphocreatine (PCr²⁻) + MgADP⁻ + H⁺. CKs are considered to play a key role in the energy homeostasis of muscle and brain cells, by keeping ATP/ADP ratios at distinct subcellular locations functionally balanced. In mammals the isoforms of CK are distributed in a tissue dependent manner and located in different cellular compartments (1, 2). The cytosolic isoforms brain CK (B-CK) and muscle CK (M-CK) are enzymatically active as BB-CK and MM-CK homodimers or as BM-CK heterodimers. The ubiquitous (Ub) and sarcomeric (Sc) isoforms act as dimers or octamers and are located in the intermembrane space of mitochondria.

Brain tissue, despite its complex structure and cellular heterogeneity, contains mostly only B-CK and UbCKmit isoforms. These CK-family members are, however, not uniformly co-distributed: B-CK is present in white and gray matter, while UbCKmit is mainly found in gray matter, at the sites of highest mitochondrial density (3). B-CK appears to be more abundant in astrocytes and oligodendrocytes than in neurons and is highest in the cerebellum (4, 5), while UbCKmit expression is predominantly confined to the cell soma of a subset of neurons in the cortex and hippocampus (6, 7). The expression of both CK family members is regulated in accordance with functional specialization in development, hormonal status, and energy demand.

Knowledge on the functional significance of the CK/PCr system in brain is lagging behind that in muscle not only because approaching the CNS *in vivo* is technically more demanding but also due to our limited knowledge of the effects of the blood-brain barrier and the extent of energy compartmentalization, such as in organellar networks in cell bodies or in axonal-dendritic projections. For example, feeding β-guanidinopropionic acid to mice, a competitive inhibitor of creatine transport and a poor substrate for CK, results in a complete replacement of PCr by phosphorylated β-guanidinopropionic acid in muscle (8), but gives only partial replacement in brain (9). Unlike in muscle, severe challenges of the brain energy system did not result in total depletion of PCr, pointing to the existence of different pools of PCr in brain (e.g. (9)).

Although the Cr-PCr/CK system is commonly seen as an integral part of the energy network in brain, it remains unclear what fractions of oxidative and glycolytic derived ATP actually flow through this circuit. Flux direction in this network is probably strongly determined by specific ATP demand. To investigate the biological significance of brain CK isoenzymes we have generated mice deficient for UbCKmit, referred to as UbCKmit^{-/-} (10, 11) or for cytosolic B-CK, referred to as B-CK^{-/-} (7). As neither of these genotypes is lethal it

seemed that pathways involved in the maintenance of energy homeostasis in brain, like in muscle (12, 13), are – at least partial - redundant. However, further studies of mice lacking CK isoforms showed behavioral deficits, changes in seizure susceptibility (for B-CK-/-), and anatomical abnormalities, indicating that this loss is indeed only partially compensated for by other systems (7, 11), leaving a distinct role for the CK circuit in neurodevelopment and in synaptic and metabolic connectivity.

Next from being a high-energy phosphate carrier, creatine also appears to act in brain osmoregulation (14-16) or as PCr in other as yet unspecified processes (17, 18). The neurological abnormalities of patients suffering from creatine deficiency syndromes indicate that adequate (phospho-)creatine levels are important for proper brain function (19-22). In the metabolic characterization of these patients magnetic resonance (MR) spectroscopy played a crucial role and recently we demonstrated that MR can also identify metabolic abnormalities in the brain of a mouse with genetic ablation of a creatine-biosynthetic pathway (23).

Here we report on the non-invasive morphologic and metabolic comparison of wild-type, B-CK-/- and UbCKmit-/- single knockout mice, and B-CK/UbCKmit-/- double knockout mice by quantitative ^1H and ^{31}P MR. Measurements of specific brain locations in animals lacking B-CK and/or UbCKmit revealed distinct changes in their metabolic profiles. The brain of mice completely devoid of CK iso-enzymes, the only model in which the entire CK system is rendered truly non-functional, showed normal ATP, Pi and pH levels, in spite of complete absence of an MR signal for PCr.

MATERIALS AND METHODS

Animals

The generation and phenotyping of knockout mice with mutations in the gene(s) encoding the ubiquitous mitochondrial creatine kinase (UbCKmit^{-/-}) or the cytosolic brain specific creatine kinase (B-CK^{-/-}) have been described in detail (7, 10, 11). The breeding and phenotyping of double knockout mice lacking both B-CK and UbCKmit has been described recently (24). In short, B-CK^{-/-} and UbCKmit^{-/-} mice (both on a mixed genetic background of 75% C57BL/6 - 25% 129/Ola) were interbred to obtain heterozygous B-CK/UbCKmit^{+/-} offspring. Siblings with only one wild-type CK allele (either B-CK^{+/-}UbCKmit^{-/-} or B-CK^{-/-}UbCKmit^{+/-}) were mated with double knockout (B-CK^{-/-}UbCKmit^{-/-}) partners resulting in the generation of mice lacking both CK isoforms (further referred to as B-CK/UbCKmit^{-/-} double knockout mice) in sufficiently high numbers. Mating between double mutant partner animals gave only an occasional litter and a majority of these B-CK/UbCKmit^{-/-} mice had a reduced body weight.

All mice examined in this study were females at 4-7 months or 2 years of age. Wild-type littermates were used as controls. As the brain morphology of the two parental background strains C57BL/6 and 129/Ola differ significantly (see (25)), mice with the pure parental background were also examined. Verification of genotypes was done by PCR analysis (7, 10, 11). All animal procedures were approved by the Animal Care Committee of the University of Nijmegen, and conformed to the Dutch Council for Animal Care.

During the MR experiments animals were anesthetized with 1.3% isoflurane in a gas mixture of 50% O₂ / 50% N₂O delivered through a facemask. The rectal temperature was monitored using a fluoroptic thermometer (Luxtron 712, California, USA) and maintained at 36.8±0.5 °C using a warm water circuit. Respiratory frequency and amplitude were monitored optically (Sirecust 401/ Siemens).

MR equipment

The MR experiments were performed on a 7.0 T horizontal magnet (Magnex Scientific, Abingdon, England) equipped with 150 mT/m shielded gradients and interfaced to a S.M.I.S. spectrometer (Surrey Medical Imaging Systems, Surrey, England) operating at 300.22 MHz for ¹H and at 121.53 MHz for ³¹P. Details of the RF probes are described below and in (26).

Localized ^1H MR Spectroscopy and Imaging

An elliptically shaped surface coil (15 x 11 mm) adapted to the geometry of the mouse brain was used. Localized ^1H MR spectroscopy was performed by the STEAM sequence (27) with an echo time (TE) of 10 ms, a mixing time (TM) of 15 ms and a repetition time (TR) of 5000 ms. The spectral width was 5000 Hz and 512 scans were averaged (43 minutes measurement time). Water suppression was achieved using CHESS (28). Voxels of 4 μl nominal volume were placed in three locations, i.e. thalamus (with some striatal contribution), cortex / hippocampus and cerebellum. The localization of this voxel was guided by T_2 -weighted spin echo images acquired in three oblique, perpendicular directions (TE=50 ms, TR=2000 ms, slice thickness 0.5 mm, bandwidth 50 kHz, matrix size 512x256, 24 slices). Field shimming on this voxel was performed until a line width (FWHM) of typically 12 Hz (0.04 ppm) or less was reached.

Localized ^{31}P MR Spectroscopy

For ^{31}P MRS two slightly overlapping, 16-mm diameter, surface coils operating in quadrature mode inside the brain were used (29). Both coils were anatomically shaped to fit the mouse brain. This configuration was shifted inside a cylindrical ^1H -volume coil with a diameter of only 33 mm to maintain good image quality. Localized ^{31}P MR spectroscopy was performed with an ISIS sequence (30) (TR=7 s, 512 scans). Voxel selection was guided by gradient echo images (FOV 20mm, TE=5ms, TR=500ms, slice thickness 1 mm, bandwidth 100 kHz, 128x128 matrix, 12 slices) and shimming was performed on this voxel using a STEAM sequence (27) until a water line width < 0.12 ppm. The largest possible VOI while still excluding unwanted contributions from surrounding skin and muscle tissue was 7x7x5 mm^3 covering most of the brain except the cerebellum. The 6.5 kHz bandwidth adiabatic hyperbolic secant RF pulses were sufficiently B_1 -insensitive. The maximum chemical shift displacement for the β -ATP is less than 1 mm when the observe frequency is set at the PCr resonance.

Data analysis

To circumvent problems with automatic segmentation of MR images obtained with the inhomogeneous B_1 -field of the surface coil, the following procedure was applied. All MR images of contiguous slices parallel to the RF-coil were edited so that only brain tissue remained visible and pixels inside the ventricles were manually selected in each slice and then set to a maximum intensity value of 255. Subsequently, using IDL software (RSI, Boulder, Co), the ventricle shape was segmented in 3-dimensions and the amount of pixels forming the

ventricles was counted. Since the pixel volume is known ($3.05 \times 10^{-3} \mu\text{l}$), an absolute value for the ventricle volume can be obtained.

The ^1H MR spectra were analyzed in the frequency domain with the LCModel 5.1-7 software package (31), which uses a linear combination of model metabolite spectra obtained under identical experimental conditions. Eddy current correction was performed with LCModel and no further fit constraints were used. Direct absolute quantification of metabolite levels by LCModel requires the use of a homogeneous RF coil. Since a surface coil was used, tissue water was taken as internal reference. The water signal was fitted in the time domain using the MRUI 97.1 software package (32) and a factor was determined relating the amplitudes calculated in MRUI to those in LCModel. A mean tissue water content of 78% was assumed as determined for mouse brain (33, 34).

The ^{31}P MR spectra were evaluated in the time domain also using the MRUI 97.1 software package. Peaks were fitted using a Gaussian line shape function with no further prior knowledge. Tissue pH was calculated from the Pi-PCr shift and also from the Pi- α NTP shift (35). For quantification, the signals were related to the amplitude of the ^{31}P MR signal from a 100 mM Pi solution acquired under identical experimental conditions including coil loading.

Estimation of the free creatine pool by the combination of ^1H and ^{31}P MRS

The combination of quantitative ^{31}P and ^1H MR spectroscopy provided the possibility to estimate the free Cr levels by subtracting the PCr pool (^{31}P) from the total Cr pool (^1H). Although the selected volumes for the ^1H and ^{31}P MR measurements were not identical the volume selected using ^{31}P MR covers two different voxel locations in which ^1H MR found identical Cr+PCr levels. Moreover, by chemical means the same Cr + PCr level was derived (vide infra).

Chemical analysis of the total creatine pool

For analysis of the creatine concentration in the mouse brain, mice were anaesthetized with Avertine. The mouse brain was removed and quickly frozen in liquid nitrogen. The tissue was powdered and extracted with 0.6 M HClO_4 and the resulting extract was neutralized with 3M KOH. The PCr and free Cr levels in this solution were assayed via coupled enzymatic reactions (36).

Statistics

An unpaired t-test was used to test if metabolite levels were significantly different between animal groups. Differences were considered significant when $p < 0.05$.

RESULTS

Enlarged ventricles in B-CK^{-/-} mice

To determine possible anatomical differences in mice lacking B-CK, UbCKmit or both, high-resolution T₂-weighted MR images were acquired in three perpendicular directions and compared to similar images of wild-type animals of different genetic backgrounds (figure 5.1).

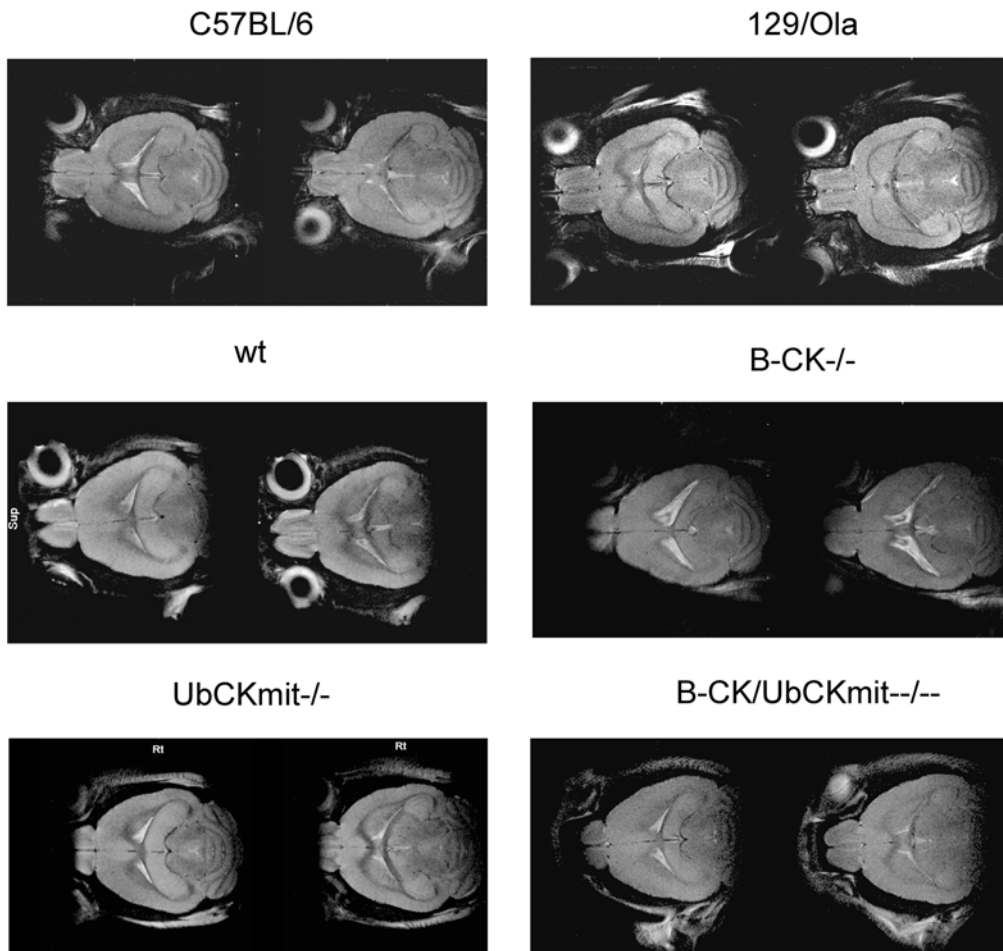


Figure 5.1: Morphology of the mouse brain as studied by T₂-weighted spin-echo MR images in two different horizontal planes.

Images are shown for the two parental background strains (top row), wild-type (wt), B-CK^{-/-} and UbCKmit^{-/-} single knockouts and B-CK/UbCKmit^{-/-/-} double knockout. Note the larger ventricles in the B-CK^{-/-} panel.

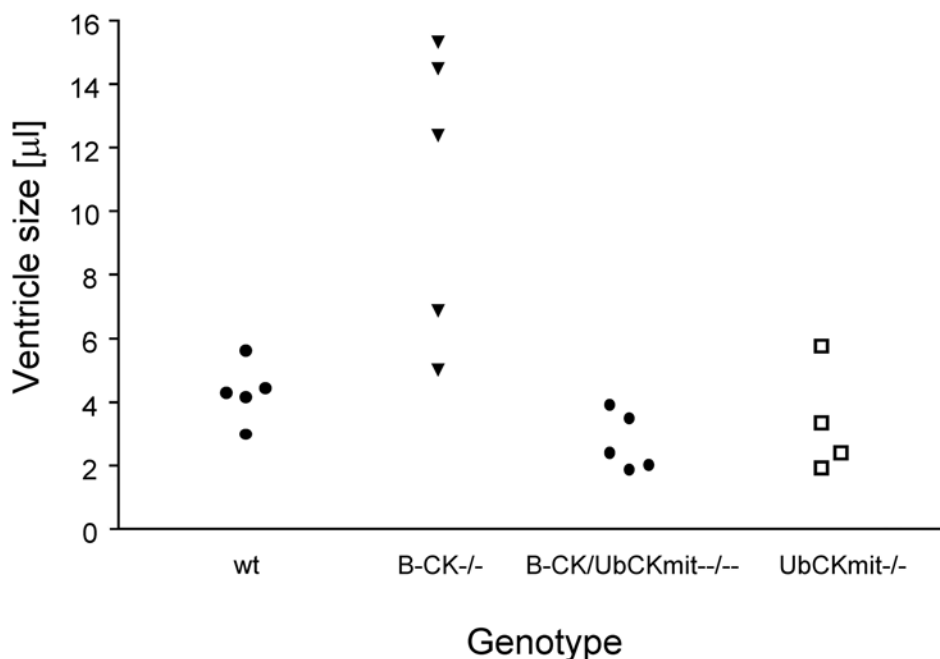


Figure 5.2: Ventricle volume size in microliter (μl) for wild-type, *B-CK*^{-/-}, *B-CK/UbCKmit*^{-/-} double knockouts and *UbCKmit*^{-/-} mice, as determined from MR images of their brains.

When compared to the wild-type controls, 3 out of 5 *B-CK*^{-/-} mice showed an increase in ventricle volume by about a factor of 2 to 3 (figure 5.2). We consider the effects on ventricle size a serious phenotype although the volume increase was not evident in all *B-CK*^{-/-} animals. This could be due to developmental masking or incomplete penetrance by compensating activity of genes that make up the volume regulatory system in brain. To analyze this possibility more closely we measured the same five *B-CK*^{-/-} mice also at an age of 7 months, but found no progressive effects on ventricle volume (i.e. the volume of the enlarged ventricles remained at 10 to 16 μl , compared to a ventricle volume between 2 to 6 μl in wild-type brains). In another group of 2 year old *B-CK*^{-/-} mutants enlarged ventricles (> 8 μl) were found again in 3 out of 6 mice, whereas all 5 wild-type mice of the same age had normal sized ventricles (< 8 μl). It is of note here that all *UbCKmit*^{-/-} and *B-CK/UbCKmit*^{-/-} double mutants had apparently normal ventricle sizes (figures. 5.1 and 5.2).

Lack of PCr in *B-CK/UbCKmit*^{-/-} double knockout mouse brain

To investigate the effects of the lack of one or both brain creatine kinases on the high-energy phosphor-metabolite profile we performed localized ³¹P MR spectroscopy. The selected voxel of 7x7x5 mm³ covered a large part of the cerebrum, but did not include the

cerebellum. In the spectra of wild-types, *UbCKmit*^{-/-} and *B-CK*^{-/-} obtained from this voxel (figure 5.3), resonances were routinely observed for PCr (resonating at 0 ppm), nucleoside triphosphates (NTP), primarily composed of ATP (γ , α and β phosphates resonating at -2.5, -7.5 and -16.1 ppm), Pi (5 ppm) and phosphomonoesters (PME; ~6.7 ppm). Usually also signals for phosphodiester (PDE; ~3.1 ppm) were observed.

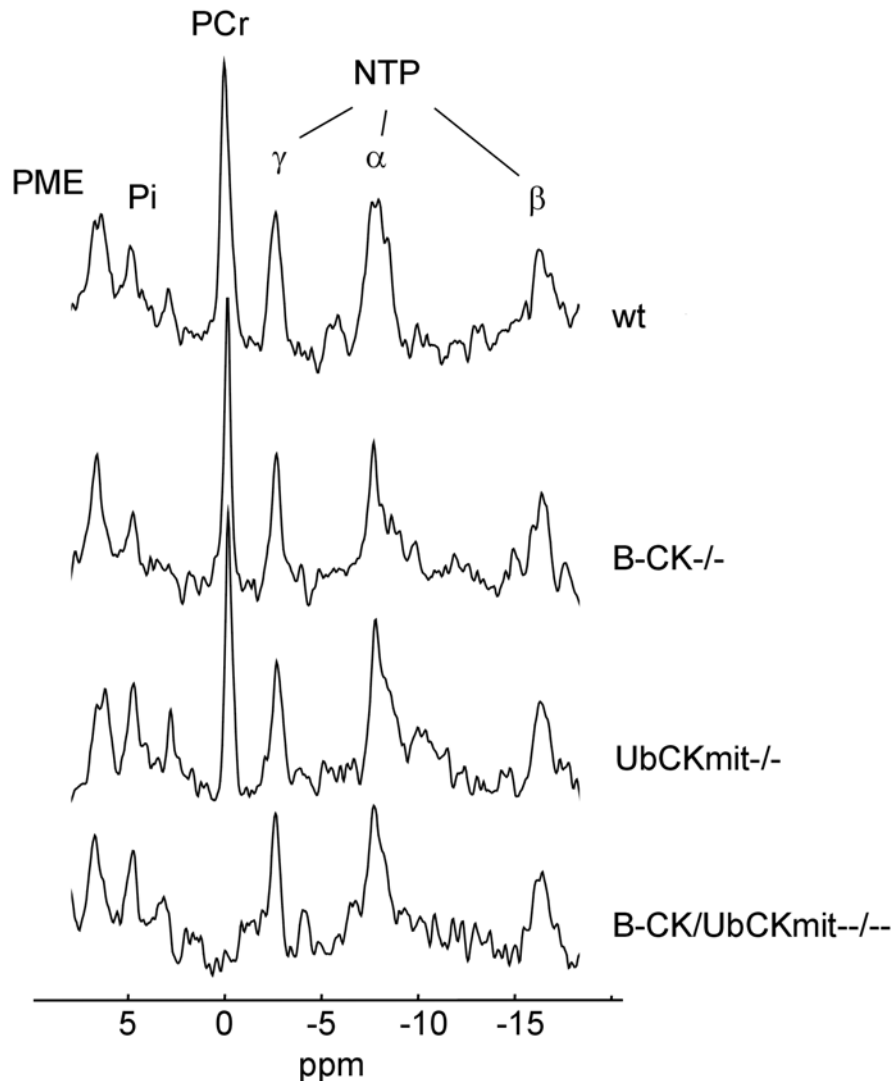


*Figure 5.3: Localized ^{31}P -MR spectroscopy of mouse brain. The spectra were obtained from a $7 \times 7 \times 5$ mm volume centered on the cerebrum, excluding contributions from cerebellum and extracranial tissue. Spectra are shown for wild-type (wt), *B-CK*^{-/-} and *UbCKmit*^{-/-} single knockouts, and a *B-CK/UbCKmit*^{-/-} double knockout mouse. Resonances are visible for phosphocreatine (PCr), phosphomonoesters (PME), inorganic phosphate (Pi) and the three phosphates of NTP (γ , α and β). Usually signals for phosphodiester (PDE) could also be detected. There are no obvious spectral differences between the groups, except for *B-CK/UbCKmit*^{-/-} double knockout mice that clearly lack PCr.*

Strikingly, but not entirely unexpected from genotype and proteome information, the PCr signal was clearly below the level of detection in the spectrum of B-CK/UbCKmit^{-/-} mice. Evaluation of the ³¹P MR data to obtain absolute average metabolite levels and tissue pH (calculated from the Pi-PCr resonance shift) revealed that PCr levels and tissue pH in B-CK^{-/-} and in UbCKmit^{-/-} mice were not deviant from those in wild-type (table 5.1). Interestingly, also NTP and Pi levels were the same in all mice, even in B-CK/UbCKmit^{-/-} brain. As B-CK/UbCKmit^{-/-} mice have no detectable PCr signal the pH in these mice was calculated on basis of the Pi- α NTP resonance shift. This pH in the B-CK/UbCKmit^{-/-} brain was not significantly different from those in other genotypes (table 5.1).

Table 5.1: Brain tissue levels of phosphoryl metabolites and tissue pH for wild-type and different CK mutant mice by ³¹P MR spectroscopy.

	Wild-type (n=5)	B-CK ^{-/-} (n=5)	UbCKmit ^{-/-} (n=4)	B-CK/UbCKmit ^{-/-} (n=3)
NTP	2.3 ± 0.3	2.4 ± 0.5	2.4 ± 0.5	2.3 ± 0.5
PCr	3.7 ± 0.6	4.4 ± 0.7	4.0 ± 0.3	ND
Pi	1.9 ± 0.6	2.0 ± 0.7	2.0 ± 0.7	1.9 ± 0.6
pH (Pi-PCr)	7.14 ± 0.07	7.10 ± 0.10	7.10 ± 0.02	-
pH (Pi- α NTP)	7.22 ± 0.16	7.18 ± 0.18	7.09 ± 0.06	7.20 ± 0.08

Phosphoryl metabolite levels (in mM) and tissue pH values are presented as mean ± SD and derived from localized ³¹P MR spectroscopy measurements from a 7 x 7 x 5 mm³ brain voxel.

NTP: nucleoside triphosphate, mostly ATP

ND: not detectable.

pH (Pi-PCr): tissue pH derived from shift of Pi signal with respect to that of PCr

pH (Pi- α NTP): tissue pH derived from shift of Pi signal with respect to that of α NTP.

Local metabolite levels in mouse brain as assessed by ^1H MR spectroscopy

While ^{31}P MR spectroscopy primarily gives an indication of the bio-energetic state of brain tissue, ^1H MR spectroscopy can provide a somewhat more diverse picture of brain metabolic content. Moreover, because of its higher sensitivity, much smaller volumes of interest can be measured. To compare data from areas of the brain with different functionality, grey matter and/or CK content, we selected voxels with a nominal volume of $4\ \mu\text{l}$ positioned in three distinct regions, i.e. thalamus, cortex/hippocampus and cerebellum (figure 5.4).

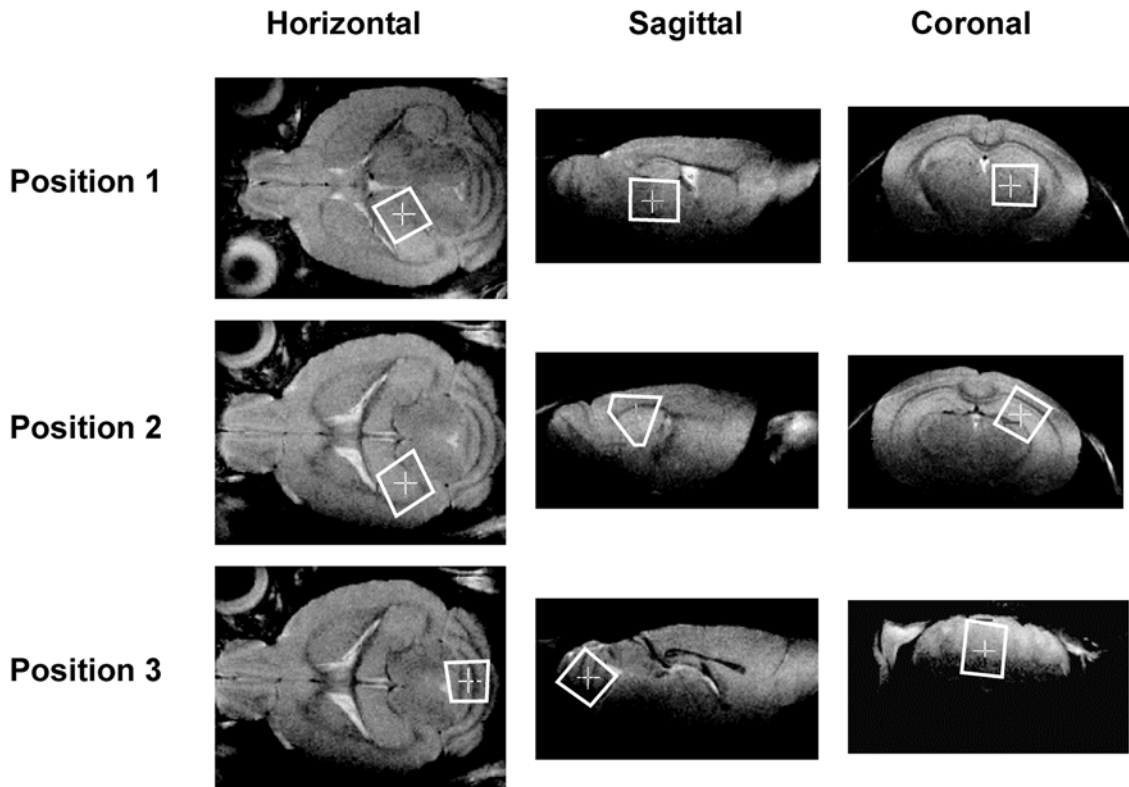


Figure 5.4: Spin echo MR images of the mouse brain depicting the projection in three perpendicular directions (horizontal, sagittal, coronal) of three selected brain tissue voxels from which for ^1H MR spectra were obtained. Position 1, thalamus; position 2, cortex/hippocampus; position 3, cerebellum. Nominal voxel volume: $4\ \mu\text{l}$.

The ^1H MR spectra acquired from these locations in the brain of a wild-type and a B-CK/UbCKmit $^{-/-}$ double mutant (figure 5.5) show various resonance of which the three most prominent ones represent the CH_3 protons of total creatine (PCr + Cr) at 3.03 ppm, of N-acetyl aspartate (NAA) at 2.03 ppm, and of phosphorylcholine (PC) and glycerol-phosphorylcholine (GPC) at ≈ 3.2 ppm. Signals for protons of other compounds such as glutamate, glutamine, taurine and myo-inositol are also visible (figure 5.5). The results of the quantitative spectral analysis for a subset of major metabolites are given in table 5.2. Total

NAA (tNAA) is presented as the sum of NAA and NAA-glutamate levels. NAA-glutamate content was about 0.5 mM for all mouse strains, mutants and investigated brain regions.

Wild-type mice showed regional variations for creatine content, which is higher in the cerebellum, and for choline compounds, which is lower in the cortex/ hippocampus as compared to the other investigated areas. Total NAA levels did not significantly differ between the three areas. For a proper comparison of mixed background wild-types with the other genotypes also metabolite levels in the parent strains were assessed in the cortex/hippocampus/thalamus region. Brain levels of the major metabolites appeared not significantly different for C57BL/6, 129/Ola and mixed background wild-type controls, with the exception of glutamate that was increased in 129/Ola mice to 9.0 ± 1.9 mM (n=3).

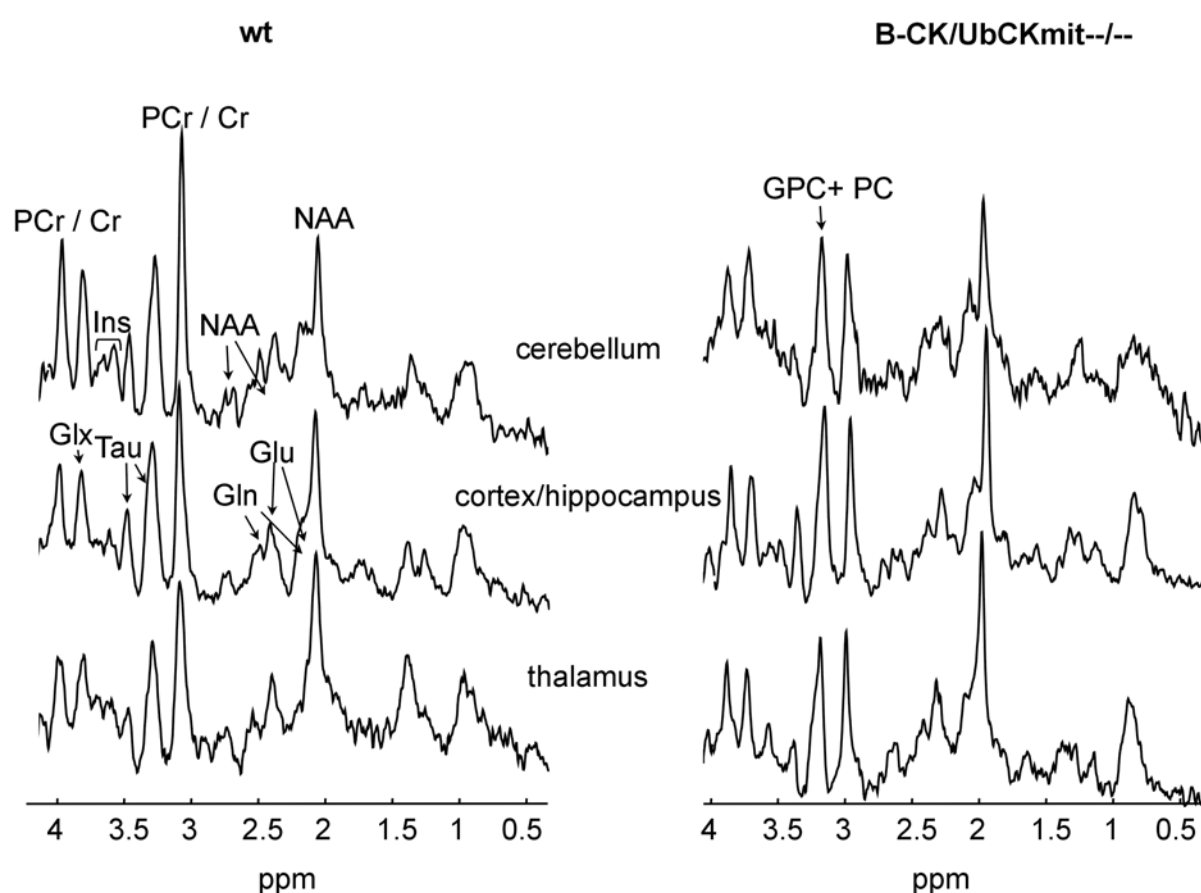


Figure 5.5: Proton MR spectra of the three selected locations (see figure 5.4) in the brain of wild-type littermate (left) and B-CK/UbCKmit^{-/-} double knockout mice (right).

Resonances are indicated for protons of phosphocreatine + creatine (PCr + Cr), glutamate (Glu), glutamine (Gln), N-acetyl-aspartic acid (NAA), taurine, glycerophosphorylcholine (GPC) and phosphorylcholine (PC) and myo-inositol (Ins). Between wild-type and B-CK/UbCKmit^{-/-} double knockout mice, the differences in NAA levels (higher) and creatine levels (lower) are the most prominent.

Table 5.2: Metabolite levels at 3 locations in the mouse brain for wild-type and different CK mutant mice as determined by ^1H MR spectroscopy.

Metabolite & location	Littermate (n=5)	B-CK-/- (n=5)	UbCKmit-/- (n=6)	B-CK/UbCKmit-/- (n=5)
Total Creatine				
Thalamus	8.5 ± 0.6	9.1 ± 0.4	8.4 ± 0.9	6.5 ± 0.5 [#]
Cortex/hippocampus	8.3 ± 0.5	8.9 ± 0.5	8.8 ± 0.8	6.7 ± 0.5 [#]
Cerebellum	10.0 ± 2.1	10.3 ± 3.0	11.2 ± 2.0	7.9 ± 1.5 [#]
Total NAA				
Thalamus	7.3 ± 1.0	5.9 ± 0.3 [#]	6.3 ± 0.4	8.8 ± 0.9 [#]
Cortex/hippocampus	6.3 ± 1.1	6.5 ± 0.5	6.4 ± 0.7	8.4 ± 1.0 [#]
Cerebellum	6.4 ± 0.9	6.2 ± 0.7	7.0 ± 0.7	8.1 ± 0.6 [#]
GPC + PC				
Thalamus	2.3 ± 0.4	1.8 ± 0.4	2.2 ± 0.6	2.6 ± 0.7
Cortex/hippocampus	0.9 ± 0.4	0.9 ± 0.5	1.4 ± 0.7	0.8 ± 0.4
Cerebellum	2.3 ± 1.2	1.4 ± 0.6	3.0 ± 1.1	2.8 ± 1.5
Myo-inositol				
Thalamus	4.3 ± 1.2	3.1 ± 0.4	2.9 ± 1.2	2.9 ± 0.6
Cortex/hippocampus	2.9 ± 1.0	3.0 ± 0.5	3.0 ± 0.5	2.8 ± 1.3
Cerebellum	3.7 ± 0.6	2.0 ± 0.4 [#]	3.8 ± 0.7	2.0 ± 1.1 [#]
Glutamate				
Thalamus	6.3 ± 0.4	6.4 ± 0.5	7.9 ± 0.4 ^{\$}	8.8 ± 1.0 ^{\$}
Cortex/hippocampus	6.6 ± 1.2	6.4 ± 0.4	7.4 ± 0.8	7.3 ± 1.0
Cerebellum	6.1 ± 0.7	5.8 ± 0.8	8.3 ± 0.7 ^{\$}	7.0 ± 0.7

All values are presented in mM (mean ± SD). The voxel centered at the thalamus had a small contribution from the striatum.

significantly different ($p < 0.05$) from wild-type and (one of the) single mutant mice

\$ significant different ($p < 0.05$) from wild-type and B-CK-/- mice
(i.e., those containing mitochondrial UbCK)

Total creatine is PCr + free creatine

Total NAA is NAA + NAA-glutamate

Differences in metabolite levels of creatine kinase deficient brain detected by ^1H MR

The most obvious changes detected by ^1H MR spectroscopy, were the significant higher tNAA and a lower total creatine levels in the B-CK/UbCKmit $^{-/-}$ double knockouts compared to wild-types (figure 5.5, table 5.2). Although absolute metabolite levels differed between genotypes, the relative spatial distribution across brain regions remained unchanged for Cr + PCr, choline compounds and tNAA.

Comparison of glutamate signals between the 3 different CK mutants for all three voxel areas (table 5.2), revealed that mice that carried mutations in the mitochondrial UbCKmit gene (i.e. either UbCKmit $^{-/-}$ or B-CK/UbCKmit $^{-/-}$ animals) had significantly higher levels of this important metabolite. Glutamate values for all three areas combined in UbCK $^{-/-}$ and B-CK/UbCKmit $^{-/-}$ mice were approximately 25 % higher than in B-CK $^{-/-}$ or wild-type animals ($p < 0.001$). Conversely, in the cerebellum of mice lacking cytosolic B-CK (i.e. in either B-CK $^{-/-}$ or B-CK/UbCKmit $^{-/-}$) the level of myo-inositol was consistently decreased by about 40 %. Other metabolites which also have been evaluated (not listed in table 5.2) showed no significantly different tissue levels between the three voxel locations and between the different mouse genotypes. These included GABA (1-2 mM), glutamine (2-3 mM) and taurine (about 6 mM).

In addition, measurements were performed on a cohort of 2 years old wild-type and B-CK $^{-/-}$ mice ($n = 5$ each). Proton MR spectra obtained from the cortex / hippocampus area showed no significant differences for any of the metabolites studied, except for tNAA in the older B-CK $^{-/-}$ mice (5.2 ± 0.6 mM), which was significantly ($p < 0.01$) decreased compared to tNAA in adult B-CK $^{-/-}$ mice (6.5 ± 0.5 mM), or in adult (see table 5.2) and aged wild-types (6.4 ± 0.9 mM).

Abnormal creatine levels in B-CK/UbCKmit $^{-/-}$ double knockout brain

Absolute total creatine levels in wild-type and B-CK/UbCKmit $^{-/-}$ mouse brain derived by non-invasive ^1H MRS are in good agreement with those obtained by chemical analysis (table 5.3). The free Cr pool, estimated from the total creatine and PCr levels, was the same in wild-type, B-CK $^{-/-}$ and UbCKmit $^{-/-}$ mice (table 5.3). Interestingly, the total Cr level is decreased only by about 25% in B-CK/UbCKmit $^{-/-}$ double knockouts. Since PCr is essentially undetectable in this mouse, we assume that the signal at the PCr + Cr position in the ^1H MR spectrum represents only Cr. It follows that the level of free Cr in B-CK/UbCKmit $^{-/-}$ double knockout animals is about 30% higher than that in B-CK $^{-/-}$, UbCK $^{-/-}$ or wild-type mice (6.6 mM vs. ~ 4.6 mM).

Table 5.3: Total creatine, phosphocreatine and free creatine tissue levels in the brain of wild-type and different CK mutant mice

	wild-type	B-CK-/-	UbCKmit-/-	B-CK/UbCKmit-/-
Chem. anal. → total Cr	8.5 ± 1.0 (n=4)	-	-	6.4 ± 0.2 [#] (n=3)
¹ H MRS → total Cr	8.4 ± 0.4 (n=5)	9.0 ± 0.3 (n=5)	8.6 ± 0.6 (n=6)	6.6 ± 0.4 [#] (n=5)
³¹ P MRS → PCr	3.7 ± 0.6 (n=5)	4.4 ± 0.7 (n=5)	4.0 ± 0.3 (n=4)	0 * (n=3)
free Cr	4.7 ± 0.7	4.6 ± 0.8	4.6 ± 0.7	6.6 ± 0.4 [#]

All values are presented in mM (mean ± SD).

Total creatine content was derived by chemical analysis of the brain of wild-type and B-CK/UbCKmit-/- double knockout mice, and by ¹H MR spectroscopy, averaging the values obtained from thalamus and cortex/hippocampus areas (see table 2)

Free creatine tissue levels were derived from the total creatine pool (as obtained by ¹H-MRS) and the PCr levels (as obtained by ³¹P MRS).

Significantly different from all other mouse genotype groups

* Because no PCr signal is detectable in ³¹P MR spectra of B-CK/UbCKmit-/- mice its level was set to 0. However, as the detection limit of our ³¹P MR spectra is estimated to be about 0.5 mM in principle PCr can be present at any tissue concentration below 0.5 mM.

DISCUSSION

As the creatine kinase reaction is considered to be an integral part of the cellular energy network in the brain, facilitating both ATP production and consumption, the ablation of any brain isoenzyme (B-CK or UbCKmit) was anticipated to result in a severe phenotype. However, earlier we reported that B-CK^{-/-} or UbCKmit^{-/-} mice are overtly normal and rather sophisticated analysis and challenging conditions were needed to reveal that these single CK mutants showed slower learning, diminished habituation, reduced acoustic startle reflex responses and (only tested for B-CK^{-/-}) a different susceptibility to seizures (7, 11). In B-CK/UbCKmit^{-/-} double knockout mice behavioral and learning problems were more clearly manifest (24).

Because changes in metabolite content upon CK depletion are expected to be the cause or the consequence of these phenotypes, the main goal of this study was to type metabolic effects in CK deficient brains *in vivo*. Substrates of the CK reaction can be monitored non-invasively in the living brain by quantitative MR spectroscopy and therefore this method is particular attractive to study CK knockout mice, although the application of this approach to the mouse brain is still challenging due to its small size. Below, we therefore also emphasize the significance of MR spectroscopic findings in wild-type mice, before addressing the effects of CK deficiency. As imaging is an inherent part of the applied MR methods also a view on brain morphology was obtained complementary to histology, which is discussed first.

Effects on brain morphology and ventricle size

As variations in genetic background are a known cause of differences in neurological properties of mice, e.g. (37, 38) and thus a potential source of errors and confusion in MR studies, we validated the “reporter-value” of our MR data by comparing mixed inbred strain and parental strains C57BL/6 and 129/Ola. Although ventricles in these animals may vary in size, see also (38), the ventricle volume seen in 3 out of 5 adult and in 3 out of 6 aged B-CK^{-/-} mice was far outside the range of ventricle sizes seen in any of the other groups with mixed and pure inbred background, rendering the finding of enlarged ventricles in these mice very significant. Enlarged ventricles have also been observed by MRI in L1 cell adhesion molecule knockout mice (39) and in mice with altered copies of the Huntington disease gene homolog (40). In two mutant lines about 50% of these latter mice had enlarged ventricles, a defect that also did not worsen with age. Apparently this phenomenon is not fully penetrant and can be compensated for by other gene functions. The enlargement of ventricles, possibly implicating a mild form of hydrocephalus, might result from a defective process of neuronal extension or cell loss in specific regions during brain development.

Elsewhere we have reported (7) that B-CK^{-/-} brains also show a significantly larger intra-infrapyramidal (LIIP) mossy fiber area. It is of particular interest here that our combined MRI and histo-anatomical analyses (not shown) did not reveal gross morphological abnormalities in the brains of double mutant B-CK/UbCKmit^{-/-} or single mutant UbCKmit^{-/-} mice, except for a 7% reduction in overall brain weight in only the double knockouts, suggesting a role of the CK system in neuronal cell differentiation or brain growth.

Absolute levels of metabolites in the in vivo mouse brain

Quantitative localized in vivo ¹H MR spectroscopy to assess metabolite levels in the brain has been little applied yet to the mouse. The levels of some metabolites have been estimated for a volume in the forebrain of 3 mouse strains (41) and a central brain volume in other mouse types (23). The tissue levels of most metabolites in wt mouse brain, as assessed in the present study by ¹H MRS, are comparable to those for the adult rat brain (42).

Total creatine content in the cerebrum of mice (7 - 9 mM) is somewhat higher than in human cerebrum (5 - 7 mM). There is more Cr in mice cerebellum than in its cerebrum, as also observed in humans, e.g. (43, 44), and which is associated with a relative high CK level (4).

Levels of total NAA for wt mouse cerebrum observed in the present study (about 6 - 7 mM) are comparable to those reported elsewhere for mouse brain (41), but somewhat lower than commonly observed for adult human and rat cerebrum (8 - 11 mM). Biochemical assessments indicate similar lower values for NAA in the mouse brain: i.e. about 5 - 6 mM (45, 46). NAA contributes to the most prominent peak in ¹H MR spectra of the CNS and because it is primarily synthesized and stored in neurons, the intensity of this peak is widely used as a marker for neuronal viability (47). However, NAA can also act as an osmolyte and its tissue level may reflect the degree of cellular integration in the CNS (48). Different NAA contents in rat and mouse brain may be related to species specific brain organization such as reflected in the 2-fold difference in cholinergic neurons per section of equal thickness of mouse and rat brain (49).

Another prominent peak in ¹H MR spectra of the brain is that of choline compounds. The tissue content of these compounds in the thalamus region is comparable to that reported for larger brain volumes (23, 41). The occurrence of lower choline levels in cortical regions is generally also observed in rats and humans (42, 43).

The brain level of the neurotransmitter glutamate in 129/Ola mice is similar to that in the rat (42), but is lower in wt littermates and the C57Bl/6 strain, more similar to values found for human white matter (43). Brain levels of myo-inositol in wt mice are close to those in rat (42). Myo-inositol is considered to be a major cellular osmolyte and a marker for the astrocyte

content of brain tissue (e.g. (15, 50, 51)), although it is not exclusively associated with glia cells (52, 53).

Absolute quantification of phosphate metabolites by localized ^{31}P MR spectroscopy has not yet been performed for mouse brain to our knowledge. The global NTP amount (primarily composed of ATP) estimated in this study (~ 2.4 mM), is comparable to global ATP levels in the brain tissue of adult mice assessed by biochemical means; e.g.(54), and absolute PCr levels closely resemble those determined by MRS for rat brain (3.9 mM; (55)).

Creatine kinase deficient mouse brain

Our regional metabolite profiling revealed that mice with complete brain CK deficiency, but not those with only B-CK or UbCKmit mutations, exhibited a higher tNAA content across all brain regions, with concentrations clearly outside the range found in mixed and pure inbred controls. One could postulate that, in analogy to mice that lack both muscle-specific CK isoforms, M-CK and ScCKmit (12, 56, 57), B-CK/UbCKmit $^{-/-}$ double knockouts show the most profound adaptations as a result of physiological and developmental responses that serve to mask the effects of the genetic lesion. A higher NAA signal most likely reflects an increase of this compound in individual neurons or an increase in relative neuronal volume (58). NAA is synthesized in mitochondria (47, 59, 60) and implicated in lipid synthesis (61) and acetyl-CoA buffering (60, 62). Thus increases in tNAA levels may reflect adaptations in any of the intracellular pathways involved (e.g. an up-regulation of mitochondrial capacity). The concomitant increase in total NAA and decrease in total creatine content may also reflect a redistribution of cerebral osmolites (14, 15). In turn, any shift in osmolite levels could promote or block ventricle enlargement. In this respect it is interesting to mention that the thalamus of B-CK $^{-/-}$ mice, the only mutant with an enlarged ventricle phenotype, shows a “reverse” shift in the levels of tNAA and creatine (Table 5.2). Finally, It is also conceivable that changes in cell size or cell-type distribution across brain regions due to adaptive neuronal plasticity or neurogenesis, e.g. (63), are the cause of alterations in NAA content. Such a generalized effect at the cellular level would corroborate the 7% change in brain weight for animals in the B-CK/UbCKmit $^{-/-}$ cohort (11).

In this context it is of note that we did observe changes in myo-inositol and glutamate content as more localized events in B-CK and UbCKmit single knockouts, respectively. Unfortunately, the variation in glutamate level in mice with different genetic backgrounds, obfuscates a clear correlation between changes in glutamate concentration and the local absence or presence of UbCKmit activity. Our glutamate findings are consistent with both (i) simple metabolic alterations in the mitochondrial capacity for glutamate synthesis, as mitochondria may have a prominent role in setting the cellular level of glutamate (64) or with

(ii) overall changes in cell differentiation and growth. Likewise, the myo-inositol findings in B-CK^{-/-} and B-CK/UbCKmit^{-/-} double knockout mice could be equally well ascribed to (i) changes in neuronal physiology such as osmoregulatory adaptations, or to (ii) specific local changes in cell type distribution or differentiation, correlated to the unequal distribution of CK isoforms across the brain.

Finally, it is interesting to discuss the role of Cr and PCr proper. In the single knockout mice there is little difference in PCr and free Cr content with respect to wild-types, but in B-CK/UbCKmit^{-/-} double knockout brain PCr is undetectable and the level of free creatine higher than normal. This renders B-CK/UbCKmit^{-/-} mice a unique model to study the biological significance of Cr in isolation, separated from the role of PCr in brain energetics. In muscle we observed that even at very low CK activities the amount of total creatine was not affected (65) indicating that the uptake of creatine in muscle cells occurs independent of its phosphorylation to PCr or CK activity. In the brain our results show that in the extreme case of total CK and PCr absence a response does occur, but it only results in a partial depletion of total creatine. Taken combined, these data suggest that the presence of free creatine is important in both tissues, but that its uptake is not directly correlated to PCr formation and hence, the cellular energy charge. This could point to a role that is independent from that as acceptor of high-energy \sim P groups in cellular energetics.

Also the observation that mice without any CK activity in brain were viable, corroborated previous findings in other cellular and animal models with CK deficiencies, and effectively challenges the proposed energy shuttling role of the CK reaction (66) as absolutely vital for life. Instead, a new picture emerges, in which compensatory shifts in associated reactions in the whole phosphotransfer network (67) safeguard maintenance of cellular energetic homeostasis. What then could be the other possible (i.e. non-energetic) physiological roles of Cr proper? All that is known is that Cr may act as an osmolyte, e.g. (15), or as co-solvent (in analogy to other amino acid-like compounds (68)). The increased level of free Cr may therefore explain the apparent masking of ventricle problems (often synonymous with cell volume changes) in B-CK/UbCKmit^{-/-} mice, but further study is needed to clarify this issue.

The relevance of homeostasis in the entire Cr and PCr system for normal brain function has been emphasized by findings in patients lacking (P)Cr due to transporter or biosynthetic pathway problems (20, 21). Here the accumulation of neurotoxic precursors, such as guanidinoacetate in cases with guanidino-methyltransferase deficiency (69), perhaps together with the absence of PCr, but also the lack of free Cr, may have contributed to the pathology in these patients.

In summary, our data presented here, in combination with the behavioral and histological phenotyping reported elsewhere and the clinical findings in humans, point to the importance of homeostasis of total and free pools of Cr as an essential factor in the regulation of physiological functioning and development of the CNS. Whether we can completely separate this from PCr's role as a buffer for high-energy phosphates during strenuous conditions or phases of cell differentiation and maturation during brain growth remains subject for further study.

ACKNOWLEDGEMENTS

We thank A.W. Simonetti for testing MR pulse sequences and J. van Asten for assistance with data processing. This work was supported by an investment grant (to A.H.) and a program grant from the Dutch Organization for Scientific Research (to B.W. from ZON-Mw).

REFERENCES

1. Wallimann, T. and Hemmer, W. Creatine kinase in non-muscle tissues and cells. *MolCellBiochem* 1994;133-134:193-220.
2. Wyss, M. and Kaddurah-Daouk, R. Creatine and creatinine metabolism. *Physiol Rev* 2000;80:1107-213.
3. Wong-Riley, M.T. Cytochrome oxidase: an endogenous metabolic marker for neuronal activity. *Trends Neurosci* 1989;12:94-101.
4. Ilyin, S.E., Sonti, G., Molloy, G. and Plata-Salaman, C.R. Creatine kinase-B mRNA levels in brain regions from male and female rats. *Brain Res Mol Brain Res* 1996;41:50-6.
5. Shen, W., Willis, D., Zhang, Y., Schlattner, U., Wallimann, T. and Molloy, G.R. Expression of creatine kinase isoenzyme genes during postnatal development of rat brain cerebellum: evidence for transcriptional regulation. *Biochem J* 2002;367:369-80.
6. Boero, J., Qin, W., Cheng, J., Woolsey, T.A., Strauss, A.W. and Khuchua, Z. Restricted neuronal expression of ubiquitous mitochondrial creatine kinase: changing patterns in development and with increased activity. *Mol Cell Biochem* 2003;244:69-76.
7. Jost, C.R., Van Der Zee, C.E., In 't Zandt, H.J., Oerlemans, F., Verheij, M., Streijger, F., Franssen, J., Heerschap, A., Cools, A.R. and Wieringa, B. Creatine kinase B-driven energy transfer in the brain is important for habituation and spatial learning behaviour, mossy fibre field size and determination of seizure susceptibility. *Eur J Neurosci* 2002;15:1692-706.
8. van Deursen, J., Jap, P., Heerschap, A., ter Laak, H., Ruitenbeek, W. and Wieringa, B. Effects of the creatine analogue beta-guanidinopropionic acid on skeletal muscles of mice deficient in muscle creatine kinase. *Biochim Biophys Acta* 1994;1185:327-35.
9. Holtzman, D., Meyers, R., O'Gorman, E., Khait, I., Wallimann, T., Allred, E. and Jensen, F. In vivo brain phosphocreatine and ATP regulation in mice fed a creatine analog. *Am J Physiol* 1997;272:C1567-C1577.
10. Steeghs, K., Oerlemans, F. and Wieringa, B. Mice deficient in ubiquitous mitochondrial creatine kinase are viable and fertile. *Biochim Biophys Acta* 1995;1230:130-8.
11. Streijger, F., Jost, C.R., Oerlemans, F., Ellenbroek, B.A., Cools, A.R., Wieringa, B. and Van der Zee, C.E. Mice lacking the UbCKmit isoform of creatine kinase reveal slower spatial learning acquisition, diminished exploration and habituation, and reduced acoustic startle reflex responses. *Mol Cell Biochem* 2004;256-257:305-18.
12. Steeghs, K., Benders, A., Oerlemans, F., de Haan, A., Heerschap, A., Ruitenbeek, W., Jost, C., van Deursen, J., Perryman, B., Pette, D., Bruckwilder, M., Koudijs, J., Jap, P., Veerkamp, J. and Wieringa, B. Altered Ca²⁺ responses in muscles with combined mitochondrial and cytosolic creatine kinase deficiencies. *Cell* 1997;89:93-103.
13. van Deursen, J., Heerschap, A., Oerlemans, F., Ruitenbeek, W., Jap, P., ter Laak, H. and Wieringa, B. Skeletal muscles of mice deficient in muscle creatine kinase lack burst activity. *Cell* 1993;74:621-31.
14. Bluml, S., Zuckerman, E., Tan, J. and Ross, B.D. Proton-decoupled 31P magnetic resonance spectroscopy reveals osmotic and metabolic disturbances in human hepatic encephalopathy. *J Neurochem* 1998;71:1564-76.
15. Ross, B. and Bluml, S. Magnetic resonance spectroscopy of the human brain. *Anat Rec* 2001;265:54-84.
16. Videen, J.S., Michaelis, T., Pinto, P. and Ross, B.D. Human cerebral osmolytes during chronic hyponatremia. A proton magnetic resonance spectroscopy study. *J Clin Invest* 1995;95:788-93.
17. Xu, C.J., Klunk, W.E., Kanfer, J.N., Xiong, Q., Miller, G. and Pettegrew, J.W. Phosphocreatine-dependent glutamate uptake by synaptic vesicles. A comparison with atp-dependent glutamate uptake. *J Biol Chem* 1996;271:13435-40.
18. Hirose, Y. and Manley, J.L. Creatine phosphate, not ATP, is required for 3' end cleavage of mammalian pre-mRNA in vitro. *J Biol Chem* 1997;272:29636-42.
19. Bianchi, M.C., Tosetti, M., Fornai, F., Alessandri, M.G., Cipriani, P., De Vito, G. and Canapicchi, R. Reversible brain creatine deficiency in two sisters with normal blood creatine level. *Ann Neurol* 2000;47:511-3.

20. Salomons, G.S., van Dooren, S.J., Verhoeven, N.M., Cecil, K.M., Ball, W.S., Degrauw, T.J. and Jakobs, C. X-linked creatine-transporter gene (SLC6A8) defect: a new creatine-deficiency syndrome. *Am J Hum Genet* 2001;68:1497-500.
21. Schulze, A., Bachert, P., Schlemmer, H., Harting, I., Polster, T., Salomons, G.S., Verhoeven, N.M., Jakobs, C., Fowler, B., Hoffmann, G.F. and Mayatepek, E. Lack of creatine in muscle and brain in an adult with GAMT deficiency. *Ann Neurol* 2003;53:248-51.
22. Stöckler, S., Holzbach, U., Hanefeld, F., Marquardt, I., Helms, G., Requart, M., Hanicke, W. and Frahm, J. Creatine deficiency in the brain: a new, treatable inborn error of metabolism. *Pediatr Res* 1994;36:409-13.
23. Renema, W.K., Schmidt, A., Van Asten, J.J., Oerlemans, F., Ullrich, K., Wieringa, B., Isbrandt, D. and Heerschap, A. MR spectroscopy of muscle and brain in guanidinoacetate methyltransferase (GAMT)-deficient mice: Validation of an animal model to study creatine deficiency. *Magn Reson Med* 2003;50:936-43.
24. Streijger, F., Oerlemans, F., Ellenbroek, B.A., Jost, C.R., Wieringa, B. and Van der Zee, C.E. Structural and behavioural consequences of double deficiency for creatine kinases BCK and UbCKmit. *Behav Brain Res* 2005;157:219-34.
25. <http://www.nervenet.org/mbl/mbl.html>
26. Heerschap, A., Sommers, M.G., Zandt, H.J., Renema, W.K., Veltien, A.A. and Klomp, D.W. Nuclear magnetic resonance in laboratory animals. *Methods Enzymol* 2004;385:41-63.
27. Frahm, J., Merboldt, K.D. and Hanicke, W. Localized proton spectroscopy using stimulated echoes. *J Magn Reson* 1987;72:502-508.
28. Haase, A., Frahm, J., Hanicke, W. and Matthaei, D. 1H NMR chemical shift selective (CHESS) imaging. *Phys Med Biol* 1985;30:341-344.
29. Adriany, G. and Gruetter, R. A half-volume coil for efficient proton decoupling in humans at 4 tesla. *J Magn Reson* 1997;125:178-84.
30. Ordidge, R.J., Connely, A. and Lohman, J.A.B. Image-selected in vivo spectroscopy (ISIS). A new technique for spatially selective NMR spectroscopy. *J Magn Reson* 1986;66:293-294.
31. Provencher, S.W. Estimation of metabolite concentrations from localized in vivo proton NMR spectra. *Magn Reson Med* 1993;30:672-9.
32. <http://www.mrui.uab.es/mrui/>
33. Schwarcz, A., Berente, Z., Osz, E. and Doczi, T. In vivo water quantification in mouse brain at 9.4 Tesla in a vasogenic edema model. *Magn Reson Med* 2001;46:1246-9.
34. Kinouchi, H., Epstein, C.J., Mizui, T., Carlson, E., Chen, S.F. and Chan, P.H. Attenuation of focal cerebral ischemic injury in transgenic mice overexpressing CuZn superoxide dismutase. *Proc Natl Acad Sci U S A* 1991;88:11158-62.
35. Moon, R.B. and Richards, J.H. Determination of intracellular pH by 31P magnetic resonance. *J Biol Chem* 1973;248:7276-8.
36. Bergmeyer, H.U. *Methods of Enzymatic Analysis*. New York: Academic Press; 1974.
37. Lipp, H.P. and Wolfer, D.P. Genetically modified mice and cognition. *Curr Opin Neurobiol* 1998;8:272-80.
38. Livy, D.J. and Wahlsten, D. Tests of genetic allelism between four inbred mouse strains with absent corpus callosum. *J Hered* 1991;82:459-64.
39. Fransen, E., D'Hooge, R., Van Camp, G., Verhoye, M., Sijbers, J., Reyniers, E., Soriano, P., Kamiguchi, H., Willemsen, R., Koekkoek, S.K., De Zeeuw, C.I., De Deyn, P.P., Van der Linden, A., Lemmon, V., Kooy, R.F. and Willems, P.J. L1 knockout mice show dilated ventricles, vermis hypoplasia and impaired exploration patterns. *Hum Mol Genet* 1998;7:999-1009.
40. Auerbach, W., Hurlbert, M.S., Hilditch-Maguire, P., Wadghiri, Y.Z., Wheeler, V.C., Cohen, S.I., Joyner, A.L., MacDonald, M.E. and Turnbull, D.H. The HD mutation causes progressive lethal neurological disease in mice expressing reduced levels of huntingtin. *Hum Mol Genet* 2001;10:2515-23.
41. Schwarcz, A., Natt, O., Watanabe, T., Boretius, S., Frahm, J. and Michaelis, T. Localized proton MRS of cerebral metabolite profiles in different mouse strains. *Magn Reson Med* 2003;49:822-7.

42. Tkac, I., Rao, R., Georgieff, M.K. and Gruetter, R. Developmental and regional changes in the neurochemical profile of the rat brain determined by in vivo ¹H NMR spectroscopy. *Magn Reson Med* 2003;50:24-32.
43. Pouwels, P.J.W. and Frahm, J. Regional metabolite concentrations in human brain as determined by quantitative localized proton mrs. *Magn Reson Med* 1998;39:53-60.
44. Jacobs, M.A., Horska, A., van Zijl, P.C. and Barker, P.B. Quantitative proton MR spectroscopic imaging of normal human cerebellum and brain stem. *Magn Reson Med* 2001;46:699-705.
45. Marcucci, F. and Giacalone, E. N-acetyl aspartic, aspartic and glutamic acid brain levels in aggressive mice. *Biochem Pharmacol* 1969;18:691-2.
46. Fleming, M.C. and Lowry, O.H. The measurement of free and N-acetylated aspartic acids in the nervous system. *J Neurochem* 1966;13:779-83.
47. Birken, D.L. and Oldendorf, W.H. N-acetyl-L-aspartic acid: a literature review of a compound prominent in ¹H-NMR spectroscopic studies of brain. *Neurosci Biobehav Rev* 1989;13:23-31.
48. Baslow, M.H., Suckow, R.F., Gaynor, K., Bhakoo, K.K., Marks, N., Saito, M., Duff, K., Matsuoka, Y. and Berg, M.J. Brain damage results in down-regulation of N-acetylaspartate as a neuronal osmolyte. *Neuromolecular Med* 2003;3:95-104.
49. Hagg, T., Van der Zee, C.E.E.M., Ross, G.M. and Riopelle, R.J. Response to "Petersen et al.: Basal forebrain neuronal loss in mice lacking neurotrophin receptor p75". *Science* 1997;277:838-839.
50. Brand, A., Leibfritz, D., Hamprecht, B. and Dringen, R. Metabolism of cysteine in astroglial cells: synthesis of hypotaurine and taurine. *J Neurochem* 1998;71:827-32.
51. Brand, A., Richter-Landsberg, C. and Leibfritz, D. Metabolism of acetate in rat brain neurons, astrocytes and cocultures: metabolic interactions between neurons and glia cells, monitored by NMR spectroscopy. *Cell Mol Biol (Noisy-le-grand)* 1997;43:645-57.
52. Moore, G.J., Koch, S., Chen, G., Santalucia Jr., J. and Manji, H.K. Myo-inositol is not exclusively glial in the human CNS. *Proc Intl Soc Magn Res Med* 1999;7:33.
53. Godfrey, D.A., Hallcher, L.M., Laird, M.H., Matschinsky, F.M. and Sherman, W.R. Distribution of myo-inositol in the cat cochlear nucleus. *J Neurochem* 1982;38:939-47.
54. Tsao, J.W., Paramanathan, N., Parkes, H.G. and Dunn, J.F. Altered brain metabolism in the C57BL/Wld mouse strain detected by magnetic resonance spectroscopy: association with delayed Wallerian degeneration? *J Neurol Sci* 1999;168:1-12.
55. Pfeuffer, J., Tkac, I., Provencher, S.W. and Gruetter, R. Toward an in vivo neurochemical profile: quantification of 18 metabolites in short-echo-time (¹H) NMR spectra of the rat brain. *J Magn Reson* 1999;141:104-20.
56. de Groof, A.J., Oerlemans, F.T., Jost, C.R. and Wieringa, B. Changes in glycolytic network and mitochondrial design in creatine kinase-deficient muscles. *Muscle Nerve* 2001;24:1188-96.
57. de Groof, A.J., Smeets, B., Groot Koerkamp, M.J., Mul, A.N., Janssen, E.E., Tabak, H.F. and Wieringa, B. Changes in mRNA expression profile underlie phenotypic adaptations in creatine kinase-deficient muscles. *FEBS Lett* 2001;506:73-8.
58. Serles, W., Li, L.M., Antel, S.B., Cendes, F., Gotman, J., Olivier, A., Andermann, F., Dubeau, F. and Arnold, D.L. Time course of postoperative recovery of N-acetyl-aspartate in temporal lobe epilepsy. *Epilepsia* 2001;42:190-7.
59. Bates, T.E., Strangward, M., Keelan, J., Davey, G.P., Munro, P.M. and Clark, J.B. Inhibition of N-acetylaspartate production: implications for ¹H MRS studies in vivo. *Neuroreport* 1996;7:1397-400.
60. Patel, T.B. and Clark, J.B. Synthesis of N-acetyl-L-aspartate by rat brain mitochondria and its involvement in mitochondrial/cytosolic carbon transport. *Biochem J* 1979;184:539-46.
61. Burri, R., Steffen, C. and Herschkowitz, N. N-acetyl-L-aspartate is a major source of acetyl groups for lipid synthesis during rat brain development. *Dev Neurosci* 1991;13:403-11.
62. Berlinguet, L. and Laliberte, M. Biosynthesis of N-acetyl-L-aspartic acid in vivo and in brain homogenates. *Can J Biochem* 1970;48:207-11.

63. Eriksson, P.S., Perfilieva, E., Bjork-Eriksson, T., Alborn, A.M., Nordborg, C., Peterson, D.A. and Gage, F.H. Neurogenesis in the adult human hippocampus. *Nat Med* 1998;4:1313-7.
64. Maechler, P. and Wollheim, C.B. Mitochondrial glutamate acts as a messenger in glucose-induced insulin exocytosis. *Nature* 1999;402:685-9.
65. in 't Zandt, H.J., Groof, A.J., Renema, W.K., Oerlemans, F.T., Klomp, D.W., Wieringa, B. and Heerschap, A. Presence of (phospho)creatine in developing and adult skeletal muscle of mice without mitochondrial and cytosolic muscle creatine kinase isoforms. *J Physiol* 2003;548:847-58.
66. Bessman, S.P. and Geiger, P.J. Transport of energy in muscle: the phosphorylcreatine shuttle. *Science* 1981;211:448-52.
67. Dzeja, P.P., Terzic, A. and Wieringa, B. Phosphotransfer dynamics in skeletal muscle from creatine kinase gene-deleted mice. *Mol Cell Biochem* 2004;256-257:13-27.
68. Tyagi, R. and Gupta, M.N. Chemical modification and chemical cross-linking for protein/enzyme stabilization. *Biochemistry (Mosc)* 1998;63:334-44.
69. Schulze, A., Hess, T., Wevers, R., Mayatepek, E., Bachert, P., Marescau, B., Knopp, M.V., De Deyn, P.P., Bremer, H.J. and Rating, D. Creatine deficiency syndrome caused by guanidinoacetate methyltransferase deficiency: diagnostic tools for a new inborn error of metabolism [see comments]. *J Pediatr* 1997;131:626-31.

6

IN VIVO ^{13}C MRS RECORDINGS POINT TO ALTERED GLUCOSE METABOLISM IN BRAIN OF MICE WITH CREATINE KINASE DEFICIENCY

KlaasJan Renema

Dennis Klomp

Andor Veltien

Frank Oerlemans

Bé Wieringa

Arend Heerschap

ABSTRACT

In vivo ^{13}C MRS using ^{13}C labeled compounds is a useful technique to provide a window on energy metabolism and neurotransmitter recycling in mammalian brain. Thus far, however, the application of ^{13}C MRS was restricted to use in brains of humans or rats, but not feasible for mice, due to problems with small brain volume and low SNR.

Here we present a new experimental framework for MR studies in the mouse brain in vivo, with the use of specially designed procedures and dedicated hardware to monitor incorporation and transfer of [1- ^{13}C] label from glucose into lactate, alanine, and several C-atom positions in glutamate, glutamine and aspartate with relatively high temporal resolution. Using this experimental setup, transfer of label from glucose to other metabolites was compared between mice lacking both cytosolic and mitochondrial brain-type creatine kinases (B-CK/UbCKmit^{-/-} mice) and wild-type controls. Direct comparison without calibration of glucose input and MR signals revealed that B-CK/UbCKmit^{-/-} mice displayed an earlier or faster conversion of glucose, and less accumulation of label into lactate, suggesting a more efficient coupling of aerobic glycolysis and mitochondrial activity in brain energetics. Advantages and disadvantages of the current setup and caveats of the experimental protocols are discussed.

INTRODUCTION

Creatine kinase (CK) plays an important role in storage and intracellular transfer of high-energy phosphoryls (~P) in tissues with high energy demand. By catalyzing the reaction creatine (Cr) + ATP \leftrightarrow phosphocreatine (PCr) + ADP + H⁺, CK provides a spatial and temporal energy buffer by keeping local ATP/ADP ratios balanced. The same reaction also facilitates that this enzyme can act as a regulator of intracellular tissue pH (see e.g. (1-3)). Based on these functions, the Cr-CK system was proposed to play an important role in neuroprotection in energy failure in brain (2).

In the brain of mammalian species CK production is developmentally regulated. Only two of the four known CK isoform subunit genes are expressed. The B-CK gene encodes the B-CK subunit isoform, which assembles into dimers mainly located in the cytosol. The ubiquitous CK (UbCKmit) gene specifies the UbCKmit subunit, which forms di- or octameric enzymes located between the inner and outer membranes of mitochondria (4, 5). B-CK, which represents more than 70-80% of total CK activity in brain, is presumed to work in close association with ATPases in the cytosol and cell membranes. There it provides ATPases with preferential access to ~P in ATP (from PCr) for work in ion-based electrogenic activity and (intra)cellular transport (1), which is important for neuronal communication, morphogenesis and plasticity of spines and synapses (6). Conversely, UbCKmit normally transfers ~P from ATP from oxidative phosphorylation (OXPHOS) directly onto PCr before shunting it into the cytoplasmic pool; this isoform is mainly present at sites of highest mitochondrial activity. The ~P flux through the combined B-CK and UbCKmit reactions appears to be higher in gray matter than in white matter (7).

Compared to skeletal muscle, our knowledge on the functional role of CK in brain energetics is lagging far behind. The main reason for this discrepancy is that metabolic study of the brain, especially *in vivo*, is technically much more challenging. In contrast to muscle, brain tissue consists of a very complex, interwoven, heterogeneous mixture of cell types, each with their own metabolic characteristics. Currently, there is intense debate on the design of energy metabolism of the brain, both in the field of cellular neurosciences and in the area where behavioral neurosciences, psychology and fMRI (functional magnetic resonance imaging) meet (see e.g. (8)). Main themes in this ongoing discussion are the cooperation between astrocytes and neurons, the relative contribution of glucose, lactate and ketone-bodies as fuels, cell-type dependence of glycolysis and lactate production, and the role of the mitochondrial TCA cycle plus associated pathways in the coupling to OXPHOS (9-11) during rest and when the brain is challenged (12). Also the coupling of ATP generation to the Cr-CK circuit in brain energetics is still not very well elucidated. Regional distribution and cell-type

involvement of Cr import across the blood brain barrier has not been studied in great detail (1) and also the contribution of endogenous creatine synthesis (1, 13, 14) is not very well understood. At the cellular level, B-CK itself has been found to be present in both glial and neuronal cell types, while UbCKmit expression is mainly confined to specific types of neurons (15). Unfortunately, details about the distribution profiles are lacking.

To study the role of CK in the brain we have generated mice deficient in both B-CK and UbCKmit (B-CK/UbCKmit^{-/-} mice) (15-17). Although these mice had a lower body and brain weight (18) and displayed abnormal behavioral and cognitive functions (partly also seen in single BCK or UbCKmit knock-outs), their basal brain functions were still intact, despite the complete absence of PCr (17). Levels of ATP, inorganic phosphate (Pi) and intracellular tissue pH were normal, as were most metabolites observed from ¹H MR spectra. The total creatine pool, however, was lower than in wt animals while NAA and glutamate (Glu) were elevated.

Although ¹H and ³¹P MR measurements yield specific metabolic information, they are often not suitable to follow the dynamic process of metabolite import, conversion and clearance from brain tissue. To study the routing or adaptation of metabolic fluxes in cellular energetics, *in vivo* ¹³C MRS with ¹³C labeled compounds is a more appropriate technique. Flux rates for several relevant metabolic pathways in the brain can be investigated simultaneously, as has been convincingly demonstrated in studies of coupling of energy pathways and the process of neurotransmitter cycling in brains of humans and rats (see e.g. (19-24)). ¹³C MRS studies in mouse brain, however, were thus far limited due to problems with the small sample size of tissue and intrinsically lower SNR .

Here, we present an experimental paradigm to perform *in vivo* ¹³C MRS with high temporal resolution especially designed for the mouse brain. Experimental monitoring of glucose uptake, lactate formation, synthesis and break-down of several neurotransmitters and other metabolites in mouse brain was demonstrated for the first time and used to compare flux rates through glycolysis and mitochondrial pathways in B-CK/UbCKmit^{-/-} and wt mice.

MATERIALS AND METHODS

Animals

B-CK/UbCKmit^{-/-} mice and wild-type (wt) animals of the same mixed genetic background (50% C57Bl/6 and 50% 129/Ola and age (3-4 months) were compared. Directly before the MR experiments, the mice were cannulated in the tail vein after which they were anaesthetized using isoflurane (1-2%) in a gas mixture of 50% O₂ and 50% N₂O delivered through a facemask. Breathing frequency was monitored, and kept constant during the experiment (100 ± 20 min⁻¹). Rectal temperature was monitored during the experiments using a fluoroptic thermometer and maintained at 38 ± 1 °C using a warm water circuit. After the experiments, animals were killed using cervical dislocation while under anesthesia. All experiments were in accordance with rules of the local animal ethics committee.

MR equipment and methods

The experiments were performed on a 7.0 T magnet (Magnex Scientific, Abingdon, England) interfaced to a S.M.I.S spectrometer (Surrey Medical Systems, Surrey, England) operating at 300 MHz for ¹H and at 75.5 MHz for ¹³C. The horizontal magnet has a free bore size of 120 mm.

A specially for mouse brain designed ¹H birdcage coil (length: 45 mm, Ø 40 mm) was used for shimming, imaging and ¹H decoupling, together with a ¹³C surface coil (Ø 12 mm) for ¹³C excitation and acquisition. Pulse-acquire experiments were performed using a WALTZ4 decoupling scheme during acquisition (90° pulse length ¹³C: 30 ms; 90° pulse length ¹H: 650 ms; TR=1.2 s).

Before glucose infusion, a natural abundance ¹³C MR spectrum was measured in 30 minutes (5 blocks of 256 averages). Subsequently, 80 spectra with a time resolution of 2.6 min were acquired (128 averages). After two spectra, [1-¹³C] labeled glucose (1 M, diluted in normal saline) was infused (STC-521, Terumo, Tokyo, Japan) using a protocol adopted from Peled-Kamar et al. (25). Infusion speeds were set at 1.2 ml/h for 1 min; 12 ml/h for 45 s; 3.6 ml/h for 5 min; and 1.2 ml/h for 4 min which in total infused 0.55 mmol in 10 minutes and 45 seconds.

Data processing

The glucose ¹³C-1 signals were fitted directly in the MR spectra obtained with high temporal resolution (2.6 min) using the AMARES method, with Lorentzian lineshape functions, in the MRUI software package (26). Signals were normalized to the maximum β-glucose signal per mouse. To be able to follow label incorporation into glutamate (Glu) and

glutamine (Gln), individual spectra were automatically corrected for frequency drifts and phase distortions with respect to each other by principal component analysis (27) implemented in home build software programmed in IDL (Research Systems inc., Boulder, Co, USA). Four spectra were added to enhance SNR, yielding a ten minute temporal resolution. The basal spectra, i.e. the spectra recorded before infusion of glucose, were averaged and subtracted from spectra obtained during the infusion of glucose. Incorporation of ^{13}C label into several metabolites was quantified by fitting signals for the third carbon position of lactate (Lac_3) and alanine (Ala_3), the third and fourth carbon positions of glutamate (Glu_3 and Glu_4) and the third and fourth position of glutamine (Gln_3 and Gln_4). Since the resonance frequencies of ^{13}C label on the second position of Glu and Gln are too close to be distinguished in our experiments (about 0.5 ppm; (28)), both signals were fitted with a single resonance and denoted as Glx_2 . Furthermore, signals for ^{13}C label at the second and third position of aspartate (Asp_2 and Asp_3) just as the 3-carbon and 4-carbon position in GABA (GABA_3 , GABA_4) could be discerned. All subtracted signals were fitted using a Gaussian lineshape function. The linewidths of Glu_3 and Gln_3 were equalized and the first order phase was fixed to an empirically determined value. No other prior knowledge was used. The signals fitted in the subtraction spectra were all scaled to the maximum intensity of the Glx_2 signal per mouse to normalize acquisition parameters.

Statistics

All data is presented as mean \pm SEM unless stated otherwise. Differences in metabolite levels were tested for significance using a t-test per time point. Evolution of metabolite or neurotransmitter levels during specific time intervals was tested for significant differences between wt and B-CK-UbCKmit $^{-/-}$ using a repeated measures test in SPSS (LEAD technologies Inc, Chicago, USA). Using this test, the last time-point in the time series ($t = 200$ min) was excluded to prevent list-wise deletion of animals. In all statistical tests, differences were considered to be significant at $p < 0.05$.

RESULTS

For the duration of the entire experiment, which lasted for over 3.5 hours, the experimental setup enabled good physiological control over the mouse as assessed from the steady condition of the body temperature and breathing frequency. All signals in the ^{13}C MR spectra originated from tissue close to the surface coil, predominantly representing the cortex.

Upon infusion of glucose labeled with 99% ^{13}C at the C1 position, two signals for β - and α -glucose appeared in the ^{13}C MR spectra (figure 6.1a).

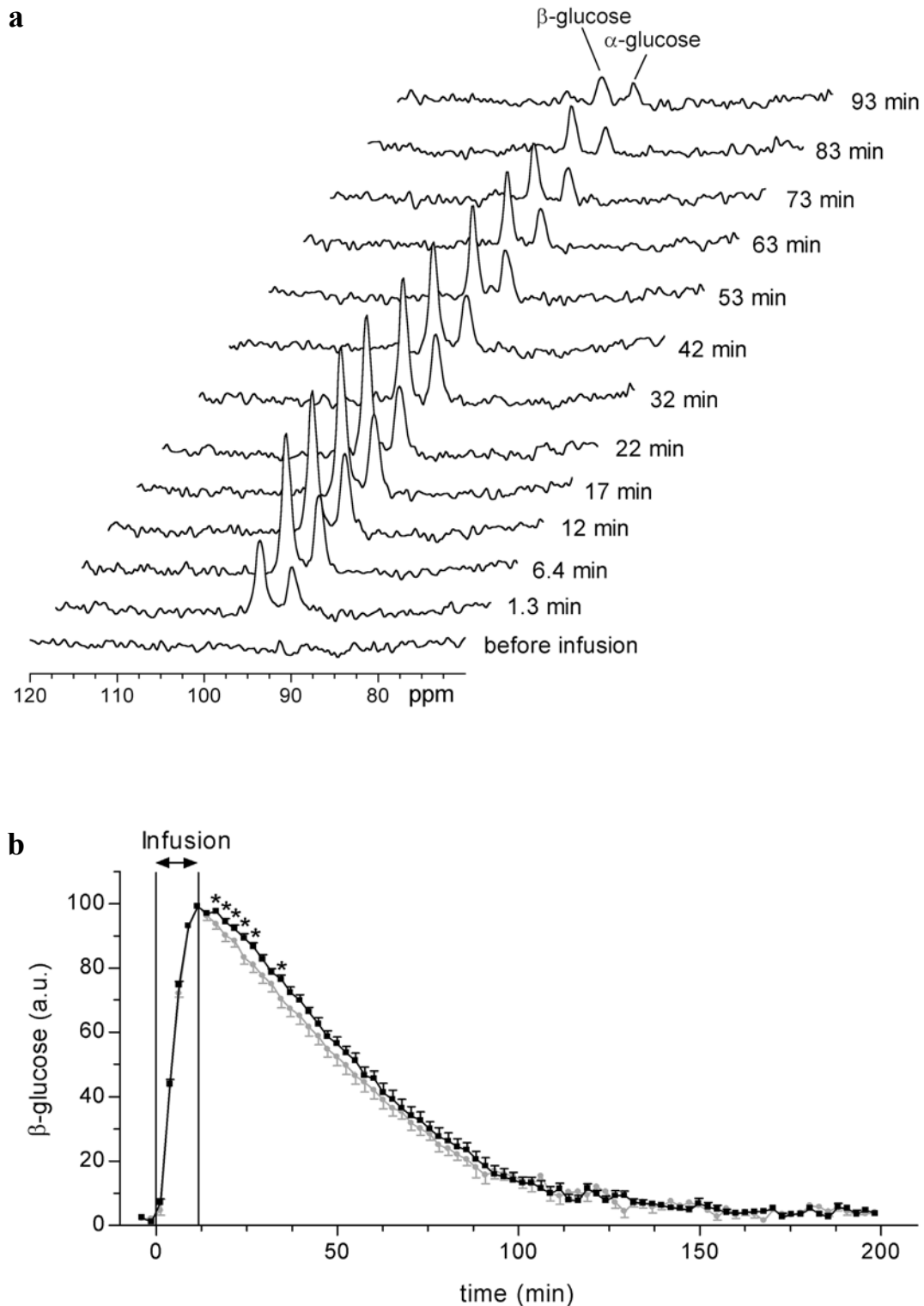


Figure 6.1: ^{13}C labeled glucose infusion and clearance in the mouse brain at different time points (a) and the difference of normalized glucose signals between *B-CK/UbCKmit*^{-/-} (grey dots) and *wt* (black squares) mice (b). Data is presented as mean \pm SEM, asterisks indicate a significant difference between *wt* and *B-CK/UbCKmit*^{-/-} mice for that time point.

After the infusion, these signals decreased, but were still detectable for more than two hours after the infusion was terminated. A difference appeared in the time dependent curves of the β -glucose signal between wt and B-CK/UbCKmit $^{-/-}$ mice (figure 6.1b). After the maximum of glucose accumulation is reached at the end of the infusion period, glucose values per time point were significantly lower in knock-out mice. Towards the end of the experiment, i.e. from approximately 100 minutes after glucose infusion until the termination of the experiment ($t=200$ min), glucose values in wt and knock-out animals became identical again.

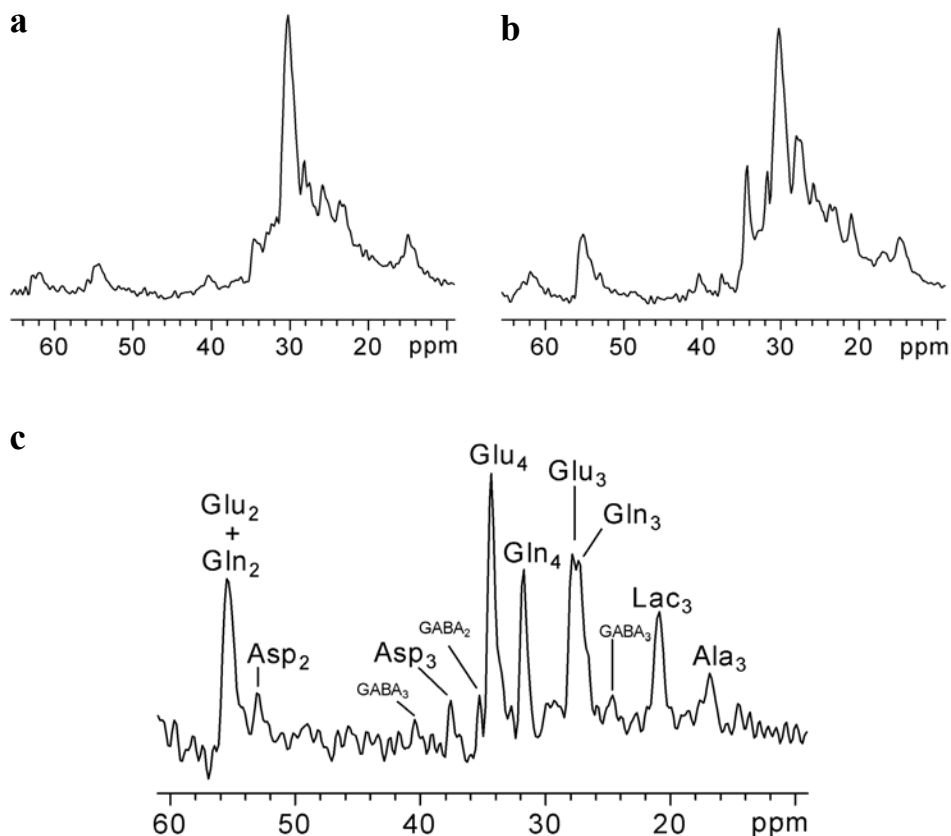


Figure 6.2: ^{13}C spectrum (30 min. average) of the mouse brain before infusion (a), after infusion (b) and subtraction spectrum (c). The horizontal and vertical scaling in the difference spectrum is enlarged to appreciate all visible resonances.

Subtraction of a spectrum acquired before infusion (figure 6.2a) from a average spectrum acquired over a time period of 30 minutes during infusion (figure 6.2b) revealed multiple MR signals of which the large ones were identified as Glu (Glu₃, Glu₄), Gln (Gln₃, Gln₄), Glx₂ and Lac. Furthermore, smaller distinct signals for Asp (Asp₂, Asp₃), GABA (GABA₂, GABA₃, GABA₄) and Ala were observed (figure 6.2c).

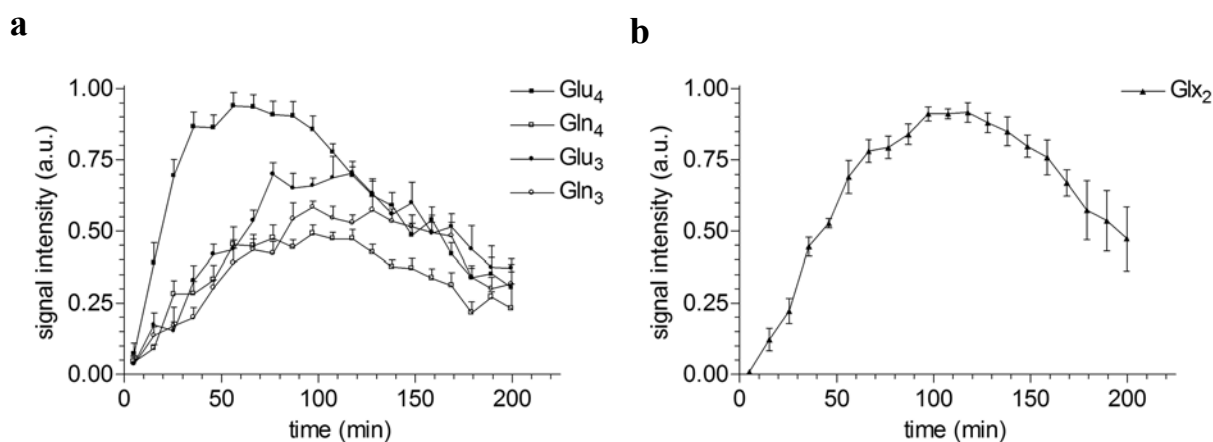


Figure 6.3: Sequential incorporation of ^{13}C label into the fourth and third position of Glu and Gln (A) and into the second position of both Glu + Gln (B) in wt mice. All signal intensities are scaled to the maximum signal intensity of the Glx₂. Data is presented as mean \pm SEM.

Sequential incorporation of ^{13}C label into several positions of Glu and Gln (figure 6.3), just as into GABA, Asp, Lac and Ala was followed over time. The signal of the carbon-4 in glutamate was the first to appear in the ^{13}C MR spectra, and reached the highest amplitude of all metabolites that accumulate ^{13}C label at approximately 60 minutes after the start of infusion. Subsequent conversion of glutamate into glutamine by glutamine synthetase is reflected by the decrease of the Glu₄ signal and the increase of signal originating from ^{13}C -label at the 4-carbon position of glutamine. If the C4 label is not transferred from α -ketoglutarate to Glu₄, it will remain in the Krebs cycle and be transferred to succinate (29, 30). Because this molecule is symmetrical of structure, the C4 label has an equal chance to be transferred to either the C3 or the C2 position. The signal of Glu₃ therefore increased with a slower pace (maximum at approx. $t=100$ min.) than Glu₄ as this compound is generated during the second turn of the Krebs cycle. Label of Glu₃ is then transferred to Gln₃ (maximum at approx. $t=115$ min.) by glutamine synthetase. Incorporation of label at the second carbon position of the combined glutamate and glutamine pool (figure 6.3b) occurred also more slowly than incorporation of Glu₄ label, with a maximum at approximately 110 minutes.

Comparing label incorporation into several metabolites between wt and B-CK/UbCKmit^{-/-} mice revealed interesting differences and similarities. Incorporation of ^{13}C label from glucose into lactate was significantly decreased in B-CK/UbCKmit^{-/-} mice (figure 6.4). Similar results were observed for the temporal incorporation of label into Ala (figure 6.4b), with a clear trend to higher accumulation in wt animals.

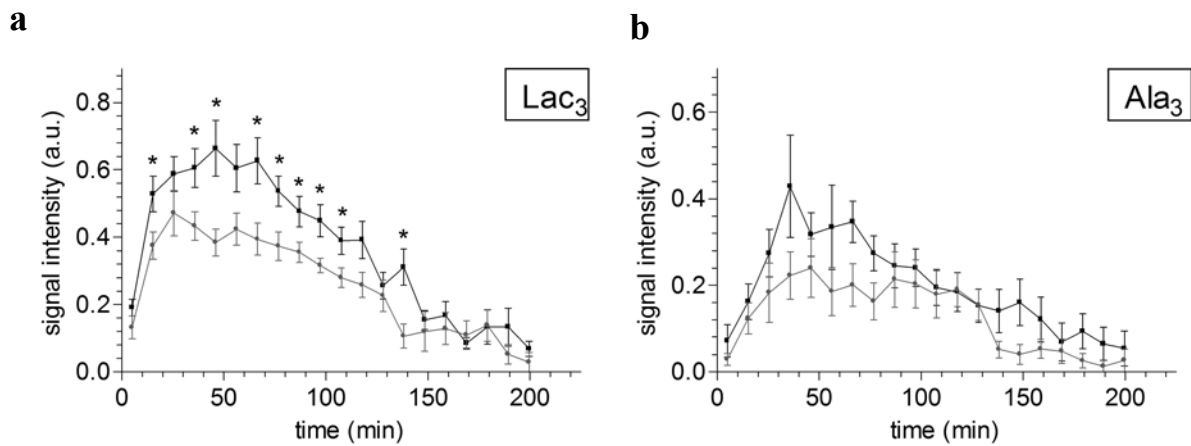


Figure 6.4: Comparison of sequential build-in of ^{13}C label in Lac_3 (a) and Ala_3 (b) between wt (black squares) and B-CK/UbCKmit $-/-$ (grey dots) mice. All signal intensities are scaled to the maximum signal intensity of the Glx_2 . Data is presented as mean \pm SEM; asterisks indicate a significant difference between wt and B-CK/UbCKmit $-/-$ mice for that time point.

Temporal evolutions of several ^{13}C labeled Glu and Gln pools were monitored and compared between wt and knock-out animals (figure 6.5). The total amount of signal measured in each pool, e.g. of Glu_4 , is the summed result of both incorporation of new ^{13}C label into Glu and breakdown of Glu_4 to Gln_4 . During the measurement period, both processes will simultaneously contribute to the temporal evolution of the total Glu_4 signal. At 55 minutes after the start of the infusion period, Glu_4 breakdown is larger than the generation of newly formed Glu_4 signal resulting in a decrease in the total Glu_4 pool (figure 6.5a). The evolution of this decrease was significantly faster in B-CK/UbCKmit $-/-$ mice. Besides this observation, no distinct differences in the time courses of transfer of label into several positions in Glu and Gln were detected (figure 6.5).

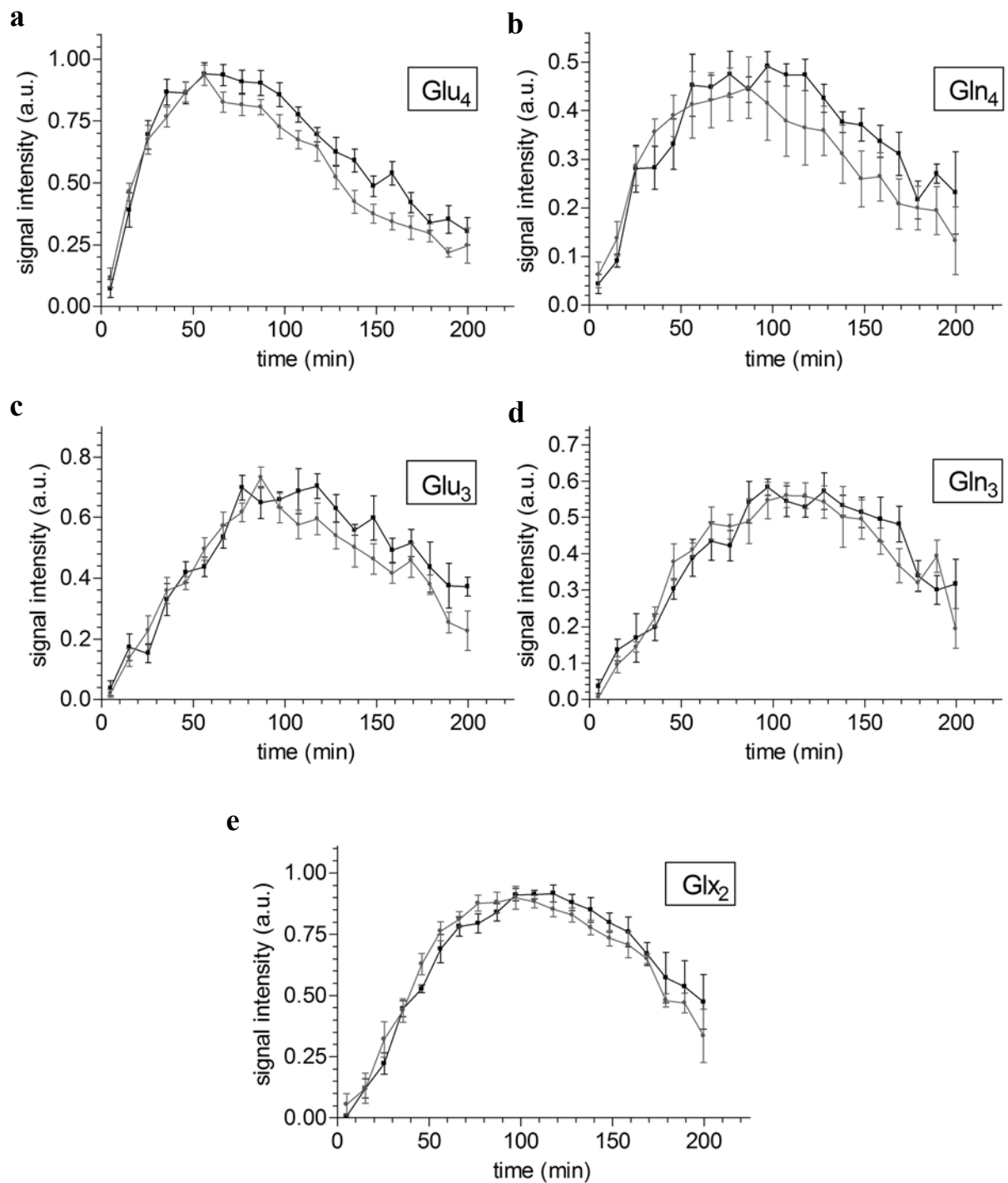


Figure 6.5: Profiles of incorporation of sequential build-in of ^{13}C label incorporation in *Glu₄* (a), *Gln₄* (b), *Glu₃* (c), *Gln₃* (d) and *Glx₂* (e) between wt (black squares) and *B-CK/UbCKmit -/-* (grey dots) mice. All signal intensities are scaled to the maximum signal intensity of *Glx₂*. Data is presented as mean \pm SEM.

DISCUSSION

The present study is the first demonstration that ^{13}C MRS can be used as a tool to study metabolic conversions in (transgenic) mouse brain *in vivo*. Both glucose uptake and amino acid formation were analyzed in one experiment with high temporal resolution using dedicated home-made equipment for signal acquisition. A broad range of signals for metabolites involved in oxidative metabolism and neurotransmitter recycling could be identified in the ^{13}C MR spectra. These results open up new prospects for the study of existing and new mouse models for brain disease.

The temporal resolution of ^{13}C label detection in amino acid signals achieved in the present study attained the temporal resolution obtained in other studies with larger animals and humans (28, 31, 32). Still, in the rat and human studies more metabolites could be discerned at this resolution as larger brain volumes can be selected resulting in a better SNR. In addition, less tissue-air transitions occur close to the selected volume providing a more optimal magnetic homogeneity within the volume of interest. Clearly, the small brain size of the mouse will remain an inherent challenge for future studies and a problem that can only be tackled with further sophistication of hard- and software and experimental procedures.

Limitations of the current infusion- and data processing protocols

Since the main goal of the current work is to optimize the technical feasibility of ^{13}C MRS in the mouse brain, we first address this aspect of our study. The current experimental approach yielded reproducible spectral profiles with clear peaks for relevant carbohydrates (glucose, lactate) in the glycolytic pathway and mitochondrial TCA-cycle. Furthermore, signals for amino acids (and derivatives) providing information on the TCA-cycle and the Glu/Gln neurotransmitter cycle were easily detected. The infusion protocol for the ^{13}C glucose label was adopted from a ^{13}C MRS study on glucose uptake in mice (25). Both the total amount of glucose infused in this study and the infusion rate appears to be rather high; other non-MRS studies on glucose metabolism in mice report values which are lower (see e.g. (33-36)). Assuming a blood plasma glucose concentration of approximately 7 mM (34, 37) and a blood volume in the mouse of about 2 ml (38), the total glucose in the blood can be calculated to be in the order of 14 μmol . Infusion of 0.55 mmol glucose in 11 minutes will therefore give a severe rise in blood glucose concentration causing a significant metabolic challenge. To approach conditions in which the glucose concentrations are closer to physiological levels, it is important to further optimize the infusion protocol.

During the measurement of ^{13}C labeled glucose it is not possible to discriminate between glucose signal originating from the brain and glucose signals originating from the

blood vessels in the brain. Although there appears to be a linear relationship between blood and brain glucose as was shown in rat (39), this relation may very well be altered during infusion in genetically modified mice (25). Unlike can be done for humans and rats, for mice it is difficult to acquire blood samples while the animal is inside the magnet during an MR protocol as the blood volume is too low compared to the volume of the connecting infusion lines. Therefore, separate parallel experiments under identical conditions have to be performed in order to obtain reliable $^{13}\text{C}/^{12}\text{C}$ ratios and glucose concentrations. Also future use of an external phantom of known concentration as a reference may add to a better comparison of absolute metabolite levels in wt and knock-out mice.

Larger glycolytic capacity in B-CK/UbCKmit^{-/-} mice

In the absence of absolute values for glucose uptake and conversion, we now took the approach to normalize all signals for one mouse to the maximum intensity of the glucose signal observed in that same animal. Using this approach, relative differences in ^{13}C label incorporation between B-CK/UbCKmit^{-/-} and wt animals were observed.

The significant lower glucose values per time point suggest a faster or earlier clearance rate of glucose in B-CK/UbCKmit^{-/-} mice. As glucose clearance from the brain reflects the rate of glycolysis (25), this points to an earlier onset of glycolysis or a larger glycolytic capacity, possibly by transcriptional or post-translational up-regulation of specific enzymes in the glycolytic pathway. Although this picture matches the results found in CK deficient muscle (40-42), also other physiological parameters - including altered mitochondrial function in brain or altered lipid and carbohydrate metabolism in other organs in the body - have to be considered. It has been shown, for instance, that B-CK/UbCKmit^{-/-} mice have a lower average body weight than wt animals (18) and show size adaptations in fat pads and in liver (Strejiger, unpublished results). Furthermore, basal glucose levels in B-CK/UbCKmit^{-/-} mice appear to be decreased and the levels of metabolic hormones have changed (Strejiger, unpublished result). Infusion of identical quantities of glucose may therefore not necessarily yield similar blood glucose concentrations in wild-type and knock-out animals. The extend to which these changes in other tissues affect glucose levels in circulation and in brain is not known.

Besides direct measurement of the total ^{13}C labeled glucose pool, i.e. of signal originating both from blood and brain glucose, indirect determination of incorporation of label in the brain glucose pool only is also possible. Pfeuffer and coworkers showed that the incorporation of ^{13}C label from glucose into lactate mirrors the kinetics of the incorporation of label in brain glucose (43). The reduced accumulation of lactate would therefore point to lower brain glucose levels - or lower glucose uptake - in knock-out mice. It is also feasible,

however, that changes in mitochondrial Krebs cycle turnover rate augmented lactate demand and that increased uptake of pyruvate coupled to more intense mitochondrial activity explains the lower glucose signal for the B-CK/UbCKmit^{-/-} mice.

Adaptations in oxidative metabolism in B-CK/UbCKmit^{-/-} mice

In the subtraction spectra, signals were normalized per mouse to the maximum of the Glx₂ signal. This normalization was preferred over normalizing to the maximum of the glucose signal, as was done in the processing of the glucose data itself, because glucose signals likely do not originate only from within the cell. Glx₂ was chosen for this normalization because it has a relatively large signal with no other large signal in the spectral neighborhood which makes it ideal for a robust fit. It represents a summed signal of the 2-carbon positions in both glutamate and glutamine, each mainly originating from a different compartment because glutamate is mainly present in neurons while glutamine is mainly present in glial cells (see e.g. (29, 30)). Normalizing to this signal therefore appears more robust and reliable than normalizing to one of the Glu or Gln signals alone.

The only significant difference when comparing Glu neurotransmitter generation and breakdown in B-CK/UbCKmit^{-/-} mice to that in control animals, is in the faster decrease of the Glu₄ signal. Indeed, the most likely position to find differences when looking at the oxidative side of the metabolism is in Glu₄, since this compound is the first MR visible metabolite to be generated after ¹³C label has entered the Krebs cycle. Generation of all other metabolites takes longer, and differences in generation rate or breakdown may therefore be obscured by dilution of label both in time and to other compounds.

Taken together, both our findings of an earlier onset of glycolysis or an increased flux through glycolysis and a reduced accumulation of ¹³C label into lactate in B-CK/UbCKmit^{-/-} mice suggest a faster transfer of label into the Krebs cycle. Although no differences could be observed in the generation of Glu₄, its breakdown was significantly faster in knock-out mice. Also this observation can be explained by altered mitochondrial activity. To avoid that evidence remains merely circumstantial and indirect, future experiments need to be designed that will enable us to follow ¹³C label transfer into several amino acid pools in such a way that dilution of label is maximally prevented. This can be accomplished by adapting infusion protocols and optimizing measurement protocols to obtain quantitative values of MR signal intensities and chemical concentrations of all relevant metabolites.

ACKNOWLEDGEMENTS

The authors would like to thank Femke Streijger for helpful discussions. This study was supported by the Netherlands Organization for Scientific Research (NWO-ZONMW).

REFERENCES

1. Wyss, M. and Kaddurah-Daouk, R. Creatine and creatinine metabolism. *Physiol Rev* 2000;80:1107-213.
2. Wyss, M. and Schulze, A. Health implications of creatine: can oral creatine supplementation protect against neurological and atherosclerotic disease? *Neuroscience* 2002;112:243-60.
3. in 't Zandt, H.J., Oerlemans, F., Wieringa, B. and Heerschap, A. Effects of ischemia on skeletal muscle energy metabolism in mice lacking creatine kinase monitored by in vivo 31P nuclear magnetic resonance spectroscopy. *NMR Biomed* 1999;12:327-34.
4. Wyss, M., Smeitink, J., Wevers, R.A. and Wallimann, T. Mitochondrial creatine kinase: a key enzyme of aerobic energy metabolism. *Biochim Biophys Acta* 1992;1102:119-66.
5. Wallimann, T., Wyss, M., Brdiczka, D., Nicolay, K. and Eppenberger, H.M. Intracellular compartmentation, structure and function of creatine kinase isoenzymes in tissues with high and fluctuating energy demands: the phosphocreatine circuit for cellular energy homeostasis. *Biochem J* 1992;281:21-40.
6. Li, Z., Okamoto, K., Hayashi, Y. and Sheng, M. The importance of dendritic mitochondria in the morphogenesis and plasticity of spines and synapses. *Cell* 2004;119:873-87.
7. Cadoux-hudson, T.A., Blackledge, J.M. and Radda, G.K. Imaging of human brain creatine kinase activity in vivo. *FASB Journal* 1989;3:2660-2666.
8. Jaffe, S. Fake method for research impartiality (fMRI). *The Scientist* 2004;18:64.
9. Pellerin, L. and Magistretti, P.J. Glutamate uptake into astrocytes stimulates aerobic glycolysis: a mechanism coupling neuronal activity to glucose utilization. *Proc Natl Acad Sci U S A* 1994;91:10625-9.
10. Magistretti, P.J. Brain Energy metabolism. in: *Fundamental neuroscience* Eds.: M. J. Zigmond, F. E. Bloom, S. C. Landis, J. L. Roberts and L. R. Squire San Diego, CA: Academic Press: 2003. 339-360
11. Magistretti, P.J., Pellerin, L., Rothman, D.L. and Shulman, R.G. Energy on demand. *Science* 1999;283:496-7.
12. Pellerin, L. and Magistretti, P.J. Food for thought: challenging the dogmas. *J Cereb Blood Flow Metab* 2003;23:1282-6.
13. Braissant, O., Henry, H., Loup, M., Eilers, B. and Bachmann, C. Endogenous synthesis and transport of creatine in the rat brain: an in situ hybridization study. *Brain Res Mol Brain Res* 2001;86:193-201.
14. Wyss, M. and Wallimann, T. Creatine metabolism and the consequences of creatine depletion in muscle. *MolCellBiochem* 1994;133-134:51-66.
15. Jost, C.R., Van Der Zee, C.E., In 't Zandt, H.J., Oerlemans, F., Verheij, M., Streijger, F., Fransen, J., Heerschap, A., Cools, A.R. and Wieringa, B. Creatine kinase B-driven energy transfer in the brain is important for habituation and spatial learning behaviour, mossy fibre field size and determination of seizure susceptibility. *Eur J Neurosci* 2002;15:1692-706.
16. Steeghs, K., Oerlemans, F. and Wieringa, B. Mice deficient in ubiquitous mitochondrial creatine kinase are viable and fertile. *Biochim Biophys Acta* 1995;1230:130-8.
17. in 't Zandt, H.J., Renema, W.K., Streijger, F., Jost, C., Klomp, D.W., Oerlemans, F., Van der Zee, C.E., Wieringa, B. and Heerschap, A. Cerebral creatine kinase deficiency influences metabolite levels and morphology in the mouse brain: a quantitative in vivo 1H and 31P magnetic resonance study. *J Neurochem* 2004;90:1321-30.

18. Streijger, F., Oerlemans, F., Ellenbroek, B.A., Jost, C., Wieringa, B. and Van Der Zee, C.E. Structural and behavioural consequences of double deficiency for creatine kinases BCK and UbCKmit. *Behav Brain Res* 2004;in press.
19. Sibson, N.R., Dhankhar, A., Mason, G.F., Behar, K.L., Rothman, D.L. and Shulman, R.G. In vivo ^{13}C NMR measurements of cerebral glutamine synthesis as evidence for glutamate-glutamine cycling. *Proc Natl Acad Sci U S A* 1997;94:2699-704.
20. Sibson, N.R., Mason, G.F., Shen, J., Cline, G.W., Herskovits, A.Z., Wall, J.E., Behar, K.L., Rothman, D.L. and Shulman, R.G. In vivo (^{13}C) NMR measurement of neurotransmitter glutamate cycling, anaplerosis and TCA cycle flux in rat brain during. *J Neurochem* 2001;76:975-89.
21. Gruetter, R., Novotny, E.J., Boulware, S.D., Rothman, D.L., Mason, G.F., Shulman, G.I., Shulman, R.G. and Tamborlane, W.V. Direct measurement of brain glucose concentrations in humans by ^{13}C NMR spectroscopy. *Proc Natl Acad Sci U S A* 1992;89:1109-12.
22. Gruetter, R., Seaquist, E.R., Kim, S. and Ugurbil, K. Localized in vivo ^{13}C -NMR of glutamate metabolism in the human brain: initial results at 4 tesla. *Dev Neurosci* 1998;20:380-8.
23. Bluml, S., Moreno, A., Hwang, J.H. and Ross, B.D. $1-(^{13}\text{C})$ glucose magnetic resonance spectroscopy of pediatric and adult brain disorders. *NMR Biomed* 2001;14:19-32.
24. Shulman, R.G., Hyder, F. and Rothman, D.L. Cerebral energetics and the glycogen shunt: neurochemical basis of functional imaging. *Proc Natl Acad Sci U S A* 2001;98:6417-22.
25. Peled-Kamar, M., Degani, H., Bendel, P., Margalit, R. and Groner, Y. Altered brain glucose metabolism in transgenic-PFKL mice with elevated L-phosphofructokinase: in vivo NMR studies. *Brain Res* 1998;810:138-45.
26. <http://www.mrui.uab.es/mrui/>
27. Witjes, H., Melssen, W.J., in 't Zandt, H.J., van der Graaf, M., Heerschap, A. and Buydens, L.M. Automatic correction for phase shifts, frequency shifts, and lineshape distortions across a series of single resonance lines in large spectral data sets. *J Magn Reson* 2000;144:35-44.
28. Henry, P.G., Oz, G., Provencher, S. and Gruetter, R. Toward dynamic isotopomer analysis in the rat brain in vivo: automatic quantitation of ^{13}C NMR spectra using LCMoDel. *NMR Biomed* 2003;16:400-12.
29. Gruetter, R., Seaquist, E.R. and Ugurbil, K. A mathematical model of compartmentalized neurotransmitter metabolism in the human brain. *Am J Physiol Endocrinol Metab* 2001;281:E100-12.
30. Cruz, F. and Cerdan, S. Quantitative ^{13}C NMR studies of metabolic compartmentation in the adult mammalian brain. *NMR Biomed* 1999;12:451-62.
31. Gruetter, R., Adriany, G., Choi, I.Y., Henry, P.G., Lei, H. and Oz, G. Localized in vivo ^{13}C NMR spectroscopy of the brain. *NMR Biomed* 2003;16:313-38.
32. Ross, B., Lin, A., Harris, K., Bhattacharya, P. and Schweinsburg, B. Clinical experience with ^{13}C MRS in vivo. *NMR Biomed* 2003;16:358-69.
33. Voshol, P.J., Jong, M.C., Dahlmans, V.E., Kratky, D., Levak-Frank, S., Zechner, R., Romijn, J.A. and Havekes, L.M. In muscle-specific lipoprotein lipase-overexpressing mice, muscle triglyceride content is increased without inhibition of insulin-stimulated whole-body and muscle-specific glucose uptake. *Diabetes* 2001;50:2585-90.
34. Kim, J.K., Zisman, A., Fillmore, J.J., Peroni, O.D., Kotani, K., Perret, P., Zong, H., Dong, J., Kahn, C.R., Kahn, B.B. and Shulman, G.I. Glucose toxicity and the development of diabetes in mice with muscle-specific inactivation of GLUT4. *J Clin Invest* 2001;108:153-60.
35. van den Hoek, A.M., Heijboer, A.C., Corssmit, E.P., Voshol, P.J., Romijn, J.A., Havekes, L.M. and Pijl, H. PYY3-36 reinforces insulin action on glucose disposal in mice fed a high-fat diet. *Diabetes* 2004;53:1949-52.
36. van Dijk, T.H., Boer, T.S., Havinga, R., Stellaard, F., Kuipers, F. and Reijngoud, D.J. Quantification of hepatic carbohydrate metabolism in conscious mice using serial blood and urine spots. *Anal Biochem* 2003;322:1-13.

37. Burcelin, R., Uldry, M., Foretz, M., Perrin, C., Dacosta, A., Nenniger-Tosato, M., Seydoux, J., Cotecchia, S. and Thorens, B. Impaired glucose homeostasis in mice lacking the alpha1b-adrenergic receptor subtype. *J Biol Chem* 2004;279:1108-15.
38. Diehl, K.H., Hull, R., Morton, D., Pfister, R., Rabemampianina, Y., Smith, D., Vidal, J.M. and van de Vorstenbosch, C. A good practice guide to the administration of substances and removal of blood, including routes and volumes. *J Appl Toxicol* 2001;21:15-23.
39. Choi, I.Y., Lee, S.P., Kim, S.G. and Gruetter, R. In vivo measurements of brain glucose transport using the reversible Michaelis-Menten model and simultaneous measurements of cerebral blood flow changes during hypoglycemia. *J Cereb Blood Flow Metab* 2001;21:653-63.
40. Steeghs, K., Benders, A., Oerlemans, F., de Haan, A., Heerschap, A., Ruitenbeek, W., Jost, C., van Deursen, J., Perryman, B., Pette, D., Bruckwilder, M., Koudijs, J., Jap, P., Veerkamp, J. and Wieringa, B. Altered Ca²⁺ responses in muscles with combined mitochondrial and cytosolic creatine kinase deficiencies. *Cell* 1997;89:93-103.
41. van Deursen, J., Heerschap, A., Oerlemans, F., Ruitenbeek, W., Jap, P., ter Laak, H. and Wieringa, B. Skeletal muscles of mice deficient in muscle creatine kinase lack burst activity. *Cell* 1993;74:621-31.
42. de Groof, A.J., Oerlemans, F.T., Jost, C.R. and Wieringa, B. Changes in glycolytic network and mitochondrial design in creatine kinase-deficient muscles. *Muscle Nerve* 2001;24:1188-96.
43. Pfeuffer, J., Tkac, I., Choi, I.Y., Merkle, H., Ugurbil, K., Garwood, M. and Gruetter, R. Localized in vivo ¹H NMR detection of neurotransmitter labeling in rat brain during infusion of [1-¹³C] D-glucose. *Magn Reson Med* 1999;41:1077-83.

7

MR SPECTROSCOPY OF MUSCLE AND BRAIN IN GUANIDINOACETATE METHYLTRANSFERASE (GAMT) DEFICIENT MICE: VALIDATION OF AN ANIMAL MODEL TO STUDY CREATINE

KlaasJan Renema
Andreas Schmidt
Jack van Asten
Frank Oerlemans
Kurt Ullrich
Bé Wieringa
Dirk Isbrandt
Arend Heerschap

This chapter is in slightly modified form published as:

Renema, W.K., Schmidt, A., Van Asten, J.J., Oerlemans, F., Ullrich, K., Wieringa, B., Isbrandt, D. and Heerschap, A. MR spectroscopy of muscle and brain in guanidinoacetate methyltransferase (GAMT)-deficient mice: Validation of an animal model to study creatine deficiency. *Magn Reson Med* 2003; 50: 936-43.

ABSTRACT

As a model for guanidinoacetate methyltransferase (GAMT) deficiency in humans, a gene knock-out mouse model was generated. Here we report on several metabolic abnormalities in these mice, observed by *in vivo* and *in vitro* MR spectroscopy.

In ^1H MR spectra of brain and hind-leg muscle a clearly reduced signal of creatine (Cr) was observed in GAMT deficient (GAMT $^{-/-}$) animals. Analysis of the ^1H MR spectra of GAMT $^{-/-}$ brain indicated little or no increase of a signal for guanidinoacetate (Gua). In proton MR spectra of muscle, a broad signal of low intensity was observed for Gua. However, substantial Gua accumulation in intact muscle tissue was unequivocally confirmed in high resolution magic angle spinning spectra, in which the Gua signal was resolved as one clear sharp singlet.

In ^{31}P MR analysis of brain and hind-leg muscle a strongly reduced phosphocreatine (PCr) content was shown. In addition, a signal of phosphorylated Gua at 0.5 ppm up-field of PCr was observed, with much higher intensity in muscle than in brain. This signal decreased when ischemia was applied to the muscle and recovered after ischemia was released. Overall the *in vivo* ^{31}P and ^1H MR spectroscopy of GAMT $^{-/-}$ mice is similar to that of human GAMT deficiency. This opens up new avenues for the fundamental study of tissue-type dependence of creatine synthesis and transport, and for diagnostic and therapeutic aspects of creatine deficiencies in humans.

INTRODUCTION

Guanidinoacetate methyltransferase (GAMT) is a key enzyme in the biosynthesis of creatine (Cr), a process that mainly occurs in pancreas and liver (1). The first step on this synthetic route involves transfer of the amidino group of arginine to glycine, to yield ornithine and guanidinoacetate (Gua). Subsequently, GAMT facilitates the methylation of Gua to Cr.

Cr is a central compound in the energy metabolism of tissues such as muscle and brain. In these tissues it can be phosphorylated to phosphocreatine (PCr) using one of the five isoenzymes of Creatine Kinase (CK). Finally, Cr and PCr are catabolized to creatinine (Crn), which is excreted through the urine. To maintain a constant body pool of Cr, its breakdown and build-up via dietary intake and endogenous synthesis must be balanced and its transport across membranes of cells in various tissues must be tightly regulated (2).

GAMT deficiency was described for the first time as a new inborn error of metabolism (3) in an infant with extrapyramidal movement disorder, who had low Crn in serum and urine (3-6). Up to now, several cases of GAMT deficiency have been reported (7-11). Patients show symptoms in a wide range of severity (12) including developmental retardation (4, 7-9, 11), muscle hypotonia (3, 5, 8, 11), extrapyramidal movement abnormalities (3-5, 7) and epileptic seizures (7, 8, 11).

Localized MR spectroscopy (MRS) of the brain of young patients has played a decisive role in the elucidation of the pathophysiology of GAMT deficiency. A strongly reduced Cr signal was revealed by ^1H MRS (3, 4, 7-11, 13). In ^{31}P MR spectra PCr was decreased and a new resonance appeared, which was assigned to phosphorylated Gua (PGua) (7, 10, 13). This assignment was confirmed by an additional resonance in the ^1H MR spectrum at 3.8 ppm, which is likely to arise from Gua protons (3, 9, 10, 13).

Oral intake of arginine resulted in an increase of the Gua signal intensity in the proton MR spectra (3, 13), while intake of Cr led to a partial restoration of the Cr signal (3, 4, 7, 9-13), decrease of the Gua signal (3, 7, 10, 13) and improvement of clinical symptoms (3-13).

To our knowledge, in only two patients with GAMT-deficiency MRS of muscle was performed. The first case study reported on a considerable signal for creatine in ^1H MR spectra of muscle but not in brain, and no peak at 3.8 ppm (10). In the ^{31}P MR spectrum only one peak was observed around 0 ppm, which was assigned to PCr. The second case study showed both PCr and PGua in ^{31}P MR spectra of muscle while no ^1H Cr resonance was observed in brain (14).

Detailed study of the pathophysiology of GAMT deficiency and possible treatment strategies is difficult in humans, as the disease is very rare. Therefore, GAMT deficient knock-out mice (GAMT $^{-/-}$) were generated (15). This article presents the first results of ^{31}P and ^1H MRS of hind-leg muscle and brain in these mice. The purpose of this work was to

validate the GAMT^{-/-} mice as useful model for creatine deficiency in human patients and to initiate a study into tissue-type and dietary-composition dependent accumulation of Gua derivatives.

METHODS

Animals

GAMT^{-/-} mice were generated by homologous recombination in embryonic stem cells (15). As a reference, heterozygous (+/-) and homozygous (+/+) wild-type-like (wt) littermates of the GAMT^{-/-} animals were used. In previous studies (not published), Isbrandt et al. showed that no differences could be observed between these groups and that animals of both genotypes can serve as control. For the determination of the T₂ of water and methyl Cr protons in hind-leg muscle, six wild-type-like mice with a randomly inbred mixed background of C57Bl/6 and 129/Ola were used. During the MR experiments, all animals were anaesthetized using 1% isoflurane in a gas mixture of 50% O₂ and 50% N₂O delivered through a facemask. Breathing frequency was monitored and a warm waterbed was used to keep the animals at normal body temperature. All experiments were approved by the local animal ethics committee.

MR equipment

The in vivo MR experiments were performed on a 7.0 T magnet (Magnex Scientific, Abingdon, England) interfaced to a S.M.I.S. spectrometer (Surrey Medical Systems, Surrey, England) operating at 300.22 MHz for ¹H and at 121.53 MHz for ³¹P. The horizontal magnet was equipped with a 150 mT/m shielded gradient set and had a free bore size of 120 mm.

High resolution magic angle spinning (HRMAS) spectroscopy experiments were performed on muscular tissues using a Bruker DRX 500 MHz spectrometer.

MR spectroscopy studies

To get a good overview of the phenotype of the GAMT^{-/-} mice, ¹H and ³¹P MR spectroscopy studies of both hind-leg muscle and of brain were performed. In the ¹H MR experiments Cr refers to the sum of Cr and PCr.

For the ¹H MR studies on the mouse brain, a 12 mm surface coil anatomically shaped for mouse brain was used. Additional perspex earbars provided stereotactic fixation. Localized spectroscopy was performed using a STEAM sequence (TE=10 ms, TM=15 ms, TR=5000 ms, 64 averages) with VAPOR water suppression (16) and outer volume suppression. A 3x3x3 mm³ (27μl) voxel was positioned in the center of the brain guided by

gradient echo images. In this study, measurements were performed in seven GAMT^{-/-} and five wt animals.

The ³¹P MR brain measurements were done using two surface coils, tuned to the ³¹P frequency and working in quadrature mode. A large ¹H surface coil was utilized for shimming, imaging and localization. To prevent contamination with signal from the masseter muscles, an ISIS sequence (17) was used (TR=7000 ms, 8 step phase cycle, 512 averages), consisting of a 6.5 kHz adiabatic hyperbolic secant pulse for inversion, together with a 50 μs rectangular 90° RF pulse for excitation. A voxel with size 6.5x6.5x4.5 mm³ (190 μl) was positioned in the brain guided by gradient echo images. The mouse head was fixated using the quadrature surface coil and earbars.

¹H MR measurements on the mouse hind leg were done using an Alderman-Grant type of coil (18), oriented at the magic angle (55°) with respect to the main magnetic field to reduce dipolar interactions (19). The same STEAM sequence was used as in the ¹H brain measurements (voxel size 1.8x1.8x3.4 mm³, TR=5 s, 128 averages). For absolute quantification, the T₂ for water and Cr protons was determined by acquiring a suppressed and water suppressed ¹H spectra at six different echo times in a separate experiment.

³¹P MR pulse acquire experiments (TR=7000 ms, 64 averages) on the hind leg were done using a three-turn solenoid coil, together with a proton Alderman-Grant type of coil for shimming. ³¹P MR experiments on hind-leg muscle and brain, and ¹H MR experiments on hind-leg muscle were performed in seven GAMT^{-/-} and seven wt animals. Ischemic occlusion of skeletal muscle was applied to two GAMT^{-/-} animals by clamping with a diaphragm plate, which allowed reversible and reproducible obstruction of blood flow through the hind limb (20). ³¹P MR spectra were obtained using a pulse-acquire sequence (TR=1400 ms, 76 averages). After four reference spectra an ischemic period of 25 minutes was applied (14 spectra), followed by a recovery period of 16 minutes (9 spectra).

Three GAMT^{-/-} and three wt animals were sacrificed, their hind-leg muscles were removed and snapshot frozen in liquid nitrogen. The intact tissue was measured in a 12 μl rotor using HRMAS spectroscopy at 4 °C with a spinning rate of 5 kHz. Residual rotor space was filled with a PBS-buffer/D₂O mixture (30/70). For 1-D ¹H MR a CPMG pulse sequence was employed with a 90° pulse of 7.2 μs, while the time between the 180° pulses was one rotor period. Water was suppressed by presaturation and a T₂ filter of 50 ms was applied.

Chemical analysis of total Cr pool

To serve as a reference to the ¹H MR spectroscopy brain metabolite values, the size of the total Cr pool (i.e. Cr plus PCr) was determined by chemical analysis. Five C57Bl/6 mice and five mice with a randomly inbred mixed background of C57Bl/6 and 129/Ola were

sacrificed after which their brains were snapshot frozen in liquid nitrogen. These frozen brains were crushed and extracted with 0.6 M HClO₄. The extracts were neutralized with 3 M KOH, and the PCr and Cr were assayed via coupled enzymatic reactions (21). PCr and Cr concentrations were added to yield the total Cr pool size.

Data processing

The ¹H MR data of brain were analyzed using the LCModel 5.2-2 software package (22). The unsuppressed water signal was used for eddy current correction, phasing and normalization. The chemically determined Cr value was used to scale the MR determined metabolite values of the wt mice such that Cr values agreed. This scaling factor was also applied to the MR spectra of the GAMT mice yielding absolute quantitative levels for all metabolites in the ¹H MR brain spectra.

The ³¹P MR data of brain and muscle and the ¹H MR data of hind-leg muscle were analyzed using the MRUI software package (23). In the data processing of ³¹P MR brain spectra, the first order phase was constrained. In GAMT -/- animals the damping of the PGua signal was set equal to the damping of the PCr signal. All signals were fitted assuming a Lorentzian line shape model function, and normalized to the γ -NTP signal since the β -NTP signal was affected by a chemical shift artefact caused by the 6.5 kHz excitation pulse.

For the ¹H MR spectra of muscle, the first order phase was constrained to zero because the first acquired data point was obtained at the top of the echo. Signals were eddy current corrected using the unsuppressed water signal. The ratio of the linewidths of taurine and Cr was determined in wt animals. Cr linewidths were constrained to this ratio in both GAMT-/- and wt animals. All signals were fitted assuming a Gaussian line shape model function. Absolute quantification of the Cr concentration in muscle was performed using the unsuppressed water signal. To correct for T₂ relaxation, the obtained water and methyl Cr spectra at six different echo times were fitted using MRUI (23), and the results at different echo times were fitted using a mono exponential curve. The protons signals in hind leg muscle are considered to be fully relaxed at a TR of 5 s, and hence no T₁ corrections needed to be applied. Tissue water content was assumed to be 77% (24).

In the fitting procedure of the ³¹P MR spectra data of hind-leg muscle, the first order phase was constrained. No other prior knowledge was used. Signals were fitted assuming a Lorentzian line shape model function and normalized to the β -NTP signal. For brain and muscle, the pH was calculated from the shift in resonance position (S) of the inorganic phosphate (Pi) signal compared to the resonance position of PCr (25) using the equation $\text{pH}=6.75 + \log((3.27-S)/(S-5.63))$. A two-tailed Mann-Whitney test was used to test if GAMT-/- from wt metabolite levels were significantly different ($p < 0.05$).

RESULTS

Muscle

The ^{31}P MR spectra of GAMT $^{-/-}$ animals showed striking differences with respect to wt spectra: PCr was significantly reduced and a new resonance appeared 0.5 ppm up-field of PCr (figure 7.1), which was assigned to PGua (13). Signal intensities of the residual PCr and newly formed PGua showed large fluctuations between animals. However, in all individual mice the ratio PGua / PCr was larger than 1, ranging from 1.4 to 8.8 (mean 3.4 ± 3). We observed that with higher PGua levels PCr levels tended to be equally lower, however, significance was not reached for this observation. Other metabolite levels (normalized to the β -NTP signal) and tissue pH were not significantly different between GAMT $^{-/-}$ animals and their littermates (table 7.1).

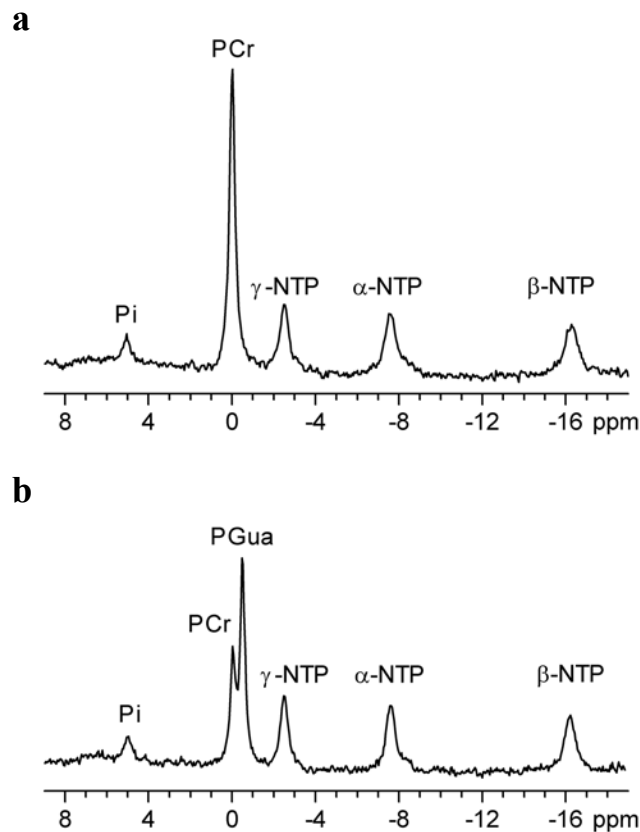


Figure 7.1: ^{31}P MRS of hind-leg muscle of wt (a) and GAMT $^{-/-}$ mice (b) in vivo. Peak assignments: inorganic phosphate (Pi); phosphocreatine (PCr); phosphorylated guanidinoacetate (PGua)

Table 7.1: Ratios of integral values of phosphorous metabolite signals and pH in muscle and brain.

	PME/NTP	Pi/NTP	PCr/NTP	PGua/NTP	PGua/PCr	pH
Muscle						
wt	-	0.40 ± 0.06	2.66 ± 0.11	-	-	7.24 ± 0.09
GAMT ^{-/-}	-	0.40 ± 0.08	0.76 ± 0.33	1.78 ± 0.42	3.4 ± 3	7.18 ± 0.06
Brain						
wt	1.1 ± 0.5	0.59 ± 0.16	1.36 ± 0.46	-	-	7.03 ± 0.08
GAMT ^{-/-}	1.4 ± 0.7	0.71 ± 0.26	0.31 ± 0.10	0.28 ± 0.07	0.90 ± 0.2	7.11 ± 0.04

All values are presented as mean ± s.d. PME: phosphomonoesters.

Muscle metabolite signal values are normalized to the resonance of β -NTP, brain metabolite signals to γ -NTP (see materials and methods section for details).

In order to find out whether PGua was metabolically active, ischemia of hind-leg muscle was applied, and monitored by ^{31}P MRS (figure 7.2). The spectrum before ischemia showed hardly any PCr signal, but a large PGua signal was apparent, especially in animals that were completely deprived of Cr. During ischemia the PGua signal decreased while Pi signals increased. After ischemia PGua increased again to its initial value. The time course of PGua depletion and recovery was of similar order as that of PCr in wt animals during and after ischemia (20).

The mono exponential fits of the water and Cr signals at different echo times yielded T_2 values for water and Cr proton spins of 21.9 ± 0.1 ms and 83 ± 4 ms respectively. Those values were used to calculate absolute Cr concentrations. Cr was significantly reduced in hind-leg muscle of GAMT^{-/-} animals (8.9 ± 3.8 mM) compared to wt animals (28.4 ± 2.6 mM) (figure 7.3). Despite the presence of PGua in the ^{31}P spectra, we observed hardly any signal for Gua in the ^1H MR spectra. Even though the spectra were obtained at the magic angle (55°) to reduce dipolar interactions, the Gua signal appeared at best as a broad line (figure 7.3c) in the spectra where Cr was largely reduced. It is of note that, although we did not explicitly study the relation between Cr content of the food and (P)Cr and PGua signals in muscle, the muscle ^1H MR spectrum showing largely reduced Cr (figure 7.3c) was taken in the same period, i.e. in mice eating the same batch of chow, as the ^{31}P MR spectrum which shows hardly any PCr (figure 7.2a).

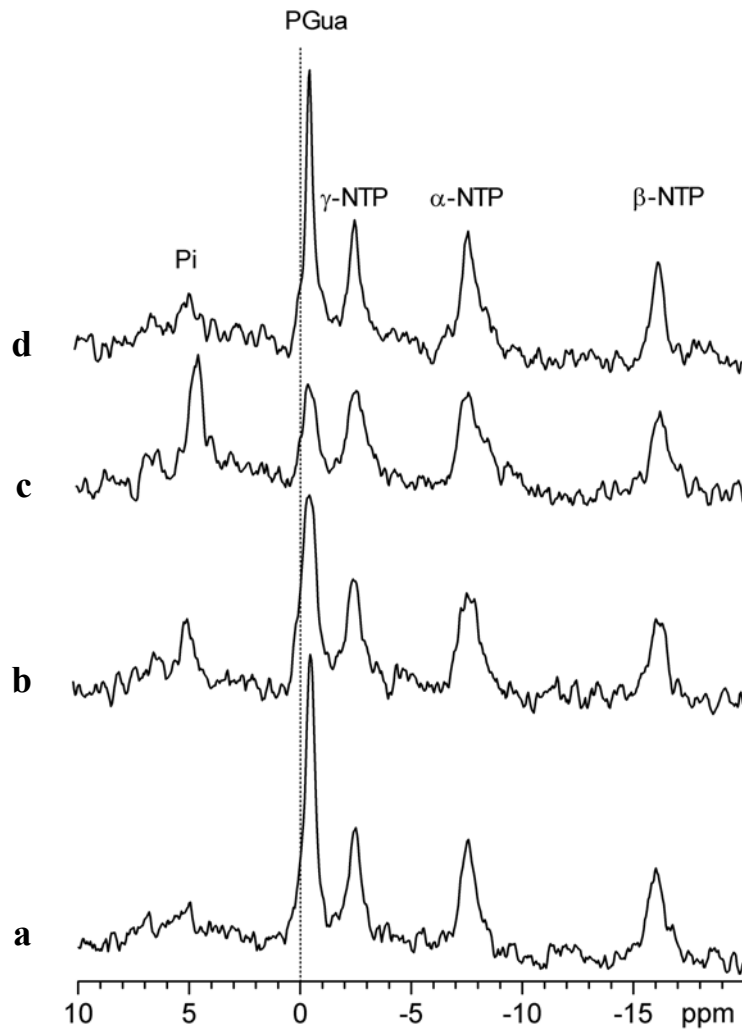


Figure 7.2: *in vivo* ^{31}P MRS of hind-leg muscle of GAMT deficient mouse before (a) ischemia, after 5 minutes (b) and 25 minutes (c) of ischemia, and 5 minutes after releasing the ischemic clamp (d). A vertical line is positioned at 0 ppm to show that the large resonance is not PCr but PGua at -0.5 ppm

In an attempt to clarify the apparent discrepancy of the broad Gua signal, HRMAS experiments on muscular tissue of GAMT^{-/-} and wt animals were performed. This approach yielded again a clearly reduced Cr signal, but now at 3.78 ppm a clear signal for Gua appeared as a distinct singlet (figure 7.4).

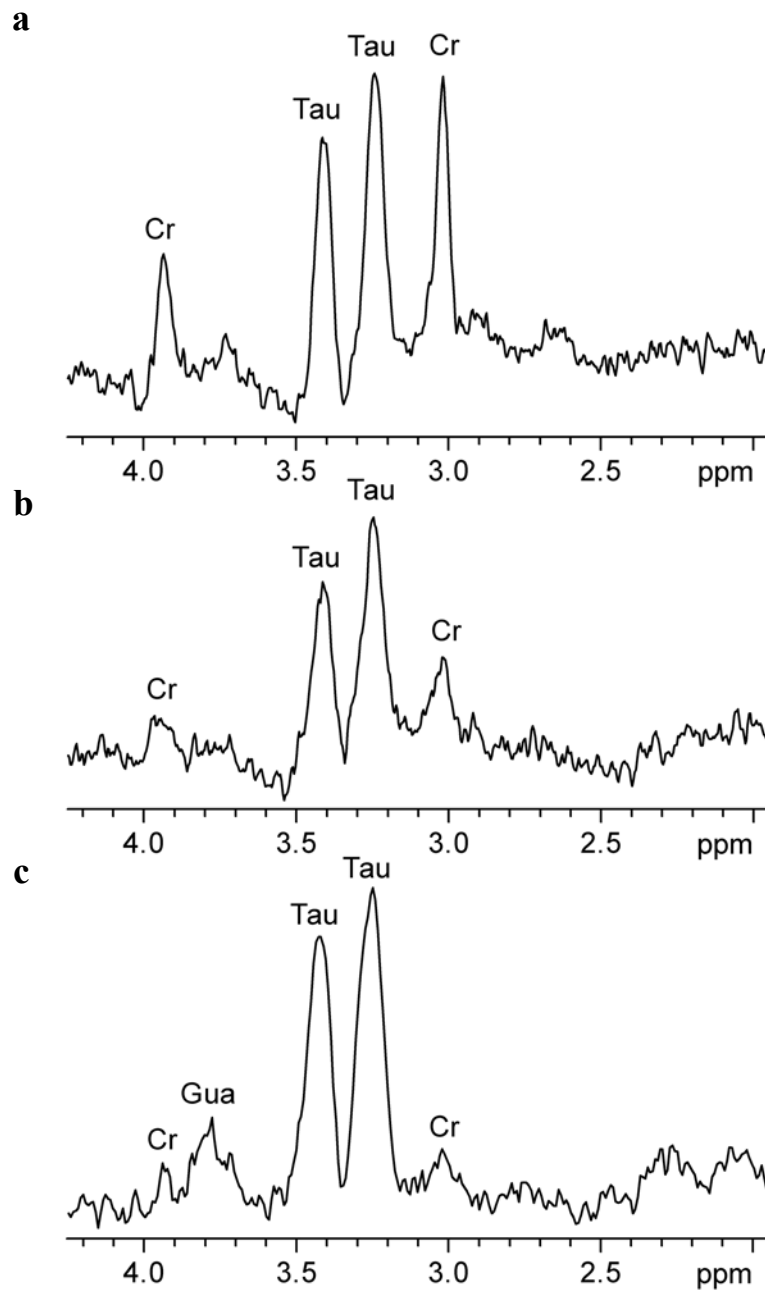


Figure 7.3: localized ^1H MRS of wt mice (a) and two $\text{GAMT}^{-/-}$ mice (b,c) hind-leg muscle in vivo.

Peak assignments: total creatine (Cr); taurine (Tau) guanidinoacetate (Gua). Gua is not observed in all $\text{GAMT}^{-/-}$ mice, only when Cr levels are very low (c).

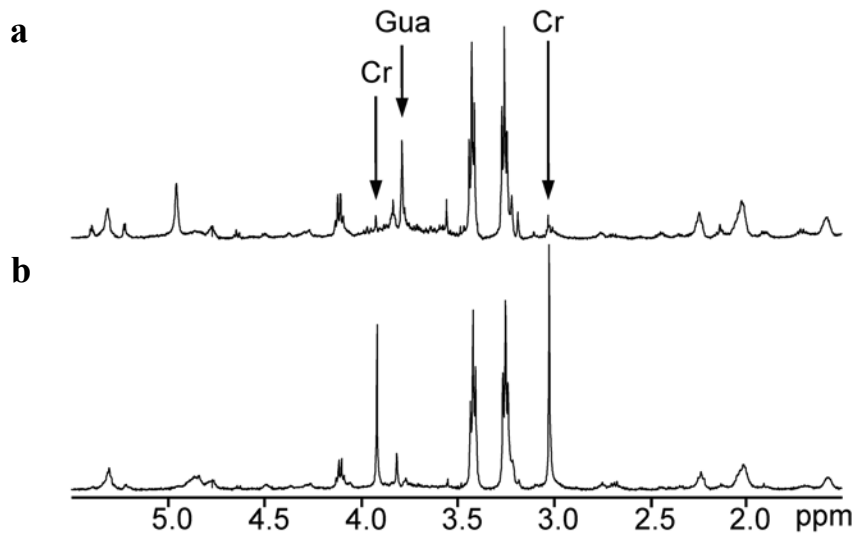


Figure 7.4: proton HRMAS MR spectra of intact *GAMT*^{-/-} (a) and wt (b) muscle tissue in vitro. Peak assignments: methyl (3.0 ppm) and methylene (3.9 ppm) signals of total creatine (Cr); methylene signal of guanidinoacetate (Gua).

Brain

Next we used ¹H and ³¹P MRS to establish whether the brains of *GAMT*^{-/-} animals show the same metabolic features as brains of *GAMT* deficient patients.

The chemical determined values of the total Cr pool were 8.7 ± 1.0 and 8.6 ± 1.4 $\mu\text{mol/g}$ wet weight for C57Bl/6 and mice with a randomly inbred mixed background of C57Bl/6 and 129/Ola, respectively. Using a brain density of 1.05 g/cm^3 (26), this could be converted to tissue concentrations of 8.3 ± 1.0 and 8.2 ± 1.3 mM respectively.

Compared to wt, the Cr signal was significantly reduced in brain of *GAMT*^{-/-} mice although some broad signals remained present at 3.0 and 3.9 ppm (figure 7.5). No other metabolites analyzed from the ¹H MR brain spectra were significantly different between wt and *GAMT*^{-/-} animals (table 7.2). In addition, no significant increase could be observed at 3.8 ppm, where Gua resonates. Other metabolites resonate around this position and might obscure the Gua signal. However, in some wt and *GAMT*^{-/-} animals there was a residual signal present at approximately 3.8 ppm after fitting the spectra. This residue was of low SNR and could not be quantified properly.

To see whether the residual Cr in *GAMT*^{-/-} animals could result from intake via the mother milk of heterozygous mother animals, ¹H MR spectra of brain of *GAMT*^{-/-} animals born to *GAMT*^{-/-} mothers were also obtained.

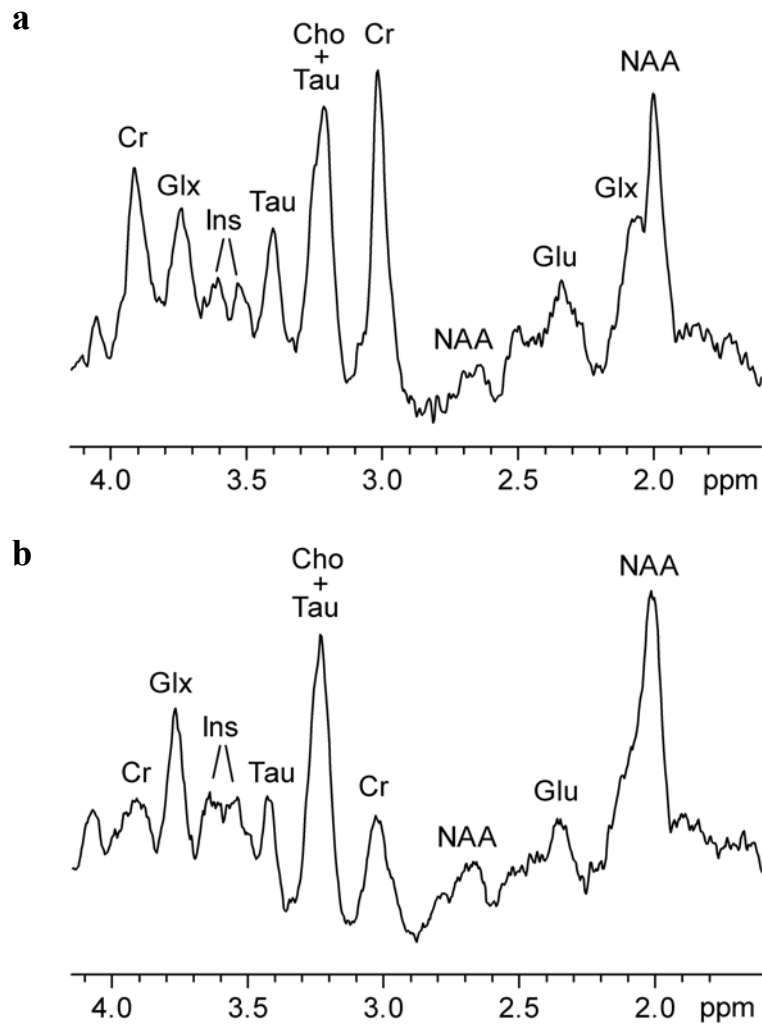


Figure 5: localized *in vivo* ^1H MR brain spectra of wt (a) and $\text{GAMT}^{-/-}$ (b) mice. Peak assignments: total creatine (Cr); choline (Cho); taurine (Tau); glutamate (Glu); glutamine and glutamate (Glx); myo-inositol (Ins); N-acetylaspartate (NAA).

There was no distinction between ^1H MR spectra from $\text{GAMT}^{-/-}$ animals nourished by heterozygous or homozygous mutant females (data not shown), indicating that the genotype of the mother is not an important parameter for the metabolic profile of the offspring.

In ^{31}P MR spectra of the brain of $\text{GAMT}^{-/-}$ animals, a strongly reduced PCr signal was evident compared to the ^{31}P MR spectra of brain of wt animals (figure 7.6). In addition, a signal for PGua was observed 0.5 ppm up-field of PCr in $\text{GAMT}^{-/-}$ animals, at a much lower intensity than in muscle. The mean ratio of PGua / PCr in brain was smaller than 1 (0.9 ± 0.2). Other metabolite levels, normalized to $\gamma\text{-NTP}$, did not differ between $\text{GAMT}^{-/-}$ and wt animals in brain (table 7.2).

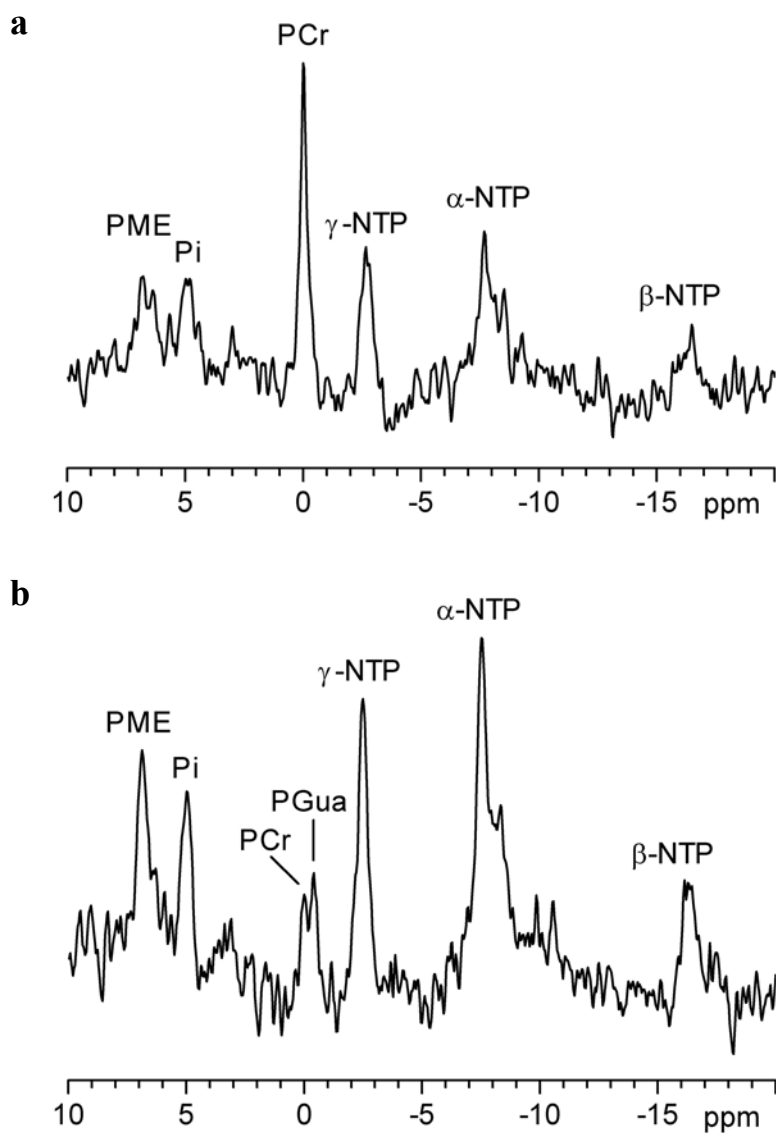


Figure 7.6: localized ^{31}P MRS of brain of wt (a) and $\text{GAMT}^{-/-}$ mice (b) in vivo. Peak assignments: phosphomonoesters (PME); inorganic phosphate (Pi); phosphocreatine (PCr); phosphorylated guanidinoacetate (PGua). Vertical scaling is arbitrary.

Table 7.2: Tissue concentrations of brain metabolites.

	wt (mM)	GAMT ^{-/-} (mM)	Rat (mM) (16)
taurine	5.8 ± 1.3	5.7 ± 1.6	6.0
total choline ^a	1.9 ± 0.4	1.9 ± 0.4	0.5
NAA	5.3 ± 1.3	5.4 ± 0.8	8.9
total creatine ^b	8.2 ± 1.2	1.4 ± 0.4 *	8.5
myo-inositol	2.2 ± 1.7	2.7 ± 0.9	4.4
Glutamate	3.9 ± 0.3	4.4 ± 0.6	8.3
Glutamine	1.8 ± 0.5	2.4 ± 0.7	2.7

All values are determined by ¹H MRS and scaled to biochemically determined Cr values (see material and methods) and presented as mean ± s.d.

^a phosphocholine + glycerol-phosphocholine

^b creatine + phosphocreatine

* significantly different from wt ($p < 0.05$)

DISCUSSION

In this study we showed that combined use of in vivo and in vitro MR spectroscopy is a valuable tool in elucidating the metabolic status of tissues of animal models for creatine deficiency. In combination with the introduction of the new GAMT knock-out mouse model this opens up many possibilities for studying the integral-physiological fate of precursors and products at various steps in the Cr-biosynthetic pathway, in much more detail than is possible in human patients.

MR spectra of brain and muscle of GAMT deficient mice

¹H MR spectra of both brain and muscle of GAMT^{-/-} mice showed reduced levels compared to wt animals, but no complete absence of Cr. The Cr concentration in the food of the mice likely accounts for the continued presence of Cr. There is evidence that the permeability of the blood-brain barrier for Cr is limited and that the brain partially relies on its own Cr synthesis (1, 27, 28). Therefore it is interesting to note that the reduction of Cr in GAMT^{-/-} mice relatively to the signal in wt animals appeared to be larger in brain than in muscle, which could be explained by a slower uptake of orally ingested Cr in the brain.

As absolute concentration data from proton MR spectroscopy of mouse brain metabolites have, to our knowledge, not been published, we compared our inferred values to metabolite concentrations measured in rat brain (16). Cr concentrations found in wt animals are almost similar to those found in rat. Strikingly, NAA and glutamate values are

significantly lower in mouse brain than in rat brain. NAA is considered to be a neuronal marker (29) and the observed concentration is in agreement with other biochemical studies done in mice (29). The difference in rat and mouse NAA levels corresponds well with the factor of about two-fold difference in cholinergic neurons per section of equal thickness in mouse and rat brain (30). Glutamate, important for synaptic signaling activity in brain, is stored mainly in neurons (31, and references therein) which explains the lower concentration found in mouse brain compared to rat brain. Although the concentration of choline compounds is in good agreement with values found in the human brain (32), it is higher than the concentration observed in rat brain. Why the concentration of choline compounds occurs at higher levels in mouse brain than in rat brain is currently not known.

A remarkable observation from MR spectra of GAMT^{-/-} compared to wt was that the PGua content in muscle was much higher than in brain, although in brain we observed a more constant level of PGua and PCr. GAMT transcript and protein was found to be present in several normal human and mouse tissues, including in muscle at high levels (15). In muscle also the enzyme AGAT, involved in synthesis of Gua, occurs at high levels (33). However, since the GAMT enzyme is lacking in GAMT^{-/-} mice this does not necessarily mean that Gua will accumulate. Altered transport or change in feedback control of metabolic steps may also affect the rate of accumulation of precursors, and these factors may vary between tissues. Currently, we lack proper explanations for the differences in PGua and PCr levels between tissues. It has been suggested that brain is relatively self-sufficient in terms of Cr biosynthesis (34), whereas muscle is not. However, no data are available about the relative capacities of the different biosynthetic steps leading to the formation of Gua (and the conversion to Cr) or for the relative import capacities for Cr in different tissues. The permeability of the blood-brain barrier is suggested to be limited for creatine (1) and throughout the brain, creatine transporters are not equally distributed. Cr uptake capacity almost surely differs between neural and glial cell types (28). In muscle fibers Cr transporters may be more equally distributed.

Visibility of guanidinoacetate

If brain tissue ATP concentration is assumed to be approximately 3 mM (35) also in GAMT mice, PGua levels in brain can be estimated from the observed signal ratios (table 7.1) to be around 1 mM. Assuming that about 75% of the total pool is phosphorylated, as is the case for Cr, the total Gua pool in the brain would be in the order of 1.3 mM. At this low concentration the signal of Gua may be hard to detect especially as it occurs at 3.8 ppm in a spectral area with several other overlapping resonances.

In muscle, by using analogous reasoning, Gua levels can be estimated to be approximately 19 mM, based on an assumed ATP concentration of 8 mM (36) and a phosphorylated fraction of 75%. Despite this high Gua tissue concentration, hardly any signal could be observed at the resonance position of Gua in our *in vivo* ^1H muscle spectra. In cases where a signal for Gua was observed, this signal appeared at best as a broad line. Because the muscle ^1H spectra of the GAMT $^{-/-}$ animals were obtained at the magic angle, dipolar interactions cannot account for the large linewidth (19). However, HRMAS spectra of intact muscle of GAMT $^{-/-}$ animals showed a clear singlet for Gua at 3.78 ppm. As HRMAS spectra were obtained at a temperature of 4 °C, the difference could possibly be due to conformational or environmental changes *in vivo*.

Remarkably, the Gua signal appeared to be more distinct in the ^1H MR spectra of muscle if a low Cr signal was present, and sometimes very low PCr and high PGua concentrations were observed in the ^{31}P spectrum of muscle. Whether the PGua concentration decreases on increasing PCr concentration should be investigated further using controlled Cr feeding of GAMT $^{-/-}$ animals.

Phosphorylated guanidinoacetate as a substitute for phosphocreatine

The large variation in the amount of PGua and residual PCr observed in GAMT $^{-/-}$ muscle is most likely caused by fluctuations in creatine intake via the food, or fluctuation in cellular import capacity, which in muscle is dependent on the feeding status and presumably other physiological parameters (2).

Based on the observation that CK can play a role in the phosphorylation of Cr analogues (37-39) it is likely that CK activity is the source of PGua in GAMT $^{-/-}$ animals. The utilization of PGua during ischemia was very similar to that of PCr in wt mice (20) despite the fact that the conversion rate may be lower as was shown in brain (13). We do not know, however, if the cytosolic BB-CK in brain and MM-CK in muscle have equal *in vivo* capacity to convert Gua to PGua. A role of mitochondrial CKs (which also occur at quite different concentrations in muscle and CNS) in this process can be excluded. Study of the utilization of creatine analogues by mitochondrial CKs in (permeabilized) tissue has demonstrated that these isoforms have no role in Gua phosphorylation (37, 38).

Comparison with patient case studies

The reduction of (P)Cr in the ^{31}P and ^1H MR spectra, and the appearance of PGua in the ^{31}P MR spectra of the brain in our mouse model revealed a striking similarity to the metabolic findings in human patients (3, 4, 7-11, 13). For muscle, however, only two case studies have been reported so far to our knowledge (10, 14). In one case, the ^{31}P MR spectrum

showed PCr and PGua, as observed in our study in GAMT^{-/-} mice (14). In the other case, however, a large signal at about 0 ppm in the ³¹P MR spectrum was assigned to PCr (10). No signal for Gua was found in the human ¹H MR spectrum (10). As shown in the present study, Gua in muscle gives rise to a broad signal which is hard to detect in vivo even at very low Cr concentrations. Brain MRS in GAMT deficient patients showed different levels of Cr after oral administration of Cr (3, 4, 7, 9-13). Variable creatine levels were also found in GAMT^{-/-} mice and attributed to differences in oral intake of Cr.

Although different inborn errors of Cr metabolism give rise to a reduction of the Cr signal in MR spectra (40-43), the simultaneous observation of reduced Cr signals and new signals for PGua is highly indicative for GAMT deficiency and can be diagnostically applied.

In summary, our results indicate that Cr synthesis is blocked in GAMT deficient mice providing evidence for the existence of only one biosynthetic pathway for Cr production in mammals. We can now use this model for an in-depth study of the effects of oral intake of Cr, the pathophysiological thresholds in the Gua levels in different tissues and the monitoring of treatment of this disease using MRS.

ACKNOWLEDGEMENTS

The authors would like to thank Claudia Soede-Huijbregts for obtaining HRMAS spectra of muscular tissues and Dennis Klomp for fruitful discussions. The study was supported by a grant of the Deutsche Forschungsgemeinschaft to D.I. and K.U. (SFB 545, Project A3) and the Netherlands Organization for Scientific Research (NWO-ZONMW).

REFERENCES

1. Wyss, M. and Kaddurah-Daouk, R. Creatine and creatinine metabolism. *Physiol Rev* 2000;80:1107-213.
2. Zhao, C.R., Shang, L., Wang, W. and Jacobs, D.O. Myocellular creatine and creatine transporter serine phosphorylation after starvation. *J Surg Res* 2002;105:10-6.
3. Stöckler, S., Holzbach, U., Hanefeld, F., Marquardt, I., Helms, G., Requart, M., Hanicke, W. and Frahm, J. Creatine deficiency in the brain: a new, treatable inborn error of metabolism. *Pediatr Res* 1994;36:409-13.
4. Stöckler, S., Hanefeld, F. and Frahm, J. Creatine replacement therapy in guanidinoacetate methyltransferase deficiency, a novel inborn error of metabolism. *Lancet* 1996;348:789-90.
5. Stöckler, S., Isbrandt, D., Hanefeld, F., Schmidt, B. and von Figura, K. Guanidinoacetate methyltransferase deficiency: the first inborn error of creatine metabolism in man. *Am J Hum Genet* 1996;58:914-22.
6. Stöckler, S., Marescau, B., De Deyn, P.P., Trijbels, J.M. and Hanefeld, F. Guanidino compounds in guanidinoacetate methyltransferase deficiency, a new inborn error of creatine synthesis. *Metabolism* 1997;46:1189-93.
7. Schulze, A., Hess, T., Wevers, R., Mayatepek, E., Bachert, P., Marescau, B., Knopp, M.V., De Deyn, P.P., Bremer, H.J. and Rating, D. Creatine deficiency syndrome caused by guanidinoacetate methyltransferase deficiency: diagnostic tools for a new inborn error of metabolism [see comments]. *J Pediatr* 1997;131:626-31.
8. van der Knaap, M.S., Verhoeven, N.M., Maaswinkel-Mooij, P., Pouwels, P.J., Onkenhout, W., Peeters, E.A., Stöckler-Ipsiroglu, S. and Jakobs, C. Mental retardation and behavioral problems as presenting signs of a creatine synthesis defect. *Ann Neurol* 2000;47:540-3.
9. Ganesan, V., Johnson, A., Connelly, A., Eckhardt, S. and Surtees, R.A. Guanidinoacetate methyltransferase deficiency: new clinical features. *Pediatr Neurol* 1997;17:155-7.
10. Thiel, T., Ensenauer, R., Hennig, J. and Lehnert, W. In vivo magnetic resonance spectroscopy in a patient with Creatine deficiency syndrome: new aspects on mechanism of Creatine uptake in brain and muscle. *Proc Intl Soc Mag Reson Med* 9 2001;582.
11. Leuzzi, V., Bianchi, M.C., Tosetti, M., Carducci, C., Cerquiglioni, C.A., Cioni, G. and Antonozzi, I. Brain creatine depletion: guanidinoacetate methyltransferase deficiency (improving with creatine supplementation). *Neurology* 2000;55:1407-9.
12. von Figura, K., Hanefeld, F., Isbrandt, D. and Stöckler-Ipsiroglu, S. Guanidinoacetate methyltransferase deficiency. in: *The Metabolic and Molecular Bases of Inherited Disease* Eds.: C. R. Scriver, A. L. Beaudet, W. S. Sly, D. Valle and V. Childs 2001. chapter 84
13. Frahm, J. and Hanefeld, F. Localized proton magnetic resonance spectroscopy of brain disorders in childhood. *Magnetic Resonance Spectroscopy and Imaging in Neurochemistry* 1997;Volume 8 of *Advances in Neurochemistry*: Plenum Press, New York.
14. Schulze, A., Bachert, P., Schlemmer, H., Harting, I., Polster, T., Salomons, G.S., Verhoeven, N.M., Jakobs, C., Fowler, B., Hoffmann, G.F. and Mayatepek, E. Lack of creatine in muscle and brain in an adult with GAMT deficiency. *Ann Neurol* 2003;53:248-51.
15. Isbrandt, D., Schmidt, A., Neu, A., Röper, J., Steinfeld, R. and Ullrich, K. Generation of a knockout mouse model for guanidinoacetate methyltransferase (GAMT) deficiency. *J Inherit Metab Dis* 2002;23, suppl.1:212.
16. Pfeuffer, J., Tkac, I., Provencher, S.W. and Gruetter, R. Toward an in vivo neurochemical profile: quantification of 18 metabolites in short-echo-time (1)H NMR spectra of the rat brain. *J Magn Reson* 1999;141:104-20.
17. Ordidge, R.J., Connely, A. and Lohman, J.A.B. Image-selected in vivo spectroscopy (ISIS). A new technique for spatially selective NMR spectroscopy. *J Magn Reson* 1986;66:293-294.
18. Alderman, D.W. and Grant, D.M. An efficient decouple coil design which reduces heating in conductive samples in superconducting spectrometers. *J Magn Reson* 1979;36:447-451.

19. in 't Zandt, H.J.A., Klomp, D.W.J., Oerlemans, F., Wieringa, B., Hilbers, C.W. and Heerschap, A. Proton MR Spectroscopy of wild-type and creatine kinase deficient mouse skeletal muscle: dipole-dipole coupling effects and post-mortem changes. *Magn Reson Med* 2000;43:517-524.
20. in 't Zandt, H.J., Oerlemans, F., Wieringa, B. and Heerschap, A. Effects of ischemia on skeletal muscle energy metabolism in mice lacking creatine kinase monitored by in vivo ³¹P nuclear magnetic resonance spectroscopy. *NMR Biomed* 1999;12:327-34.
21. Bergmeyer, H.U. *Methods of Enzymatic Analysis*. New York: Academic Press; 1974.
22. Provencher, S.W. Estimation of metabolite concentrations from localized in vivo proton NMR spectra. *Magn Reson Med* 1993;30:672-9.
23. <http://www.mrui.uab.es/mrui/mruiHomePage.html>
24. Sjogaard, G. and Saltin, B. Extra- and intracellular water spaces in muscles of man at rest and with dynamic exercise. *Am J Physiol* 1982;243:R271-80.
25. Moon, R.B. and Richards, J.H. Determination of intracellular pH by ³¹P magnetic resonance. *J Biol Chem* 1973;248:7276-8.
26. Torack, R.M., Alcala, H., Gado, M. and Burton, R. Correlative assay of computerized cranial tomography CCT, water content and specific gravity in normal and pathological postmortem brain. *J Neuropathol Exp Neurol* 1976;35:385-92.
27. Wyss, M. and Wallimann, T. Creatine metabolism and the consequences of creatine depletion in muscle. *Mol Cell Biochem* 1994;133-134:51-66.
28. Braissant, O., Henry, H., Loup, M., Eilers, B. and Bachmann, C. Endogenous synthesis and transport of creatine in the rat brain: an in situ hybridization study. *Brain Res Mol Brain Res* 2001;86:193-201.
29. Birken, D.L. and Oldendorf, W.H. N-acetyl-L-aspartic acid: a literature review of a compound prominent in ¹H-NMR spectroscopic studies of brain. *Neurosci Biobehav Rev* 1989;13:23-31.
30. Hagg, T., Van der Zee, C.E.E.M., Ross, G.M. and Riopelle, R.J. Response to "Petersen et al.: Basal forebrain neuronal loss in mice lacking neurotrophin receptor p75". *Science* 1997;277:838-839.
31. Cruz, F. and Cerdan, S. Quantitative ¹³C NMR studies of metabolic compartmentation in the adult mammalian brain. *NMR Biomed* 1999;12:451-62.
32. Pouwels, P.J.W. and Frahm, J. Regional metabolite concentrations in human brain as determined by quantitative localized proton mrs. *Magn Reson Med* 1998;39:53-60.
33. van Pilsum, J.F., Olsen, B., Taylor, D., Rozycki, T. and Pierce, J.C. Transamidinase activities, in vitro, of tissues from various mammals and from rats fed in protein-free, creatine-supplemented and normal diets. *Arch Biochem and Biophys* 1963;100:520-524.
34. Wyss, M. and Schulze, A. Health implications of creatine: can oral creatine supplementation protect against neurological and atherosclerotic disease? *Neuroscience* 2002;112:243-60.
35. Gorell, J.M., Dolkart, P.H. and Ferrendelli, J.A. Regional levels of glucose, amino acids, high energy phosphates, and cyclic nucleotides in the central nervous system during hypoglycemic stupor and behavioral recovery. *J Neurochem* 1976;27:1043-9.
36. van Deursen, J., Heerschap, A., Oerlemans, F., Ruitenbeek, W., Jap, P., ter Laak, H. and Wieringa, B. Skeletal muscles of mice deficient in muscle creatine kinase lack burst activity. *Cell* 1993;74:621-31.
37. van Deursen, J., Jap, P., Heerschap, A., ter Laak, H., Ruitenbeek, W. and Wieringa, B. Effects of the creatine analogue beta-guanidinopropionic acid on skeletal muscles of mice deficient in muscle creatine kinase. *Biochim Biophys Acta* 1994;1185:327-35.
38. Boehm, E.A., Radda, G.K., Tomlin, H. and Clark, J.F. The utilisation of creatine and its analogues by cytosolic and mitochondrial creatine kinase. *Biochim Biophys Acta* 1996;1274:119-28.
39. Holtzman, D., McFarland, E., Moerland, T., Koutcher, J., Kushmerick, M.J. and Neuringer, L.J. Brain creatine phosphate and creatine kinase in mice fed an analogue of creatine. *BrainRes* 1989;483:68-77.
40. de Grauw, T.J., Cecil, K.C., Salomons, G.S., van Doornen, S.J.M., Verhoeven, N.M., Ball, W.S. and Jakobs, C., The clinical syndrome of creatine transporter deficiency, in "Abstracts of 6th international conference on guanidino compounds in biology and medicine, Cincinnati, Ohio, VS, 2001.

41. Cecil, K.M., Salomons, G.S., Ball, W.S., Jr., Wong, B., Chuck, G., Verhoeven, N.M., Jakobs, C. and DeGrauw, T.J. Irreversible brain creatine deficiency with elevated serum and urine creatine: a creatine transporter defect? *Ann Neurol* 2001;49:401-4.
42. Bianchi, M.C., Tosetti, M., Fornai, F., Alessandri, M.G., Cipriani, P., De Vito, G. and Canapicchi, R. Reversible brain creatine deficiency in two sisters with normal blood creatine level. *Ann Neurol* 2000;47:511-3.
43. Item, C.B., Stockler-Ipsiroglu, S., Stromberger, C., Muhl, A., Alessandri, M.G., Bianchi, M.C., Tosetti, M., Fornai, F. and Cioni, G. Arginine:glycine amidinotransferase deficiency: the third inborn error of creatine metabolism in humans. *Am J Hum Genet* 2001;69:1127-33.

8

MAGNETIZATION TRANSFER EFFECT ON THE CREATINE METHYL RESONANCE STUDIED BY CW OFF-RESONANCE IRRADIATION IN HUMAN SKELETAL MUSCLE ON A CLINICAL MR SYSTEM

KlaasJan Renema

Dennis Klomp

Mariëlle Philippens

Erik van den Bergh

Bé Wieringa

Arend Heerschap

This chapter is in slightly modified form published as:

Renema, W.K., Klomp, D.W., Philippens, M.E., van den Bergh, A.J., Wieringa, B. and Heerschap, A. Magnetization transfer effect on the creatine methyl resonance studied by CW off-resonance irradiation in human skeletal muscle on a clinical MR system. *Magn Reson Med* 2003; 50: 468-73.

ABSTRACT

Transfer of magnetization (MT) between the mobile (MR visible) spin pool and immobile (MR invisible) spin pool of creatine (Cr) was studied on a clinical 1.5 T MR scanner in human skeletal muscle using continuous wave (CW) pre-irradiation as saturation method for the immobile pool. For this purpose, only slight modifications to the MR system were made. A specially designed electronic circuit was used to couple a CW amplifier to the RF channel of the scanner. CW pulse power ($\gamma B_2/2\pi$) and pulse length were determined to be approximately 550 Hz and 3 s respectively for optimal signal attenuation of the Cr methyl signal. The bound Cr fraction in human gastrocnemius muscle was determined to be between 0.4% and 1.3% using a two-pool exchange model function describing the MT effect.

INTRODUCTION

Magnetization transfer (MT) methods are frequently used in MRI (1) and MR spectroscopy (2). Proton spin systems of small metabolites in tissues may show an off-resonance MT effect: magnetization from an immobile, MR invisible pool is transferred to a mobile, MR visible pool. For the first time this was demonstrated in rat brain, where the methyl signal of creatine (Cr) showed attenuation after off-resonance irradiation (3). Subsequently, several other studies have been published on MT of Cr in rat brain (4-6), rat and mice skeletal muscle (7-9) and human brain (10, 11). While ^1H spins of some metabolites, e.g. Cr and ethanol, showed a clear MT effect in brain (3, 12), for others like N-acetylaspartate, glutamine/glutamate, myo-inositol, taurine and alanine only small effects were detected (4, 5).

The exact mechanism of the transfer of magnetization from an immobile to a mobile Cr pool is still unknown. It has been demonstrated that both Cr and phosphocreatine (PCr) contribute to an MT effect (8). The role of exchangeable protons is negligible (9), even as interaction with creatine kinase (8). Using the inversion transfer technique in human brain and skeletal muscle, a significant transient reduction in the methyl signal of Cr was found indicative of magnetic coupling between protons of water and those of Cr / PCr (13).

Saturation of the immobile fraction can be achieved by pulsed pre-irradiation, which can be applied on or off-resonance, or by off-resonance continuous wave (CW) pre-irradiation (14). In theory, these three methods are expected to give similar results as long as the relevant experimental parameters are properly optimized (15). However, in practice off-resonance CW pre-irradiation offers some advantages, especially for the quantitative analysis of the data in terms of an exchange model; the pulse length, saturation power and pulse offset frequency in CW pre-irradiation can be calibrated accurately (14). In MT studies in humans, however, no CW irradiation has been used so far. In order to obtain full magnetization transfer effects, long saturation pulses are required at sufficient strength. Based on earlier CW MT experiments in animal muscle and brain, pulse duration and strength of more than 2 seconds and $\gamma B_2/2\pi$ of more than 200 Hz respectively should be applied (4, 7, 8). Standard clinical MR scanners have an RF pulse-amplifier, which cannot handle these long pulses.

In the present study, MT of the Cr methyl group was studied in human skeletal muscle using CW pre-irradiation for the first time. For this purpose we designed an electronic circuit to couple a CW amplifier to the RF channel of the clinical 1.5 T MR scanner, which required only slight modifications to the transmit/receive switch on the clinical system. The different parameters involved in obtaining maximal signal attenuation, e.g. CW pulse power and pulse length, were calibrated. With this approach the bound Cr fraction in human gastrocnemius

muscle was determined using a two-pool exchange model function describing the MT effect (16).

MATERIALS AND METHODS

MR equipment and modifications

A circular polarized ^1H coil with a diameter of 15 cm was used for both excitation and reception. The coil was interfaced to a Siemens Vision 1.5 T clinical MR scanner (Siemens, Erlangen, Germany). The amplifier of the second RF channel was replaced by a 35 W CW amplifier (GRF5071-10-100, OPHIR-RF, Los Angeles, USA) and connected to the first channel by an electronic switch just before it enters the transmit receive switch. To prevent damage to the CW amplifier during transmission with the 15 kW pulse amplifier, a damping of at least 26 dB of the switch is required. For this purpose, a Pi-circuit for both amplifiers in combination with high power pindiodes (Macom) tuned to a quarter wave at 63.6 MHz was implemented (figure 8.1). Because the transmit-receive switch of the 1st channel is by default in receive mode and cannot be changed to transmit mode by sequence programming for longer than 2 seconds, a trigger signal is added to the driver signal using diodes (figure 8.1).

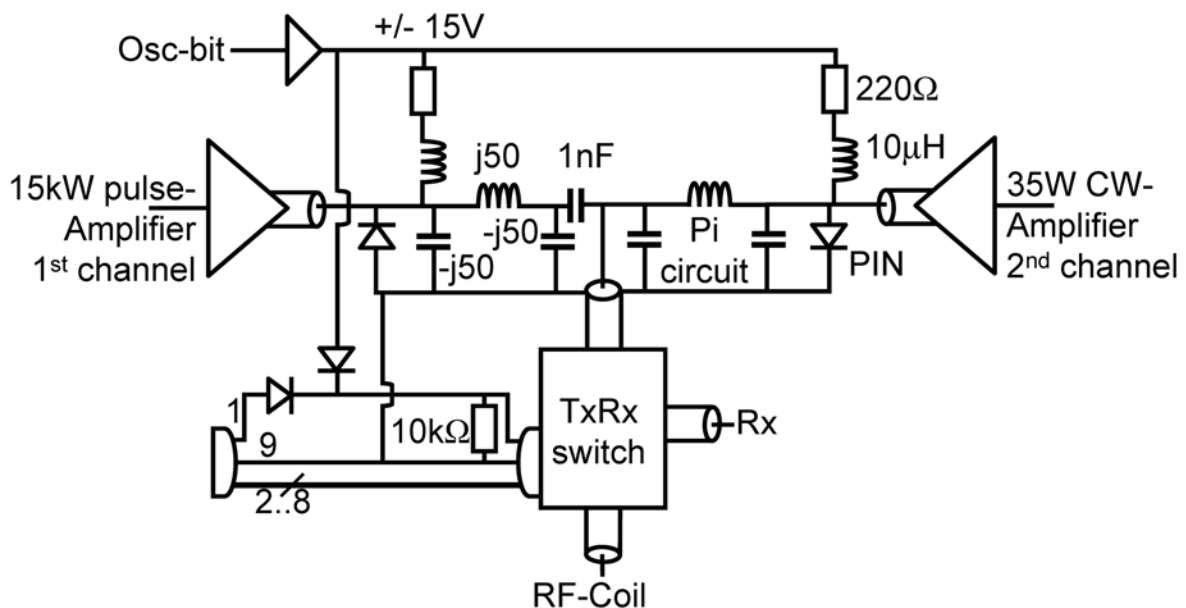


Figure 8.1: Electronic circuit that switches either the original 15 kW peak amplifier or the 35 W CW amplifier to the transmit-receive switch. The Pi-circuits are tuned to a quarter wavelength at 63.6 MHz and connects or isolates the desired amplifier. A trigger bit from the scan gates a circuit that drives the PIN-diodes and sets the transmit-receive switch in transmit mode by a diode adder.

Calibration of the CW amplifier

The isolation of the switch to both amplifiers was measured by a network-analyzer (8752A, Hewlett-Packard). The function of the switch was first tested by on and off-resonance irradiation on a phantom containing 50 mM Cr solution. The forward and reflected RF power to both coil elements was measured by an RF peak power analyzer (8542B, Gigatronics, San Ramon, USA) to calibrate the 2nd channel to the first and to estimate the Specific Absorption Ratio (SAR). Since the coil has an inhomogeneous electromagnetic field, the RF power was optimized to maximum signal intensity using point resolved spectroscopy (PRESS) localization. In this way, the value $\gamma B_2/2\pi$ per square root of power was determined at the location of the selected voxel of interest.

MT experiments

For every volunteer (n=6), the right calf muscle was placed in the coil, after which a voxel of interest (27 cc) was selected in the gastrocnemius muscle.

The magnetization transfer sequence starts with a variable length (1-5 s) CW irradiation pulse, followed by a single Gaussian shaped RF pulse for water suppression (25.6 ms pulse length) and PRESS localization (TE=135 ms; TR=6 s; 12 averages). Since the timing in the sequence is sequential, an electronic triggered switch can be included which connects either the standard pulse amplifier or the commercially available CW amplifier via the transmit-receive switch to the coil. Three series of MT measurements were performed for each subject. Firstly, a series consisting of 9 experiments with an MT pulse duration of 3 seconds and offset frequency of +10 kHz with amplitudes ($\gamma B_2/2\pi$) ranging from 0 until 900 Hz. Secondly, 7 experiments with a fixed MT pulse amplitude of 550 Hz and offset frequency of +10 kHz with variable duration from 0 until 5 seconds, acquired interleaved to reduce maximum SAR. The third series of measurements consisted of 27 experiments with a fixed MT pulse duration of 3 seconds and amplitude of 550 Hz with offset frequencies ranging from -100 kHz until +100 kHz. Although the estimated maximum local SAR is below 12 W/kg (17), additional temperature measurements were performed on the leg at the position closest to the conductors (18).

Data processing and model fitting

Trimethylammonium and creatine methyl signals were analyzed using MRUI (19) and normalized to the spectra with no MT irradiation. Lorentzian line shapes with constant line-widths were assumed.

The bound Cr fraction was determined from the experimental data series with a fixed MT pulse power and duration, at 27 different offset frequencies. The data of all six volunteers were averaged, and the mean Cr signal was fitted using a two-pool model function based on previous water MT modeling (16, 20, 21) as extensively described by Kruiskamp et al. (7). A Lorentzian line shape function for the description of the free Cr signal (pool A), and a Gaussian line shape function for the description of the bound pool (pool B) were assumed (21). Fitting of the observed Cr signal (M_Z^A), normalized to the Cr intensity without irradiation (M_0^A), involves six parameters and is described by equation 8.1 (21):

$$\frac{M_Z^A}{M_0^A} = \frac{R_A \left(\frac{R}{M_0^B} + R_B + R_{rfB} \right) + R_B \cdot R}{\left(R + R_A + R_{rfA} \right) \cdot \left(\frac{R}{M_0^B} + R_B + R_{rfB} \right) - \frac{R \cdot R}{M_0^B}} \quad [8.1]$$

in which R_{rfA} and R_{rfB} represent the rate of loss of longitudinal magnetization due to saturation with a pulse of power ω_1 ($=\gamma B_2/2\pi$) (Hz) at an offset Δ (Hz):

$$R_{rfA} = \omega_1^2 \cdot \frac{T_{2A}}{\pi \cdot \left(1 + (2\pi\Delta T_{2A})^2 \right)} \quad [8.2]$$

$$R_{rfB} = \omega_1^2 \cdot \frac{T_{2B}}{\sqrt{2\pi}} \cdot e^{-2(\pi T_{2B})^2} \quad [8.3]$$

T_{2A} and T_{2B} are the transverse relaxation times of respectively the mobile and immobile Cr pool. The six different parameters yielded from the fit of the data to equation 8.1 are the longitudinal relaxation rate ($=1/T_1$) of the mobile and immobile pool (R_A and R_B); T_{2A} and T_{2B} ; the size of the maximal magnetization of the immobile pool, relatively to the mobile pool M_0^B and a fundamental rate constant R , which describes the rate of exchange between pool A and B. Curve-fitting was performed in IDL (Interactive Data Language: RSI, Boulder, Co) using a Levenberg-Marquardt algorithm. The normalized mean Cr signals with their standard deviations were used as an input for the curve-fitting procedure, which yielded a fitted parameter with a one standard deviation confidence interval and correlation coefficients of the parameters derived from the covariance matrix. Two evaluation methods for the fitted parameters were used. Since the value of the parameter fit appeared to be highly dependent on the initial estimate of the parameter, 1000 randomly calculated initial values were used as an

initial estimate for each parameter to investigate the influence of the input. Secondly, the standard deviation of each parameter was derived from the covariance matrix. The fit was performed with none of the six parameters fixed, or with either R_A or T_{2A} fixed. The quality of the fit was determined by obtaining the root mean square deviation (*rmsd*) from the fit with respect to the experimental data.

A curve of theoretical spill over was calculated using a theoretical T_1 and T_2 for Cr of 1.35 s and 0.18 s respectively (22), and a power of 550 Hz as input parameters (4, 14). All data is presented as mean \pm standard deviation.

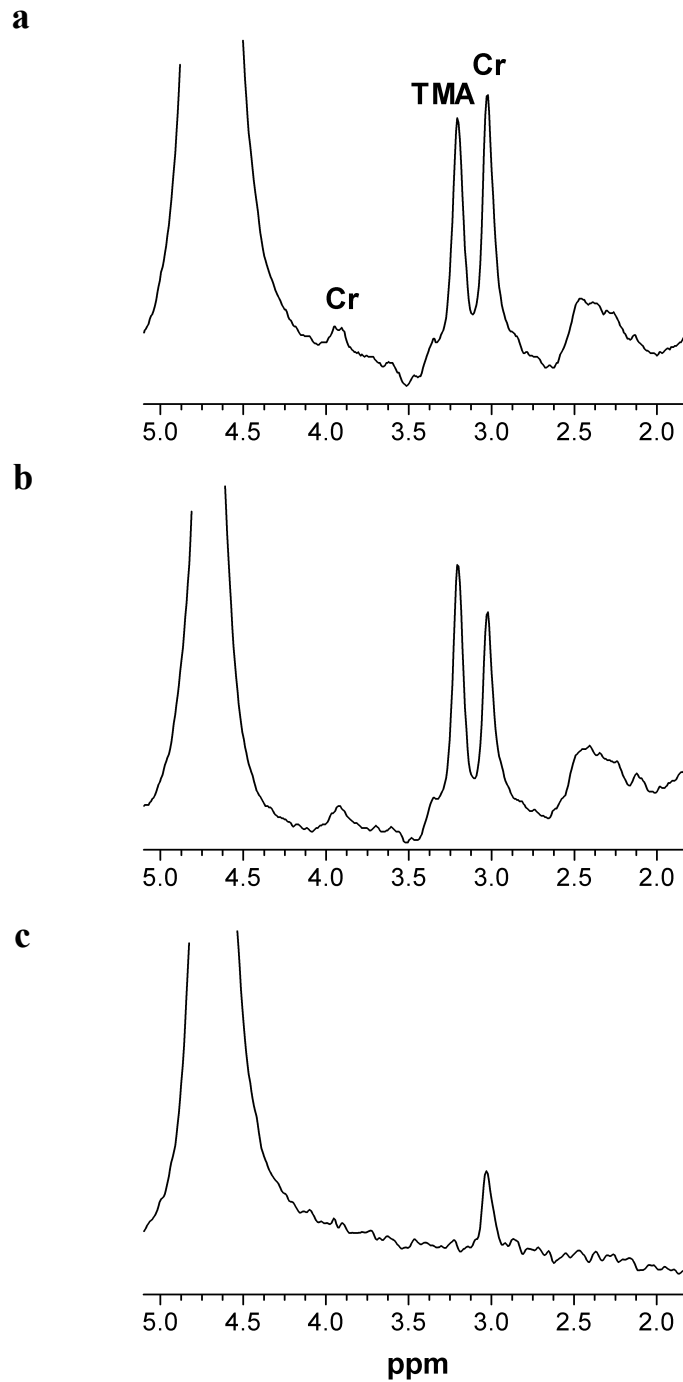


Figure 8.2 : Total Cr methyl signal measured with a pre-saturation pulse of 3 s. and a power of 550 Hz at +100 kHz (a) and +10kHz (b) offset with respect to the Cr methyl resonance and the difference spectrum (c). Vertical scaling is equal in all three spectra. Peak annotations: total creatine (Cr) and trimethylammonium (TMA).

RESULTS

The efficiency of the circular polarized coil used in these studies was found to be 900 Hz ($\gamma B_2/2\pi$) in human gastrocnemius muscle for an input power of 30 W. Power loss due to insertion of the Pi-circuit was reduced to only 0.15 dB. The RF power of the pre-irradiation pulse was monitored in all experiments and kept within SAR limits; temperature sensors showed no tissue heating. A clear MT effect on the methyl resonance of Cr (3.0 ppm) in the ^1H MR spectra of human gastrocnemius muscle was observed after pre-saturation during 3 seconds at 10 kHz offset (figure 8.2). In addition, an MT effect on the residual water signal was observed.

To optimize the CW power needed for maximal saturation, powers ($\gamma B_2/2\pi$) ranging from 0 to 900 Hz were used for a pre-saturation pulse of 3 s at an offset of +10 kHz (figure 8.3). It is clearly demonstrated that the relative Cr signal intensity reaches a plateau value at approximately 500 Hz. In the same way the optimal pulse length was calibrated using seven different pre-saturation pulse lengths (0-5 s) with fixed power (550 Hz) and offset (+10 kHz) (figure 8.4). Accordingly, a plateau is reached at a pulse length of approximately 3 seconds.

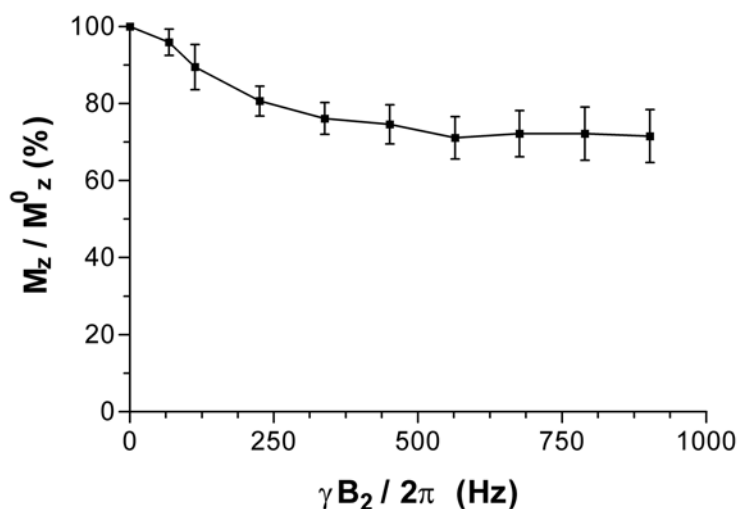


Figure 8.3: Total Cr methyl signal as a function of saturation pulse power (expressed in $\gamma B_2/2\pi$). The saturation pulse was applied at an offset frequency of +10 kHz with respect to the Cr methyl signal with a duration of 3 s. Datapoints are given as mean \pm s.d. scaled to the fit of the Cr signal without pre-irradiation.

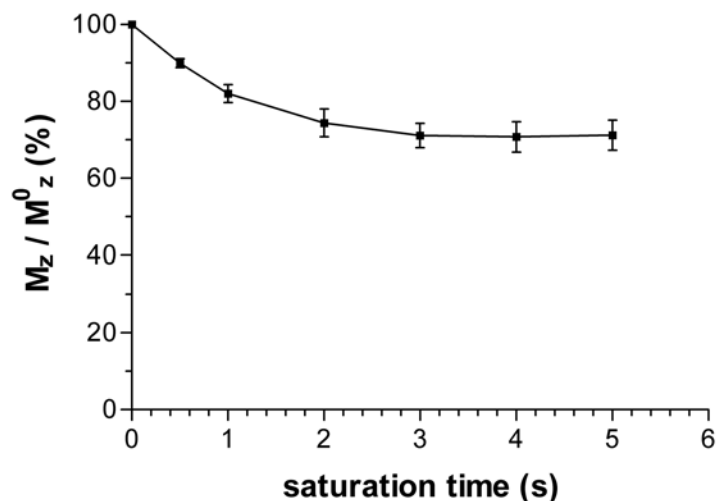


Figure 8.4: Total Cr methyl signal as a function of saturation pulse length. The saturation pulse was applied at an offset frequency of +10 kHz with respect to the Cr methyl signal and a $\gamma B_2/2\pi$ pulse power of 550 Hz. Datapoints are given as mean \pm s.d. scaled to the fit of the Cr signal without pre-irradiation

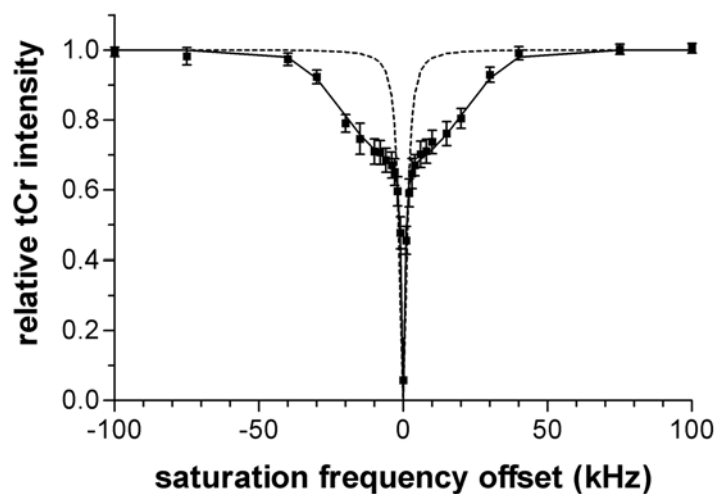


Figure 8.5: Total Cr methyl signal as a function of saturation pulse offset with respect to the Cr resonance. The saturation pulse was applied with a pulse length of 3 seconds and a $\gamma B_2/2\pi$ pulse power of 550 Hz. Datapoints are given as mean \pm s.d scaled to the Cr signal without pre-irradiation. Solid line is the fitted curve; the dotted line is the theoretical spill over curve.

In order to calculate the bound Cr fraction, a frequency sweep was done where a pre-saturation pulse was swept from an offset of -100 kHz to +100 kHz in 27 steps (see figure 8.5). For the saturation pulse power and length, the optimized values of 550 Hz and 3 s were used. When comparing the Cr signal intensity curve to the curve of theoretical RF spill over (figure 8.5, dotted line), a clear MT effect can be observed between an offset of approximately 0 and ± 40 kHz with respect to the Cr resonance. The mean relative Cr signal intensity at different offset frequencies of the pre-irradiation pulse is fitted using equation 8.1. When the fit was performed with none of the six parameters fixed, the values yielded for each parameter appeared highly dependent on the initial estimate of the parameters used as input for the fit. Besides this, the parameters derived were highly correlated and had a very large standard deviation; for the immobile fraction, for example, this may be of the order of 5000 %. In contrast, T_{2B} could be estimated accurately because it is independent of the initial parameter estimation, has a small standard deviation and a small correlation coefficient with the other parameters.

To average the influence of the initial estimation of each parameter, 1000 randomly calculated initial values were used as an initial estimate for each parameter. The resulting parameters of the converging fits ($\text{rmsd} < 0.016$) were averaged and the mean parameter value together with the standard deviation of this mean value, caused by differences in initial parameter estimation, is given in table 8.1. Because the standard deviation of each parameter derived from a single fit was large when six parameters were fitted, R_A and T_{2A} were fixed to values found in human skeletal tissue by standard relaxation time measurements at 1.5 T (22). In these cases, parameter standard deviations were within acceptable ranges (table 8.1) and appeared not dependent on the initial estimate of the parameters.

Overall, the immobile fraction of Cr in human skeletal muscle was determined to be small, between 0.4% and 1.3% depending on which parameter is fixed. The value of R_B appeared to have no influence on the value of the other parameters derived from the fit, but could not accurately be estimated as was previously observed in other MT studies (7, 8). Therefore, this parameter is not included in table 8.1.

Table 8.1: Parameter values obtained by a model fit of the mean Cr signal attenuation due to off-resonance irradiation.

	present study			other studies		relaxation studies	
	no fix ^a	fixed R_A ^b	fixed T_{2A} ^c	rat ^d	mouse ^e	human ^f	human ^g
R_A (s^{-1})	1.7 ± 0.4	0.74	2.4 ± 0.4	1.1	0.83	0.74	0.59-0.83
T_{2A} (s)	0.28 ± 0.08	0.58 ± 0.1	0.18	0.12	0.20	0.18	0.12-0.15
T_{2B} (μs)	11.5 ± 0.0	11.5 ± 1.5	11.5 ± 1.5	12	10		
M_0^B (%)	0.9 ± 0.2	0.4 ± 0.2	1.3 ± 0.6	2.5	1.3		
R (s^{-1})	1.4 ± 0.3	0.6 ± 0.4	2.0 ± 1.4	2.3	1.56		
<i>rmsd</i>	< 0.016	0.015	0.015	0.011	0.017		

Fitting was performed on the mean MT data using a two-pool model function. The value of R_B is not shown because it could not be fitted accurately; it did not affect the value of the other parameters.

^a Values obtained with none of the six parameters fixed. Data are presented as the mean of the fitted parameter with random initial parameter values \pm s.d. of the mean fitted value.

^b R_A is fixed to $0.74 s^{-1}$. Data are presented as the parameter derived from the fit \pm s.d. of this parameter due to the fit.

^c T_{2A} is fixed to 0.18 s. Data are presented as the parameter derived from the fit \pm s.d. of this parameter due to the fit.

^d Values for rat skeletal muscle derived from (7).

^e Values for mouse skeletal muscle derived from (8).

^{f,g} Proton relaxation times of the Cr signal in human skeletal muscle obtained by standard relaxation time measurements at 1.5 T obtained from ^f: (22) and ^g: (23).

DISCUSSION

The present results demonstrate that MT effects can be studied using CW pre-irradiation on a standard clinical MR machine after a relatively simple modification. Water suppression may also lead to an MT effect, however, a CHESS sequence consisting of three 15 ms Gaussian shaped RF pulses did not show this (4). In the present study, only one 26 ms Gaussian shaped RF pulse was used for water suppression and therefore the MT effect observed must be solely attributed to the irradiation pulse.

In the calibration of the pre-irradiation pulse parameters to obtain an MT effect on the methyl resonance of Cr we observed plateau values for the attenuation of this resonance when increasing CW pulse length or pulse power. The pre-irradiation pulse length of 3 s used in the present study is in good agreement with similar calibrations on rat and mouse skeletal muscle (7, 8). The calibration of the $\gamma B_2/2\pi$ pulse power dictated that we had to use somewhat more pulse power (550 Hz) than used in animal studies (325 - 400 Hz) (4, 7, 8). Signal attenuation due to the MT effect is clearly demonstrated when the CW pre-irradiation pulse is between an offset of 0 and ± 50 kHz with respect to the Cr methyl resonance. This frequency range is also observed in other MT studies on Cr (4, 7, 8). In both saturation–time and saturation–power curves (figure 8.3 and 8.4) the intensity of the Cr signal maximally decreased to a value of 70% of its original intensity. This is less than found in rat skeletal muscle, where Cr is decreased to 60% of its original intensity (7), and it corresponds with a calculated immobile Cr fraction of 0.4%-1.3% in our study which is slightly less than observed in the same rat study (2.5%). Similar differences in signal attenuation at 10 kHz frequency offset can be interpolated from frequency sweep plots to correspond to small changes in calculated bound fraction (8, 24). Overall, we conclude from our results that the size of the immobile Cr fraction is small in human skeletal muscle and of the same order of magnitude as observed in mouse and rat skeletal muscle. This small size of the immobile and therefore MR invisible Cr signal indicates that absolute quantification of the Cr content in skeletal muscle by ^1H MR spectroscopy using the Cr methyl signal is justified. Rat and mouse skeletal muscle are used as a reference (table 8.1) because, to our knowledge, no fit of MT data to a two-pool model has been performed in humans before. The goodness of the fit, expressed as the rmsd, is similar to the fits on rat and mouse Cr data. Until now, no ^1H MT by saturation transfer has been performed on human muscle although the existence of an MT effect in human muscle was demonstrated using ^1H inversion transfer experiments (13).

The parameters describing the mobile Cr pool, R_A and T_{2A} , appeared to be somewhat higher than values determined by other methods than MT in human muscle at 1.5 T (table 8.1). The only two parameters that are available from other MR techniques are R_A and T_{2A} .

When R_A is fixed, T_{2A} yields a value that is higher than found in literature. On the other hand, if T_{2A} is fixed, R_A is higher than expected from literature. These observations suggest that further research of the model itself is necessary.

When none of the parameters were fixed, the parameters are highly correlated, except for T_{2B} . Fixing one of the parameters, the fit to this model resulted in smaller standard deviations while the rmsd remained the same. This indicates that this model may consist of too many parameters to properly describe this type of data. Combining CW MT experiments with other techniques, like pulsed on-resonance pre-irradiation, could improve the ability of the mathematical model to derive the relevant parameters (6).

In conclusion, our method of integrating a CW power supply into a clinical scanner opens up possibilities to perform detailed studies of the MT effect on various metabolites in human muscle and brain and may even be integrated in other MR (imaging) techniques involving spin saturation.

ACKNOWLEDGEMENTS

The authors would like to thank Marijn Kruiskamp and Gerard van Vliet for providing their software to fit the MT frequency sweep curve. This work was supported by a program grant of the Dutch Organisation for Scientific Research (Medical Sciences).

REFERENCES

1. Wolff, S.D. and Balaban, R.S. Magnetization transfer contrast (MTC) and tissue water proton relaxation in vivo. *Magn Reson Med* 1989;10:135-44.
2. Rudin, M. and Sauter, A. Measurement of Reaction rates in vivo using magnetization transfer techniques. *NMR Basic Principles and Progress* 1992;27:257-293.
3. Dreher, W., Norris, D.G. and Leibfritz, D. Magnetization transfer affects the proton creatine/phosphocreatine signal intensity: in vivo demonstration in the rat brain. *Magn Reson Med* 1994;31:81-4.
4. de Graaf, R.A., van Kranenburg, A. and Nicolay, K. Off-resonance metabolite magnetization transfer measurements on rat brain in situ. *Magn Reson Med* 1999;41:1136-44.
5. Roell, S.A., Dreher, W., Busch, E. and Leibfritz, D. Magnetization transfer attenuates metabolite signals in tumorous and contralateral animal brain: in vivo observations by proton NMR spectroscopy. *Magn Reson Med* 1998;39:742-8.
6. Roell, S.A., Dreher, W. and Liebfriz, D. Combining CW and pulsed saturation allows in vivo quantitation of magnetization transfer observed for total creatine by ¹H-NMR Spectroscopy of rat brain. *MRM* 1999;42:222-227.
7. Kruiskamp, M.J., de Graaf, R.A., van Vliet, G. and Nicolay, K. Magnetic coupling of creatine/phosphocreatine protons in rat skeletal muscle, as studied by (¹H)-magnetization transfer MRS. *Magn Reson Med* 1999;42:665-672.
8. Kruiskamp, M.J., van Vliet, G. and Nicolay, K. ¹H and (³¹P) magnetization transfer studies of hindleg muscle in wild- type and creatine kinase-deficient mice. *Magn Reson Med* 2000;43:657-64.
9. Kruiskamp, M.J. and Nicolay, K. On the importance of exchangeable NH protons in creatine for the magnetic coupling of creatine methyl protons in skeletal muscle. *J Magn Reson* 2001;149:8-12.
10. Helms, G. and Frahm, J. Magnetization transfer attenuation of creatine resonances in localized proton MRS of human brain in vivo. *NMR Biomed* 1999;12:490-4.
11. Meyerhoff, D.J. Proton magnetization transfer of metabolites in human brain. *Magn Reson Med* 1999;42:417-20.
12. Meyerhoff, D.J., Rooney, W.D., Tokumitsu, T. and Weiner, M.W. Evidence of multiple ethanol pools in the brain: an in vivo proton magnetization transfer study. *Alcohol Clin Exp Res* 1996;20:1283-8.
13. Kruiskamp, M.J., de Graaf, R.A., van Der Grond, J., Lamerichs, R. and Nicolay, K. Magnetic coupling between water and creatine protons in human brain and skeletal muscle, as measured using inversion transfer (¹H)-MRS. *NMR Biomed* 2001;14:1-4.
14. Leibfritz, D. and Dreher, W. Magnetization transfer MRS. *NMR Biomed* 2001;14:65-76.
15. Hua, J. and Hurst, G.C. Analysis of on- and off-resonance magnetization transfer techniques. *J Magn Reson Imaging* 1995;5:113-20.
16. Caines, G.H., Schleich, T. and Ryzewski, J.M. Incorporation of magnetization transfer into the formalism for rotating-frame spin-lattice proton NMR relaxation in the presence of an off-resonance-irradiation field. *J Magn Reson* 1991;95:558-566.
17. <http://www.fda.gov/cdrh/ode/95.html>
18. van den Bergh, A.J., van den Boogert, H.J. and Heerschap, A. Skin temperature increase during local exposure to high-power RF levels in humans. *Magn Reson Med* 2000;43:488-90.
19. <http://www.mrui.uab.es/mrui/>
20. Quesson, B., Thiaudiere, E., Delalande, C., Dousset, V., Chateil, J.F. and Canioni, P. Magnetization transfer imaging in vivo of the rat brain at 4.7 T: interpretation using a binary spin-bath model with a superLorentzian lineshape. *Magn Reson Med* 1997;38:974-80.
21. Morrison, C. and Henkelman, R.M. A model for magnetization transfer in tissues. *Magn Reson Med* 1995;33:475-82.

22. Bottomley, P.A., Lee, Y. and Weiss, R.G. Total creatine in muscle: imaging and quantification with proton MR spectroscopy. *Radiology* 1997;204:403-10.
23. Bongers, H., Schick, F., Skalej, M., Jung, W.I. and Stevens, A. Localized in vivo ¹H spectroscopy of human skeletal muscle: normal and pathologic findings. *Magn Reson Imaging* 1992;10:957-64.
24. Dresselaers, T., Bergans, N., Van Hecke, P. and Vanstapel, F. Proton magnetization transfer effect in rat liver lactate. *Magn Reson Med* 2002;47:880-7.

9

SUMMARY

In tissues of all living organisms, energy production and utilization are tightly balanced in a dynamic fashion to be able to comply to fluctuating energy demands. In this homeostatic process, adenosine triphosphate (ATP) is the most important biochemical energy carrier, which fulfills a key role as the main source of fuel for cellular processes. Elaborate systems for the production, use and distribution of ATP work in close conjunction with specific enzymes, like creatine kinase (CK) and adenylate kinase (AK), for energy buffering and transmission. CK stores high-energy phosphoryls (~P) by catalyzing the reaction: creatine (Cr) + ATP <-> phosphocreatine (PCr) + ADP + H⁺, while AK enables reformation of ATP from 2 ADP by catalyzing the reaction: 2 ADP-> ATP + AMP. Together, these circuits provide an integrated metabolic network with high flexibility to meet sudden and large fluctuations in energy demand in tissues like muscle and brain. Disabling one or more enzymes in these circuits, e.g. by genetic knock-out, will promote a re-routing of fluxes through the remaining systems to re-establish the balance between energy production and utilization.

Transgenic mice have become a valuable tool to study the (patho)biological significance of metabolic conversion by individual enzymes and their role in integral physiological pathways. Various tools have been developed to study these mouse models of which magnetic resonance spectroscopy (MRS), monitoring ¹H, ³¹P, or ¹³C nuclei in metabolites is now increasingly applied since it enables a unique view on metabolomics of tissues such as muscle and brain. In particular when the enzymes that are targeted employ MR visible metabolites as substrates, MRS is a very powerful approach. Various MR spectroscopy methods are now available for longitudinal and non-invasive measurements to acquire useful information about structure and function of metabolic networks, cells and tissues in these models. A broad introduction into this theme is presented in **chapter 1**.

The general aim of this thesis was to elucidate the role of CK and AK systems in energy metabolism of muscle and brain as they function in living animals. The specific possibilities and limitations of MR spectroscopy studies on (transgenic) mice with alterations in the high-energy phosphoryl transfer systems are reviewed in **chapter 2**. These first two chapters present the basis to understand the remainder of this thesis which addresses the following specific issues.

Insight in postnatal development of (P)Cr in wild-type (wt) mice and mice lacking both the cytosolic and mitochondrial isoforms of muscle creatine kinase (M-CK/ScCKmit-/-) is of crucial importance in understanding maturation of (P)Cr levels in relation to CK activity. Therefore, PCr and total Cr (tCr) concentration in hind-limb muscles of M-CK/ScCKmit-/- and control mice were determined by in vivo MR spectroscopy and by biochemical means during postnatal growth and adulthood in **chapter 3**. Furthermore, in vitro

CK activity was determined at different ages for both wt and knock-out mice. In wild-type muscle [tCr], the PCr/ATP ratio and CK activity increased rapidly in the first 4 - 7 weeks of age. Remarkably, M-CK/ScCKmit^{-/-} mice showed a similar increase in the PCr/ATP ratio during the first month of age in the presence of only minor brain-type BB-CK activity. Uptake of Cr in muscle appeared to be unrelated to CK activity as tCr increased in the same way in the muscles of both mice types. At older age the PCr/ATP ratio decreased in M-CK/ScCKmit^{-/-} muscles in contrast to wild-type where it still slowly increased, whereas [tCr] was similar for muscle of both mice. Using ¹³C-4 labeled Cr, also a lower PCr/tCr ratio was observed in ¹³C MR spectra of M-CK/ScCKmit^{-/-} muscle. From these data it followed that in vivo global ATP levels at rest are similar in presence or absence of CK. Although Cr could still be converted to PCr in mature M-CK/ScCKmit^{-/-} muscle, the immediate availability of PCr decreased, and PCr became partly inconvertible at older age. Apparently catalysis of the CK reaction by BB-CK, although significant in muscles of newborn mice, gradually declines to very low levels in adulthood. Part or all of this BB-CK may arise from satellite cells fusing with myotubes, a process which is most active during the first months of life. Finally, our observation that the MR and the chemical assessment of muscle [tCr] and PCr/tCr ratio were similar for all mice does not support the existence of a significant MR-invisible or immobile pool of Cr, with a role of CK in this phenomenon.

Because actions of CK are likely concerted with metabolic activity of other enzymes, in particular AK, the collaboration between CK and AK was investigated in **chapter 4** by studying energy-metabolite behavior in hind leg muscles of mice lacking both cytosolic creatine kinase (M-CK) and adenylate kinase (AK1) (MAK^{-/-}) before, during and after an ischemic challenge. Data of similar MR experiments in M-CK and AK1 single knock-out mice were reevaluated and compared to MAK^{-/-} mice to gain insight in the complementary role that these enzyme may have. During the ischemic period, both inorganic phosphate (Pi) accumulation and PCr depletion in MAK^{-/-} were faster than in wild-type mice, but total [PCr + Pi] remained constant in both types of animals. After ischemia, MAK^{-/-} mice had a significant slower recovery of PCr and Pi than wild-type mice, reflecting a severely compromised phosphoryl transfer efficiency. Although basal tissue pH levels were similar, upon ischemia pH started to decline immediately in MAK^{-/-} mice while in wt mice basal tissue pH was initially maintained. Therefore, MAK^{-/-} mice had a lower intracellular pH during most of the ischemic period, suggesting earlier turn-on of glycolysis. As ATP levels appeared similar and were essentially homeostatic in both types of animals, our results suggest that the communication between supply-demand pathways for ~P metabolites, reflected by the pool-dynamics thereof, is deviant in MAK^{-/-} mice.

Cytosolic B-CK and mitochondrial ubiquitous CK (UbCKmit) are the only two isoforms of CK present in the brain. Knocking out both these enzymes fully erases the possibility to phosphorylate Cr, unlike in muscle where trace amounts of CK remain present in double knock-out mice. In light of the current debate in literature on energy metabolism of the brain, analysis of mice with a partial or double deletion of CK may add to this discussion by highlighting the role of CK in neurometabolic coupling to hemodynamic effects of brain activation. To provide a basis for further MR research on the brain of CK deficient mice, **chapter 5** starts with assessing the metabolic and anatomical consequences of partial or complete depletion of this system. Transgenic mice without cytosolic B-CK (B-CK^{-/-}), mitochondrial ubiquitous CK (UbCKmit^{-/-}), or both isoenzymes (B-CK/UbCKmit^{-/-}), were studied by non-invasive quantitative MR imaging and spectroscopy. MR imaging revealed an increase in ventricle size in a subset of B-CK^{-/-} mice, but not in animals with UbCKmit or compound CK mutations. Mice lacking single CK isoenzymes had normal levels of high-energy metabolites and tissue pH. In the brains of CK double knock-outs pH and ATP and Pi levels were also normal, even though PCr had become completely undetectable. Moreover, a 20 – 30% decrease was observed in the level of total creatine and a similar increase in the level of neuronal N-acetyl-aspartate compounds. Although CKs themselves are not evenly distributed throughout the CNS, these alterations were uniform and concordant across different brain regions. Changes in myo-inositol and glutamate peaks did appear mutation-type and brain area specific. Our results challenge current models for the biological significance of the PCr/CK energy system and suggest a multifaceted role for creatine in the brain.

A method to investigate the dynamics of energy metabolic pathways in vivo is by ¹³C MRS using ¹³C labeled compounds. It has proven to be a very useful technique in the brain to provide a window on both energy metabolism and neurotransmitter recycling in humans and rats. Thus far, however, this technique has not been applied yet to the mouse brain to study these processes due to lower SNR in these smaller animals, although it could enhance further knowledge on whether glycolysis is up-regulated in CK deficient mice. Besides up-regulation of glycolysis, also other metabolic adaptation like a faster flux through the Krebs cycle may be possible for CK knock-out mice to comply to their energy needs. To answer these and other questions, ¹³C MRS on the mouse brain had to be developed. **Chapter 6** demonstrates a specifically designed experimental setup to perform in vivo ¹³C MRS of the mouse brain, which enabled monitoring of glucose uptake, lactate and alanine formation, and synthesis of several other compounds including some neurotransmitters with high temporal resolution for the first time in the mouse brain. Furthermore, build-in of label from [1-¹³C] labeled glucose to lactate, alanine and several positions in glutamate and glutamine was compared between wt

mice and mice lacking both B-CK and UbCKmit. It was shown that B-Ck/UbCKmit^{-/-} mice appeared to utilize glucose faster or with an earlier onset than wt animals, although lactate production is significantly less pronounced. Since build-in of label into neurotransmitter seems to be more rapid, these results may point to an earlier onset or a faster glycolysis and a up-regulation of the oxidative processes of energy production in the brain. Although it is still too early to fully clarify the role on CK in physiology and energy metabolism of the brain, the current results enable further in vivo studies using ¹³C MRS e.g. under metabolic stress situations.

Instead of deleting one or more CK isoforms, the generation of Cr itself can be prevented by knocking out the enzyme that catalyzes the final step in the formation of Cr: guanidinoacetate methyltransferase (GAMT). As a model for deficiency of this enzyme as it occurs in humans, a gene knock-out mouse model was generated that yielded mice which completely lack the ability to synthesize Cr. Both for the research on GAMT deficiency in humans as for further exploration on the role of Cr in comparison to role of CK which is depicted by CK deficient mice, this new knock-out model could provide new insights. In **chapter 7**, we report on several metabolic abnormalities in these mice, observed by in vivo and in vitro MR spectroscopy. ¹H MR spectra of brain and hind leg muscle showed a clearly reduced signal of Cr in GAMT deficient (GAMT^{-/-}) animals. Analysis of the ¹H MR spectra of GAMT^{-/-} brain indicated little or no increase of a signal for guanidinoacetate (Gua). In proton MR spectra of muscle, a broad signal of low intensity was observed for Gua. However, substantial Gua accumulation in intact muscle tissue was unequivocally confirmed in high resolution magic angle spinning spectra, in which the Gua signal was resolved as one clear sharp singlet. In ³¹P MR analysis of brain and hind leg muscle a strongly reduced PCr content was shown. In addition, a signal of phosphorylated Gua at 0.5 ppm up-field of PCr was observed, with much higher intensity in muscle than in brain. This signal decreased when ischemia was applied to the muscle and recovered after ischemia was released. Overall the in vivo ³¹P and ¹H MR spectroscopy of GAMT^{-/-} mice is similar to that of human GAMT deficiency.

The presentation of experimental data closes with the description of a study in humans dealing with the visibility of Cr in ¹H MR spectra of human skeletal muscle (**chapter 8**). In rat and mice tissues it has already been demonstrated that the proton invisible pool of Cr is very small. In humans, however, due to technical limitations of clinical MR scanners this was thus far not possible. We retrofitted a clinical 1.5 T MR scanner, and studied the transfer of magnetization (MT) between the mobile (MR visible) spin pool and immobile (MR invisible) spin pool of Cr using continuous wave (CW) pre-irradiation as saturation method for the immobile pool. For this purpose, only slight modifications to the MR system were made. A

specially designed electronic circuit was used to couple a CW amplifier to the RF channel of the scanner. CW pulse power ($\gamma B_2/2\pi$) and pulse length were determined to be approximately 550 Hz and 3 s respectively for optimal signal attenuation of the Cr methyl signal. The bound Cr fraction in human gastrocnemius muscle was determined to be between 0.4% and 1.3% using a two-pool exchange model function describing the MT effect.

10

SAMENVATTING

In weefsels van alle levende organismen is de dynamische balans tussen productie en verbruik van metabole energie nauwkeurig gereguleerd. Zo kan goed worden ingespeeld op de vaak sterk fluctuerende vraag naar energie. Binnen dit homeostatische proces heeft adenosine trifosfaat (ATP) als belangrijkste biochemische energiedrager een sleutelrol. Metabole systemen voor de productie, het gebruik en de distributie van ATP werken nauw samen met specifieke enzymen, zoals de creatine kinases (CK) en adenylate kinases (AK). Deze enzymen zorgen voor de opslag en de verdeling van de energie die verkregen wordt uit ATP. CK slaat hoogenergetische fosfaten ($\sim P$) op door middel van katalyse van de reactie: creatine (Cr) + ATP \leftrightarrow fosfocreatine (PCr) + ADP + H^+ . AK hergebruikt 2 ADP moleculen om één ATP molecuul te vormen door katalyse van de reactie: 2 ADP \rightarrow ATP + AMP. Samen vormen deze systemen een integraal metabool netwerk dat een hoge mate van flexibiliteit bezit om plotselinge grote fluctuaties in activiteit van weefsels, zoals brein en spier, op te vangen. Als één of meer enzymen in dit netwerk functioneel onklaar wordt gemaakt - of helemaal niet meer wordt aangemaakt - bijvoorbeeld door middel van genetische uitschakeling (knock-out), zal dit leiden tot herschikking van de metabole fluxen door de resterende systemen. Een nieuw evenwicht tussen energieproductie en -vraag zal zich dan instellen.

Transgene muizen zijn een belangrijk instrument geworden bij de studie van omzettingsreacties door individuele enzymen binnen integrale metabole netwerken. Er zijn verschillende technieken ontwikkeld om deze muis-modellen te bestuderen. Magnetische resonantie spectroscopie (MRS) is hier één van en biedt de mogelijkheid de aanwezigheid van bepaalde metaboliëten te bestuderen aan de hand van de daarin aanwezige 1H , ^{31}P of ^{13}C atoomkernen. Deze techniek wordt steeds vaker gebruikt omdat het een uniek zicht biedt op het metabole patroon van weefsels zoals brein en spier terwijl het proefdier geheel intact blijft. Met name indien één van de gemodificeerde enzymen MR zichtbare substraten heeft, is MRS een zeer krachtige techniek. Verschillende MRS methoden zijn heden ten dage beschikbaar voor onderzoek in longitudinale niet-invasieve studies naar structuur en functie van metabole netwerken in cellen en weefsels. Een globaal overzicht hiervan wordt gegeven in **hoofdstuk 1**.

De algemene doelstelling voor de promotiestudie beschreven in dit proefschrift was het ophelderen van de rol van het CK en AK systeem in het energie metabolisme van spier en brein in levende dieren. De specifieke mogelijkheden - en de beperkingen - van MR spectroscopie studie aan (transgene) muizen met een veranderde hoogenergetische fosfaat overdracht is beschreven in **hoofdstuk 2**. Deze eerste twee hoofdstukken vormen daarmee de basis om het vervolg van dit proefschrift te kunnen begrijpen. In de daarop volgende hoofdstukken komen meer specialistische onderwerpen aan bod.

Inzicht in de postnatale ontwikkeling van (P)Cr niveaus in de spieren van normale controle muizen en muizen waarbij zowel de cytosolische als de mitochondriële spier isovormen van CK ontbreken (M-CK/ScCKmit--/--) is cruciaal voor het begrip van de relatie tussen (P)Cr niveaus en CK activiteit tijdens ontwikkeling. Zoals beschreven in **hoofdstuk 3** is daarom in spieren van de achterpoot van M-CK/ScCKmit--/-- en controle muizen zowel het PCr gehalte als ook de totale creatine concentratie (tCr) met behulp van een biochemische aanpak en met MRS gemeten. Deze metingen werden zowel tijdens postnatale groei als bij volwassen muizen uitgevoerd. Daarnaast is bij verschillende leeftijden ook nog de in vitro CK activiteit in de spieren van normale en knock-out muizen bepaald. In spieren van normale muizen nam de [tCr], de PCr/ATP ratio, en de CK activiteit snel toe tot ongeveer 4 tot 7 weken na de geboorte. Opmerkelijk was dat tijdens de eerste maand van ontwikkeling in M-CK/ScCKmit--/-- muizen een vergelijkbare PCr/ATP ontwikkeling werd waargenomen. Dit trad op in de afwezigheid van spier-specifieke CKs en vermoedelijk door aanwezigheid van zeer kleine hoeveelheden brein-type BB-CK. De opname van Cr in spier bleek niet gerelateerd te zijn aan de aanwezige CK activiteit omdat tCr in spieren van beide muis typen op een gelijke wijze toenam. In tegenstelling tot de situatie bij normale muizen nam de PCr/ATP verhouding af in CK deficiënte muizen naarmate ze ouder werden, terwijl de [tCr] gelijk bleef in spieren van beide typen muizen. Door gebruik te maken van ^{13}C -4 gelabelde Cr hebben we een lagere PCr/tCr verhouding vast kunnen stellen aan de hand van ^{13}C MR spectra van M-CK/ScCKmit--/-- spieren. Hieruit konden we opmaken dat de globale ATP niveaus in rust niet veranderde bij afwezigheid van CK. Hoewel Cr in de spieren van volwassen CK deficiënte muizen nog steeds kon worden omgezet naar PCr, was de directe beschikbaarheid van PCr afgenomen en werd PCr gedeeltelijk onomzetbaar. Katalyse van de CK reactie door BB-CK was blijkbaar belangrijk in pasgeboren M-CK/ScCKmit--/-- muizen, maar geleidelijk afnemend naar zeer lage waarden bij volwassen muizen. BB-CK in jonge spieren zou kunnen worden ingebracht door satelliet cellen, welke tot celfusie kunnen overgaan tijdens de vorming van nieuwe spiervezels. Satellietcellen komen in grote aantallen voor met name tijdens de eerste levensmaanden. Tot slot kunnen we uit de observatie dat de chemische en MRS bepalingen van spier [tCr] dezelfde waarden opleverden voor alle muizen, concluderen dat er geen bewijs is voor het bestaan van een MR-onzichtbare (of MR-immobile) voorraad van – al dan niet aan CK gebonden - creatine.

Omdat CK aktiviteit zeer waarschijnlijk nauw verweven is met de activiteit van andere enzymen, in het bijzonder met AK, is de metabole samenwerking tussen CK en AK onderzocht in **hoofdstuk 4**. Daartoe hebben wij voor, tijdens, en na een ischemische proef energie metabolieten bestudeerd in spieren van de achterpoot van muizen die zowel de cytosolische CK isovorm (M-CK) als adenylaat kinase (AK) (MAK--/--) misten. Eerder hier

gegenereerde data van soortgelijke experimenten in M-CK en AK1 ‘enkelvoudige’ knock-out muizen werden geheranalyseerd om meer inzicht te krijgen in de aanvullende rol die deze enzymen kunnen hebben. Tijdens een ischemische periode bleek de toename van zowel inorganisch fosfaat (Pi) als de afname van PCr in MAK^{-/-} muizen sneller te verlopen dan in controle muizen, maar de totale voorraad Pi en PCr bleef in beide constant. Na afloop van de ischemie periode hadden MAK^{-/-} muizen een significant langzamer herstel van PCr en Pi waarden, wat een weerspiegeling is van een ernstig verstoorde efficiëntie van fosforyl overdracht. Hoewel de basale pH uitgangswaarden gelijk waren, bleek de pH in MAK^{-/-} muizen tijdens de ischemische periode direct te dalen, terwijl deze bij normale muizen eerst tijdelijk op het beginniveau bleef na inzet van de ischemie. Hierdoor hadden MAK^{-/-} muizen een lagere intracellulaire pH gedurende het grootste deel van de ischemische periode, wat een sneller aktivering van de glycolyse suggereert. Omdat de ATP niveaus gelijk waren en niet veranderden in beide groepen muizen lijken onze resultaten te wijzen op een veranderde communicatie tussen de aanmaak en het verbruik van ~P metabolieten in MAK^{-/-} muizen.

Cytosolische B-CK en één van de twee mitochondriële isovormen van CK, het zogenaamde ubiquitous CK (UbCKmit), zijn de enige twee isovormen van CK die in het brein voorkomen. Met het genetisch uitschakelen van deze twee enzymen is de mogelijkheid om Cr te fosforyleren volledig weggenomen. Dit is dus anders dan in de spier, waar immers kleine hoeveelheden niet-spier CK (B-CK) achterblijven in CK ‘dubbel knock-out’ muizen. Muizen met een gedeeltelijke of totale verwijdering van het CK systeem uit het brein zijn interessant in het licht van een heden ten dage bij voortdurend gevoerde discussie over het karakter van het energie metabolisme van het brein. Met name de mogelijke rol van CK in neurometabole koppeling met hemodynamische effecten in het brein is hierbij interessant. **Hoofdstuk 5** start met de beschrijving van de metabole en anatomische consequenties van een gedeeltelijke of volledige depletie van CK als basis voor verder MR onderzoek. Transgene muizen zonder cytosolische B-CK (B-CK^{-/-}), zonder mitochondriële CK (UbCKmit^{-/-}) of zonder beide enzymen (B-CK/UbCKmit^{-/-}) werden bestudeerd met niet-invasieve quantitative MRI en MR spectroscopie. MRI liet een toename zien in het volume van de hersenventrikels in een subpopulatie van de B-CK^{-/-} muizen, terwijl in muizen met UbCKmit of een samengestelde CK mutatie dergelijke afwijkingen niet werden gevonden. Muizen zonder B-CK of zonder UbCKmit hadden normale niveaus van hoog-energetische metabolieten en een normale intracellulaire pH. Het brein van muizen met een dubbele CK knock-out hadden ook normale ATP en Pi niveaus, evenals een normale pH, maar hier was het PCr niveau zo laag geworden dat deze niet meer te detecteren viel. Daarnaast werd een 20-30% afname in de totale creatine concentratie gedetecteerd, welke samenging met een

soortgelijke toename in componenten die N-acetyl-aspartaat bevatten. Hoewel CK's zelf niet uniform verdeeld zijn over de cellen van het centrale zenuwstelsel waren deze veranderingen wel uniform over de verschillende breinregio's. Veranderingen in myo-inositol en glutamaat waren mutatie en breinregio specifiek. Onze resultaten plaatsen een kritische noot bij de huidige modellen voor de biologische betekenis van het PCr/CK energie systeem en suggereren dat Cr in het brein meerdere functies heeft.

^{13}C MRS met infusie van ^{13}C gelabelde substraten is een methode die de mogelijkheid biedt om de dynamiek van metabole paden te onderzoeken welke te maken hebben met de energievoorziening in vivo. Het is bewezen zeer nuttig te zijn bij onderzoek naar het humane brein en het brein van ratten, waar het een licht werpt op zowel het energie metabolisme als ook op de kringloop van neurotransmitters. Tot op heden is deze techniek echter nog niet toegepast voor studie van het muizenbrein. Hoewel juist deze aanpak ons dus informatie kan verschaffen over de toename van glycolysesnelheid in CK deficiënte muizen blijft het verkrijgen van spectra met een goede gevoeligheid een groot probleem, met name omdat de hersenen van muizen heel klein zijn. Om de mogelijkheid te onderzoeken of naast toename van de glycolyse snelheid ook andere metabole aanpassingen optreden, zoals bijvoorbeeld een verhoogde flux door de Krebs cyclus, moest een verbeterde aanpak van ^{13}C MRS voor het muizenbrein worden ontwikkeld. **Hoofdstuk 6** beschrijft een hiervoor speciaal ontwikkelde opstelling. Hierbij werd het mogelijk om met een hoge tijdsresolutie te kijken naar glucose opname en naar lactaat en alanine productie, en de synthese van verscheidene andere substraten waaronder een aantal neurotransmitters. Overdracht van ^{13}C label van glucose naar lactaat, alanine, en verschillende posities in het glutamaat en glutaminemolecuul werd vergeleken tussen normale muizen en muizen zonder B-CK en UbCKmit. Er bleek dat B-CK/UbCKmit $^{-/-}$ muizen glucose sneller of eerder na de start van de infusie gebruikten dan normale muizen, maar dat de lactaat productie in deze muizen minder was. Omdat ook de inbouw van label in neurotransmitters sneller leek te verlopen, duiden deze voorlopige resultaten op een snellere of eerdere aanschakeling van glycolyse samen met een hogere snelheid van oxidatieve processen in het brein van CK deficiënte muizen. Hoewel het nog te vroeg is om de rol van CK in de fysiologie en het energie metabolisme van het brein volledig inzichtelijk te kunnen maken, bieden de huidige resultaten aanknopingspunten voor verdere in vivo studies met ^{13}C MRS, bijvoorbeeld in situaties met metabole stress.

In plaats van het genetisch uitschakelen van één of meerdere CK isovormen is het ook mogelijk om de vorming van Cr zelf te verhinderen. Dit blijkt mogelijk in muizen waar het enzym dat de laatste stap in de Cr synthese katalyseert, guanidinoacetaat methyltransferase (GAMT), is uitgeschakeld. Deze muizen dienen als model voor humane GAMT deficiëntie en kunnen een bijdrage leveren aan het verkrijgen van nieuwe inzichten in humane GAMT

deficiëntie en de verdere verkenning van de functie van Cr. In **hoofdstuk 7** wordt een verslag gegeven van verscheidene abnormaliteiten die in deze muizen zijn gevonden met in vivo en in vitro MR spectroscopie. ^1H MR spectra van het brein en van spieren uit de achterpoot lieten duidelijk verlaagde Cr signalen zien in GAMT deficiënte (GAMT-/-) muizen. Bij analyse van de ^1H MR spectra van het brein van GAMT-/- muizen werd weinig tot geen toename van guanidinoacetaat (Gua), het initiële substraat van de GAMT reactie, gevonden. In proton MR spectra van de skeletspier daarentegen werd wel een Gua signaal met grote lijnbreedte aangetroffen, maar dit signaal had een kleine amplitude. Duidelijke Gua stapeling werd bevestigd in hoge resolutie ‘magic angle spinning’ spectroscopie van intacte GAMT spieren. In deze spectra verscheen een Gua signaal als een duidelijk en scherp enkelvoudig signaal. ^{31}P MRS van GAMT brein en skelet spier lieten een duidelijk verlaagde aanwezigheid van PCr zien. Daarnaast was - 0.5 ppm verschoven in de richting van het signaal voor γ -ATP - een signaal van gefosforyleerde Gua verschenen. Dit signaal had een duidelijk hogere intensiteit in de skeletspier dan in het brein en nam in skeletspier af op het moment dat de spier ischemisch werd gemaakt. Het signaal nam weer toe nadat de ischemie was opgeheven. In het algemeen lieten de ^1H en ^{31}P MR spectra in GAMT-/- muizen een beeld zien dat overeenkomt met het beeld van patiënten met GAMT deficiëntie.

De presentatie van onze experimentele data eindigt met een beschrijving van een studie naar de zichtbaarheid van Cr in ^1H MR spectra van menselijke skeletspieren (**hoofdstuk 8**). In ratten en muizen was al aangetoond dat de fractie van de totale Cr hoeveelheid die onzichtbaar is in proton MR spectra klein is. Bij mensen was een soortgelijke studie door technische beperkingen van klinische scanners echter niet mogelijk. Wij hebben daarom een klinische 1.5T MR scanner aangepast zodat we overdracht van magnetisatie (MT) van spins van de immobiele Cr fractie (MR onzichtbaar) naar de mobiele fractie (MR zichtbaar) konden volgen. Hierbij hebben we gebruik gemaakt van continue (CW) instraling als verzadigingsmethode van de immobiele fractie. Om dit te bereiken moesten een aantal aanpassingen aan de MR scanner worden verricht. Een speciaal ontwikkeld elektronisch schema werd gebruikt om de CW versterker te koppelen met het RF kanaal van de scanner. De CW pulslengte en het CW vermogen ($\gamma B_2/2\pi$) werden geoptimaliseerd (naar een waarde van ongeveer 3 s en 550 Hz respectievelijk) voor een maximale verzwakking van het creatine methyl signaal. De gebonden fractie van de Cr in de humane gastrocnemius spier werd bepaald middels een uitwisselingsmodel met twee compartimenten dat de overdracht van magnetisatie beschrijft. Een waarde tussen de 0.4% en 1.3% werd gevonden, in overeenstemming met de proefdierstudies.

DANKWOORD

CURRICULUM VITAE

LIST OF PUBLICATIONS

DANKWOORD

Het schrijven van een goed dankwoord is misschien wel één van de lastigste opdrachten bij de afronding van het proefschrift. Niet eens zozeer omdat er de afgelopen jaren veel mensen zijn geweest, zowel privé als op het werk, die een bijdrage hebben geleverd aan het tot stand komen van dit manuscript, dat ze onmogelijk allemaal te noemen zijn. Eerder nog omdat het bedanken van enkele mensen voor een specifieke bijdrage hen tekort zou doen. Het meeste wat mij bij zal blijven van mijn promotietijd is de openheid van de mensen om mij heen en de bereidheid van hen om elkaar verder te helpen bij uitdagingen die een ieder in zijn onderzoek tegen komt. De hierdoor ontstane onderzoekssfeer is niet in een kort dankwoord te vatten.

Met dit in het achterhoofd wil ik toch een aantal mensen even bij naam noemen, te beginnen bij mijn promotores Arend Heerschap en Bé Wieringa. Arend, jouw tomeloze enthousiasme is inspirerend. Het leuke onderzoek dat je me geboden hebt met alle vrijheid daarbinnen maakt dat ik geen moment spijt heb gehad van de keuze om in Nijmegen te komen promoveren. Bé, jou wil ik met name bedanken voor jouw wetenschappelijk scherpe blik op de dingen waar ik mee bezig was. De goede inhoudelijke discussies die we hebben gehad over de verschillende onderwerpen binnen mijn promotie waren zeer leerzaam voor mij en hebben me frequent aangezet tot opnieuw nadenken over de resultaten.

Naast de promotores wil ik alle (ex)leden van de MR spectroscopie groep bedanken voor de geweldige tijd die ik tijdens mijn promotie heb gehad. Verschillende mensen, allen met hun eigen expertise, hebben me geholpen in het opzetten en uitvoeren van mijn onderzoek. Daarnaast hebben we een hoop plezier beleefd in Nijmegen en elders tijdens congressen. Een unieke combinatie van werk en ontspanning op het werk die de al eerder genoemde onderzoekssfeer in belangrijke mate bepaalt. Zonder iemand te kort te willen doen, wil ik Rene in 't Zandt even noemen. Hoewel we maar een half jaar overlap hebben gehad, waarin ik zoveel mogelijk moest leren om 'jouw' onderzoek te kunnen overnemen, was je de daarop volgende jaren altijd bereid vragen te beantwoorden, data op te zoeken, of uit je tenen te halen welk protocol je nou precies had gevolgd voor een bepaalde meting.

Bij celbiologie wil ik de CK groep bedanken. Jullie wisten altijd tijd vrij te maken als deze natuurkundige weer voor een (cel)biologisch raadsel stond. Ook tijdens de vrijdagochtend besprekingen, eerst in het Trigon, later in de research-toren, wilden jullie altijd meedenken met de resultaten van mijn MR-metingen aan jullie muizen. Frank bedankt voor het altijd maar weer beschikbaar hebben van voldoende muizen van meestal ☺ het juiste genotype voor mijn experimenten.

Voor de verzorging van ‘mijn’ muizen wil ik de medewerkers van het dierenlab, en dan in het bijzonder Henk Arnts, bedanken. Naast verzorging kon ik voor diertechnische handelingen, zoals het zetten van een canule in de staart van de muis (waar menig lab jaloers op is), altijd op hen terug vallen.

Mijn paranimfen ben ik zeer erkentelijk dat ze mij terzijde willen staan tijdens de verdediging van mijn proefschrift. Hugo, ik vind het erg leuk dat we na onze studie in een soortgelijk vakgebied terecht zijn gekomen. Dank dat ik altijd stoom bij je mocht afblazen als dat nodig was. Hermien, doordat jij met jouw fysiologische achtergrond een andere kijk hebt dan ik, en door jouw prettige manier van samenwerken, heb ik genoten van het samen met jou opstarten van jouw onderzoek en het afronden van het mijne. Ik hoop dat we nog vele discussies zullen hebben.

Er kan geen fijne werksituatie bestaan zonder een goede warme basis in de privé sfeer. Ik wil daarom alle vrienden bedanken voor hun steun en geduld de afgelopen tijd. Het afronden van een proefschrift slokt flink wat vrije uurtjes op in de weekenden. Komende tijd halen we het in. Dit geldt ook voor de tijd met mijn ouders, schoonouders, broer, zussen en de ‘kolt kent’. Mijn ouders wil ik bedanken voor hun onvoorwaardelijke steun. Al wisten jullie op een gegeven moment tijdens mijn studie en promotie inhoudelijk niet meer precies waar het over ging, ik vind het fijn dat jullie altijd geïnteresseerd bleven en naar de voortgang blijven vragen.

Monique, als laatste wil ik jou bedanken voor alles. Weer een stap in ons leven, de volgende is al gepland. Ik zie er naar uit, en naar wat er weer achter die horizon ligt.

CURRICULUM VITAE

KlaasJan Renema werd geboren op 19 augustus 1975 te Winterswijk. Hij groeide op in Hoogeveen, waar hij in 1992 zijn HAVO- en in 1994 zijn VWO-diploma behaalde aan het Menso Alting College. Aansluitend ging hij Technische Natuurkunde studeren in Groningen. Tijdens deze studie kwam hij in aanraking met protontherapie, een techniek op het raakvlak van natuurkunde en geneeskunde. In een stage van 3 maanden aan het National Accelerator Center (Faure, Zuid-Afrika) kon hij aan dit werkveld proeven. Hij studeerde af aan het Kernfysisch Versneller Instituut te Groningen. Hier werkte hij aan de ontwikkeling van een apparaat dat tijdens protonbestralingen de positie van de protonbundel kan bepalen.

Na afronding van zijn studie startte hij met zijn promotie onderzoek onder leiding van Prof. Dr. A. Heerschap en Prof Dr. B. Wieringa, waarvan de resultaten zijn beschreven in dit proefschrift. Sinds november 2003 is hij in opleiding tot Klinisch Fysicus radiologie, met eerst als opleider Dr. M.A.O. Thijssen, en sinds begin 2005 als opleider Dr. R.L. Kamman.

LIST OF PUBLICATIONS

H.J.A. in 't Zandt, A.J.C. de Groof, W.K.J. Renema, F.T.J.J. Oerlemans, D.W.J. Klomp, B. Wieringa and A. Heerschap. Presence of (phospho)creatine in developing and adult skeletal muscle of mice without mitochondrial and cytosolic muscular creatine kinase isoforms. *J Physiol* 2003; 548 (3): 847-858.

W.K.J. Renema, D.W.J. Klomp, M.E.P. Philippens, A.J. van den Bergh, B. Wieringa and A. Heerschap. Magnetization Transfer Effect on the Creatine Methyl Resonance Studied By CW Off-resonance Irradiation in Human Skeletal Muscle on a Clinical MR System. *Magn Reson Med* 2003; 50: 468-473.

W.K.J. Renema, A Schmidt, J.J.A. van Asten, F. Oerlemans, K. Ullrich, B. Wieringa, D. Isbrandt and A. Heerschap. MR Spectroscopy of muscle and brain in guanidinoacetate methyltransferase (GAMT) deficient mice: validation of an animal model to study creatine deficiency. *Magn Reson Med* 2003; 50: 936-943.

A. Schmidt, B. Marescau, E.A. Boehm, W.K.J. Renema, R. Peco, A. Das, R. Steinfeld, S. Chan, J. Wallis, M. Davidoff, K. Ullrich, R. Waldschütz, A. Heerschap, P.P. De Deyn, S. Neubauer, and D. Isbrandt. Severely altered guanidino compound levels, disturbed body weight homeostasis, and impaired fertility in a mouse model of guanidinoacetate N-methyltransferase (GAMT) deficiency. *Hum Mol Gen* 2004; 14: 905-921.

A. Heerschap, M.G. Sommers, H.J.A. in't Zandt, W.K.J. Renema, A.A. Veltien and D.W.J. Klomp. NMR in laboratory animals. *Methods Enzymol* 2004; 385: 41-63.

H.J.A. in 't Zandt, W.K.J. Renema, F. Streijger, C. Jost, D.W.J. Klomp, F. Oerlemans, C.E.E.M. van der Zee, B. Wieringa and A. Heerschap. Cerebral creatine kinase deficiency influences metabolite levels and morphology in the mouse brain: a quantitative in vivo ¹H and ³¹P Magnetic Resonance study. *J Neurochem* 2004; 90 (6): 1321-1330.

H.E. Kan, W.K.J. Renema, D. Isbrandt and A. Heerschap. Creatine deficient knockout mice use phosphorylated guanidinoacetate for high energy phosphoryl transfer despite lower reaction rates. *J Physiol* 2004; 560(Pt 1): 219-229.

G. Gambarota, M. Philippens, B.E. Cairns, X.D. Dong, W.K.J. Renema, A. Heerschap. MRS assessment of glutamate clearance in a novel masticatory muscle pain model. NMR Biomed 2005, in press.

D.W.J. Klomp, W.K.J. Renema, M. van der Graaf, B.E. de Galan, A.P.M. Kentgens, A. Heerschap. Sensitivity enhanced ^{13}C MR Spectroscopy of the human brain at 3 Tesla. Magn Reson Med 2005, in press.

Invited lectures

W.K.J. Renema, R.L. Kamman, A. Heerschap. Principles of MRI. Annual congress of the european association of nuclear medicine, Helsinki, 2004.

W.K.J. Renema, R.L. Kamman, M.A.O. Thijssen. Principles of CT. Annual congress of the european association of nuclear medicine, Helsinki, 2004.

Abstracts

W.K.J. Renema, A.J. v.d. Bergh, J.A. Pikkemaat, F. Oerlemans, B. Wieringa and A. Heerschap; poster walking tour: 'Short TE CSI at 7T of the mouse brain.' ESMRMB '00 17th Annual meeting, Paris; Mag*ma, supplement to Vol 11 2000.

H.J.A. in 't Zandt, D.W.J. Klomp, F. Oerlemans, C.E.E.M. van der Zee, C. Jost, W.K.J. Renema, B. Wieringa and A. Heerschap; poster walking tour: 'Altered metabolite levels and morphology in creatine kinase deficient mouse brain revealed by quantitative ^1H and ^{31}P MR.' ESMRMB '00 17th Annual meeting, Paris; Mag*ma, supplement to Vol 11 2000.

W.K.J. Renema, A. Schmidt, D. Isbrandt, K. Ulrich, B. Wieringa and A. Heerschap; Oral presentation: ' ^{31}P and ^1H MRS of brain and muscle in Guanidino Acetate Methyltransferase deficient mice.' ISMRM 9th and ESMRMB 18th joint meeting, Glasgow, 2001.

A.J. van den Bergh, W.K.J. Renema, D. Klomp, A. Heerschap; poster: 'Creatine magnetization transfer effect studied by CW off resonance irradiation in human skeletal muscle.' ISMRM 9th and ESMRMB 18th joint meeting, Glasgow, 2001

W.K.J. Renema, A. Schmidt, J.J.A. vanAsten, D. Isbrandt, K. Ulrich, B. Wieringa and A. Heerschap; Oral presentation and poster: ' ^{31}P and ^1H MRS reveal differences between brain and muscle metabolism in guanidino acetate methyltransferase deficient mice.' International Workshop on Non Invasive Investigation of Muscle Function, Marseille, 2001 Mag*ma volume 14(2), 2002.

A. Heerschap, W.K.J. Renema, R. in 't Zandt, A. de Groof, E. Janssen, F. Oerlemans, A. Schmidt, D. Isbrandt, B. Wieringa; Plenary session: 'Genetic modification of energy metabolic pathways in mice assessed by MRS.' International Workshop on Non Invasive Investigation of Muscle Function, Marseille, 2001
Mag*ma volume 14(2), 2002.

W.K.J. Renema, A. Schmidt, J. van Asten, C. Soede, D. Isbrandt, K. Ulrich, B. Wieringa and A. Heerschap; oral presentation: 'Phosphorylated guanidinoacetate is present and metabolic active in muscle of guanidinoacetate methyltransferase deficient mice'
ISMIRM 10th meeting, Hawaii, 2002.

W.K.J. Renema, E.E.W. Janssen, J.F.A. Janssen, F. Oerlemans, B. Wieringa and A. Heerschap; poster: '31P MRS reveals a compromised phosphoryl transfer system in mice lacking both cytosolic CK and AK'
ISMIRM 10th meeting, Hawaii, 2002.

W.K.J. Renema, D.W.J. Klomp, A.J.van den Bergh, B. Wieringa and A. Heerschap; poster: 'Off resonance magnetization transfer of creatine in human gastrocnemius muscle studied by CW irradiation'
ESMRMB '02 19th Annual meeting, Cannes; Mag*ma, supplement to Vol 15 2002.

E. Janssen, W.K.J. Renema, P.P Dzeja, A. Heerschap, A. Terzic and B. Wieringa; oral presentation: 'Disturbed intracellular energetic communication in muscles of mice with combined creatine kinase and adenylate kinase (M-CK/AK1) deficiency.'
European muscle conference, Lunteren, 2003.

G. Gambarota, M. Philippens, B.E. Cairns, W.K.J. Renema, J. Pikkemaat, A. Heerschap; oral presentation: 'MRS Assessment of Glutamate Clearance in a Novel Pain Model'
ISMIRM 11th meeting, Toronto, 2003.

W.K.J. Renema, D.W.J. Klomp, G. Gambarota, F. Oerlemans, B. Wieringa and A. Heerschap; poster: 'In vivo 13C MRS recording of glucose uptake and neurotransmitter metabolism in mouse brain'
ISMIRM 11th meeting, Toronto, 2003.

H.E. Kan, W.K.J. Renema, D. Isbrandt, A. Heerschap; poster: 'GAMT deficient mice compensate lack of (phospho)creatine by using phosphorylated guanidinoacetate for high energy phosphoryl transfer.'
12th Biochemistry of exercise conference, Maastricht, 2003.

H.E. Kan, W.K.J. Renema, D.W.J. Klomp, D. Isbrandt and A. Heerschap; 'Phosphorylated guanidinoacetate is used for high energy phosphoryl transfer in creatine deficient knockout mice despite lower reaction rates.'
ESMRMB '03 20th Annual meeting, Rotterdam; Mag*ma, supplement to Vol 16 2003.

B. Wieringa, W.K.J. Renema, R. in 't Zandt, A. de Groof, E. Janssen, A. Terzic and A. Heerschap; plenary session: 'State-of-the-art in genetic manipulation of rodents.'
ESMRMB '03 20th Annual meeting, Rotterdam; Mag*ma, supplement to Vol 16 2003.

W.K.J. Renema, A.A. Veltien, F. Oerlemans, B. Wieringa and A. Heerschap; oral presentation: 'Development of in vivo ^{13}C MRS to study alterations in glucose uptake and neurotransmitter metabolism in CK deficient mouse brain.'

Workshop on dynamic Dynamic Spectroscopy and Measurements of Physiology, Metabolism and Function, Orlando, 2003.

H.E. Kan, W.K.J. Renema, D.W.J. Klomp, D. Isbrandt and A. Heerschap; oral presentation: 'Effects of creatine supplementation on phosphorylated guanidinoacetate recovery after ischemia in creatine deficient knockout mice.'

Workshop on dynamic Dynamic Spectroscopy and Measurements of Physiology, Metabolism and Function, Orlando, 2003.

H.E. Kan, W.K.J. Renema, D. Isbrandt and A. Heerschap; poster presentation: 'Phosphorylated Guanidinoacetate in muscle of GAMT deficient mice only partly compensates for PCr as assessed by ^3P MRS and functional measurements'

ISMIRM 12th meeting, Kyoto, 2004.

H.E. Kan, W.K.J. Renema, D. Isbrandt and A. Heerschap; oral presentation: 'Magnetic resonance spectroscopy in the validation of a mouse model of guanidinoacetate methyltransferase deficiency'

SSIEM Amsterdam 2004.

W.K.J. Renema, D.W.J. Klomp, A.A. Veltien, F. Oerlemans, B. Wieringa and A. Heerschap; oral presentation: 'Faster glucose conversion with no change in neurotransmitter synthesis rate found in creatine kinase deficient mouse brain using ^{13}C MRS in vivo.'

ESMRMB '04 21st Annual meeting, Copenhagen; Mag*ma, supplement to Vol 17 2004.

H.E. Kan, W.K.J. Renema, D. Isbrandt, and A. Heerschap; oral presentation: 'Cr supplementation results in a shift in relative Pi levels in creatine deficient knockout mice.'

ESMRMB '04 21st Annual meeting, Copenhagen; Mag*ma, supplement to Vol 17 2004.

H.E. Kan, W.K.J. Renema, A. Veltien, D. Isbrandt, A. Heerschap; poster presentation: ' ^{13}C MRS detection of 1- ^{13}C - glycogen in mouse muscle in vivo.'

ESMRMB '04 21st Annual meeting, Copenhagen; Mag*ma, supplement to Vol 17 2004.

D.W.J. Klomp, W.K.J. Renema, M. van der Graaf, B.E. de Galan, A.P.M. Kentgens and A. Heerschap; oral presentation: 'Coil for optimal ^{13}C sensitivity in the human brain at 3T.'

ESMRMB '04 21st Annual meeting, Copenhagen; Mag*ma, supplement to Vol 17 2004.

D.W.J. Klomp, W.K.J. Renema, M. van der Graaf, B.E. de Galan, A.P.M. Kentgens, and A. Heerschap; oral presentation: 'Broadband ^1H to ^{13}C cross polarization in the human brain at 3T.'

ISMIRM 13th Annual meeting, Miami Beach, 2005.